# The Amundsen Sea Expedition 2015 – 2016
# (ANA06B)

Chief Scientist: SangHoon Lee

IBRV Araon, 6 January − 23 February 2016

(Christchurch to Christchurch, New Zealand)

# Prologue

This was the longest Amundsen cruise with the largest number of the cruise participants onboard; 48 of us, scientists and engineers altogether, spent 49 days at sea. This was also the first cruise we failed to recover a few of our moorings, which seemed due probably to dislocation or destruction by iceberg. We grieved more over the lost data that could be restored by no means, unlike the insurance-covered instruments. Radar deployment on the Amundsen glacier was half way achieved because of the tenacious low-pressure front in the Amundsen shelf area, which frequently discouraged the airborne operation. Despite the instrument casualties and aborted air missions, we managed to accomplish most of the planned operations and samplings.

The KOPRI Amundsen project in the phase one and two is to study the warming mechanism of the Western Antarctic, and to establish the basis of the long-term monitoring on the changes of the ecosystem and biogeochemical cycles incurred by the warming. Beginning from 2017, the phase three of the KOPRI Amundsen project will focus more on the ocean-ice interactions, i.e., the ice melting and glacier retreat by oceanic heating. Along with the temperature rise, fresh water discharge and subsequent biochemical changes will affect the ecosystem and biogeochemical cycles; these are also in the phase 3 research objectives. As part of the priming studies, we planted 4 ice radars (ApRES; Autonomous phase-sensitive Radio Echo Sounder) on the Western Getz in this season. Six of ApRES, of which deployment on the Eastern Getz and the Thwaites glacier was given up due to inclement weather during this season, will be planted in the 2017/2018 season. We conducted airborne gravimeter survey over the Western Getz area, in preparation for the future AUV operation. Three mooring lines were installed across the Antarctic Circumpolar Current in the Udintsev Fracture Zone, in order to study the heat flux from mid-latitude ocean to the Amundsen Sea. Many of the ecosystem studies in this season shifted from static profiling of the standing stock to manifesting specific biological processes in situ. Although the loss of sediment trap samples of K1 (sea-ice margin) and K2 (polynya) left a critical blank in the serial data set, we have obtained instead sediment cores from the area, which will reveal the organic sediment accumulation rates.

This cruise report catalogues the scientific activities we have performed during the 4$^{th}$ field expedition, which wraps up the second phase of the KOPRI Amundsen project. This report provides readers with valuable information on the multinational research effort ongoing in the Amundsen Sea. Credits and gratitude should go to the entire members of the Amundsen team, officers and crew of IBRV Araon.

Chief Scientist of the 2016 Amundsen Expedition, SangHoon Lee

# Contents

**1. Physical Oceanography in Amundsen Sea** ..... **4**

1.1. Hydrographic Survey .....5

1.2. Long-term Mooring Systems .....9

1.3. Glider Operations .....25

1.4. Surface Drifter Deployment .....27

1.5. XCTD Launching .....29

1.6. T-pops Deployments .....29

Appendix 1.1. ANA06B cruise log spread sheet .....32

Appendix 1.2. All design diagrams of moorings .....41

Appendix 1.3. Multibeam survey results .....60

Appendix 1.4. Triangulation results .....64

Appendix 1.5. ADCP deployment files .....76

**2. Chemical Oceanography** ..... **82**

2.1. Nutrient measurements .....82

2.2. Dissolved and particulate matters .....83

2.3. Sulfur species in marine aerosols .....85

2.4. Dissolved oxygen determined by automated amperometric titrator .....87

2.5. Continuous $O_2$/Ar measurement as a proxy of net community production .....90

2.6. Underway measurement of DMS using MIMS system .....93

2.7. Water sampling for the measurement of noble gases .....95

2.8. On-board measurements of noble gases using a membrane inlet mass spectrometer .....96

2.9. Inorganic Carbon System and Dissolved Trace Gases .....100

2.10. Greenhouse gases other than $CO_2$ .....103

2.11. Clean sampling for trace metals (Fe, Cd) .....106

2.12. Carbon cycling on the Amundsen Shelf: Insights from radiocarbon analysis .....107

2.13. Sediment trap .....110

2.14. Sediment sample by Box-core .....112

**3. Biological Oceanography** ..... **116**

3.1. Phytoplankton community ..... 116

3.2. Primay production and macromolecular composition of phytoplankton ..... 120

3.3. Phytoplankton physiology by photochemistry ..... 124

3.4. Abundance and distribution of mesozooplankton ..... 128

3.5. Acoustics ..... 131

3.6. Grazing impacts and community structure of heterotrophic protists ..... 135

3.7. Bacterial respiration ..... 138

3.8. Metagenome and production of virus ..... 140

3.9. Transcriptome samples from phytoplankton ..... 145

3.10. Live/dead status of the heterotrophic prokaryote community ..... 146

3.11. Mixotrophy and selectivity of bacteria *in situ* by CARD-FISH ..... 148

3.12. Bacterivory ..... 150

**4. Physical Oceanography in Udintsev Fracture Zone** ..... **152**

**5. Geophysics on Getz** ..... **160**

5.1. Introduction ..... 161

5.2. Automous Phase-sensitive Radio Echo Sounders (ApRES) ..... 163

5.3. Seismic surveys at the ApRES sites ..... 168

5.4. Airborne gravimetry ..... 171

**6. Atmospheric Science and Glaciology** ..... **177**

**7. Ocean Optics** ..... **183**

**Appendix I. Cruise Participants and Contact information** ..... **187**

**Appendix II. Group photo** ..... **188**

# Chapter 1

# Physical Oceanography in Amundsen Sea

T.W. Kim[1], K.H. Cho[1], C.S. Kim[1], H.W. Yang[1], H.S. La[1], J.H. Lee[2], D.K. Kim[2], J.H. Jung[2], A.K. Wåhlin[3], K.M. Assmann[3], E. Darelius[4], E.P. Abrahamsen[5], and N. Waite[6]

[1]Korea Polar Research Institute (KOPRI), Incheon 406-840, Korea
[2]Korea Institute of Ocean Science and Technology (KIOST), Ansan 425-600, Korea
[3]University of Gothenburg (UGOT), Gothenburg, Sweden
[4]University of Bergen (UiB), Bergen, Norway
[5]British Antarctic Survey (BAS), Cambridge, UK
[6]Rutgers University (RU), New Brunswick, NJ 08901, USA

## 요약문

2015/16년 겨울, 쇄빙연구선 아라온호를 이용하여 남극 아문젠 해에서 4번째 종합적인 해양탐사를 실시하였다. 해양물리 분야의 주된 연구주제는 아문젠 해(Amundsen Sea) 에서 남극순환심층수(circumpolar deep water) 분포의 시공간적인 변동성을 규명하고 빙붕 융해수의 분포 및 해양순환에 미치는 영향을 규명하는 것이다. 총 81개의 CTD정점에서 수리적 자료와 해수샘플을 획득하였다. 2014년도에 설치된 6기의 계류시스템 중 닷슨 빙붕(Dotson Ice Shelf) 전면 및 서쪽에 설치된4기의 계류시스템을 회수하여 갯츠 빙붕(Getz Ice Shelf)에 다시 계류하였으며, 닷슨 골(Dotson Trough)에 설치된 2기의 계류시스템 중 1기는 전체 망실 1기는 시스템의 상부가 망실되었다. 이중 아문젠 해 폴리냐 (Amundsen Sea Polynya)에는 여분의 장비를 활용 다시 계류하였다.

국제공동연구의 일환으로, 스웨덴 고덴버그 대학, 노르웨이 베르겐 대학, 영국 남극연구소, 미국 럿거스 대학과 공동 현장조사를 실시하였다. 고덴버그 대학에서 기존에 설치한 2기의 계류시스템 중 1기를 회수하였으나, 1기는 망실되었다. 그리고 새롭게 2기의 계류시스템을 설치하였다. 베르겐대학에서는 새롭게 4기의 계류시스템을 갯츠 빙붕 전면에 설치하였으며, 영국 남극연구소에서는 기존 설치된 6기의 계류 시스템 중 4기를 성공적으로 회수하였으며 재 계류하였다. 또한 럿거스 대학에서 제공한 글라이더를 닷슨 빙붕 부근에서 약 16일간 운영하였으며, 공간적인 해상도가 높은 자료를 획득하는 데 성공하였다.

## Abstract

In order to monitor the temporal and spatial variation of circumpolar deep water (CDW) and its effect on the rapid melting of glaciers in the Amundsen Sea, an extensive oceanographic survey was conducted on the 2016 expedition (ANA06B). The overall aims in the field of physical oceanography were: (1) to identify the temporal and spatial variation of Circumpolar Deep Water (CDW) in the Amundsen Sea and (2) to estimate the effect of meltwater from glaciers on the ocean circulation. During the 2016 Amundsen Sea cruise (ANA06B) by IBRV Araon, a total of 81 CTD stations were visited, 9 moorings were successfully recovered and 6 moorings were newly deployed on the shelf

troughs and near the ice shelf fronts. Three moorings were partially (one mooring) or entirely (two moorings) lost. A total of seven moorings installed in front of Getz Ice Shelf will reveal the circulation pattern, variability and pathways of CDW and meltwater that have not yet been observed. One Teledyne Webb Slocum glider provided by RU was operated in front of Dotson Ice Shelf to obtain high-resolution data of the Dotson Glacier inflow and outflow of CDW.

# 1.1 Hydrographic Survey

## Introduction

The widespread thinning of the West Antarctic Ice Sheet and its floating ice shelves along the Amundsen Sea coast has been recorded in recent decades and recently attributed to intrusions of warm circumpolar deep water (CDW) onto the continental shelf (Jenkins et al., 2010). The intrusion of relatively warm CDW supplies heat to the ice shelves and has led to increased ice shelf melting (Walker et al., 2007; Wåhlin et al., 2010). The spreading of meltwater from the glaciers probably influences water mass properties and ocean circulation in the polynya. Despite the importance of the spatial-temporal variability of CDW in the continental shelf, vital knowledge for assessing the role of various forcing mechanisms is very limited, primarily due to a lack of in-situ data in this remote area with harsh weather, sea and ice conditions. In order to understand the CDW's role in the hydrodynamics in the Amundsen Sea, shipborne measurements were conducted during the 2015/16 expedition (ANA06B). The overall aims of the physical oceanography group are:

- To identify the temporal and spatial distribution of CDW on the Amundsen shelf,
- To reveal the main forcing that affects the flow rate of CDW onto the Amundsen shelf, and
- To identify the spreading of meltwater from ice shelves and its effect on the ocean circulation.

From these measurements, the oceanic heat transport to the glacier and its effect on the meltwater production will be estimated. The spreading of glacier meltwater to the adjacent sea will cause changes in water mass properties and ocean circulation patterns.

## Materials and methods

An intensive oceanographic survey was conducted in the period of January 6, 2016 - February 23, 2016 using the IBRV Araon to understand the spatial and temporal variability of CDW on the Amundsen Shelf and poleward heat flux across the ACC in Udintsev Fracture Zone (Figure 1.1). A total of 81 CTD stations were visited to collect hydrographic data as well as water samples. At each hydrographic station, at least one cast of the CTD/Rosette system with additional probes (e.g., dissolved oxygen, fluorometer, transmissometer, PAR, etc.) was conducted to measure the vertical profiles of temperature, salinity and other related biochemical parameters. The serial numbers and calibration information of each sensor are given in Table 1.1. During the CTD upcasts, water samples were collected at several depths. For improved accuracy the salinities of collected water samples were further analyzed by an Autosal salinometer (Guildline, 8400B). The measurement was performed when the temperature of water samples was stabilized to a laboratory temperature, usually within 48h after the collection. A lowered acoustic Doppler current profiler (LADCP, RDI, 300 kHz) was attached to the CTD frame to measure the full profile of current velocities. The bin size was chosen as 5 m, and the number of bins was 20. On the cruise track, the vessel-mounted ADCP (RDI, 38 kHz) was continuously operated.

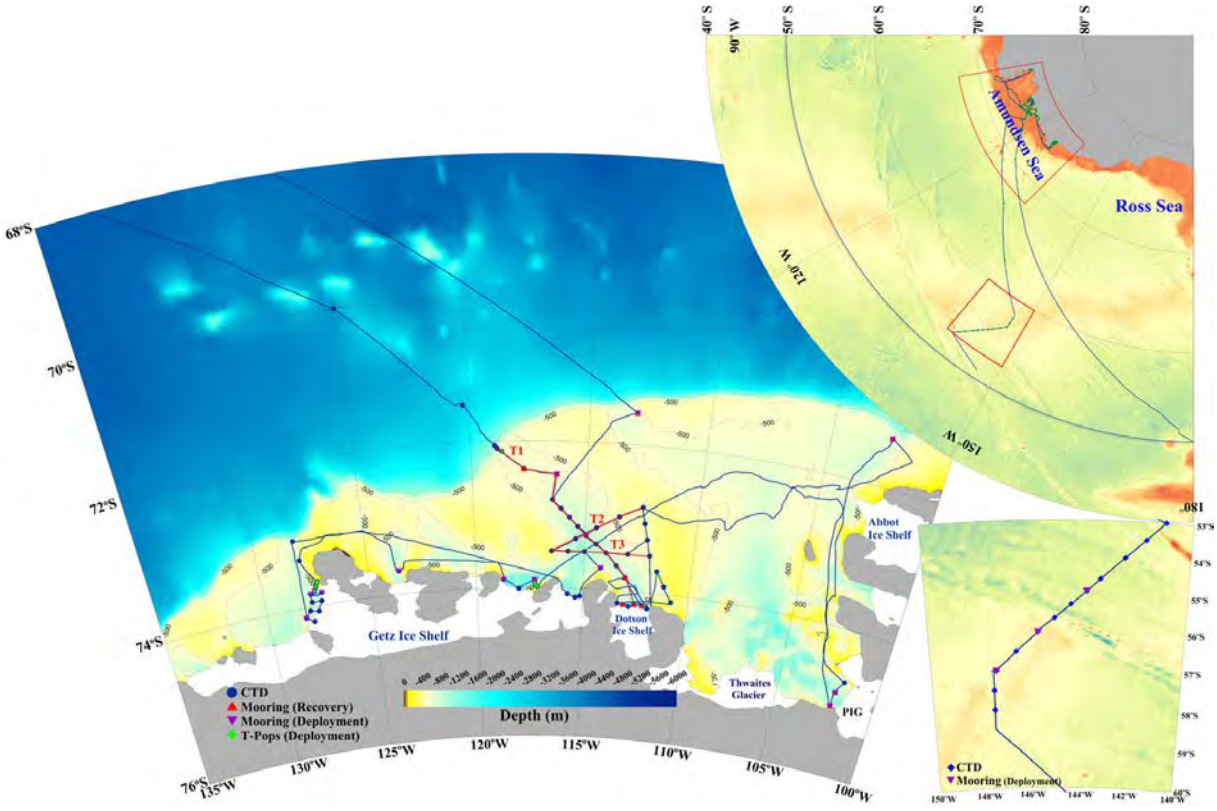


Figure 1.1. Map of study area. Blue dots denote the CTD stations visited during ANA06B expedition. Triangles are the mooring sites. Three transects (T-1, T-2 and T-3) were selected to reveal the spatial distribution of CDW along and cross the Dotson Trough.

Table 1.1. Configuration of CTD (SBE 911plus) sensors used during ANA06B cruise

| Sensor | S/N | Calibration date |
|---|---|---|
| Temperature 1 (SBE 3Plus) | 6017 | July 2015 |
| Temperature 2 (SBE 3Plus) | 5111 | July 2014 |
| Conductivity 1 (SBE 4C) | 4415 | July 2015 |
| Conductivity 2 (SBE 4C) | 3587 | July 2014 |
| Pressure | 1241 | July 2015 |
| Oxygen (SBE 43) | 3190 | July 2015 |
| Fluorometer (WET Labs ECO-AFL/FL) | 3864 | July 2015 |
| Transmissometer (Chelsea/Seatech) | CST-1734DR | July 2015 |
| PAR (Biospherical/Licor) | 1023 | July 2015 |
| Altimeter | 1306 | Nov. 2010 |

## Preliminary results

In January and February 2016, a total of 16 CTD stations were visited along the Dotson trough to investigate the spatial CDW variability along the trough (Fig_1.2). Offshore of the Amundsen Shelf (St.2) the CDW was observed to be warmer than 1.6 °C, and the salinity was 34.7 psu. As the CDW enters onto the shelf region, CDW is modified (colder and fresher) by mixing with cold surface water as well as meltwater from glaciers and sea ice. There is a strong inter-annual variability of the intruded

MCDW. The thickness of CDW (defined by 0°C isotherm) was much thinner in 2014 than in 2012 (Figure 1.2). However, the thickness of CDW layer at continental shelf break had rebounded back in 2016 and the CDW layer thickness was large compared to 2012. This inter-annual variability of CDW thickness probably depends on the local wind pattern and Ekman transport at the shelf break (Kim et al, submitted). The main reasons should be revealed by analyzing long-term ocean moorings and atmospheric data.

Two transects (T-2 and T-3) across the Dotson Trough show the intrusion of warm CDW, tilting toward the eastern side of the trough (Figure 1.3 and Figure 1.4). The existence of the warm, salty water mass suggests that the trough bathymetry plays an important role in defining the inflow/outflow pattern of CDW. Warm and salty southward MCDW inclines toward the eastern flank of the trough by the effect of the Coriolis force and local cyclonic circulation pattern along the east boundary of the polynya. Therefore, the slope of isohalines across the trough was steepest in 2016 when the thickness of warm layer at shelf break was thickest (compared with 2012 and 2014).

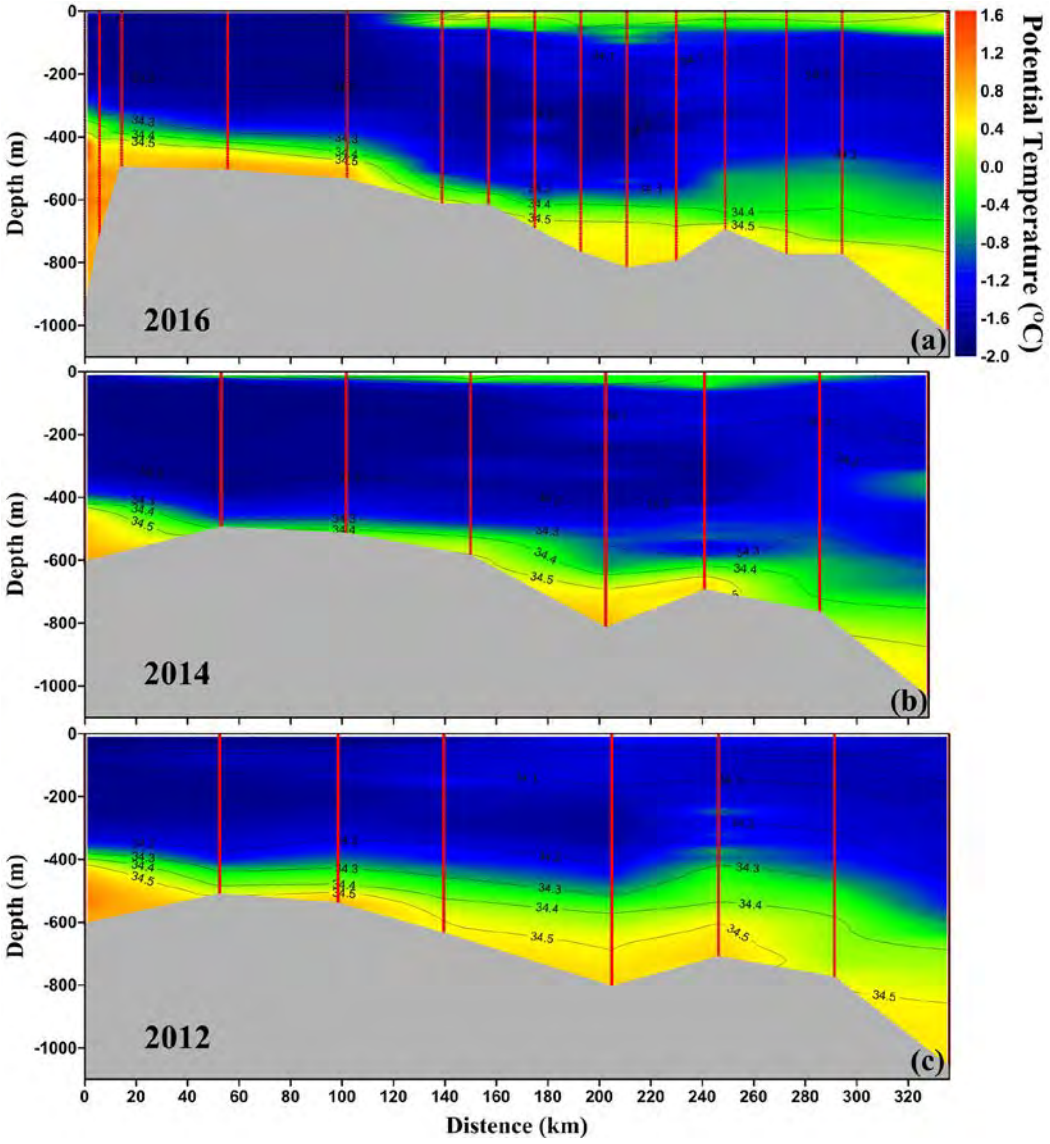


Figure 1.2. Vertical distribution of water mass properties along the Dotson Trough (T-1): (a) 2016 expedition, (b) 2014 expedition, and (c) 2012 expedition. The color indicates the potential temperature, and the contour indicates the isohaline.

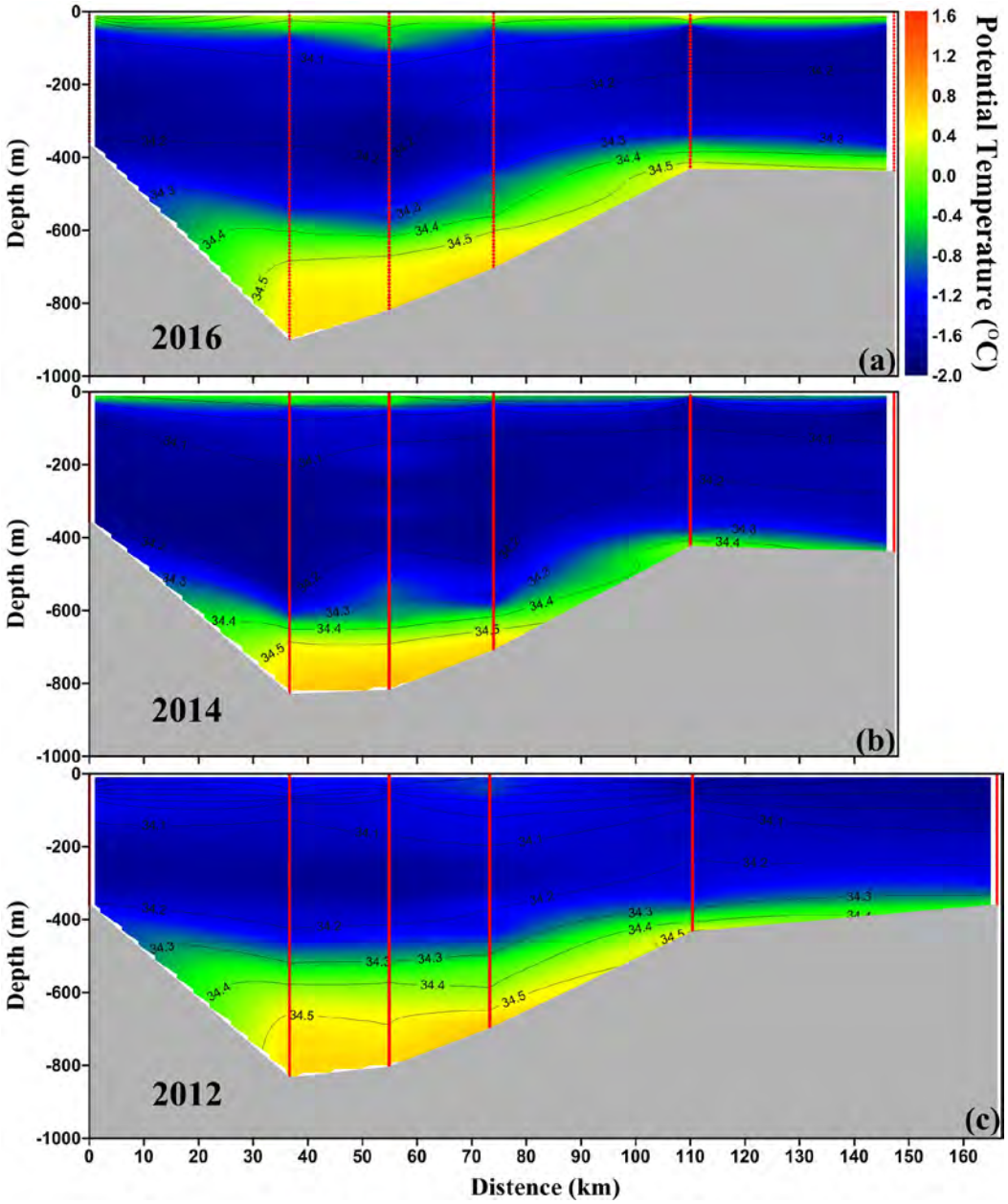


Figure 1.3. Vertical distribution of water mass properties across the Dotson Trough (T-2): (a) 2016 expedition, (b) 2014 expedition, and (c) 2012 expedition. The color indicates the potential temperature, and the contour indicates the isohaline.

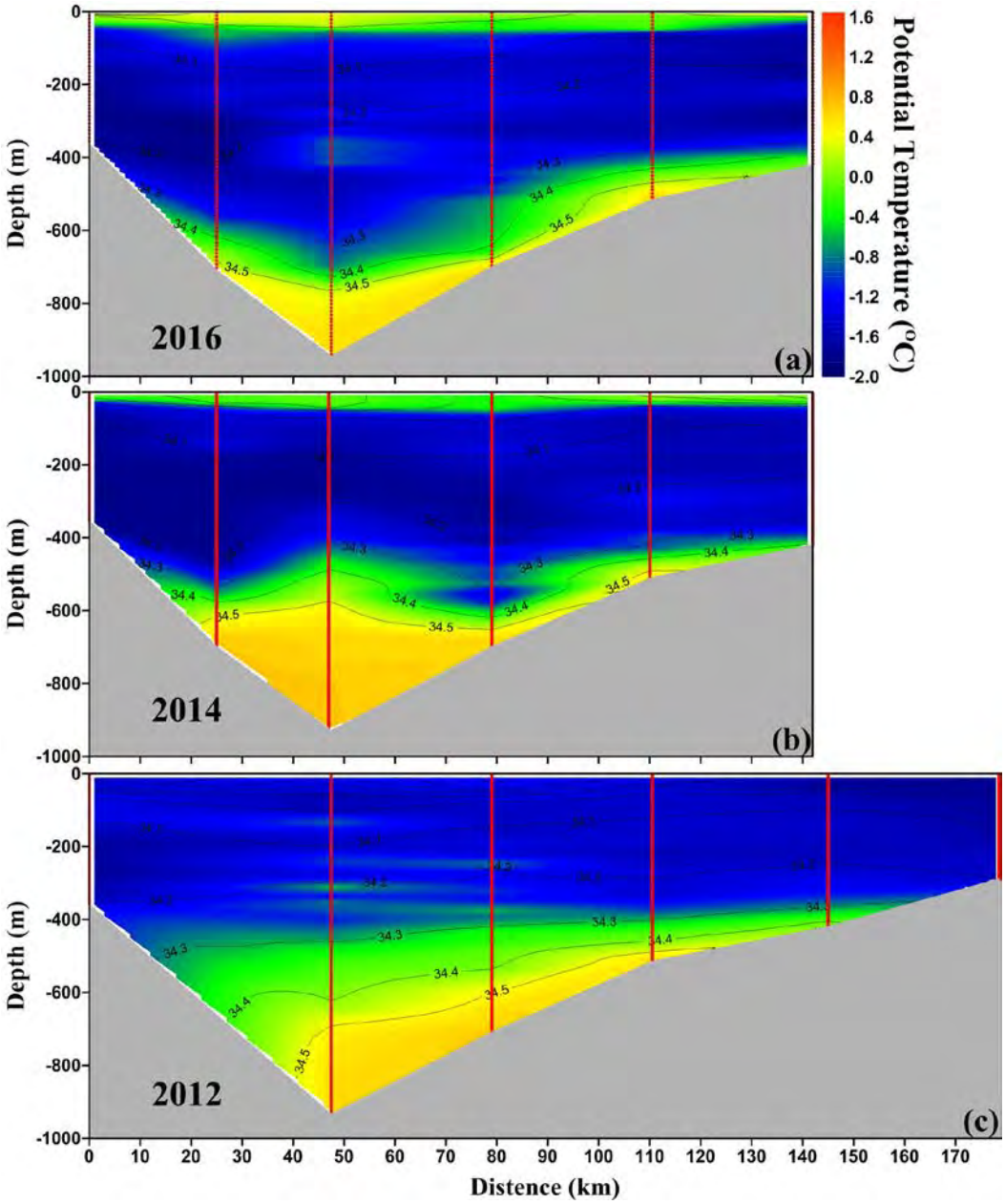


Figure 1.4. Vertical distribution of water mass properties across the Dotson Trough (T-3): (a) 2016 expedition, (b) 2014 expedition, and (c) 2012 expedition. The color indicates the potential temperature, and the contour indicates the isohaline.

## 1.2 Long-term Mooring Systems

### KOPRI moorings

Six mooring systems, installed in 2014 at the northern entrance (K1), the center of polynya (K2), in front of Dotson Ice Shelf (DIS; K3, K4, K5), and western flank of DT (K6?) were attempted to be recovered during ANA06B. However, 2 moorings were partially (K1) or entirely (K2) lost while the rest of the moorings were successfully recovered. Detailed information on the time table for recovery is given in Table 1.2. Four recovered moorings were redeployed in front of Getz Ice Shelf and Bear

Peninsula to reveal the circulation pattern and pathways of CDW and meltwater from the glacier.

**Recovery**

The K1 mooring system including a sediment trap, Microcats, and current meters was installed in the center of DT in 2014 (for the detailed information, see the ANA04B cruise report). For recovery and redeployment of the K1 mooring system, Araon arrived at the mooring location (72° 23.188' S, 117° 42.757' W) on January 16, 2016 14:23 (UTC). First we sent the enable code to wake up the Acoustic Release and checked the distance between Acoustic Transducer and Acoustic Release. We confirmed that the mooring system had been located with same position during last 2 years. On January 16, 2016 15:05 (UTC), we sent the release code to the Acoustic Release and waited for the float groups on the mooring to rise to the sea surface. We only found one float group at sea surface, of a total of 4 float groups, within 40 minutes after release. After recovering the mooring system, we confirmed that the mooring line had been cut (418 m). Also, to measure the biochemical process in Polynya, one mooring system had been installed at center of Amundsen Sea Polynya in 2014. In January 18, 2016, we tried to recover for redeployment but we didn't receive any signal from the acoustic release when we sent the enable code. A line survey using the EK60 and multibeam was executed to confirm the presence of the mooring line in the water but the mooring system had disappeared completely from the mooring location that was determined by triangulation after release of the weight in 2014 (Figure 1.5). Detailed information on the recovered and lost mooring contents was given in Table 1.3. Other moorings (K3, K4, K5, K6) were successfully recovered and measured the time series variation of temperature, salinity and current over more than one seasonal cycle.

Table 1.2. Time table for recovery of mooring systems in ANA06B

| Mooring Recovery | K1 | K2 | K3 | K4 | K5 | K6 |
|---|---|---|---|---|---|---|
| Date | 01/16/2016 | 01/18/2016 | 01/19/2016 | 01/19/2016 | 01/20/2016 | 01/21/2016 |
| Latitude (S) | 72° 23.188' | 73° 16.790' | 74° 10.292' | 74° 10.576' | 74° 10.946' | 73° 49.176' |
| Longitude (W) | 117° 42.757' | 114° 57.024' | 112° 31.699' | 112° 08.083' | 113° 03.823' | 113° 02.712' |
| Arrive station | 14:23 | 2:18 | 17:17 | 9:55 | 5:55 | 1:35 |
| Wakeup AR | 14:45 | 02:27<br>03:09 | 17:18 | 9:57 | 6:01 | 1:35 |
| Release | 15:05 | | 17:21 | 10:43 | 6:20 | 1:36 |
| Find a Buoy | 15:15 | | 17:33 | 10:45 | 6:27 | 1:42 |
| Finish recovery | 16:05 | | 19:18 | 13:41 | 7:37 | 3:59 |

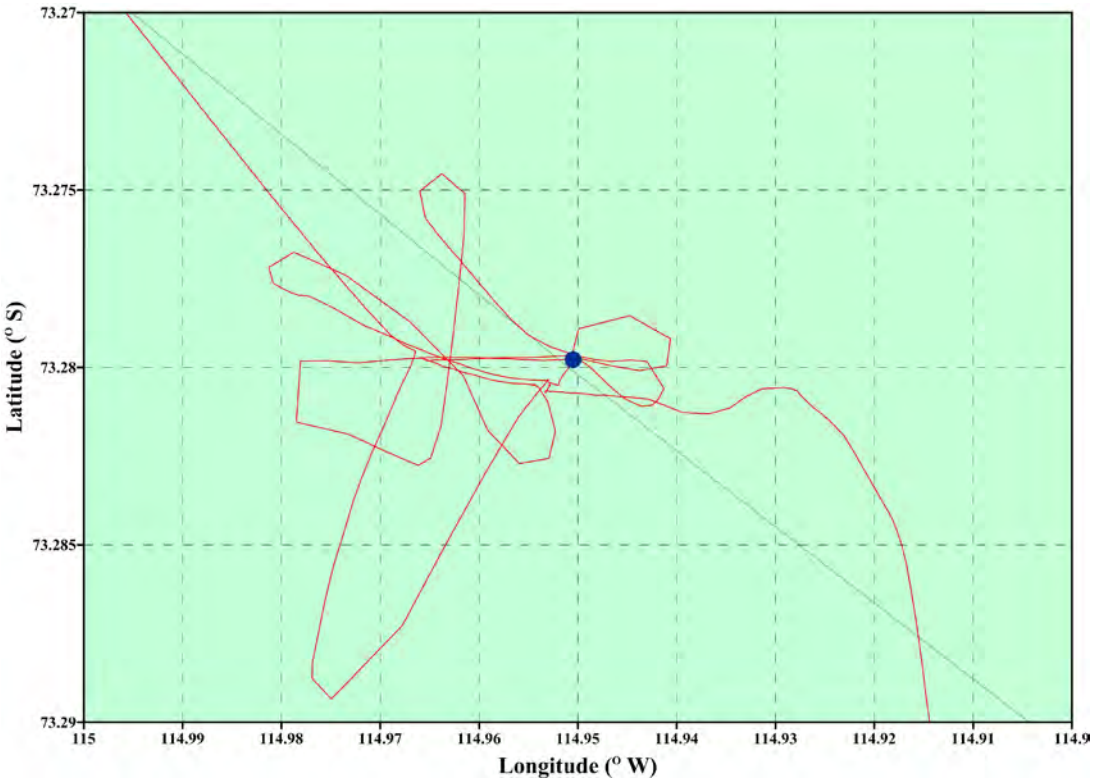


Figure 1.5. Survey line of EK60 and multibeam to confirm the existence of mooring line at K2.

Table 1.3. Lost mooring contents at mooring station K1 and K2

| Mooring St. | Depth | Lost Instrument | Remarks |
|---|---|---|---|
| K1 | 219m | Xenon Flasher, Radio Beacon | KIOST |
| | 266m | RCM-11 | KIOST |
| | 267m | SBE 37 SM | KOPRI |
| | 414m | Sediment Trap | KOPRI |
| | 417m | RCM-11 | KIOST |
| | 419m | SBE 37 SM | KOPRI |
| K2 | 238m | Xenon Flasher, Radio Beacon | KIOST |
| | 265m | Acoustic Zooplankton Fish Profiler | KOPRI |
| | 430m | Sediment Trap | KOPRI |
| | 433m | RCM-11 | KIOST |
| | 434m | SBE 37 SM | KOPRI |
| | 733m | RCM-11 | KIOST |
| | 734m | SBE 37 SM | KOPRI |
| | 814m | Dual Acoustic Release | KOPRI |

**Deployment**

As an international collaboration for monitoring the circumpolar deep water (CDW) and associated rapid melting of glaciers in front of Getz Ice Shelf, three institutes (KOPRI, UGOT and UiB) launched a resource-sharing program. KOPRI is in charge of the monitoring of the eastern part of the Getz Ice Shelf (K4, K5, K6). Another mooring system (K3) was installed just in front of Bear Peninsula to measure the temporal variation of the meltwater fraction from the Dotson Ice Shelf and the Antarctic coastal current (for location, see Figure 1.1). Although the recovery failed, the long-term monitoring station, K2 is a key position for improving the understanding on the biochemical process in Amundsen Sea Polynya. Therefore, we decided to maintain the K2 mooring station using a short mooring design to protect the mooring from icebergs. The setups for MicroCats and ADCP were summarized in Table 1.4 (ADCP) and Table 1.5 (MicroCat). Detailed information on the deployment is given in Table 1.6. After the deployment, the triangulation was made to confirm the settlement status of moorings and record the exact GPS location for future recovery. The design diagrams, Multi survey, and triangulation results for individual moorings are given in Appendix Ⅱ, Ⅲ, and Ⅳ.

Table 1.4. Summary of setups for moored ADCP

| ADCP | | | | |
|---|---|---|---|---|
| | | 75 kHz | 150 kHz | 300 kHz |
| Deployment Timing Setup | Duration(days) | 800 | 800 | 800 |
| | Ensemble interval | 15 min | 15 min | 30 min |
| | Ping int. | 2.5 | 2 sec | 2 sec |
| Profiling Setup | Pings Per | 20 | 20 | 20 |
| | Number of Depth | 60 | 44 | 37 |
| | Depth Cell size | 8 | 8 | 4 |
| Environmental Setup | Transducer Depth | 450 | 450 | 560 |
| | Salinity (ppt) | 35 | 35 | 35 |
| | Transducer Variation | 0 | 0 | 0 |
| | Temperature | -1 | -1 | -1 |
| Deployment Consequences | First cell range | 15.03 | 12.21 | 6.17 |
| | Last cell range | 487.03 | 356.21 | 150.17 |
| | Max range | 478.58 | 355.47 | 105.61 |
| | Standard deviation | 3.27 | 1.59 | 0.79 |
| | Ensemble size | 1354 | 1034 | 894 |
| | Storage required | 99.17 | 75.73 | 32.74 |
| | Power usage | 1510.05 | 1568.77 | 401.68 |
| | Battery usage | 3.4 | 3.5 | 0.9 |
| | Processing Bandwidth (BW) | Narrow BW | Narrow BW | Narrow BW |
| | Power | Low | | |

Table 1.5. Summary of setups for moored MicroCat

| MicroCat | | | |
|---|---|---|---|
| | **37-SM** | **37-SMP** | **37-SMP & IMP (Support By UGOT)** |
| **Sample Interval** | **10 min** | **60 min** | **30min** |
| **Deployment Endurance Calculator** | 1.5 | 1.5 | 1.5 |
| **Model Name** | SBE 37 SM RS-232 | SBE 37 SMP RS-232 | SBE 37 SM RS-232 |
| **Firmware** | Firmware 3.0 and Higher | Firmware 1.0 and Higher | Firmware 3.0 (IMP : 1.0) and Higher |
| **Pressure Sensor** | Strain gauge | Strain gauge | Strain gauge |
| **Sample Interval (sec)** | 600 | 3600 | 1800 |
| **Sampling Type** | Autonomous | Autonomous | Autonomous |
| **Transmit Real time** | Not Enabled | Not Enabled | Not Enabled |
| **Deployment Temperature** | - | -1 | IMP : -1 |
| **Deployment Pressure** | - | 500 | IMP : 500 |
| **Oxygen Time Constant (tau 20)** | - | 5.5 | IMP : 5.5 |
| **Battery Type** | AA Lithium | AA Lithium | AA Lithium |
| **Battery Capacity** | 8.8 Amp-Hours | 257040 Joules | 8.8 Amp-Hours (IMP : 257040 Joules) |
| **Battery Endurance** | 5670 Days | | 5670 Days |
| | Batteries are not expected to last longer 2 years | Pump on before sampling 110.2 seconds | |

Table 1.6. Detail information on deployed KOPRI moorings. GPS location was determined by triangulation after finishing the deployment.

| St. | Latitude (s) | Longitude (w) | Depth(m) | Release Date & Time (UTC) | | CTD St. |
|---|---|---|---|---|---|---|
| | | | | Date (YYYY/MM/DD) | Time (UTC) | |
| K2 | 73° 16.801' | 114° 56.680' | 831 | 2016/02/06 | 21:57 | 12 |
| K3 | 73° 42.680' | 114° 12.916' | 593 | 2016/01/25 | 02:26 | 36 |
| K4 | 73° 53.325' | 118° 43.681' | 688 | 2016/01/30 | 18:56 | 55 |
| K5 | 73° 56.265' | 117° 16.520' | 658 | 2016/01/31 | 10:16 | 58 |
| K6 | 73° 53.990' | 117° 16.368' | 1095 | 2016/01/31 | 06:25 | 57 |

## UGOT moorings

One mooring was recovered and two moorings were deployed during the cruise – see Figure 1.1 for mooring sites. In addition, two attempted recoveries of mooring UGOT5 were performed without success. The mooring had moved 800 m from its original deployment position, into a shallow region and it was only 400 m deep at the site where the releases were now located. The initial recovery attempt on 26/01/2016 had to be aborted due to an approaching storm. On the second attempt on 30/01/2016, contact was obtained with both releases and successful release commands were sent, but

the mooring did not surface. We also searched for the buoys with the multibeam as well as the EK60, but there was no trace of either the top or the ADCP buoys. There was one strong return close to the bottom at one occasion from the EK60, but it was unclear if that was the ADCP buoy or not.

Table 1.7. Information about UGOT moorings

| | UGOT1 | UGOT5 | UGOT6 |
|---|---|---|---|
| **Anchor Release** | | | |
| **Latitude** | 72° 27.2552S | 73° 39.545 S | 73°S 49.9010’ |
| **Longitude** | 116° 21.270 W | 118° 58.445 W | 127°W 16.5232’ |
| **Depth** | 552 m | 480 m | 605 m |
| **Time** | 20160116 | 20140116 | 20160128 |
| **Triangulation** | | | |
| **Sound velocity** | 1453 m/s | 1453 m/s | 1453 m/s |
| **Lat1** | 72° 27.1047 S | 73° 39.5973 S | 73° S 50.0524 |
| **Lon1** | 116° 20.664 W | 118° 57.999W | 127° 15.9098 |
| **Range1** | 778 m | 1133 m | 774 m |
| **Lat2** | 72° 27.5506 S | 73° 39.4785S | 73°S 49.990’ |
| **Lon2** | 116° 20.9664 W | 118° 59.2021W | 127°W 17.5901’ |
| **Range 2** | 821 m | 556 m | 783 m |
| **Lat3** | 72° 27.1549 S | 73° 39.2658S | 73°S 49.6239’ |
| **Lon3** | 116° 21.9667 W | 118° 59.2230W | 127°W 16.5462’ |
| **Range 3** | 714 m | 582 m | 818 m |
| **Mooring Position** | | | |
| **Latitude** | **72° 27.250' S** | **73° 39.403’ S** | **73°S 49.913’** |
| **Longitude** | **116° 21.270' W** | **118° 59.857’W** | **127°W 16.5462’** |
| **2-D error** | 6 m | 4 m | 1 m |
| **Depth, multi-beam** | 552 m | 400 | 605 m |
| **Acoustic Releases** | | | |
| **SN1** | 48122 | 50773 | 50774 |
| **E/R codes** | D/A | G/H | E/F |
| **Rx/Tx** | 10/12 | 14.0/12.5 | 15.0/13.0 |
| **SN2** | - | 55012* | 55048* |
| **E/R codes** | - | B/C | H/G |
| **Rx/Tx** | - | 8.0/10.0 | 9.0/10.0 |
| **Station info** | | | |
| **Station name** | ANA06B07 | - | ANA06B47 |

* Releases marked with * are long-life option (4 years of battery)

The location of mooring UGOT1 (552 m depth) was chosen to continue the long time series at S1 that has been maintained since 2009. The location of UGOT6 (600 m depth) was chosen to study the inflow of warm water towards the Getz ice shelf between Siple and Dean Island, and complement the three UiB moorings deployed there. UGOT6 was placed only 0.5 nautical miles out from the ice shelf front while the UiB moorings were placed about 7 nautical miles away from the front. By comparing the moorings it will be made clear how much of the water flowing towards the ice shelf front actually enters into the ice shelf cavity. The final position of the moorings was chosen after undertaking a bathymetric survey using the multibeam. Details about mooring deployment and triangulation are given in Table 1.7. For mooring design see Appendix 2 and for triangulation results see Appendix 4.

The moorings are equipped with SBE37SMP, SBE37IMP, SBE56, and an RDI ADCP 150 kHz and single or double acoustic releases from Benthos, see Table 1.7 and Appendix 2. All MicroCats are

pumped and have pressure, conductivity and temperature sensors. Three of the SBE37 (s/n 11213, 11214 and 9018) have oxygen sensors. The releases have a guaranteed life time of either 2 (s/n 48122 and 50774) or 4 (s/n 55048) years. Both moorings have a recovery float attached with a 7 m floating rope. The sampling interval was set to 5 min for SBE56 (batteries lasting >10 yrs), 30 min for SBE37SMP (batteries lasting > 4 yrs), and 120 min for the SBE37 with oxygen sensors. The ADCP deployment files are included in Appendix 5. Instruments belonging to KOPRI are marked with asterisks in Appendix 2. Figure 1.6 shows the entire 6-year time series of bottom temperature and along-trough velocity from S1. Figure 1.7 shows the last two years of S1 temperatures and velocities as a function of time and depth.

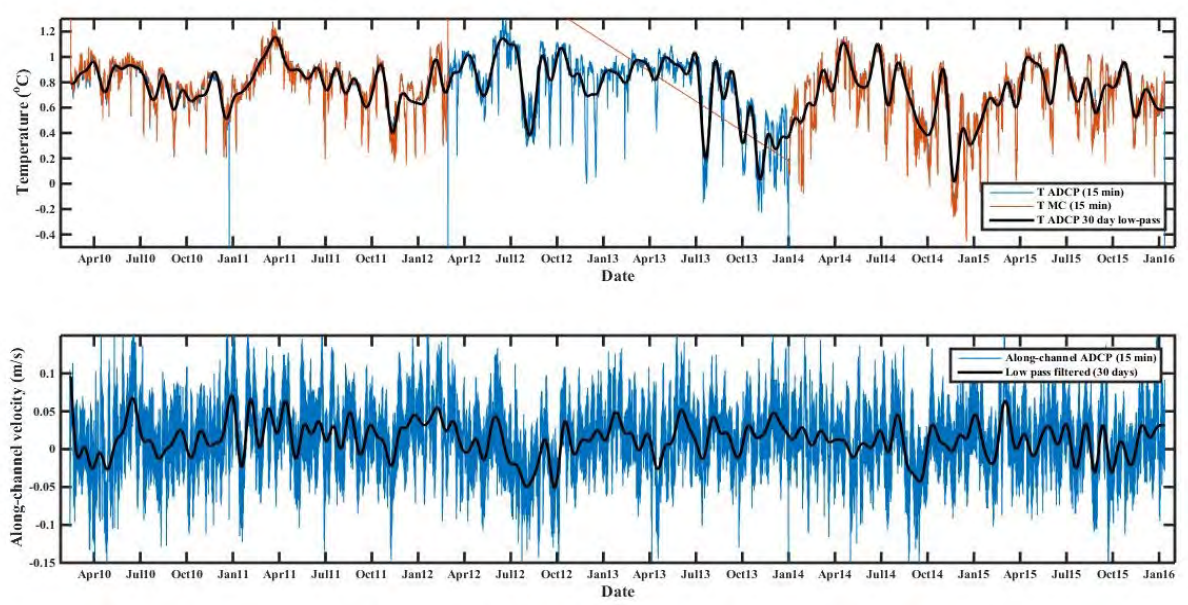


Figure 1.6. The 6-year time series from UGOT1. Top panel: Bottom temperature. Bottom panel: Along-channel velocity.

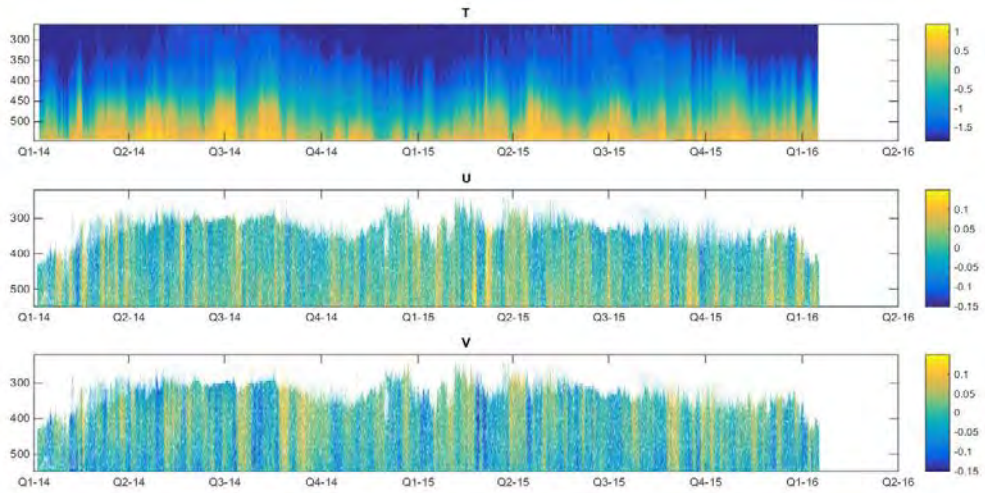


Figure 1.7. Temperature (top panel), eastward velocity (center panel) and northward velocity (bottom panel) as a function of time and depth for UGOT 1.

## UiB moorings

Four moorings were deployed during the cruise – see Figure 1.1 for mooring sites. The location of mooring UiB1 (710 m depth) and Mooring UiB4 (600 m depth) was chosen to study the inflow of warm water towards the Getz ice shelf between Siple island and Dean island, while mooring UiB2 (600 m depth) is meant to capture the outflow of warm water-meltwater mixture on the east side of the same front. The inflow moorings are complemented by the UGOT mooring S6, which is placed along the same isobaths as UiB4 but much closer (within a Rossby radius) to the ice shelf front. UiB3 is placed along the eastern slope leading into the ice shelf front between Siple Island and Carney Island to study the flow of water towards the Getz ice shelf. Summer-time hydrographic observations from this location show cool water at this location; the maximum temperature observed during ANA06B was -0.18C. The final location of the mooring was chosen after a bathymetric survey using the multibeam. The existing bathymetric charts (IBCSO) proved to be relatively poor, especially in the vicinity of UiB3. The suggested sill of about 650 m isolating the deep inner basin did not exist, and the inner basin is connected to the outer basing by a relatively narrow 850 m deep channel, see Figure 1.8. Details about mooring deployment and triangulation are given in Table 1.8. For mooring design and results from triangulation, see Appendix 1.2 and 1.4.

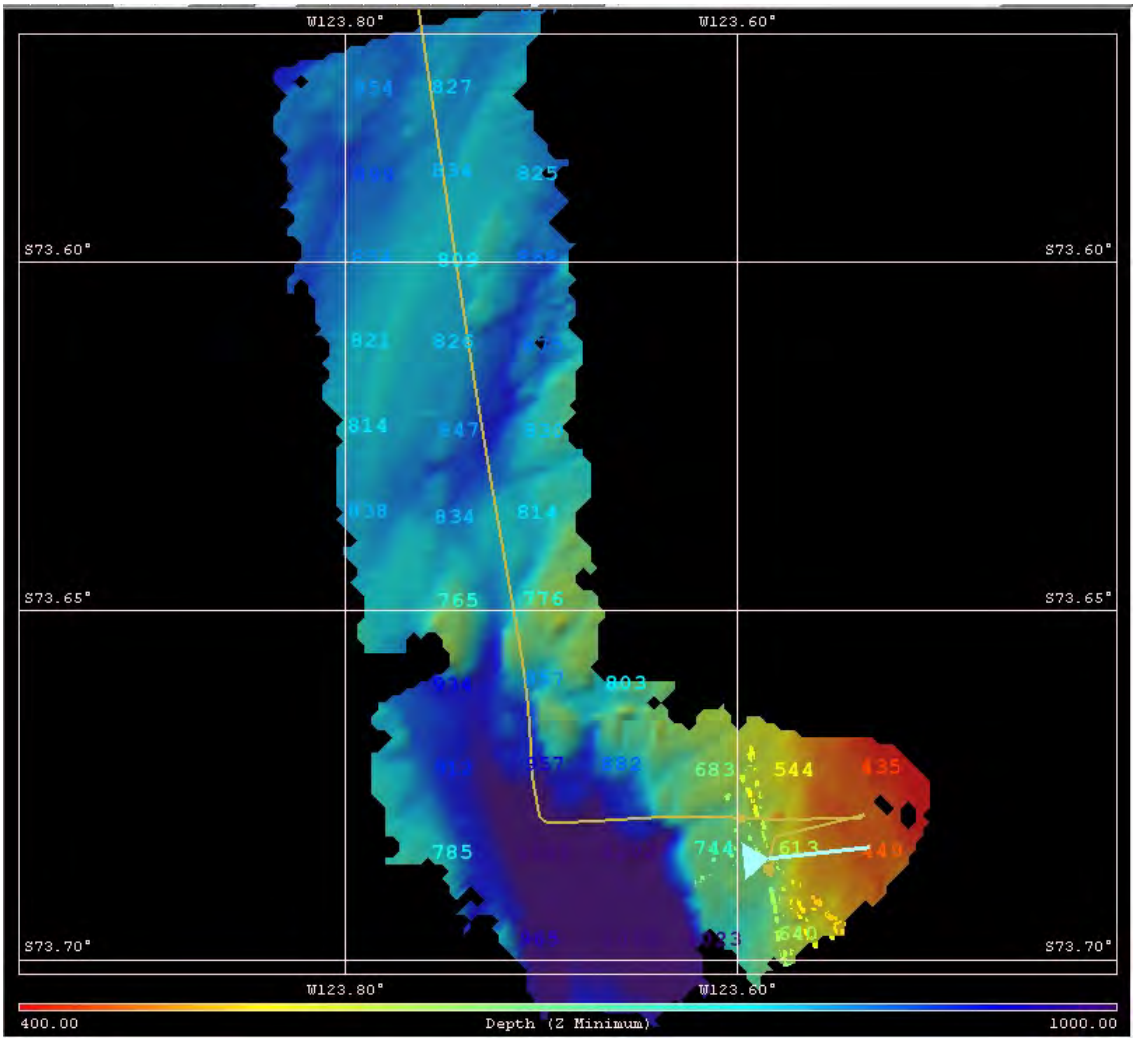


Figure 1.8. Results from bathymetric survey in the vicinity of the UiB3 deployment showing an 850 m deep channel leading into the southern basin.

The (old) deck unit used for triangulation does not account for the 20 ms delay in the response of the releasers, and the ranges given are thus 10 ms x speed of sound = 15 m too large. This has been corrected for in Table 1.8.

Table 1.8. Information about UiB mooring deployment and position. *The range as given by old deck unit using a sound velocity of 1497 m/s and including the delay in the response of the releaser of 20 ms

| | UiB1 | UiB2 | UiB3 | UiB4 |
|---|---|---|---|---|
| **Anchor Release** | | | | |
| **Latitude** | 73° 49.8241S | 74° 8.2957 S | 73°S 41.1210' | 73°S 47.570 |
| **Longitude** | 127° 47.4638 W | 128° 12.721 W | 123°W 34.855' | 127°W 35.9760 |
| **Depth** | 707 m | 600 m | 649 m | 601 m |
| **Time** | 20160128 18:58 | 20160127 23:33 | 20160130 01:44 | 20160128 22:38 |
| **Triangulation** | | | | |
| **Sound velocity** | 1450 m/s | 1447 m/s | 1448 m/s | 1450 m/s |
| **Lat1** | 73° 50.0131 S | 74° 08.4478 S | 73 41.0723 | 73° 47.4122 |
| **Lon1** | 127° 46.9162 W | 128° 12.053W | 123 34.0646 | 127° 35.3503 |
| **Range1** | 893-15 m | 802-15 m | 857-15 m | 825-15 m |
| **Lat2** | 73° 49.8461 S | 74° 8.3847S | 73°S 41.3891' | 73°S 47.875' |
| **Lon2** | 127° 48.4930 W | 128° 13.7401W | 123°W 35.2966' | 127W 35.4708' |
| **Range 2** | 867-15 m | 754-15 m | 798-15 m | 724-15 m |
| **Lat3** | 73° 49.5502 S | 74° 8.0109S | 73°S 40.9310' | 73S 47.6263 |
| **Lon3** | 127° 47.2023 W | 128° 12.7079W | 123°W 35.6510' | 127W 36.8560' |
| **Range 3** | 881-15 m | 816-15 m | 850-15 m | 835*-15 m |
| **Mooring Position** | | | | |
| **Latitude** | **73° 49.800' S** | **74° 8.296' S** | **73°S 41.159'** | **73S 47.671'** |
| **Longitude** | **127° 47.578' W** | **128° 12.916'W** | **123°W 35.048'** | **127W 35.807'** |
| **2-D error** | 0 m | 7 m | 1 m | 6 m |
| **Depth, triangulatio** | 707 m | 591 m | 648 m | 609 m |
| **Acoustic Release** | | | | |
| **SN** | 1807 | 1868 | 1806 | 1222 |
| **ARM code** | 0AE3 | 1ACC | 0AE2 | 0899 |
| **Station info** | | | | |
| **St. number** | ANA06B48 | ANA06B42 | ANA06B54 | ANA06B49 |
| **CTD-cast** | 481 | 421 | 541 | 491 |

The moorings are equipped with SBE37, SBE56, RDI ADCP (300 kHz / 150 kHz / 75 kHz) and single acoustic releases from IXSEA, see Table 1.9-12 and Appendix 2. Three of the SBE37 have oxygen sensors. The releases all have lithium batteries that have an estimated life time of 5-7 years. All moorings have a top-buoy attached with a 10 m floating rope. The sampling interval was set to 1 min for SBE56 (batteries lasting >4 yrs), 10 min for SBE37 (batteries lasting > 4 yrs), 120 min for the SBE37 with oxygen sensors, 60 min for the 300 kHz and 150 kHz ADCPs and 120 min for the 75 kHz. The ADCP deployment files are included in Appendix 5.

The following SBE37 have oxygen sensors: The following SBE37 have conductivity, temperature and pressure sensors: 5446, 5448, 7223, 7224, 8971 and 8972, and these have conductivity and temperature only: 5251, 5252 and 5409. Apart from the SBE37 with oxygen sensors, none of the UiB SBE37 is pumped. LOTUS buoy #9 (UGOT) was attached to UiB4, 250 mab. LOTUS buoy #10 was deployed in the vicinity of UiB4. Instruments belonging to UGOT are marked with asterisks in Table 1.9-12. UiB2 include an ADCP (300 kHz) from UGOT and UiB3 include an SBE37 (pumped,

conductivity, temperature and pressure) from UGOT. Note that UiB1 is referred to as mooring #3, UiB2 as mooring #4, UiB3 as mooring # 2 and UiB 4 as mooring #1 in the station plan. NB! SBE56 s/n 4592 and s/n 4594 on UiB4 might have been switched during deployment.

Table 1.9. Details of mooring UiB1, deployed 20160228

| Mab | Sn | type | Time (UTC) |
|---|---|---|---|
| 400 | 21396 | ADCP | 18:32 |
| 400 | 5446 | CTD | 18:32 |
| 350 | 1330 | T | 18:36 |
| 300 | 5252 | CT | 18:39 |
| 250 | 1331 | T | 18:41 |
| 200 | 5251 | CT | 18:44 |
| 150 | 1332 | T | 18:46 |
| 100 | 5409 | CT | 18:48 |
| 50 | 1334 | T | 18:50 |
| 25 | 12338 | CTO | 18:52 |
| 20 | 1807 | AR | 18:54 |
| 0 | - | Anchor | 18:59 |

Table 1.10. Details on UiB2, deployed 20160127

| Mab | Sn | type | Time (UTC) |
|---|---|---|---|
| **300** | 7223 | CTD | 23:00 |
| **250** | 1335 | T | |
| **200** | 5448 | CTD | |
| **200** | 21329 | ADCP* | |
| **200** | 17226 | ADCP | |
| **150** | 1338 | T | |
| **100** | 1337 | T | |
| **50** | 1339 | T | |
| **25** | 12339 | CTO | |
| **20** | 1868 | AR | 23:30 |
| **0** | - | Anchor: | 23:33 |

Table 1.11. Details of UiB3, deployed 20160130

| Mab | Sn | type | Time (UTC) |
|---|---|---|---|
| 350 | 8020 | CTD* | 01:21 |
| 300 | 1343 | T | 01:23 |
| 250 | 17227 | ADCP | 01:25 |
| 250 | 7224 | CTD | 01:26 |
| 200 | 1341 | T | 01:29 |
| 150 | 1333 | T | 01:31 |
| 100 | 4434 | T | 01:32 |
| 50 | 4589 | T | 01:34 |
| 25 | 8971 | CTD | 01:39 |
| 20 | 1806 | AR | 01:39 |
| 0 | - | Anchor | 01:44 |

Table 1.12. Details of UiB4, deployed 20160128

| Mab | Sn | Type | Time (UTC) |
|---|---|---|---|
| 255 | 9 | LOTUS* | 22:14 |
| 250 | 18595 | ADCP | 22:14 |
| 250 | 8972 | CTD | 22:14 |
| 200 | 1345 | T | 22:19 |
| 150 | 4590 | T | 22:20 |
| 100 | 4592 | T | 22:22 |
| 50 | 4594 | T | 22:23 |
| 25 | 12340 | CTO | 22:27 |
| 20 | 1222 | AR | 22:28 |
| 0 | - | Anchor | 22:38 |

## BAS moorings

The Natural Environment Research Council (NERC) / British Antarctic Survey (BAS) moorings are a continuation of the NERC iSTAR (ice sheet stability) research program. Originally nine moorings were deployed from RV Araon on ANA02C in 2012 for iSTAR. Seven of these were recovered on the iSTAR research cruise, JR294/5, on RRS James Clark Ross in 2014. One further mooring (iSTAR 3) was located, but did not rise when the release command was given; one attempt was made to drag for it, but this failed, and the mooring was left for later recovery. Five of the moorings were redeployed with slightly reduced instrumentation for a further two years, using NERC National Capability funding through the BAS Polar Oceans Long-Term Monitoring and Survey (LTMS) project.

Our objective during ANA06B was to recover and redeploy these five moorings, and recover iSTAR 3 if possible. Unfortunately, one of the moorings (mid-shelf) was located in the middle of a large area with 98%+ sea ice cover at the time when we could have attempted to recover it, so its recovery was not attempted this year. Time constraints did not allow us to drag for iSTAR 3; however, we did verify that it was still in position, the release was still communicating, and the mooring still did not rise when the release command was sent. However, four moorings were successfully turned around on the cruise, and we have extended the iSTAR time series by two years, including concurrent measurements from the central and eastern troughs leading to Pine Island Glacier. We believe this is the first successful mooring recovery from the eastern trough.

### Instrumentation

The two moorings at the PIG ice front both have one Teledyne RDI Workhorse Sentinel 300-kHz ADCP. These are mounted in Flotation Technologies syntactic foam buoys (one 33-inch, one 24-inch), and both point upward. All of the moorings have two Seabird Electronics SBE-37SM Microcat temperature-conductivity-pressure recorder (unpumped, 2000 m pressure range). The two PIG moorings have one Nortek Aquadopp DW (3000 m) each, the other moorings have two. Mid-shelf was intended to have two, but only one instrument was available when it was first deployed, so on a future cruise a second Aquadopp should be added. All of the moorings have several Aquatec Aqualogger 520T temperature loggers, and one 520PT temperature/pressure logger (all rated to 1000 m, with 512 kb memory). Instrument settings are given in the table below.

Table 1.13. Instrument settings used on the BAS moorings

| | ADCP | Aquadopp | Microcat | Aqualogger |
|---|---|---|---|---|
| Sampling interval | 1800 s | 600 s | 300 s | 300 s (temp only)<br>600 s (with press) |
| Duty cycle | 12 pings per ensemble | 60 s average interval | n/a | n/a |
| Blanking distance | 2.25 m | 0.5 m | n/a | n/a |
| Bins | 20 | 1 | n/a | n/a |
| Bin height | 8 m | 0.75 m | n/a | n/a |
| Battery (2014-16) | 1 RDI alkaline battery pack | 2 Tadiran TLP-82121/C/NO3A | 12 SAFT LS14500 | 1 EVE ER14505 |
| Battery (2016-) | 1 RDI alkaline battery pack | 1 Simpower custom battery: 36 SAFT LS14500 | 12 SAFT LS14500 | 1 SAFT LS14500 |

The Microcats have last been factory calibrated in June 2011. More recently they were attached to the rosette of RRS James Clark Ross for one cast on JR294/5 for comparison against the ship's CTD. The Aqualoggers' factory calibration is not satisfactory, and all the instruments have been calibrated in a bath at BAS against a standard thermometer over a polar temperature range of at least -2 to +4. All of the Aqualoggers were calibrated in this way in 2011, and 14 of the instruments were recalibrated in 2015, with only one instrument showing significant drift.

The ADCP buoys are mounted in-line on the mooring; all remaining instruments are clamped onto the line. Two types of rope are used: 12 mm Gleistein Tasmania double-braid polyester is used in the lower parts of the moorings, and where Aquadopps and Microcats are used. On the upper parts of the moorings where only Aqualoggers are mounted, 8 mm Samson Tenex or Maffioli Evolution Splice single-braid 12-strand polyester ropes are used. Apart from the ADCP buoys, which are syntactic foam, Vitrovex 17-inch glass floats are used as the main buoyancy, mounted on Eddygrip 3/5-m Kevlar ropes, in line with the moorings. At the top of the 8mm rope sections, a 10-m length of 12mm polypropylene (floating) rope is attached, with Neptunplast 629 9-inch trawl floats (1800 m depth rated) clamped on for buoyancy. At least one float is separate from the others, with a length of rope between for easier grappling during recovery. Where instruments or buoyancy are clamped onto the rope, a section of 12/8 mm inner diameter plastic hose/tubing is used as strain relief on the rope. The clamps for the Aquadopps are custom Delrin blocks, based on a design from Bruce Huber at LDEO. The Aqualoggers are attached directly to the rope using size 1M stainless steel Jubilee clips (hose clamps).

**Recovery of PIG_S**

When we arrived at PIG_S there was a jagged iceberg, approx. 0.3 x 0.2 nautical miles large and 20 m high, directly to the west of the mooring. This was drifting to the west, and we therefore considered a release to be safe. A single range was taken 500 m from the previously triangulated point, and this was consistent with the estimated position. However, when released, the mooring surfaced considerably closer to the iceberg than expected. Initially we did not think so much of this; however, from the instrument records it is clear that icebergs moved the mooring twice, in July 2014 and July 2015. From multibeam data gathered on this cruise and on previous USAP cruises, there is one point where the isobath of the final mooring depth nearly intersects the range – and it appears that the mooring happened to land at this spot. Had the triangulation taken place from another point, or had the mooring moved elsewhere, the ranges would have been inconsistent, and a full triangulation would have been done before the mooring was released.

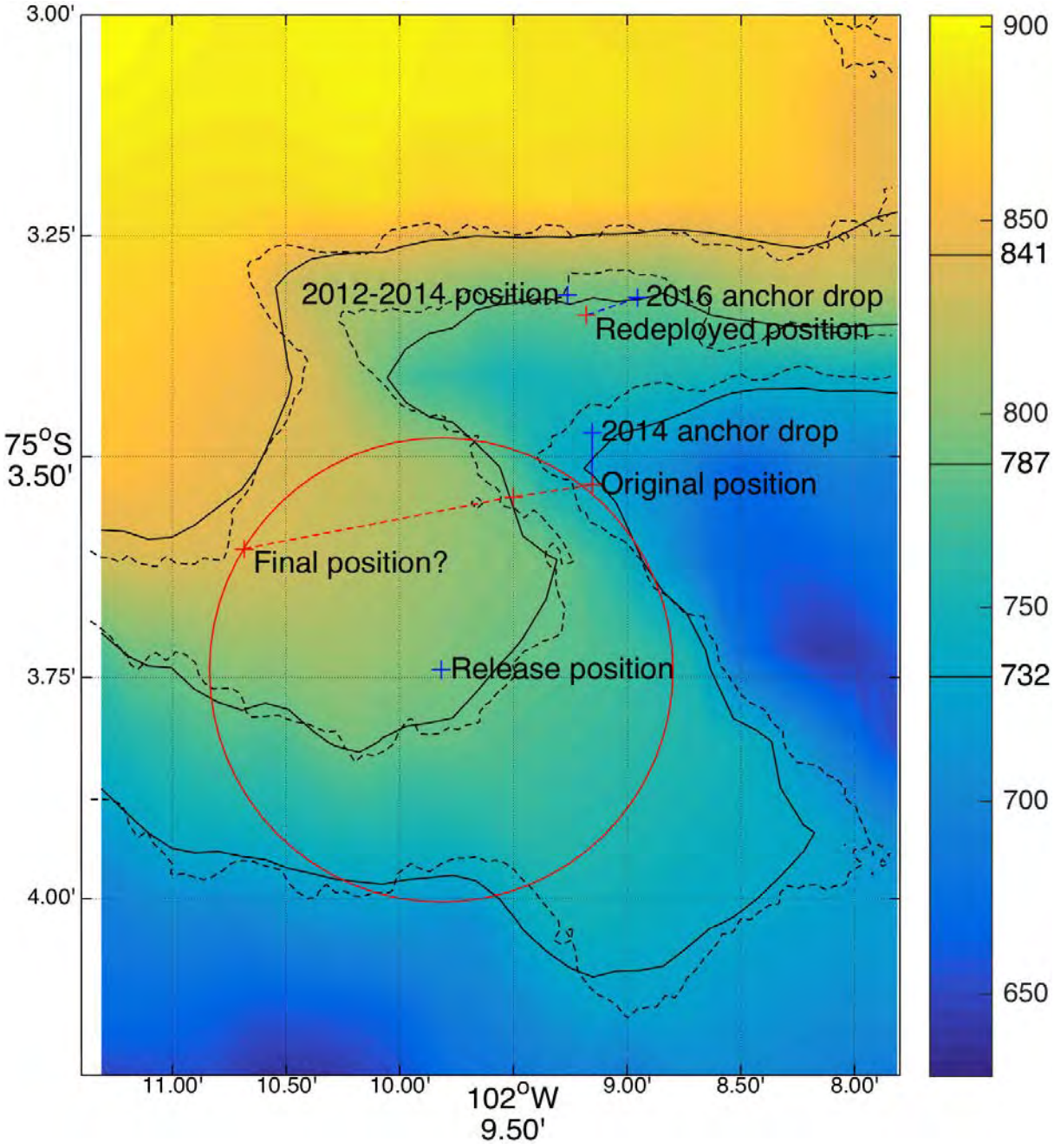


Figure 1.9. Map showing the bathymetry around PIG_S. The background shading and solid black contours are from USAP multibeam data; dashed lines are from ANA06B multibeam data.

Once the mooring surfaced, the ship moved into position to grapple the top buoy from the side deck, bringing the bow very close to the iceberg. Once it was grappled, the top buoyancy was removed along with the uppermost Aqualogger. The line was then led around to the stern, and the ship started repositioning to stream the mooring astern. At this stage the line slipped back in the water, and was pulled into the starboard propeller. The inboard end of the line was quickly cut, but the mooring line was slowly drawn into the prop. Eventually a grappling hook was brought under the line, and a bight brought back onto the deck. The end with the rest of the mooring was attached to a cleat, and the end going to the propeller was cut. Apart from the loss of ~25-30 m of rope, two shackles, and a 1/2" link, no damage appeared to have been done to the ship or instruments. The rest of the recovery went well.

All instruments on PIG_S appear to have worked well during the deployment, and were still logging on recovery.

**Redeployment of PIG_S**

The redeployment of PIG_S went smoothly, with no noteworthy events. The mooring landed close to the target position, but slightly shallower. The indicated target position was the final location of iSTAR 9 in 2012-2014; this is slightly shallower than the target depth of 810 m. In future years, I would suggest that we redeploy the mooring slightly further north, to reach the target depth of 810 m.

**Recovery and redeployment of PIG_N**

PIG_N was recovered without incident eleven hours after PIG_S. The mooring was in the expected location, and came up as planned. All instruments except one Aqualogger, s/n 1205, were logging on recovery – it had stopped on 16 Mar 2015. This instrument had its battery replaced on JR294/5 with an "EVE" battery, which had a tendency to get stuck in the instrument housing, in some cases leading to instrument or battery damage. In this case, the negative battery wire was damaged. Perhaps the added resistance in the damaged wire drained the battery faster than expected. The temperatures recorded by Aqualogger s/n 1201 appear to have drifted; the records are not consistent with the other instruments on the mooring. This instrument is being taken back to Cambridge for investigation, and will probably not be redeployed again.

**Recovery of trough_E**

When we reached the site of trough_E, there was about 8/10 sea ice cover, but with relatively large pools and leads. A large pool was near the mooring. After triangulating to confirm the location of the mooring, the captain broke ice near the mooring location, and then proceeded sideways over the mooring site under DP into the wind. This kept a large lead open on the starboard side of the ship. Once we had passed 300 m upwind of the mooring location, a release command was sent. Four (somewhat tense) minutes after the mooring was released, the green top floats were sighted on the starboard beam, with the first orange floats surfacing less than a minute later. Although small patches of ice approached the mooring after release, it was successfully recovered without incident.

Aqualogger s/n 1211 had stopped recording on 24 Mar 2015, and the battery was completely depleted (reading 0 V). This instrument had been deployed with a used LS14500 battery (from the previous two-year iSTAR deployment). Although the Aquatec battery life calculator estimates over 7 years of battery life, using a derating of 50% and sampling rate of 5 minutes, it would appear that this may be a bit too optimistic. All other instruments were logging on recovery.

**Deployment of trough_E**

There was still heavy sea ice cover in the area of trough_E during the time of redeployment. Although I indicated a strong preference for deploying the mooring in an existing lead, the captain insisted on breaking ice, bringing the ship sideways on DP downwind across the target position, then turning and steaming slowly upwind while deploying the mooring. In the beginning this went well, but soon the ice started to close in on the lead, with bits going over the mooring line. And since the ice had closed in on the ship's previous wake, the track had to be diverted toward the most open part, missing the target position anyway. At one stage a large multi-year floe passed over the top buoy. However, it

appeared that the buoy was pulled under the ice without any visible damage. When the anchor was dropped, all buoyancy was observed to be pulled through the water, and sank as expected. Both for trough_E and trough_W the anchors used were significantly heavier than required (400 kg rather than 250 kg); this led to the moorings sinking nearly vertically and landing very close to the drop positions.

In this case, an anchor first deployment would have been a better choice, as there were large pools of open water in the area; having the correct anchor weight would have made this easier and safer.

**Recovery and redeployment of trough_W**

The recovery and redeployment of trough_W were without incident. There was slightly larger swell than during the previous mooring operations, but all went well. All instruments were logging on recovery. Again, the mooring landed almost on top of the drop position.

**iSTAR 3**

Although we did not have time to drag for iSTAR 3, we did verify that it was still in the expected location. We obtained a range consistent with its last known location, and verified that the upper part of the mooring is still present using the EM122 multibeam sonar. A diagnostic command was also sent, returning a delay of 5004 ms, indicating that the release is vertical and has a battery voltage of 8.22 V. This is quite low, and the release may not be working two years from now. A release command was also sent but, similar to two years ago, the mooring did not rise.

Table 1.14. Locations and depths of BAS moorings in the Amundsen Sea. The effective speed of sound is also given, to assist with future mooring triangulations.

| Mooring | Deployment date | Recovery date | Latitude (deg/min south) | Longitude (deg/min west) | Depth (m) | $Vs_{eff}$ (m/s) | JR294 stn | ANA-06B stn |
|---|---|---|---|---|---|---|---|---|
| PIG_S (iSTAR 9) | 16/02/2014 13:29 | (20/07/2014) | 75° 03.532' | 102° 09.145' | 732 | 1453 | 51 | 62 |
| | (20/07/2014) | (30/07/2015) | 75° 03.545' | 102° 09.499' | 787 | | | |
| | (30/07/2015) | 02/02/2016 11:53 | 75° 03.604' | 102° 10.684' | 841 | | | |
| | 02/02/2016 18:45 | | 75° 03.315' | 102° 09.125' | 781 | 1453 | | 62 |
| | target position and depth: | | 75° 03.317' | 102° 09.262' | 810† | | | |
| PIG_N (iSTAR 8) | 18/02/2014 14:00 | 02/02/2016 22:42 | 74° 52.032' | 102° 04.795' | 956 | 1457 | 59 | 63 |
| | 03/02/2016 05:11 | | 74° 51.838' | 102° 05.924' | 952 | 1455 | | 63 |
| | target position and depth: | | 74° 51.790' | 102° 06.250' | 954 | | | |
| trough_E | 04/03/2014 19:38 | 04/02/2016 07:54 | 71° 19.806' | 102° 32.796' | 634 | 1452 | 106 | 65 |
| | 04/02/2016 13:01 | | 71° 20.176' | 102° 30.232' | 639 | 1451 | | 65 |
| | target position and depth: | | 71° 20.095' | 102° 30.738' | 638‡ | | | |
| trough_W (iSTAR 1) | 02/03/2014 13:41 | 07/02/2016 16:13 | 71° 33.727' | 113° 02.782' | 605 | 1451 | 97 | 67 |
| | 07/02/2016 21:09 | | 71° 33.729' | 113° 02.768' | 605 | 1452 | | 67 |
| | target position and depth: | | 71° 33.732' | 113° 02.759' | 600 | | | |
| iSTAR 3 | 05/03/2012 17:42 | | 71° 42.143' | 114° 02.769' | 542 | 1450 | 80 | |
| mid-shelf (iSTAR 6) | 22/02/2014 19:17 | | 73° 48.764' | 106° 32.062' | 958 | 1456 | 73 | |
| | target position and depth: | | 73° 48.759' | 106° 32.120' | 913 | | | |

All mooring positions are triangulated, except for the intermediate and final positions of PIG_S and the recovery position of trough_W.

† Depth at the target position is approx. 785 m. The position should be shifted northward in future years.
‡ The original target depth of this mooring was 600 m, but the trough is deeper than that.

## 1.3 Glider Operations

### Goals

The goal of this effort was to deploy a Teledyne Webb Slocum glider to collect hydrographic and bio-optical data. The data would be used to address three science issues. The first two science issues have grown out two recent manuscripts that were published using previous glider deployments in the Amundsen Sea from United States and Korean vessels (Miles et al. 2015, Schofield et al. 2015). The first is, what is the relationship between the upper mixed layer depth and the concentration of phytoplankton? The second was to map the distribution of Modified Circumpolar Deep Water and its relationship to changes in bottom bathymetry. The final was an experimental effort to record passive acoustics signals on the glider and assess the presence/absence of higher trophic levels.

### Technology

Teledyne Webb Slocum gliders are buoyancy-driven autonomous underwater vehicles. The gliders sample a sawtooth upcast and downcast pattern underwater and surface at regular intervals to transmit data and mission information via an iridium satellite connection. These instrument platforms are ideally suited to compliment shipboard sampling by significantly increasing the temporal- and spatial-resolution of a field study that uses traditional rosette sampling systems. RU25D, a deep glider, was configured to obtain high-resolution data of the Dotson Glacier inflow and outflow of Circumpolar Deep Water. The Rutgers University (RU) glider is named RU25D and is a deep glider rated to 1000 meters depth and was also equipped with a CTD, Aanderaa Optode and an additional Wetlabs Ecopuck. The Ecopuck measured Chlorophyll fluorescence, Colored Dissolved Organic Material (CDOM) and one channel of optical backscatter. This glider collected data with all sensors at a nominal 0.5 Hz on up- and down- casts continuously for the duration of the mission. Dive time is highly dependent on bathymetry, with 700 to 1000 meter dives taking approximately 3 to 4 hours. The final sensor that was deployed on the glider was a digital acoustic monitoring instrument (DMON). The DMON was not integrated into the glider and was mounted on the hull of the glider and internally recorded data.

### Mission Strategy

The glider represents a unique field asset as they are adaptively tasked based on the evolving science needs informed by the near real-time data provided via Iridium phone. The data is transmitted to the Rutgers Center of Ocean Observing Leadership (RU COOL) and this is used to adjust the piloting strategies. The other issue that influences the mission segments is the glider's ability to navigate despite variable currents and the presence of loose sea ice. The original mission was adjusted during the mission because of the prevailing currents and the clear mixing of Modified Circumpolar Deep Water to the surface associated with shallow bathymetry observed during the mission. These features were of keen interest to the science team after the discovery of bottom water outflows from the ice shelf during the previous glider deployments in the area. The central focus of the mission, despite adaptive adjustments, was to fly along the face of the ice shelf and confirm outflows observed the year before. After completing that effort, what remaining time was available for glider missions was used to access how consistent outflow dynamics were based on finding other regions of shallow bathymetry, until the science was terminated and the glider was directed back to the recovery section. The final glider mission that was conducted is provided in Figure 1.10.

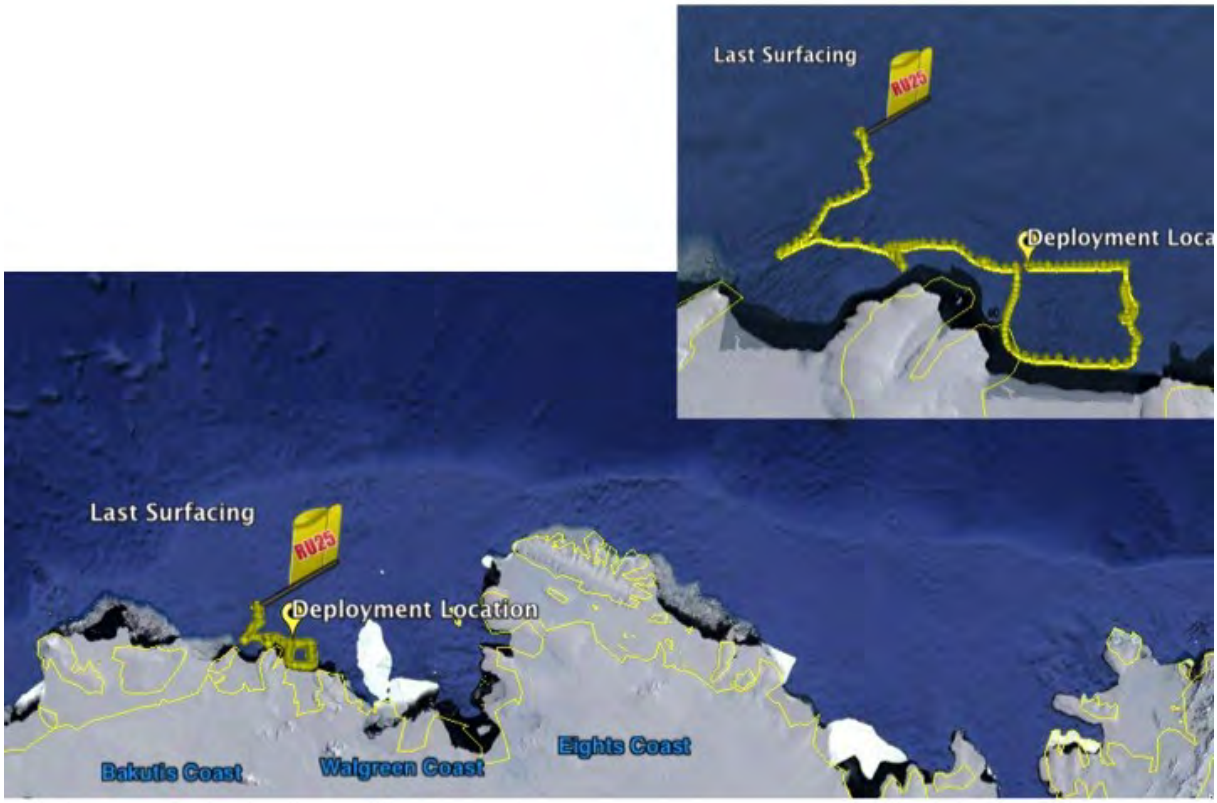


Figure 1.10. The mission conducted by during the glider mission during 2016.

## Mission Data

The Rutgers team deployed a deep Slocum glider during the KOPRI expedition. The glider was deployed on January 21st 2016 and conducted a 16.5-day mission before being recovered on February 6th 2016. During the mission the glider covered 357.8 kilometers. This was the longest glider mission to date in the Amundsen and the data provided a nice snapshot of the conditions along the front of the ice sheet. The glider operated as expected and collected a wide range of data (temperature, salinity, oxygen, optical backscatter, chlorophyll and colored dissolved organic matter fluorescence) which was posted in real-time to the web. All data is open to all KOPRI research projects. Some of the glider data is presented in Figure 1.11.

During the mission the glider encountered warm and saline bottom water likely indicating modified circumpolar water. Surface waters were also warm with evidence of low salinity surface plumes. Mid-water depths were identified with cold-water temperatures consistent with remnant winter water. The Modified Circumpolar Deep Water was characterized with low oxygen values and high values of colored dissolved organic matter fluorescence. The surface waters were characterized by high chlorophyll values.

## Lessons Learned

During the mission there was a need to recover the glider with the Araon and not by zodiac because of

prevailing weather. This was difficult and will need to be improved given the high probability of variable weather in these locations. Therefore we believe, while zodiac operations are preferred; the group must assume a high likelihood of the need to recover the gliders from the larger vessels. To that end we should incorporate a Nose Recovery (Assy G-1428) system into the gliders being deployed in the Amundsen. The nose recovery system is used to facilitate recovery from large vessels. The nose release comes with a 30 ft length of line that spools out using the nose dome as a sea anchor. A CO2 or compressed-air-powered grappling gun, hand grapple, or fishing pole is used to pass a line over the glider recovery line and haul in the nose. The recovery line is attached to the appropriate A-frame winch or block and tackle and the glider is pulled up and out of the water nose first.

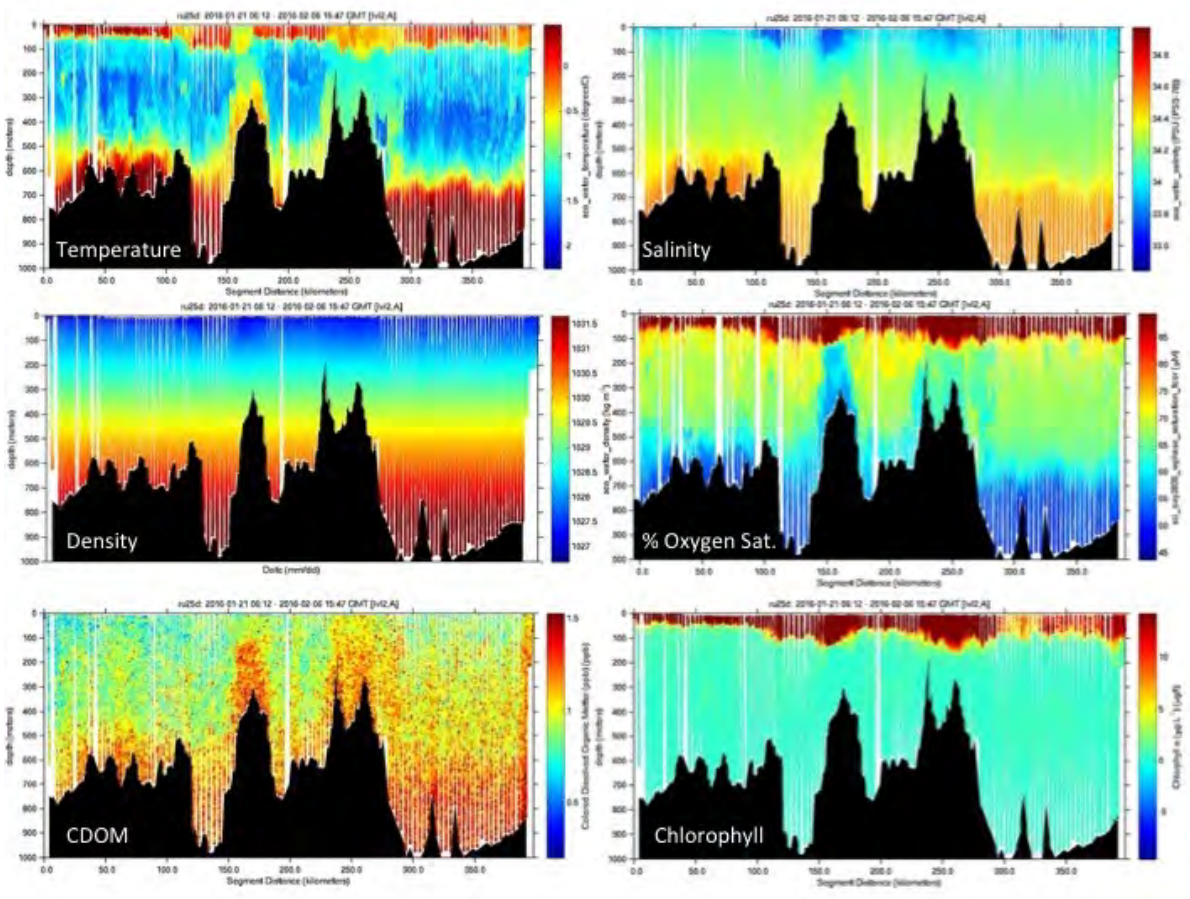


Figure 1.11. Data collected by the Rutgers glider during the 2016 Amundsen Sea experiment.

## 1.4 Surface Drifter Deployment

A total of 30 drifters provided by NOAA (Dr. Shaun Dolk) were deployed in transit between Udintsev Fracture Zone and Amundsen Sea. In particular, 4 drifters were deployed in the polynya of Amundsen Sea to investigate the surface circulation in the vicinity of Dotson Ice Shelf. The details on the drifters deployed during ANA06B were given in Table 1.15 and Figure 1.12.

Table 1.15. NOAA drifter deployed during the ANA06B

| Summary of deployment of surface drifting buoys | | | | | | |
|---|---|---|---|---|---|---|
| No | Drifter ID | Date (GMT) | | Latitude (S) | Longtitude (W) | Area |
| 1 | 139719 | 2016-01-19 | 3:35 AM | 73° 40.0′ | 113° 30.0′ | Amundsen Sea Polynya |
| 2 | 139842 | 2016-01-20 | 3:36 AM | 74° 10.3′ | 112° 31.7′ | |
| 3 | 139796 | 2016-01-22 | 6:16 AM | 74° 05.9′ | 110° 47.4′ | |
| 4 | 139812 | 2016-01-23 | 8:10 PM | 72° 50.7′ | 112° 28.9′ | |
| 5 | 139655 | 2016-02-07 | 9:13 PM | 71° 33.0′ | 113° 02.8′ | Southern Ocean (Transit) |
| 6 | 139652 | 2016-02-08 | 2:20 AM | 71° 00.0′ | 115° 20.0′ | |
| 7 | 139650 | 2016-02-08 | 6:23 AM | 70° 29.6′ | 117° 20.4′ | |
| 8 | 139832 | 2016-02-08 | 10:23 AM | 70° 01.0′ | 119° 11.3′ | |
| 9 | 139649 | 2016-02-08 | 2:55 PM | 69° 29.8′ | 121° 08.6′ | |
| 10 | 139653 | 2016-02-08 | 11:40 PM | 68° 29.9′ | 124° 46.9′ | |
| 11 | 300234063935480 | 2016-02-09 | 8:08 AM | 67° 30.0′ | 128° 17.2′ | |
| 12 | 300234063935840 | 2016-02-09 | 9:25 PM | 66° 29.9′ | 131° 36.0′ | |
| 13 | 300234063937830 | 2016-02-10 | 4:50 AM | 65° 29.8′ | 133° 49.7′ | |
| 14 | 300234063938830 | 2016-02-10 | 1:50 PM | 64° 29.8′ | 135° 57.8′ | |
| 15 | 300234063936800 | 2016-02-10 | 11:43 PM | 63° 29.8′ | 138° 01.1′ | |
| 16 | 300234063939810 | 2016-02-11 | 1:48 PM | 62° 30.0′ | 140° 00.0′ | |
| 17 | 300234063937800 | 2016-02-11 | 9:21 PM | 61° 30.0′ | 141° 52.5′ | |
| 18 | 300234063937810 | 2016-02-12 | 4:35 AM | 60° 29.9′ | 143° 52.2′ | |
| 19 | 300234063939830 | 2016-02-12 | 11:12 AM | 59° 29.7′ | 145° 43.2′ | |
| 20 | 300234063935910 | 2016-02-12 | 7:20 PM | 58° 30.0′ | 147° 30.0′ | UFZ |
| 21 | 300234063932830 | 2016-02-13 | 1:09 AM | 58° 00.0′ | 147° 30.0′ | |
| 22 | 300234063933840 | 2016-02-13 | 6:32 AM | 57° 30.0′ | 147° 30.0′ | |
| 23 | 300234063933810 | 2016-02-13 | 4:44 PM | 57° 00.0′ | 147° 30.0′ | |
| 24 | 300234063934820 | 2016-02-13 | 11:23 PM | 56° 30.0′ | 146° 34.7′ | |
| 25 | 300234063937702 | 2016-02-14 | 8:08 AM | 56° 10.0′ | 145° 42.5′ | |
| 26 | 300234063931830 | 2016-02-14 | 2:09 PM | 55° 37.8′ | 145° 03.6′ | |
| 27 | 300234063933830 | 2016-02-14 | 7:30 PM | 55° 15.8′ | 144° 25.8′ | |
| 28 | 300234063933820 | 2016-02-15 | 4:56 AM | 54° 55.4′ | 143° 52.8′ | |
| 29 | 300234063932810 | 2016-02-15 | 10:45 AM | 54° 35.1′ | 143° 19.8′ | |
| 30 | 300234063935820 | 2016-02-15 | 8:08 PM | 54° 00.0′ | 142° 25.8′ | |

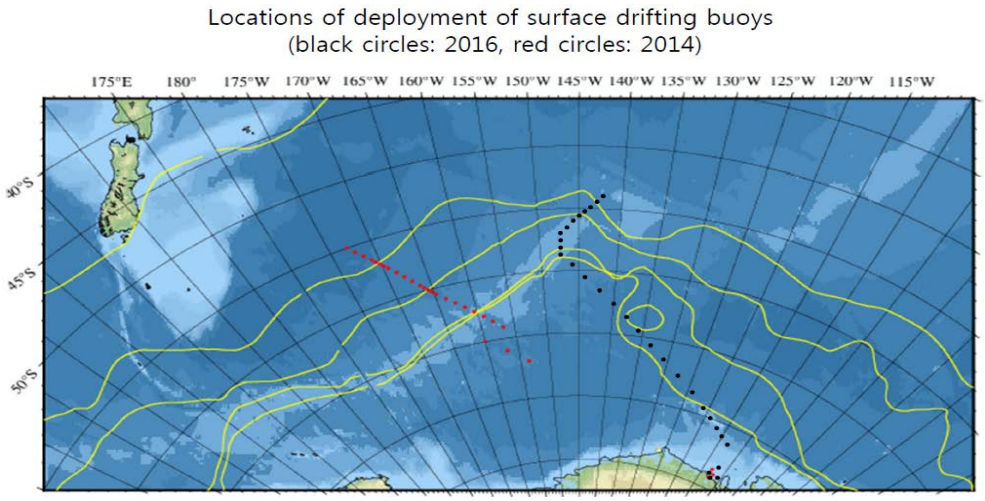


Figure 1.12. Map of NOAA drifter deployed area during the ANA06B

## 1.5 XCTD Launching

In order to measure the vertical temperature and salinity profile between Amundsen Sea and Polar Front, XCTD probes were used at several stations between regular hydrographic stations (see Table 1.16). The location of XCTD deployment was determined by the bathymetry and distance between regular stations. Also, we launched the XCTD when we were not able to operate the shipborne CTD due to the stormy weather condition. Measured vertical temperature and salinity profile will be calibrated using the observed data by shipborne CTD casts at the same positions.

Table 1.16. Detail information on XCTD casts

| St. | Latitude (s) | Longitude (w) | Deploy depth(m) | Release Date & Time (UTC) | | XCTD cast |
|---|---|---|---|---|---|---|
| | | | | Date (YYYY/MM/DD) | Time (UTC) | |
| 1 | 70° 29.871' | 117° 19.302' | 1100 | 2016/02/08 | 06:23 | 1 |
| 2 | 69° 30.014' | 121° 07.816' | 500 | 2016/02/08 | 14:45 | 2 |
| 2-1 | 69° 29.356' | 121° 10.329' | 700 | 2016/02/08 | 15:02 | 3 |
| 3 | 68° 29.770' | 124° 47.229' | 1100 | 2016/02/08 | 23:41 | 4 |
| 4 | 67° 29.939' | 128° 17.247' | 1100 | 2016/02/09 | 08:08 | 5 |
| 5 | 65° 29.890' | 133° 49.461' | 1100 | 2016/02/10 | 04:50 | 6 |
| 6 | 64° 29.905' | 135° 57.414' | 100 | 2016/02/10 | 13:50 | 7 |
| 7 | 63° 29.836' | 138° 01.081' | 200 | 2016/02/10 | 23:43 | 8 |
| 8 | 62° 30.001' | 140° 00.000' | 1100 | 2016/02/11 | 12:44 | 9 |
| 9 | 61° 30.536' | 141° 56.985' | 1100 | 2016/02/11 | 21:15 | 10 |
| 10 | 60° 29.932' | 143° 52.067' | 1100 | 2016/02/12 | 04:35 | 11 |
| 11 | 59° 29.979' | 145° 42.657' | 110 | 2016/02/12 | 11:13 | 12 |
| 12 | 58° 30.001' | 147° 30.002 | 1100 | 2016/02/12 | 19:17 | 13 |

## 1.6 T-pops Deployments

In total 12 'T-pop' devices were deployed during the cruise. T-pops are buoys that measure bottom temperature and then pop up to the surface at a given date and time, relaying the data back home via satellite. If they are trapped under sea ice upon surfacing they should fall asleep and then search for a satellite link only infrequently, saving batteries until they are eventually out in open water. We deployed 4 instruments developed by University of Rhode Island (‘T-pop’) and 9 developed by the Royal Technical University of Sweden (‘Lotus’). All 12 instruments were specially developed for this cruise and were prototypes or beta versions with the aim of obtaining commercially available products in the future, after eventual successful tests. Two of the Lotus buoys (number 9 and number 10) were deployed next to (Lotus 10) or tied to (Lotus 9) the mooring UiB4 in order to prove its temperature measurement stability. The remaining 4 T-pops and 7 Lotus were deployed in dynamically interesting

locations where it is too shallow to place moorings. They were all set to measure once per hour, and pop up in approximately one year (Table 1.17).

Table 1.17. Detail information on T-pops deployments

| Started on | Station name | Pop-up date | Deployment date | Depth | Lat | Lon | Tpop/Lotus SNR |
|---|---|---|---|---|---|---|---|
| **2016-01-14** | ANA06B05 | 2017-03-01 | 2016-01-16 | 507 | 72,141 S | 118,691 W | T-Pop016 |
| **? (Jari)** | ANA06B05 | 2016-03-15 | 2016-01-16 | 507 | 72,141 S | 118,691 W | Lotus 5 |
| **2016-02-20** | ANA06B49 | 2021-02-18 | 2016-01-28 | 601 | 73,795 S | 127,598 W | Lotus 9* |
| **2016-01-20** | ANA06B49 | 2017-02-13 | 2016-01-28 | 601 | 73,795 S | 127,598 W | Lotus 10** |
| **2016-01-28** | ANA06B50 | 2017-02-15 | 2016-01-29 | 460 | 73,738 S | 127.511 W | Tpop 15 |
| **2016-01-28** | ANA06B51 | 2017-02-15 | 2016-01-29 | 323 | 73.690 S | 127.448 W | Tpop 17 |
| **2016-01-20** | ANA06B52 | 2017-02-13 | 2016-01-29 | 206 | 73,672 S | 127.414 W | Lotus 7*** |
| **2016-01-31** | ANA06B58 | 2017-02-20 | 2016-01-31 | 663 | 73,937 S | 117.275 W | Tpop 18 |
| **2016-01-19** | ANA06B59 | 2017-02-12 | 2016-01-31 | 400 | 73,954 S | 117.252 W | Lotus 2 |
| **2016-01-20** | ANA06B60 | 2017-02-13 | 2016-01-31 | 320 | 73,962 S | 117.237 W | Lotus 3 |
| **2016-01-20** | ANA06B60 | 2017-02-13 | 2016-01-31 | 320 | 73,962 S | 117.237 W | Lotus 6 |
| **2016-01-20** | ANA06B61 | 2017-02-13 | 2016-01-31 | 206 | 73,987 S | 117.152 W | Lotus 8 |


Figure 1.13. Photography of Lotus buoy.

Figure 1.14. Photography of T-pops buoy.

## References


Miles, T. N., Lee, S., Wahlin, A.,Ha, K. H., Assmann, K., Schofield, O. 2015. Glider observations of the Dotson Ice Shelf outflow. Deep Sea Research. doi:10.1016/j.dsr2.2015.08.008

Schofield, O., Miles, T., Aldercamp A-C, Lee, S, Haskin. C., Roaglsky E., Sipler, R., Sherrell R., Yager, P. 2015. *In situ* phytoplankton distributions in the Amundsen Sea polynya measured by autonomous gliders. Elementa: Science of the Anthropocene. doi: 10.12952/journal.elementa.000073

Jenkins, A., P. Dutrieux, S. S. Jacobs, S. D. McPhail, J. R. Perrett, A. T. Webb, and D. White (2010), Observations beneath Pine Island Glacier in West Antarctica and implications for its retreat. *Nature Geosci*. 3, 468−472.

Wåhlin, A. K., X. Yuan, G. Björk, and C. Nohr (2010) Inflow of warm Circumpolar Deep Water in the Central Amundsen Shelf. *J. Phys. Oceanogr.* 40, 1427–1434.

Walker, D. P., M. A. Brandon, A. Jenkins, J. T. Allen, J. A. Dowdeswell, and J. Evans (2007) Oceanic heat transport onto the Amundsen Sea shelf through a submarine glacial trough. *Geophys. Res. Lett.* 34, L02602 (2007).


## Acknowledgements


We are very grateful to the captain and crew of IBRV Araon for their professional support with all mooring works in making successful recoveries and deployments. The UGOT part of the project has been funded by the Swedish Research Council and the Swedish Polar Research Secretariats, for which we are grateful.

## Appendix 1.1. ANA06B cruise log spreadsheet.

Scientific Cruise Daily Log

Ship: R/V Araon  Cruise: ANA06 . B  Prepared by H. W. Yang (yhw@kopri.re.kr)

| STN No. | Gear | Cast No. | Date (UTC time) | Cast start (UTC time) | Cast end (UTC time) | Latitude | Longitude | Water depth (m) | Cast depth (m) | Wind speed knot | Wind direction (°) | Ship speed knot | Heading (°) | Remarks | Device Driver |
|---|---|---|---|---|---|---|---|---|---|---|---|---|---|---|---|
| CTD; PHY: Phytoplankton net; BON: Bongo net;RTN: Rectangular net; SD:Secchi disk; MD: Mooring Deploy; MR: Mooring Recovery; FRR:fluoremeter; Trios :Radiometer; BC:Box Core; GOF:Go-flo;HS:Helicopter survey; EM: EM-APEX; GD : Glider; SDD: Surface drift; TPOP:T-POP deploy; | | | | | | | | | | | | | | | |
| E1 | EM | | 01/13/2016 | 21:20 | 21:28 | 68° 00.016' | 132° 59.991' | | | | | | | Release EM-APEX | C.S. KIM |
| 1 | CTD | 1 | 01/14/2016 | 14:51 | 17:24 | 69° 59.9971' | 125°00.00' | 3451 | 3415 | | 315.18 | 0.85 | 181.44 | First deep casting | H.W. YANG |
| | SD | 1 | | 17:30 | 17:40 | | | | 10 | | | | | Secchi disk | D. B. LEE |
| | TriOS | 1 | | 17:53 | 18:10 | | | | 110 | | | | | Radiometer | D. H. LEE |
| | PHY | 1 | | 18:19 | 18:34 | | | | 100 | | | | | Vertical towing mesh size 20 µm | H.S. LA |
| | BON | 1 | | 18:35 | 18:55 | | | | 200 | | | | | Vertical towing mesh size 330 µm, 500 µm | H.S. LA |
| | CTD | 2 | | 19:06 | 19:25 | | | | 100 | | | | | First shallow casting | H.W. YANG |
| | GOF | 1 | | 20:57 | 21:55 | | | | 800 | | | | | Go-Flo deep casting | D. J. JANG |
| | CTD | 3 | | 22:02 | 22:35 | | | | 100 | | | | | Second shallow casting | C.S. KIM |
| 2 | HS | | 01/15/2016 | 13:40 | 14:06 | | | | | | | | | Search for SEA Ice | T. S. RHEE |
| 2 | CTD | 1 | 01/15/2016 | 13:56 | 15:57 | 71° 29.4138' | 120° 15.0514' | 2560 | 2550 | 7.14 | 327.16 | 0.14 | 312.9 | First deep casting | H.W. YANG |
| | TriOS | 2 | | 16:10 | 16:30 | | | | 80 | | | | | Radiometer | D.H. LEE |
| | PHY | 1 | | 16:37 | 16:48 | | | | 100 | | | | | Vertical towing mesh size 20 µm | H.S. LA |
| | BON | 1 | | 16:50 | 17:05 | | | | 200 | | | | | Vertical towing mesh size 330 µm , 500 µm | H.S. LA |
| | CTD | 2 | | 17:18 | 17:33 | | | | 100 | | | | | First shallow casting | H.W. YANG |
| | CTD | 3 | | 18:27 | 18:38 | | | | 100 | | | | | Second shallow casting | H.W. YANG |
| 3 | CTD | 1 | 01/15/2016 | 23:34 | 0:39 | 72° 03.5998' | 118° 59.3801' | 985 | 976 | 6.59 | 353.14 | 0.82 | 125.2 | First deep casting | H.W. YANG |
| | EM | | 01/16/2016 | 0:58 | 1:01 | 72° 03.583' | 118° 59.353' | | | | | | | Release EM-APEX | C.S. KIM |
| 4 | CTD | 1 | 01/16/2016 | 1:52 | 2:46 | 72° 05.9002' | 118° 52.9697' | 745 | 736 | 4.42 | 229 | 0.1 | 157.3 | First deep casting | C.S. KIM |
| | SD | 2 | | 2:50 | 2:54 | | | | 7 | | | | | Secchi disk | D. B. LEE |
| | TriOS | 3 | | 3:00 | 3:07 | | | | 80 | | | | | Radiometer | D.H. LEE |
| | FRR | 1 | | 3:17 | 3:32 | | | | 35 | | | | | Fluoremeter | E.H. KO |
| | CTD | 2 | | 3:56 | 4:11 | 72° 06.0257' | 118° 52.6991' | 740 | 100 | 5.1 | 40 | 0.03 | 18.8 | First shallow casting | C.S. KIM |
| | PHY | 1 | | 4:22 | 4:32 | | | | 100 | | | | | Vertical towing mesh size 20 µm | H.S. LA |
| | BON | 1 | | 4:34 | 4:50 | | | | 200 | | | | | Vertical towing mesh size 330 µm, 500 µm | H.S. LA |
| | CTD | 3 | | 5:00 | 5:14 | 72° 06.1512' | 118° 52.7466' | 739 | 60 | 5 | 53 | 0.1 | 56 | Second shallow casting | C.S. KIM |
| | GOF | 1 | | 5:45 | 7:13 | | | | | | | | | Go-Flo deep casting | D. J. JANG |
| | CTD | 4 | | 7:40 | 8:19 | 71° 07.0995' | 118° 52.7238' | 717 | 500 | 6 | 77 | 0.06 | 24.5 | Second deep casting | C.S. KIM |
| | BC | 1 | | 8:30 | 9:35 | | | | 710 | | | | | Box core | S. Y. HA |
| 5 | TPOP | 1,2 | 01/16/2016 | 11:04 | 11:09 | | | | | | | | | T-POP deploy | A. K. Wåhlin |
| | CTD | 1 | | 11:21 | 12:01 | 72° 08.4715' | 118° 41.4659' | 510 | 500 | 11.15 | 91.96 | 0.03 | 92.4 | First deep casting | H.W. YANG |
| 6 | MR | 1 | 01/16/2016 | 14:45 | 16:05 | 72° 23.10' | 117° 43.39' | | | | | | | KOPRI K1 Mooring Recovery | T. W. KIM |
| | CTD | 1 | | 16:07 | 16:47 | 72° 22.8987' | 117° 44.9285' | 517 | 510 | 11.66 | 93.15 | 0.18 | 48.3 | First deep casting | H.W. YANG |
| | PHY | 1 | | 16:55 | 17:10 | | | | | | | | | Vertical towing mesh size 20 µm | H. S. LA |
| | BON | 1 | | 17:15 | 17:50 | | | | | | | | | Vertical towing mesh size 330 µm , 500 µm | H. S. LA |
| | CTD | 2 | | 18:00 | 18:16 | 72° 22.9924' | 117° 45.7952' | 514 | 100 | 12 | 82 | 0.08 | 87.1 | First shallow casting | C.S. KIM |
| | GOF | 1 | | 18:26 | 20:10 | | | | 500 | | | | | Go-Flo deep casting | D. J. JANG |
| 7 | CTD | 1 | 01/16/2016 | 22:55 | 23:36 | 72° 27.27' | 116° 20.0415' | 552 | 540 | 8.05 | 66 | 0.09 | 85.2 | First deep casting | H.W. YANG |
| | SD | 3 | | 23:38 | 23:40 | | | | 9 | | | | | Secchi disk | D. B. LEE |
| | MR | 1 | 01/17/2016 | 2:40 | 3:29 | | | | | | | | | UGOT Mooring recovery | A. K. Wåhlin |
| | CTD | 2 | | 4:01 | 4:16 | 72° 27.3337' | 116° 20.6612' | 554 | 100 | 4.97 | 350 | 0.05 | 50.6 | First shallow casting | C.S. KIM |
| | FRR | 2 | | 4:20 | 4:40 | | | | 25 | | | | | Fluoremeter | E.H. KO |

| | | | | | | | | | | | | | | |
|---|---|---|---|---|---|---|---|---|---|---|---|---|---|---|
| | TriOS | 4 | | 4:42 | 4:46 | | | | 30 | | | | | Radiometer | D.H. LEE |
| | BON | 1 | | 5:00 | 5:14 | | | | 200 | | | | | Vertical towing mesh size 330 μm, 500 μm | H. S. LA |
| | MD | 1 | | 5:20 | 6:12 | 72° 27.24' | 116° 21.42' | | | | | | | UGOT Mooring deploy | A. K. Wåhlin |
| 8 | CTD | 1 | 01/17/2016 | 9:21 | 10:11 | 72° 48.0108' | 116° 30.0450' | 630 | 617 | 6.8 | 291 | 0 | 251 | First deep casting | C.S. KIM |
| | GOF | 1 | | 10:44 | 11:46 | | | | 600 | | | | | Go-Flo deep casting | D. J. JANG |
| | CTD | 2 | | 12:28 | 12:41 | 72° 48.1520' | 116° 30.8900' | 627 | 100 | 5.55 | 333.34 | 0.69 | 22.9 | First shallow casting | H.W. YANG |
| | TriOS | 5 | | 12:59 | 13:03 | | | | 30 | | | | | Radiometer | D.H. LEE |
| | CTD | 3 | | 13:39 | 14:18 | 72° 48.1685' | 116° 30.9591' | 632 | 550 | 5.39 | 22.51 | 1.07 | 69.3 | Second deep casting | H.W. YANG |
| 9 | CTD | 1 | 01/17/2016 | 15:33 | 16:15 | 72° 55.1826' | 116° 06.7885' | 628 | 621 | 8.97 | 9.59 | 0.08 | 36.7 | First deep casting | H.W. YANG |
| 10 | CTD | 1 | 01/17/2016 | 17:22 | 18:07 | 73° 02.4011' | 115° 43.5058' | 710 | 697 | 5.58 | 5.03 | 0.05 | 33.9 | First deep casting | H.W. YANG |
| | SD | 4 | | 18:15 | 18:17 | | | | 7 | | | | | Secchi disk | D. B. LEE |
| | TriOS | 6 | | 18:26 | 18:31 | | | | 40 | | | | | Radiometer | D.H. LEE |
| | FRR | 3 | | 18:35 | 18:49 | | | | 30 | | | | | Fluoremeter | E.H. KO |
| | BON | 1 | | 18:53 | 19:10 | | | | 200 | | | | | Vertical towing mesh size 330 μm, 500 μm | H. S. LA |
| | CTD | 2 | | 19:32 | 19:46 | 73° 02.4006' | 115° 43.5049' | | 100 | 5.07 | 34.36 | 0.08 | 30.3 | First shallow casting | H.W. YANG |
| | GOF | 2 | | 20:08 | 21:20 | | | | 650 | | | | | Go-Flo deep casting | D. J. JANG |
| | CTD | 3 | | 21:43 | 21:59 | 73° 02.4034' | 115° 43.4970' | | 100 | 6.89 | 55.3 | 0.2 | 64.8 | Second shallow casting | H.W. YANG |
| | BC | 1 | | 22:10 | 22:52 | | | | | | | | | Box core | S. Y. HA |
| 11 | CTD | 1 | 01/18/2016 | 0:23 | 1:20 | 73° 09.5921' | 115° 20.2559' | 786 | 772 | 8.4 | 53 | 0.01 | 55.3 | First deep casting | C.S. KIM |
| 12 | MR | 1 | 01/18/2016 | 2:27 | 5:24 | | | | | | | | | KOPRI K2 Mooring Recovery | H. S. LA |
| | CTD | 1 | | 5:26 | 6:15 | 73° 16.7917' | 114° 57.0519' | 837 | 820 | 10 | 75.71 | 0.07 | 95 | First deep casting | C.S. KIM |
| | SD | 5 | | 6:18 | 6:19 | | | | 6 | | | | | Secchi disk | D. B. LEE |
| | TriOS | 7 | | 6:31 | 6:34 | | | | 30 | | | | | Radiometer | D.H. LEE |
| | FRR | 4 | | 6:35 | 6:45 | | | | 30 | | | | | Fluoremeter | E.H. KO |
| | CTD | 2 | | 7:22 | 7:37 | 73° 16.7870' | 114° 57.6299' | | 100 | | | | | First shallow casting | C.S. KIM |
| | PHY | 1 | | 7:45 | 8:00 | | | | 100 | | | | | Vertical towing mesh size 20 μm | H. S. LA |
| | BON | 1 | | 8:05 | 8:20 | | | | 200 | | | | | Vertical towing mesh size 330 μm, 500 μm | H. S. LA |
| | CTD | 3 | | 8:32 | 9:11 | 73° 16.7884' | 114° 57.0294' | | 500 | 10.62 | 83.63 | 0.3 | 98.9 | Second deep casting | C.S. KIM |
| | GOF | 3 | | 9:34 | 10:48 | | | | 750 | | | | | Go-Flo deep casting | D. J. JANG |
| | GOF | 4 | | 11:04 | 12:01 | | | | 750 | | | | | Go-Flo deep casting | D. J. JANG |
| | CTD | 4 | | 12:41 | 12:42 | 73° 16.8376' | 114° 55.6883' | | 0 | 8.6 | 85.5 | 0.27 | 94.6 | Second shallow casting | C.S. KIM |
| | RTN | 1 | | 12:50 | 13:35 | | | | | | | | | Rectangular net towing | H. S. LA |
| 13 | CTD | 1 | 01/18/2016 | 14:33 | 15:23 | 73° 23.3955' | 114° 28.4930' | 808 | 800 | 8.85 | 85.45 | | 111 | First deep casting | H.W. YANG |
| 14 | CTD | 1 | 01/18/2016 | 16:39 | 17:27 | 73° 29.9977' | 113° 59.9989' | 710 | 700 | 8.14 | 81.62 | 0.12 | 120.2 | First deep casting | H.W. YANG |
| | TriOS | 8 | | 17:37 | 17:40 | | | | 30 | | | | | Radiometer | D.H. LEE |
| | CTD | 2 | | 18:19 | 18:34 | 73° 30.0020' | 114° 00.0028' | 710 | 100 | 7.78 | 82.07 | 0.11 | 110.3 | First shallow casting | H.W. YANG |
| | GOF | 5 | | 18:58 | 20:05 | | | | 650 | | | | | Go-Flo deep casting | D. J. JANG |
| | BC | 1 | | 20:23 | 21:00 | | | | 689 | | | | | Box core | S. Y. HA |
| | GOF | 6 | | 21:20 | 22:30 | | | | 650 | | | | | Go-Flo deep casting | D. J. JANG |
| 15 | CTD | 1 | 01/19/2016 | 0:09 | 1:06 | 73° 40' | 113° 29.9915' | 791 | 780 | 7.57 | 91.4 | 0.24 | 109.9 | First deep casting | C.S. KIM |
| 16 | CTD | 1 | 01/19/2016 | 2:35 | 3:28 | 73° 49.1730' | 113° 02.7096' | 790 | 780 | 10.95 | 87.35 | 0.05 | 104.8 | First deep casting | C.S. KIM |
| | SDD | 1 | | 3:35 | 3:38 | | | | | | | | | Serface drift deploy | J. H. LEE |
| 17 | CTD | 2 | 01/19/2016 | 7:00 | 7:20 | 74° 12.8976' | 111° 53.5407' | 263 | 255 | 15.2 | 99.78 | 0.05 | 112.9 | First deep casting | C.S. KIM |
| | PHY | | | 7:37 | 7:48 | | | | | | | | | Vertical towing mesh size 20 μm | H. S. LA |
| | BON | | | 7:51 | 8:07 | | | | | | | | | Vertical towing mesh size 330 μm, 500 μm | H. S. LA |
| | CTD | 3 | | 8:19 | 8:39 | 74° 12.8979' | 111° 53.5583' | | 180 | 8.5 | 100.01 | 0.14 | 112.5 | First shallow casting | C.S. KIM |
| 18 | MR | | 01/19/2016 | 9:57 | 13:40 | | | | | | | | | KOPRI K4 Mooring Recovery | T. W. KIM |
| | CTD | 1 | | 14:09 | 15:05 | 74° 10.5103' | 112° 08.3233' | 943 | 933 | 4.1 | 103.97 | 0.04 | 125.5 | First deep casting | H.W. YANG |
| | RTN | 2 | | 15:25 | 16:55 | | | | | | | | | Rectangular net towing | H. S. LA |
| 19 | MR | | 01/19/2016 | 17:18 | 19:20 | 74° 10.676' | 112° 31.6999' | | | | | | | KOPRI K3 Mooring Recovery | T. W. KIM |
| | CTD | 1 | | 20:21 | 21:23 | 74° 10.2920' | 112° 09.263' | 1034 | 1026 | 6.76 | 98.1 | 0.03 | 98.2 | First deep casting | H.W. YANG |

| | | | | | | | | | | | | | | |
|---|---|---|---|---|---|---|---|---|---|---|---|---|---|---|
| | SD | 6 | | 21:29 | 21:30 | | | 8 | | | | | Secchi disk | D. B. LEE |
| | TriOS | 9 | | 21:35 | 21:39 | | | 30 | | | | | Radiometer | D.H. LEE |
| | FRR | 5 | | 21:40 | 22:00 | | | 30 | | | | | Fluoremeter | E.H. KO |
| | CTD | 2 | | 22:15 | 22:34 | 74° 10.2913' | 112° 31.6994' | 100 | 7.97 | 82.05 | 0.12 | 98.1 | First shallow casting | H.W. YANG |
| | PHY | 1 | | 22:42 | 22:54 | | | 100 | | | | | Vertical towing mesh size 20 μm | H. S. LA |
| | BON | 1 | | 22:58 | 23:17 | | | 200 | | | | | Vertical towing mesh size 330 μm, 500 μm | H. S. LA |
| | CTD | 3 | | 23:26 | 0:10 | 74° 10.2918' | 112° 31.7002' | 100 | 5.74 | 80 | 0.2 | 98.2 | Second shallow casting | C.S. KIM |
| | GOF | 7 | 01/20/2016 | 0:20 | 1:49 | | | 800 | | | | | Go-Flo deep casting | D. J. JANG |
| | BC | 2 | | 2:07 | 3:10 | | | 1532 | | | | | Box core | S. Y. HA |
| | SDD | 2 | | | | | | | | | | | Serface drift deploy | J. H. LEE |
| 20 | CTD | 1 | 01/20/2016 | 4:18 | 5:17 | 74° 12.4097' | 112° 47.7750' | 841 | 835 | 3.26 | 106.9 | 0.1 | 256 First deep casting | C.S. KIM |
| 21 | MD | | 01/20/2016 | 6:01 | 7:50 | | | | | | | | KOPRI K5 Mooring Recovery | T. W. KIM |
| | CTD | 1 | | 8:01 | 8:54 | 74° 10.9533' | 113° 03.8264' | 790 | 981 | 2.34 | 177.99 | 0.12 | 185 First deep casting | H.W. YANG |
| | RTN | 3 | | 9:15 | 10:30 | | | | | | | | Rectangular net towing | H. S. LA |
| 22 | CTD | 1 | 01/20/2016 | 10:56 | 11:47 | 74° 10.3090' | 113° 19.7151' | 633 | 625 | 3.4 | 192.71 | 0.07 | 230 First deep casting | H.W. YANG |
| | TriOS | 10 | | 11:58 | 12:01 | | | | 30 | | | | Radiometer | D.H. LEE |
| | CTD | 2 | | 12:37 | 12:51 | 74° 10.3078' | 113° 19.7099' | | 100 | 6.56 | 169.99 | 0.01 | 230.2 First shallow casting | H.W. YANG |
| | PHY | 1 | | 12:55 | 13:13 | | | | 100 | | | | Vertical towing mesh size 20 μm | H. S. LA |
| | BON | 1 | | 13:13 | 13:29 | | | | 200 | | | | Vertical towing mesh size 330 μm, 500 μm | H. S. LA |
| | CTD | 3 | | 13:40 | 13:47 | | | | 20 | 6.13 | 195.33 | 0.05 | 229.9 Second shallow casting | H.W. YANG |
| | RTN | 4 | | 16:45 | 17:20 | | | | | | | | Rectangular net towing | H. S. LA |
| | HS | | 01/20/2016 | 17:20 | 22:19 | 74° 12.66' | 112° 05.77' | | | | | | Helicopter operation for AWS | T. J. CHOI |
| | MR | | 01/21/2016 | 1:35 | 4:15 | 73° 49.274' | 113° 02.040' | | | | | | KOPRI K6 Mooring Recovery | T. W. KIM |
| 16_Revisit | CTD | 2 | 01/21/2016 | 4:17 | 5:12 | 73° 49.1630' | 113° 02.7782' | 788 | 778 | 4.3 | 230 | 0.3 | 193 Second deep casting | C.S. KIM |
| | GD | | | 5:45 | 6:47 | | | | | | | | Glider deploy | N. W |
| | SD | 7 | | 7:20 | 7:22 | | | | 7 | | | | Secchi disk | D. B. LEE |
| | FRR | 6 | | 7:30 | 7:50 | | | | 25 | | | | Fluoremeter | E.H. KO |
| | CTD | 3 | | 7:50 | 8:05 | 73° 49.1797' | 113° 02.7124' | | 100 | 7 | 175 | 0.02 | 225 First shallow casting | C.S. KIM |
| | PHY | 1 | | 8:12 | 8:27 | | | | 100 | | | | Vertical towing mesh size 20 μm | H. S. LA |
| | BON | 1 | | 8:30 | 8:45 | | | | 200 | | | | Vertical towing mesh size 330 μm, 500 μm | H. S. LA |
| | CTD | 4 | | 8:52 | 9:02 | 73° 49.1793' | 113° 02.7133' | | 20 | 5.59 | 183 | 0.1 | 225 Second shallow casting | C.S. KIM |
| | GOF | 8 | | 9:25 | 10:30 | | | | 700 | | | | Go-Flo deep casting | D. J. JANG |
| | BC | 3 | | 10:40 | 11:18 | | | | 755 | | | | Box core | S. Y. HA |
| | EK | 1 | 01/22/2016 | 11:55 | 2:15 | | | | | | | | EK 60 Line survey | H. S. LA |
| 23 | CTD | 1 | 01/22/2016 | 4:24 | 4:54 | 74° 05.8801' | 110° 47.5297' | 301 | 290 | 9.6 | 146.48 | 0.06 | 164.7 First deep casting | C.S. KIM |
| | PHY | 1 | | 5:06 | 5:18 | | | | 100 | | | | Vertical towing mesh size 20 μm | H. S. LA |
| | BON | 1 | | 5:18 | 5:33 | | | | 200 | | | | Vertical towing mesh size 330 μm, 500 μm | H. S. LA |
| | CTD | 2 | | 5:41 | 5:55 | 74° 05.8799' | 110° 47.5247' | | 100 | 0.04 | 131 | 0.1 | 144.8 First shallow casting | C.S. KIM |
| | TriOS | 11 | | 6:06 | 6:10 | | | | 30 | | | | Radiometer | D.H. LEE |
| | SDD | 3 | | 6:20 | 6:21 | | | | | | | | Serface drift deploy | J.H. LEE |
| 24 | CTD | 1 | 01/22/2016 | 7:44 | 8:18 | 73° 53.9203' | 111° 11.7285' | 401 | 390 | 6.8 | 118.12 | 0.08 | 125.2 First deep casting | C.S. KIM |
| 25 | CTD | 1 | 01/22/2016 | 9:45 | 10:22 | 73° 41.953' | 111° 35.918' | 398 | 389 | 4.2 | 115 | 0.98 | 116 First deep casting | K.H. CHO |
| | SD | 8 | | 10:25 | 10:26 | | | | 6 | | | | Secchi disk | D. B. LEE |
| | TriOS | 12 | | 10:30 | 10:34 | | | | 30 | | | | Radiometer | D.H. LEE |
| | FRR | 7 | | 10:35 | 10:50 | | | | 25 | | | | Fluoremeter | E.H. KO |
| | CTD | 2 | | 11:06 | 11:21 | 73° 41.0158' | 111° 35.867' | | 100 | 5.4 | 125 | 0.07 | 120 First shallow casting | K.H. CHO |
| | CTD | 3 | | 11:49 | 12:00 | | | | 20 | 4.59 | 113 | 0.08 | 134 Second shallow casting | K.H. CHO |
| | HS | | 01/23/2016 | 14:45 | 4:10 | 74° 10.41' | 111° 42.90' | | | | | | Helicopter operation for AWS | T. J. CHOI |
| 26 | CTD | 1 | 01/23/2016 | 7:40 | 8:16 | 73° 29.997' | 111°59.974' | 430 | 420 | 7.3 | 346 | 0.1 | 5.6 First deep casting | J.H. LEE |
| | BC | 4 | | 8:24 | 21:00 | | | | 412 | | | | Box core | S. Y. HA |
| | CTD | 2 | | 9:30 | 9:38 | 73° 29.995' | 111° 59.976' | 420 | 20 | 9.6 | 10.2 | 0.05 | 5.3 First shallow casting | K.H. CHO |

| | | | | | | | | | | | | | | |
|---|---|---|---|---|---|---|---|---|---|---|---|---|---|---|
| 27 | CTD | 1 | 01/23/2016 | 11:06 | 11:43 | 73° 17.00' | 112° 10.003' | 445 | 435 | 10.4 | 27.5 | 0.15 | 31.7 | First deep casting | K.H. CHO |
| | TriOS | 13 | | 11:55 | 11:58 | | | | 30 | | | | | Radiometer | D.H. LEE |
| | FRR | 8 | | 12:00 | 12:20 | | | | 20 | | | | | Fluoremeter | E.H. KO |
| | CTD | 2 | | 12:38 | 12:52 | | | | 100 | 11.04 | 32 | 0.07 | 40.6 | First shallow casting | K.H. CHO |
| 28 | CTD | 1 | 01/23/2016 | 14:26 | 14:58 | 73° 04.0122' | 112° 19.9493' | 453 | 442 | 14.51 | 32.02 | 0.19 | 42.5 | First deep casting | H.W. YANG |
| 29 | CTD | 1 | 01/23/2016 | 17:12 | 17:50 | 72° 50.7782' | 112° 28.8739' | 449 | 439 | 11.34 | 23.6 | 0.23 | 44 | First deep casting | H.W. YANG |
| | SD | 9 | | 17:54 | 17:55 | | | | 9 | | | | | Secchi disk | D. B. LEE |
| | TriOS | 14 | | 17:59 | 18:03 | | | | 30 | | | | | Radiometer | D.H. LEE |
| | FRR | 9 | | 18:06 | 18:25 | | | | 25 | | | | | Fluoremeter | E.H. KO |
| | CTD | 2 | | 18:39 | 18:53 | 72° 50.7768' | 112° 28.8814' | | 100 | 9.91 | 356.97 | 0.07 | 17.1 | First shallow casting | H.W. YANG |
| | PHY | 1 | | 19:03 | 19:18 | | | | 100 | | | | | Vertical towing mesh size 20 μm | H. S. LA |
| | BON | 1 | | 19:20 | 19:39 | | | | 200 | | | | | Vertical towing mesh size 330 μm, 500 μm | H. S. LA |
| | CTD | 3 | | 19:52 | 20:06 | 72° 50.7767' | 112° 28.8814' | | 92 | | | | | Second shallow casting | H.W. YANG |
| 30 | CTD | 1 | 01/23/2016 | 22:08 | 22:49 | 72° 59.992' | 113° 29.971' | 441 | 433 | 11.8 | 30 | 0.1 | 45 | First deep casting | K.H. CHO |
| | TriOS | 15 | | 23:25 | 23:29 | | | | 30 | | | | | | D.H. LEE |
| | CTD | 2 | | 23:43 | 23:58 | | | | 100 | 10.8 | 34 | 0.07 | 45 | First shallow casting | K.H. CHO |
| 31 | CTD | 1 | 01/24/2016 | 1:54 | 2:48 | 73° 9.992' | 114° 29.977' | 712 | 705 | 18.3 | 27 | 0.1 | 50.7 | First deep casting | K.H. CHO |
| | PHY | 1 | | 2:55 | 3:12 | | | | 100 | | | | | Vertical towing mesh size 20 μm | H. S. LA |
| | BON | 1 | | 3:15 | 3:31 | | | | 200 | | | | | Vertical towing mesh size 330 μm, 500 μm | H. S. LA |
| 31 | TriOS | 16 | | 3:26 | 3:39 | | | | 30 | | | | | Radiometer | D.H. LEE |
| | CTD | 2 | | 3:57 | 4:11 | | | | 100 | 7.7 | 32.2 | 0.1 | 54.8 | First shallow casting | C.S. KIM |
| 32 | CTD | 1 | 01/24/2016 | 6:04 | 7:01 | 73° 19.7021' | 115° 25.2443' | 915 | 904 | 3.12 | 46 | 0.04 | 189.7 | First deep casting | C.S. KIM |
| | CTD | 2 | | 7:50 | 8:04 | 73° 19.7017' | 115° 25.2444' | | 100 | 2 | 51 | 0.2 | 189.31 | First shallow casting | C.S. KIM |
| | CTD | 3 | | 8:23 | 8:30 | | | | 0 | | | | | Second shallow casting | C.S. KIM |
| 33 | CTD | 1 | 01/24/2016 | 10:27 | 11:02 | 73° 29.999' | 118° 29.982' | 375 | 365 | 5.03 | 45.3 | 0.1 | 49.1 | First deep casting | K.H. CHO |
| | SD | 10 | | 11:05 | 11:06 | | | | 9 | | | | | Secchi disk | D. B. LEE |
| | TriOS | 17 | | 11:11 | 11:18 | | | | 20 | | | | | Radiometer | D.H. LEE |
| | FRR | 10 | | 11:18 | 11:26 | | | | 25 | | | | | Fluoremeter | E.H. KO |
| | CTD | 2 | | 11:50 | 12:04 | | | | 100 | | | | | First shallow casting | C.S. KIM |
| | PHY | 1 | | 12:13 | 12:25 | | | | 100 | | | | | Vertical towing mesh size 20 μm | H. S. LA |
| | BON | 1 | | 12:25 | 12:43 | | | | 200 | | | | | Vertical towing mesh size 330 μm, 500 μm | H. S. LA |
| | CTD | 3 | | 12:54 | 13:02 | | | | 25 | | | | | Second shallow casting | C.S. KIM |
| | BC | 5 | | 13:18 | 13:48 | | | | 373 | | | | | Box core | S. Y. HA |
| 34 | CTD | 1 | 01/24/2016 | 15:33 | 16:20 | 73° 30.00' | 115° 45.0001' | 719 | 710 | 5.46 | 72.68 | 0.17 | 88.2 | First deep casting | H.W. YANG |
| 35 | CTD | 1 | 01/24/2016 | 17:45 | 18:45 | 73° 29.9999' | 114° 59.9970' | 953 | 945 | 9.93 | 86 | 0.26 | 85 | First deep casting | H.W. YANG |
| 36 | CTD | 1 | 01/24/2016 | 21:33 | 22:19 | 73° 42.6812' | 114° 12.9312' | 567 | 557 | 13.65 | 78.38 | 0.57 | 92.3 | First deep casting | H.W. YANG |
| | SD | 11 | | 22:23 | 22:24 | | | | 6 | | | | | Secchi disk | D. B. LEE |
| | TriOS | 18 | | | | | | | 30 | | | | | Radiometer | D. H. LEE |
| | CTD | 2 | | 23:29 | 23:45 | 73° 42.6824' | 114° 12.9290' | 567 | 100 | 18.5 | 87.66 | 0.96 | 94 | Second shallow casting | J. H. LEE |
| | PHY | 1 | | | | | | | | | | | | Vertical towing mesh size 20 μm | H. S. LA |
| | BON | 1 | | | | | | | | | | | | Vertical towing mesh size 330 μm, 500 μm | H. S. LA |
| | CTD | 3 | 01/25/2016 | 0:43 | 1:15 | 73° 42.6821' | 114° 12.9269' | | 400 | | | | | Second deep casting | J. H. LEE |
| | MD | 1 | | 2:26 | 5:18 | 73° 42.690' | 114° 12.722' | | 593 | | | | | KOPRI K3 Mooring Deploy | T. W. KIM |
| 37 | CTD | 1 | 01/25/2016 | 7:59 | 8:49 | 74° 06.3058' | 115° 08.6008' | 647 | 640 | 16.3 | 93.27 | 0.2 | 116.5 | First deep casting | C.S. KIM |
| | TriOS | 19 | | 21:00 | 21:10 | | | | 25 | | | | | Radiometer | D. H. LEE |
| | CTD | 2 | | 9:53 | 10:05 | 74° 06.3087' | 115° 08.6122' | | 100 | | | | | First shallow casting | C.S. KIM |
| 38 | CTD | 1 | 01/25/2016 | 10:47 | 11:29 | 74° 07.5099' | 115° 21.2877' | 1129 | 1106 | 20 | 130.8 | 0.2 | 115 | First deep casting | C.S. KIM |
| 39 | CTD | 1 | 01/25/2016 | 13:37 | 14:32 | 74° 04.7642' | 115° 43.3703' | 1060 | 1043 | 14 | 109.5 | 0.7 | 117 | First deep casting | C.S. KIM |
| | SD | 12 | | 14:36 | 14:38 | | | | 15 | | | | | Secchi disk | D. B. LEE |
| | TriOS | 20 | | 14:40 | 14:51 | | | | 30 | | | | | Radiometer | D. H. LEE |
| | FRR | 11 | | 14:52 | 15:04 | | | | 30 | | | | | Fluoremeter | E. H. KO |

| | | | | | | | | | | | | | | | |
|---|---|---|---|---|---|---|---|---|---|---|---|---|---|---|---|
| | PHY | 1 | | 15:08 | 15:20 | | | | 100 | | | | | Vertical towing mesh size 20 μm | H. S. LA |
| | BON | 1 | | 15:20 | 15:38 | | | | 200 | | | | | Vertical towing mesh size 330 μm, 500 μm | H. S. LA |
| | CTD | 2 | | 15:51 | 16:13 | 74° 04.9666' | 115° 43.2029' | | 200 | 12.93 | 85.62 | 0.72 | 108.6 | First shallow casting | H.W. YANG |
| | BC | 6 | | 16:20 | 17:48 | | | | 1064 | | | | | Box core | S. Y. HA |
| | CTD | 3 | | 18:09 | 18:40 | 74° 04.9860' | 115° 42.8482' | | 420 | 9 | 135 | | | Second shallow casting | H.W. YANG |
| 40 | CTD | 1 | 01/26/2016 | 17:18 | 18:02 | 73° 04.6207' | 128° 10.9042' | 561 | 550 | 9.28 | 89.29 | 0.13 | 202.6 | First deep casting | H.W. YANG |
| | FRR | 12 | | 18:20 | 18:35 | | | | 30 | | | | | Fluoremeter | E. H. KO |
| | TriOS | 21 | | 18:40 | 18:50 | | | | 30 | | | | | Radiometer | D. H. LEE |
| | CTD | 2 | | 19:08 | 19:29 | 73° 04.6164' | 128° 13.8487' | | 200 | 5.61 | 95.13 | 0.2 | 218.4 | First shallow casting | H.W. YANG |
| | PHY | 1 | | 19:39 | 19:50 | | | | 100 | | | | | Vertical towing mesh size 20 μm | H. S. LA |
| | BON | 1 | | 19:55 | 20:14 | | | | 200 | | | | | Vertical towing mesh size 330 μm, 500 μm | H. S. LA |
| | HS | 1 | 01/27/2016 | 6:23 | 16:39 | 74° 12.07' | 127° 50.45' | | | | | | | Helicopter operation for ApRES | K. H. CHO |
| 41 | CTD | 1 | 01/27/2016 | 7:04 | 7:48 | 74° 12.0741' | 127° 50.4274' | 697 | 689 | 8 | 138 | 0.06 | 115 | First deep casting | C.S. KIM |
| 42 | CTD | 1 | 01/27/2016 | 19:08 | 19:54 | 74° 08.2799' | 128° 12.8386' | 596 | 588 | 7.08 | 4.64 | 0.03 | 137.9 | First deep casting | H.W. YANG |
| | SD | 13 | | 19:58 | 19:59 | | | | 9 | | | | | Secchi disk | D. B. LEE |
| | FRR | 13 | | 20:00 | 20:22 | | | | 40 | | | | | Fluoremeter | E. H. KO |
| | TriOS | 22 | | 20:26 | 20:30 | | | | 40 | | | | | Radiometer | D. B. LEE |
| | CTD | 2 | | 20:46 | 21:00 | 74° 08.2807' | 128° 12.8387' | | 100 | 13.5 | 105.54 | 0.13 | 137.8 | First shallow casting | H.W. YANG |
| | PHY | 1 | | 21:05 | 21:17 | | | | 100 | | | | | Vertical towing mesh size 20 μm | H. S. LA |
| | BON | 1 | | 21:19 | 21:40 | | | | 200 | | | | | Vertical towing mesh size 330 μm, 500 μm | H. S. LA |
| | CTD | 3 | | 22:05 | 22:16 | 74° 08.2802' | 128° 12.8394' | | 45 | 12.13 | 104.68 | 0.1 | 137.9 | Second shallow casting | H.W. YANG |
| | MD | | | 22:57 | 23:33 | | | | | | | | | UIB Mooring Deployment | E. Darelius |
| 43 | CTD | 1 | 01/28/2016 | 1:43 | 2:32 | 74° 02.9586' | 127° 57.0071' | 710 | 695 | - | - | - | - | First deep casting | J. H. LEE |
| 44 | CTD | 1 | 01/28/2016 | 3:35 | 4:33 | 74° 04.4298' | 127° 32.7757' | 799 | 783 | 7.3 | 101.5 | 0.07 | 104.9 | First deep casting | J. H. LEE |
| 45 | CTD | 1 | 01/28/2016 | 5:32 | 6:18 | 73° 56.3760' | 127° 20.7200' | 792 | 785 | 8 | 103.01 | 0.03 | 124.9 | First deep casting | C.S. KIM |
| 46 | CTD | 1 | 01/28/2016 | 7:21 | 8:12 | 73° 56.4032' | 127° 47.9728' | 780 | 770 | 8.5 | 108.67 | 0.15 | 114.9 | First deep casting | K. H. CHO |
| | FRR | 14 | | 8:16 | 8:33 | | | | 30 | | | | | Fluoremeter | E. H. KO |
| | PHY | 1 | | 8:36 | 8:47 | | | | 100 | | | | | Vertical towing mesh size 20 μm | H. S. LA |
| | BON | 1 | | 8:51 | 9:10 | | | | 200 | | | | | Vertical towing mesh size 330 μm, 500 μm | H. S. LA |
| | CTD | 2 | | 9:22 | 9:39 | 73° 56.402' | 127° 47.974' | | 150 | 8.92 | 82.7 | 0.05 | 106.9 | First shallow casting | K. H. CHO |
| | RTN | 5 | | 9:51 | 10:18 | | | | | | | | | Rectangular net towing | H. S. LA |
| 47 | CTD | 1 | 01/28/2016 | 12:44 | 13:22 | 73° 49.8963' | 127° 16.6852' | 600 | 592 | 8.49 | 97.19 | 0.06 | 98.2 | First deep casting | H.W. YANG |
| | MD | | | 14:01 | 15:20 | 73° 49.895' | 127° 16.682' | | | | | | | UIB Mooring Deployment | E. Darelius |
| 48 | CTD | 1 | 01/28/2016 | 17:08 | 17:55 | 73° 49.8033' | 127° 47.3528' | 700 | 689 | 7.15 | 122.71 | 0.1 | 145.1 | First deep casting | H.W. YANG |
| | MD | | | 18:00 | 19:38 | 73° 49.834' | 127° 47.428' | | | | | | | UGOT Mooring Deloyment | A. K. Wåhlin |
| 49 | CTD | 1 | 01/28/2016 | 20:58 | 21:47 | 73° 47.6322' | 127° 35.8993' | 603 | 591 | 5.47 | 330.86 | 0.09 | 338.9 | First deep casting | H.W. YANG |
| | MD | | | 22:05 | 23:29 | | | | | | | | | UIB Mooring Deployment | E. Darelius |
| | TPOP | 3 | | 22:40 | 22:42 | | | | | | | | | UGOT T-POP deploy | A. K. Wåhlin |
| 50 | CTD | 1 | 01/29/2016 | 0:17 | 0:49 | 73° 44.3021' | 127° 30.6678' | 460 | 451 | 3.32 | 206.4 | 0.06 | 153.2 | First deep casting | C.S. KIM |
| | TPOP | 4 | | 0:47 | 0:48 | | | | | | | | | UGOT T-POP deploy | A. K. Wåhlin |
| 51 | TPOP | 5 | 01/29/2016 | 1:21 | 1:22 | | | | | | | | | UGOT T-POP deploy | A. K. Wåhlin |
| | CTD | 1 | | 1:31 | 1:56 | 73° 41.4311' | 127° 26.8420' | 322 | 315 | 5.46 | 130 | 0.2 | 229.7 | First deep casting | C.S. KIM |
| | SD | 14 | | 1:58 | 1:59 | | | | 6 | | | | | Secchi disk | D. B. LEE |
| | FRR | 15 | | 2:02 | 2:16 | | | | 30 | | | | | Fluoremeter | E. H. KO |
| | TriOS | 23 | | 2:19 | 2:23 | | | | 40 | | | | | Radiometer | D. H. LEE |
| | CTD | 2 | | 3:09 | 3:16 | 73° 41.4027' | 127° 26.7328' | | 15 | | | | | First shallow casting | C. S. KIM |
| | PHY | 1 | | 3:26 | 3:38 | | | | 100 | | | | | Vertical towing mesh size 20 μm | H. S. LA |
| | BON | 1 | | 3:40 | 3:55 | | | | 200 | | | | | Vertical towing mesh size 330 μm, 500 μm | H. S. LA |
| 52 | TPOP | 6 | 01/29/2016 | 4:25 | 4:37 | | | | | | | | | UGOT T-POP deploy | A. K. Wåhlin |
| | CTD | 1 | | 4:45 | 5:05 | 73° 40.2964' | 127° 24.8536' | 220 | 213 | 3.7 | 145.5 | 0.02 | 110 | First deep casting | C. S. KIM |
| 53 | CTD | 1 | 01/29/2016 | 7:28 | 8:16 | 73° 20.9998' | 128° 03.0024' | 614 | 605 | 9.97 | 44.68 | 0.05 | 69.9 | First deep casting | C. S. KIM |

| | | | | | | | | | | | | | | |
|---|---|---|---|---|---|---|---|---|---|---|---|---|---|---|
| | FRR | 16 | | 8:21 | 8:35 | | | | 25 | | | | | Fluoremeter | E. H. KO |
| | TriOS | 24 | | 8:38 | 8:42 | | | | 30 | | | | | Radiometer | D. H. LEE |
| | CTD | 2 | | 8:53 | 9:07 | 73° 20.9957' | 128° 03.0112' | | 100 | 6.48 | 18.9 | 0.06 | 57.4 | First second casting | C. S. KIM |
| 54 | CTD | 1 | 01/29/2016 | 19:45 | 20:30 | 73° 41.1313' | 123° 35.0265' | 640 | 631 | 11.88 | 64.6 | 0.06 | 85.7 | First deep casting | H. W. YANG |
| | SD | 15 | | 20:33 | 20:34 | | | | 11 | | | | | Secchi disk | D. B. LEE |
| | FRR | 17 | | 20:38 | 20:53 | | | | 35 | | | | | Fluoremeter | E. H. KO |
| | TriOS | 25 | | 20:55 | 21:00 | | | | 40 | | | | | Radiometer | D. H. LEE |
| | CTD | 2 | | 21:23 | 21:41 | 73° 41.1290' | 123° 35.0067' | | 160 | 12.72 | 67.38 | 0.04 | 76.3 | First shallow casting | H. W. YANG |
| | PHY | 1 | | 21:50 | 22:05 | | | | 100 | | | | | Vertical towing mesh size 20 μm | H. S. LA |
| | BON | 1 | | 22:07 | 22:18 | | | | 200 | | | | | Vertical towing mesh size 330 μm, 500 μm | H. S. LA |
| | CTD | 3 | | 22:29 | 22:43 | 73° 41.1296' | 123° 35.0066' | | 100 | 11.95 | 68.53 | 0.02 | 76.5 | Second shallow casting | H. W. YANG |
| | GOF | 9 | 01/30/2016 | 23:34 | 0:40 | | | | | | | | | GO-Flo deep casting | D. J. JANG |
| | MD | | | 1:19 | 2:22 | | | | | | | | | UIB Mooring Deployment | E. Darelius |
| | RTN | 6 | | 3:46 | 4:15 | | | | 300 | | | | | Rectangular net towing | H. S. LA |
| 55 | CTD | 1 | 01/30/2016 | 15:24 | 16:14 | 73° 53.3778' | 118° 43.6445' | 673 | 665 | 4.46 | 199.47 | 0.12 | 210.8 | First deep casting | H. W. YANG |
| | SD | 16 | | 16:17 | 16:18 | | | | 11 | | | | | Secchi disk | D. B. LEE |
| | FRR | 18 | | 16:39 | 16:56 | | | | 45 | | | | | Fluoremeter | E. H. KO |
| | TriOS | 26 | | 17:00 | 17:07 | | | | 70 | | | | | Radiometer | D. H. LEE |
| | CTD | 2 | | 17:23 | 17:43 | 73° 53.3781' | 118° 43.6445' | | 160 | 6.77 | 122.75 | 0.09 | 200.6 | First shallow casting | H. W. YANG |
| | PHY | | | 17:48 | 18:02 | | | | 100 | | | | | Vertical towing mesh size 20 μm | H. S. LA |
| | BON | | | 18:04 | 18:20 | | | | 200 | | | | | Vertical towing mesh size 330 μm, 500 μm | H. S. LA |
| | CTD | 3 | | 18:31 | 18:43 | 73° 53.3780' | 118° 43.6371' | | 50 | 3.39 | 143.35 | 0.06 | 165.1 | Second shallow casting | H. W. YANG |
| | MD | | | 18:50 | 20:40 | 73° 53.372' | 118° 43.649' | | | | | | | K4 Kopri mooring deploy | T. W. KIM |
| 56 | CTD | 1 | 01/30/2016 | 22:19 | 23:43 | 74° 00.8220' | 118° 01.1420' | 1119 | 1111 | 12.09 | 122.48 | 0.2 | 130.5 | First deep casting | J. H. LEE |
| | GOF | 10 | 01/31/2016 | 0:20 | 1:25 | | | | 700 | | | | | GO-Flo deep casting | D. J. JANG |
| | CTD | 2 | | 1:52 | 2:08 | 74° 00.8250' | 118° 01.1470' | | 150 | 6.56 | 30.83 | 0.08 | 130.3 | First second casting | J. H. LEE |
| | RTN | 7 | | 2:20 | 3:03 | | | | 300 | | | | | Rectangular net towing | H. S. LA |
| 57 | CTD | 1 | 01/31/2016 | 5:03 | 6:02 | 73° 53.9723' | 117° 16.5136' | 1095 | 1080 | 7.09 | 67.05 | 0.14 | 68.1 | First deep casting | C. S. KIM |
| | MD | | | 6:05 | 8:16 | 73° 53.92' | 117° 14.993' | | | | | | | K6 Kopri mooring deploy | T. W. KIM |
| 58 | CTD | 1 | 01/31/2016 | 9:12 | 9:57 | 73° 56.2501' | 117° 16.4554' | 658 | 650 | 10.48 | 63.27 | 0.22 | 82.4 | First deep casting | H. W. YANG |
| | MD | | | 10:15 | 10:45 | | | | | | | | | K5 Kopri mooring deploy | T. W. KIM |
| | SD | 17 | | 11:24 | 11:25 | | | | 12 | | | | | Secchi disk | D. B. LEE |
| | FRR | 19 | | 11:29 | 11:42 | | | | 30 | | | | | Fluoremeter | E. H. KO |
| | TriOS | 27 | | 11:44 | 11:48 | | | | 40 | | | | | Radiometer | D. H. LEE |
| | CTD | 2 | | 12:04 | 12:19 | 73° 56.5004' | 117° 16.6827' | | 150 | 12.57 | 74.07 | 0.09 | 90.3 | First shallow casting | C. S. KIM |
| | PHY | 1 | | 12:28 | 12:38 | | | | 100 | | | | | Vertical towing mesh size 20 μm | H. S. LA |
| | BON | 1 | | 12:38 | 12:54 | | | | 200 | | | | | Vertical towing mesh size 330 μm, 500 μm | H. S. LA |
| | CTD | 3 | | 13:07 | 13:16 | 73° 56.5031' | 117° 17.2517' | | 33 | 15.01 | 73.45 | 0.04 | 67.4 | Second shallow casting | C. S. KIM |
| 59 | TPOP | 7 | 01/31/2016 | 13:36 | 13:37 | | | | | | | | | UGOT T-POP deploy | A. K. Wåhlin |
| | CTD | 1 | | 13:51 | 14:21 | 73° 57.2554' | 117° 15.0352' | 390 | 380 | 0.12 | 87.5 | 17.06 | 72.32 | First deep casting | C. S. KIM |
| 60 | TPOP | 8 | 01/31/2016 | 14:44 | | | | | | | | | | UGOT T-POP deploy | A. K. Wåhlin |
| | CTD | 1 | | 14:55 | 15:21 | 73° 57.7069' | 117° 14.1617' | 310 | 300 | 15.3 | 70.7 | 0.06 | 79.5 | First deep casting | C. S. KIM |
| 61 | TPOP | 9 | 01/31/2016 | 16:03 | 16:04 | | | | | | | | | UGOT T-POP deploy | A. K. Wåhlin |
| | CTD | 1 | | 16:10 | 16:29 | 73° 59.2118' | 117° 09.0505' | 206 | 198 | 17.7 | 77.47 | 0.11 | 83.4 | First deep casting | C. S. KIM |
| | HS | | 02/02/2016 | 0:56 | 3:25 | | | | | | | | | Helicopter operation for AWS | T. J. CHOI |
| 62 | MR | 1 | 02/02/2016 | 11:43 | 13:00 | | | | | | | | | BAS Mooring recorvery | P. Abrahamsen |
| | CTD | 1 | | 13:48 | 14:37 | 75° 03.5344' | 102° 09.1377' | 743 | 735 | 0.22 | 41.21 | 0.02 | 70.3 | First deep casting | H. W. YANG |
| | SD | 18 | | 14:40 | 14:42 | | | | 13 | | | | | Secchi disk | D. B. LEE |
| | FRR | 20 | | 14:44 | 14:59 | | | | 35 | | | | | Fluoremeter | E. H. KO |
| | TriOS | 28 | | 15:02 | 15:06 | | | | 40 | | | | | Radiometer | D. H. LEE |
| | CTD | 2 | | 15:27 | 15:46 | 75° 03.5323' | 102° 09.1294' | | 100 | 7.1 | 69.48 | 0.07 | 70.5 | First shallow casting | H. W. YANG |

| | | | | | | | | | | | | | | | |
|---|---|---|---|---|---|---|---|---|---|---|---|---|---|---|---|
| | PHY | 1 | | 15:53 | 16:03 | | | | 100 | | | | | Vertical towing mesh size 20 μm | H. S. LA |
| | BON | 1 | | 16:05 | 16:40 | | | | 200 | | | | | Vertical towing mesh size 330 μm, 500 μm | H. S. LA |
| | CTD | 3 | | 16:59 | 17:10 | 75° 03.5337' | 102° 09.1303' | | 50 | 0.55 | 100.8 | 0.03 | 90.8 | Second shallow casting | H. W. YANG |
| | MD | | | 17:55 | 19:30 | 75° 03.322' | 102° 08.8440' | | | | | | | BAS Mooring deploy | P. Abrahamsen |
| | GOF | 11 | | 20:02 | 21:20 | | | | 700 | | | | | GO-Flo deep casting | D. J. JANG |
| 63 | MR | | 02/03/2016 | 22:42 | 23:57 | | | | | | | | | BAS Mooring recorvery | P. Abrahamsen |
| | CTD | 1 | | 0:20 | 1:11 | 74° 52.0320' | 102° 04.7984' | 940 | 930 | 6.62 | 131.56 | 0.08 | 151.8 | First deep casting | C. S. KIM |
| | CTD | 2 | | 2:01 | 2:17 | 74° 52.0315' | 102° 04.7996' | | 140 | | | | | First shallow casting | C. S. KIM |
| | BC | 7 | | 2:44 | 3:35 | | | | 940 | | | | | Box core | S. Y. HA |
| | MD | | | 3:55 | 6:00 | 74° 51.8380' | 102° 05.779' | | | | | | | BAS Mooring deploy | P. Abrahamsen |
| | RTN | 8 | | 6:05 | 6:48 | | | | | | | | | Rectangular net towing | H. S. LA |
| 64 | CTD | 1 | 02/03/2016 | 7:50 | 8:31 | 74° 42.2023' | 101° 45.7129' | 559 | 550 | 14.1 | 122.9 | 0.5 | 129.8 | First deep casting | C. S. KIM |
| | SD | 19 | | 8:35 | 8:36 | | | | 8 | | | | | Secchi disk | D. B. LEE |
| | FRR | 21 | | 8:38 | 8:51 | | | | 25 | | | | | Fluoremeter | E. H. KO |
| | TriOS | 29 | | 8:53 | 8:57 | | | | 30 | | | | | Radiometer | D. H. LEE |
| | CTD | 2 | 02/03/2016 | 9:10 | 9:25 | 74° 42.3994' | 101° 45.7101' | | 140 | 10.2 | 18.3 | 0.1 | 125.7 | First shallow casting | C. S. KIM |
| | PHY | 1 | | 9:30 | 9:41 | | | | 100 | | | | | Vertical towing mesh size 20 μm | Y. J. LEE |
| | BON | 2 | | 9:44 | 0:00 | | | | 200 | | | | | Vertical towing mesh size 330 μm, 500 μm | H. S. LA |
| | CTD | 3 | | 10:14 | 10:24 | 74° 42.3991' | 101° 45.7074' | 560 | 25 | 0.03 | 132 | 16.2 | 112 | Second shallow casting | C. S. KIM |
| 65 | MR | | 02/04/2016 | 7:05 | 8:48 | 71° 19.5870' | 102° 33.37' | | | | | | | BAS Mooring recorvery | P. Abrahamsen |
| | CTD | 1 | | 9:00 | 9:49 | 71° 19.5870' | 102° 33.4132' | 625 | 615 | 13.17 | 197 | 0.1 | 320.6 | First deep casting | C. S. KIM |
| | GOF | 12 | | 10:10 | 11:33 | | | | 600 | | | | | GO-Flo deep casting | D. J. JANG |
| | MD | | | 12:33 | 13:49 | 71° 19.5870' | 102° 30.252' | | | | | | | BAS Mooring deploy | P. Abrahamsen |
| | EM | | | 17:05 | 17:16 | | | | | | | | | Release EM--APEX | C. S. KIM |
| 29_revisit | CTD | 4 | 02/05/2016 | 23:20 | 23:56 | 71° 20.168' | 112° 29.9935' | 451 | 441 | 5.6 | 12 | 1.44 | 35.1 | Second deep casting | H. W. YANG |
| | SD | 20 | | 23:59 | 0:00 | | | | 8 | | | | | Secchi disk | D. B. LEE |
| | FRR | 22 | | 0:24 | 0:39 | | | | 30 | | | | | Fluoremeter | E. H. KO |
| | TriOS | 30 | | 0:42 | 0:47 | | | | 40 | | | | | Radiometer | D. H. LEE |
| | CTD | 5 | | 0:58 | 1:13 | 72° 50.9960' | 112° 29.9968' | | 100 | 6.3 | 31 | 0.2 | 33.03 | Third shallow casting | C. S. KIM |
| | PHY | 1 | | 1:20 | 1:31 | | | | 100 | | | | | Vertical towing mesh size 20 μm | Y. J. LEE BON |
| | | 1 | | 1:33 | 1:50 | | | | 200 | | | | | Vertical towing mesh size 330 μm, 500 μm | H. S. LA |
| | CTD | 6 | | 2:00 | 2:09 | 72° 50.9972' | 112° 29.9951' | | 25 | 6.53 | 32.65 | 0.2 | 33.5 | Fourth shallow casting | C. S. KIM |
| 27_revisit | CTD | 3 | 02/06/2016 | 4:35 | 5:10 | 73° 16.9973' | 112° 09.9942' | 446 | 435 | 6.7 | 36.48 | 0.28 | 64.7 | Second deep casting | C. S. KIM |
| | PHY | 1 | | 5:17 | 5:30 | | | | 100 | | | | | Vertical towing mesh size 20 μm | Y. J. LEE |
| | CTD | 4 | | 6:05 | 6:18 | 73° 17.0012' | 112° 09.9967' | | 110 | 6.7 | 10.6 | 0.5 | 55.2 | Third shallow casting | C. S. KIM |
| 66 | CTD | 1 | 02/06/2016 | 8:09 | 8:48 | 73° 30.0019' | 112° 59.9960' | 523 | 515 | 10.55 | 51.05 | 0.23 | 195.2 | First deep casting | C. S. KIM |
| 14_revisit | CTD | 3 | | 10:39 | 11:29 | 73° 29.9720' | 114° 0.0524' | 710 | 700 | 10.99 | 70 | 0.24 | 91.7 | Second deep casting | H. W. YANG |
| | CTD | 4 | | 12:29 | 12:47 | 73° 30.0015' | 114° 0.0108' | | 150 | 11.63 | 337 | 0.03 | 199.91 | Second shallow casting | H. W. YANG |
| | BC | 8 | | 13:00 | 13:35 | | | | 710 | | | | | Box core | S. Y. HA |
| | GD | 1 | 02/06/2016 | 15:50 | 17:45 | 73° 17.389' | 114° 54.348' | | | | | | | Glider recovery | H. S. LA |
| 12_revisit | CTD | 5 | | 18:00 | 18:55 | 73° 16.7931' | 114° 57.0265' | 830 | 819 | 11 | 77 | 0.49 | 99 | Third deep casting | H. W. YANG |
| | SD | 21 | | 18:59 | 19:00 | | | | 9 | | | | | Secchi disk | D. B. LEE |
| | FRR | 23 | | 19:01 | 19:16 | | | | 30 | | | | | Fluoremeter | E. H. KO |
| | TriOS | 31 | | 19:19 | 19:24 | | | | 40 | | | | | Radiometer | D. H. LEE |
| | CTD | 6 | | 19:50 | 20:08 | 73° 16.9107' | 114° 57.0265' | | 150 | 11.18 | 84.71 | 0.94 | 105.8 | Third shallow casting | H. W. YANG |
| | PHY | 1 | | 20:15 | 20:35 | | | | 100 | | | | | Vertical towing mesh size 20 μm | Y. J. LEE BON |
| | | 1 | | 20:35 | 20:55 | | | | 200 | | | | | Vertical towing mesh size 330 μm, 500 μm | H. S. LA |
| | CTD | 7 | | 21:08 | 21:18 | 73° 16.7902' | 114° 57.0196' | | 40 | 13.56 | 94.09 | 0.44 | 104.6 | Fourth shallow casting | J. H. LEE |
| | MD | | | 21:56 | 23:26 | 73° 16.8019' | 114° 56.5804' | | | | | | | K2 KOPRI Mooring deploy | T. W. KIM |
| | RTN | 9 | 02/07/2016 | 23:38 | 0:17 | | | | | | | | | Rectangular net towing | H. S. LA |
| 8 | CTD | 4 | 02/07/2016 | 4:43 | 5:28 | 72° 48.0008' | 116° 30.0021' | 631 | 617 | 12 | 86.1 | 0.07 | 104.2 | Third deep casting | K. H. CHO |

| | | | | | | | | | | | | | | | | |
|---|---|---|---|---|---|---|---|---|---|---|---|---|---|---|---|---|
| | PHY | | | 5:38 | 5:47 | | | | 100 | | | | | Vertical towing mesh size 20 μm | Y. J. LEE |
| | BON | | | 5:48 | 6:05 | | | | 200 | | | | | Vertical towing mesh size 330 μm, 500 μm | H. S. LA |
| | CTD | | 5 | 6:29 | 6:59 | 72° 48.0077' | 116° 30.0030' | | 350 | 15 | 75.4 | 0.8 | 110 | Third shallow casting | C. S. KIM |
| E2 | Ping test | | 02/07/2016 | 14:09 | 14:12 | 71° 42.01' | 114° 03.11' | | | | | | | BAS Ping test | P. Abrahamsen |
| 67 | MR | | 02/07/2016 | 16:10 | 17:12 | | | | | | | | | BAS Mooring recorvery | P. Abrahamsen |
| | CTD | | 1 | 17:41 | 18:31 | 71° 33.7271' | 113° 02.7856' | 600 | 590 | 7.6 | 92.15 | 0.22 | 100.2 | First deep casting | H. W. YANG |
| | GOF | | 13 | 19:08 | 20:13 | | | | 500 | | | | | GO-Flo deep casting | D. J. JANG |
| | MD | | | 20:38 | 21:55 | 71° 33.74' | 113° 02.66' | | | | | | | BAS Mooring deploy | P. Abrahamsen |
| | SDD | | 4 02/08/2016 | 2:20 | 2:31 | 71° 00.00 | 115° 19.58' | | | | | | | Surface drift deploy | J. H. LEE |
| | SDD | | 5 02/08/2016 | 6:15 | 6:25 | 70° 30.00 | 117° 18.74' | | | | | | | Surface drift deploy | J. H. LEE |
| | XCTD | | 1 | 6:25 | 6:30 | | | | 1100 | | | | | XCTD Launching | T. W. KIM |
| | XCTD | 2,3 | 02/08/2016 | 14:45 | 15:10 | 69° 30.00 | 121° 09.081' | | 700 | | | | | XCTD Launching | T. W. KIM |
| | SDD | | 6 | 14:45 | 14:58 | | | | | | | | | Surface drift deploy | J. H. LEE |
| | SDD | | 7 02/08/2016 | 23:38 | 23:39 | 68° 30.00 | 124° 46.52' | | | | | | | Surface drift deploy | J. H. LEE |
| | XCTD | | 4 | 23:41 | 23:47 | | | | | | | | | XCTD Launching | T. W. KIM |
| | XCTD | | 5 02/09/2016 | 8:08 | 8:15 | 67° 29.00 | | | | | | | | XCTD Launching | T. W. KIM |
| 68 | CTD | | 1 02/09/2016 | 16:47 | 20:01 | 66° 29.9988' | 131° 35.9987' | 4745 | 4700 | 4.45 | 237.07 | 0.4 | 308.7 | First deep casting | H. W. YANG |
| | PHY | | | 20:10 | 20:24 | | | | 100 | | | | | Vertical towing mesh size 20 μm | Y. J. LEE |
| | BON | | | 20:25 | 20:45 | | | | 200 | | | | | Vertical towing mesh size 330 μm, 500 μm | H. S. LA |
| | CTD | | 2 | 21:04 | 21:21 | | | | 100 | 5.27 | 261.41 | 0.27 | 308.5 | First second casting | H. W. YANG |
| | SDD | | 8 | 21:26 | 21:27 | | | | | | | | | Surface drift deploy | J. H. LEE |
| | XCTD | | 6 02/10/2016 | 4:50 | 5:00 | 65° 29.99' | 133° 49.21' | | | | | | | XCTD Launching | T. W. KIM |
| | SDD | | 9 | 4:51 | 4:52 | | | | | | | | | Surface drift deploy | J. H. LEE |
| | SDD | | 10 | 13:49 | 13:50 | 64° 30.00' | 135° 37.20' | | | | | | | Surface drift deploy | J. H. LEE |
| | XCTD | | 8 02/10/2016 | 23:43 | 23:50 | 63° 29.817' | 138° 01.143' | | 100 | | | | | XCTD Launching | T. W. KIM |
| | SDD | | 11 | 23:45 | 23:46 | | | | | | | | | Surface drift deploy | J. H. LEE |
| 69 | CTD | | 1 02/11/2016 | 9:37 | 12:37 | 62° 29.9982 | 139° 59.9999' | 4424 | 4403 | 13.5 | 280.9 | 0.5 | 279 | First deep casting | C. S. KIM |
| | XCTD | | 9 | 12:44 | 12:52 | | | | 1100 | | | | | XCTD Launching | T. W. KIM |
| | PHY | | | 12:46 | 12:56 | | | | 100 | | | | | Vertical towing mesh size 20 μm | Y. J. LEE |
| | BON | | | 12:56 | 13:16 | | | | 200 | | | | | Vertical towing mesh size 330 μm, 500 μm | H. S. LA |
| | CTD | | 2 | 13:29 | 13:45 | | | | 100 | 3.8 | 306.81 | 0.04 | 282.2 | First second casting | H. W. YANG |
| | SDD | | 12 | 13:47 | 13:48 | | | | | | | | | Surface drift deploy | J. H. LEE |
| | XCTD | | 10 02/11/2016 | 21:15 | 21:23 | 61° 30.544' | 141° 57.001' | | 1100 | | | | | XCTD Launching | T. W. KIM |
| | XCTD | | 11 02/12/2016 | 4:35 | 4:42 | 60° 29.9' | | | | | | | | XCTD Launching | T. W. KIM |
| | SDD | | 13 | 4:40 | 4:41 | | | | | | | | | Surface drift deploy | J. H. LEE |
| | XCTD | | 12 02/12/2016 | 11:13 | 11:16 | 59° 29.984' | 145° 42.706' | | 200 | | | | | XCTD Launching | T. W. KIM |
| | SDD | | 14 | 11:13 | 11:14 | | | | | | | | | Surface drift deploy | J. H. LEE |
| | XCTD | | 13 02/12/2016 | 19:17 | 19:25 | 58° 29.992' | 147° 29.991' | 2847 | 1100 | | | | | XCTD Launching | T. W. KIM |
| | SDD | | 15 | 19:20 | 19:21 | | | | | | | | | Surface drift deploy | J. H. LEE |
| 70 | CTD | | 1 02/12/2016 | 22:14 | 0:08 | 57° 59.9968' | 147° 29.9981' | 2750 | 2738 | 13.02 | 347 | 0.63 | 139.03 | First deep casting | H. W. YANG |
| | PHY | | | 12:16 | 12:26 | | | | 100 | | | | | Vertical towing mesh size 20 μm | Y. J. LEE |
| | SDD | | 16 | 13:08 | 13:09 | | | | | | | | | Surface drift deploy | J. H. LEE |
| 71 | CTD | | 1 02/13/2016 | 4:33 | 6:28 | 57° 30.0022' | 147° 29.9995' | 2756 | 2748 | 7.3 | 212 | 0.13 | 217.7 | First deep casting | C. S. KIM |
| | SDD | | 17 | 6:32 | 6:33 | | | | | | | | | Surface drift deploy | J. H. LEE |
| 72 | CTD | | 1 02/13/2016 | 11:10 | 13:12 | 56° 59.9610' | 147° 23.8176' | 2890 | 2880 | 2.6 | 349 | 1.59 | 82.92 | First deep casting | H. W. YANG |
| | MD | | | 13:48 | 17:48 | 56° 59.963' | 147° 23.815' | | | | | | | Locean Mooring deployment | Y. H. PARK |
| | SDD | | 18 | 16:42 | 16:44 | | | | | | | | | Surface drift deploy | J. H. LEE |
| 73 | CTD | | 1 02/13/2016 | 21:23 | 23:21 | 56° 30.0001' | 146° 34.6877' | 2957 | 2945 | 7.08 | 328 | 0.17 | 281.56 | First deep casting | H. W. YANG |
| | SDD | | 19 | 23:25 | 23:26 | | | | | | | | | Surface drift deploy | J. H. LEE |
| 74 | CTD | | 1 02/14/2016 | 3:34 | 5:38 | 55° 59.9963' | 145° 42.8754' | 2865 | 2845 | 10.76 | 20.99 | 1.12 | 150 | First deep casting | C. S. KIM |
| | MD | | | 6:03 | 9:23 | | | | | | | | | Locean Mooring deployment | Y. H. PARK |

| | | | | | | | | | | | | | | |
|---|---|---|---|---|---|---|---|---|---|---|---|---|---|---|
| 75 | CTD | 1 | 02/14/2016 | 12:10 | 14:06 | 55° 37.8088' | 145° 03.5977' | 2663 | 2654 | 10.19 | 48.35 | 1.48 | 12.9 | First deep casting | H. W. YANG |
| | SDD | 20 | | 14:07 | 14:08 | | | | | | | | | Surface drift deploy | J. H. LEE |
| 76 | CTD | 1 | 02/14/2016 | 17:08 | 19:24 | 55° 15.7600' | 144° 25.8013' | 3162 | 3153 | 11.25 | 66.68 | 0.18 | 61.8 | First deep casting | H. W. YANG |
| 77 | CTD | 1 | 02/14/2016 | 22:16 | 0:54 | 54° 55.2894' | 143° 50.2154' | 3780 | 3763 | 11 | 74.77 | 0.6 | 263.3 | First deep casting | H. W. YANG |
| | MD | | | 1:35 | 7:51 | 54° 35.0974' | 143° 50.5574' | | | | | | | KIOST Mooring delployment | J. H. LEE |
| | RTN | 10 | | 8:04 | 8:35 | | | | | | | | | Rectangular net towing | H. S. LA |
| 78 | SDD | 21 | 02/15/2016 | 10:45 | 10:46 | | | | | | | | | Surface drift deploy | J. H. LEE |
| | CTD | 1 | | 10:54 | 13:27 | 54° 55.5231' | 143° 19.8000' | 3668 | 3656 | 10.81 | 65.44 | 1.83 | 255.3 | First deep casting | H. W. YANG |
| 79 | CTD | 1 | 02/15/2016 | 17:40 | 20:02 | 53° 59.9988' | 142° 25.8033' | 3600 | 3586 | 5.19 | 65.15 | 1.14 | 69.4 | First deep casting | H. W. YANG |
| | SDD | 22 | | 20:08 | 20:09 | | | | | | | | | Surface drift deploy | J. H. LEE |
| 80 | CTD | 1 | 02/15/2016 | 23:27 | 1:43 | 53° 30.00' | 141° 41.0019' | 3520 | 3505 | 6.08 | 33.4 | 0.45 | 54.7 | First deep casting | C. S. KIM |
| 81 | CTD | 1 | 02/16/2016 | 5:06 | 7:25 | 52° 59.9994' | 140° 59.9970' | 3575 | 3560 | 8.5 | 67.49 | 0.62 | 51.9 | First deep casting | C. S. KIM |

## Appendix 1.2. All design diagrams of moorings

AP2_01 Mooring design K2

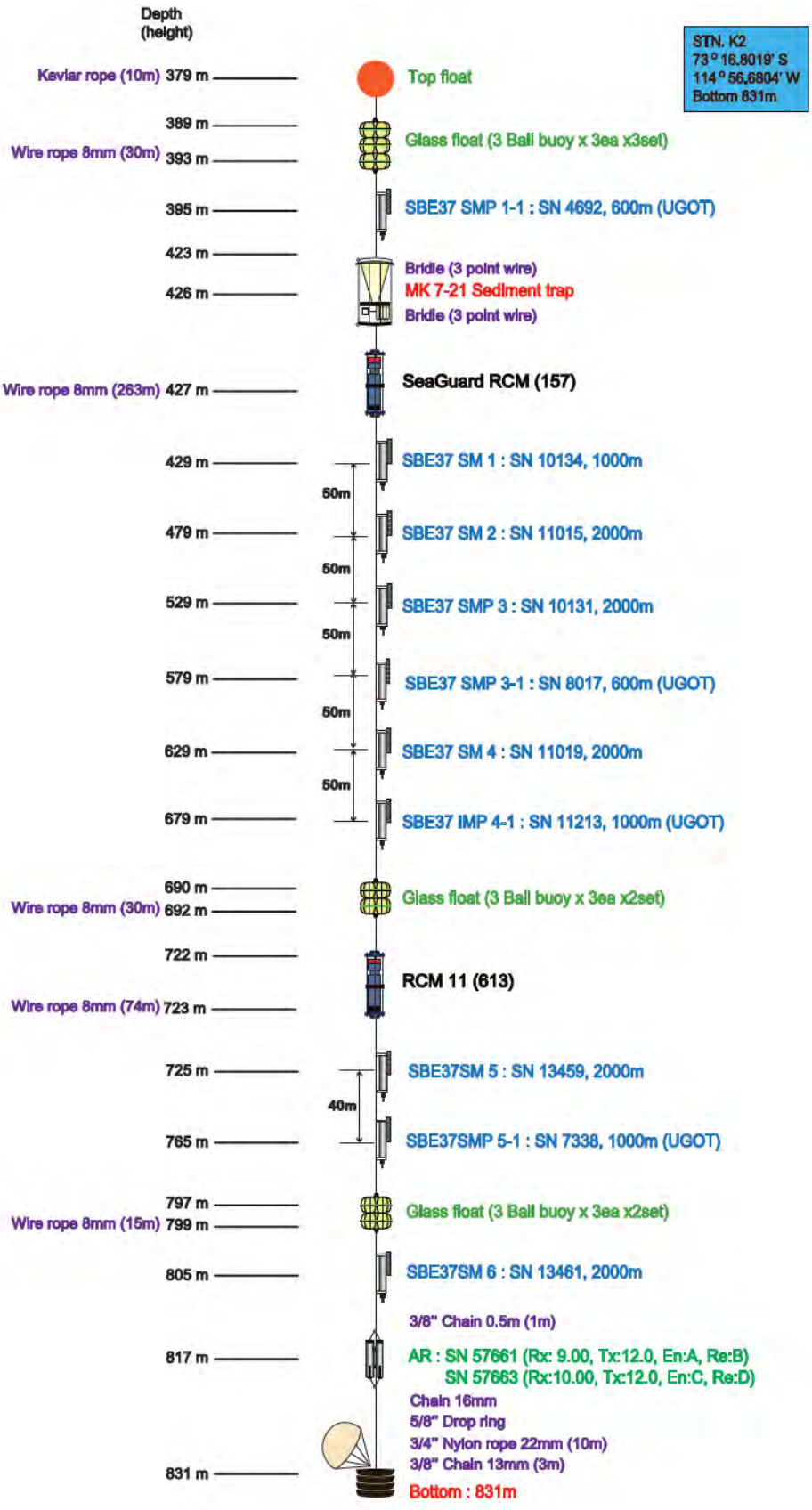

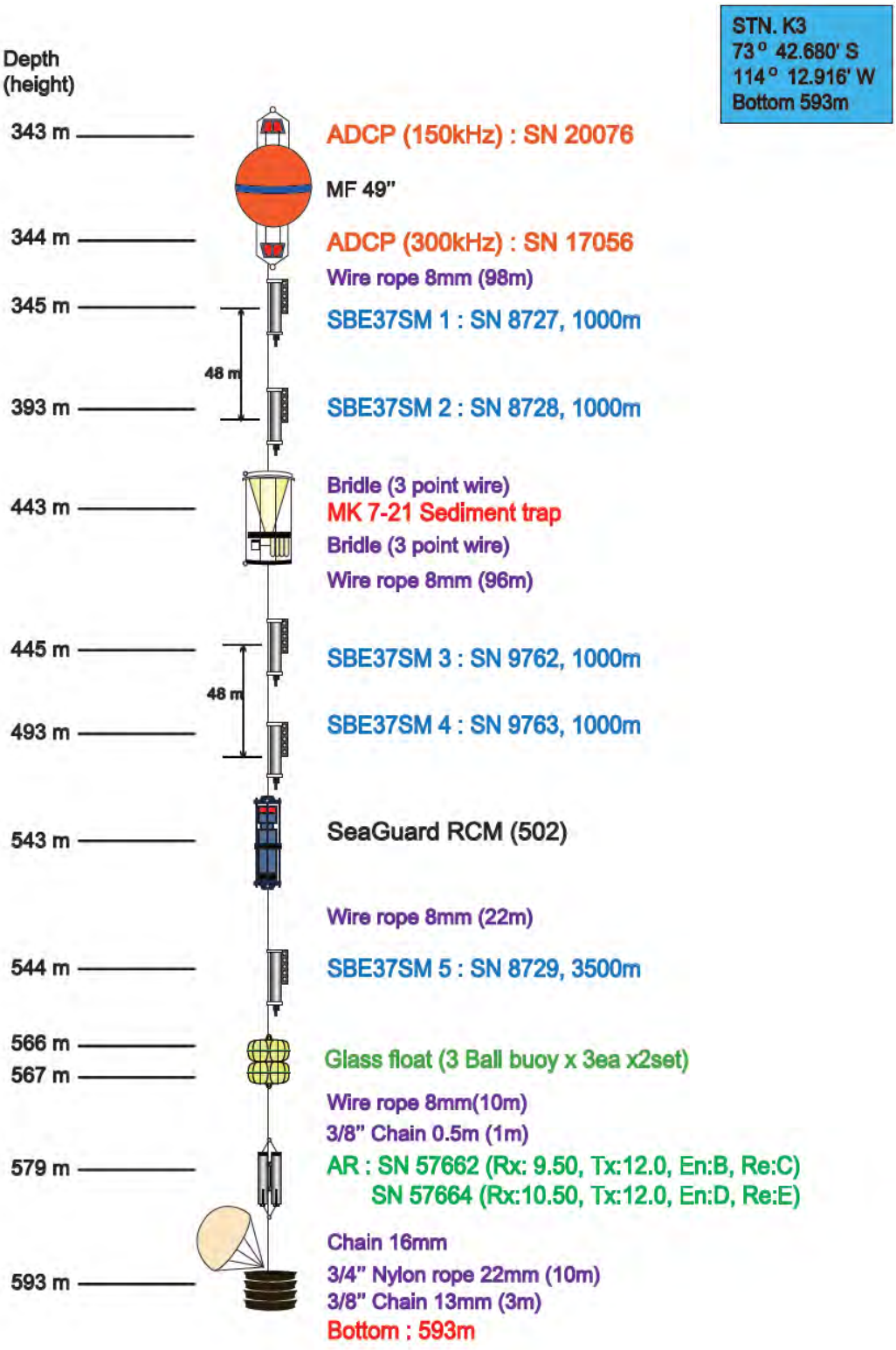
STN. K3
73° 42.680' S
114° 12.916' W
Bottom 593m
Depth
(height)
343 m
ADCP (150kHz) : SN 20076
MF 49"
344 m
ADCP (300kHz) : SN 17056
Wire rope 8mm (98m)
345 m
SBE37SM 1 : SN 8727, 1000m
48 m
393 m
SBE37SM 2 : SN 8728, 1000m
443 m
Bridle (3 point wire)
MK 7-21 Sediment trap
Bridle (3 point wire)
Wire rope 8mm (96m)
445 m
SBE37SM 3 : SN 9762, 1000m
48 m
493 m
SBE37SM 4 : SN 9763, 1000m
543 m
SeaGuard RCM (502)
Wire rope 8mm (22m)
544 m
SBE37SM 5 : SN 8729, 3500m
566 m
567 m
Glass float (3 Ball buoy x 3ea x2set)
Wire rope 8mm(10m)
3/8" Chain 0.5m (1m)
579 m
AR : SN 57662 (Rx: 9.50, Tx:12.0, En:B, Re:C)
SN 57664 (Rx:10.50, Tx:12.0, En:D, Re:E)
Chain 16mm
3/4" Nylon rope 22mm (10m)
3/8" Chain 13mm (3m)
593 m
Bottom : 593m

AP2 03 Mooring design K4

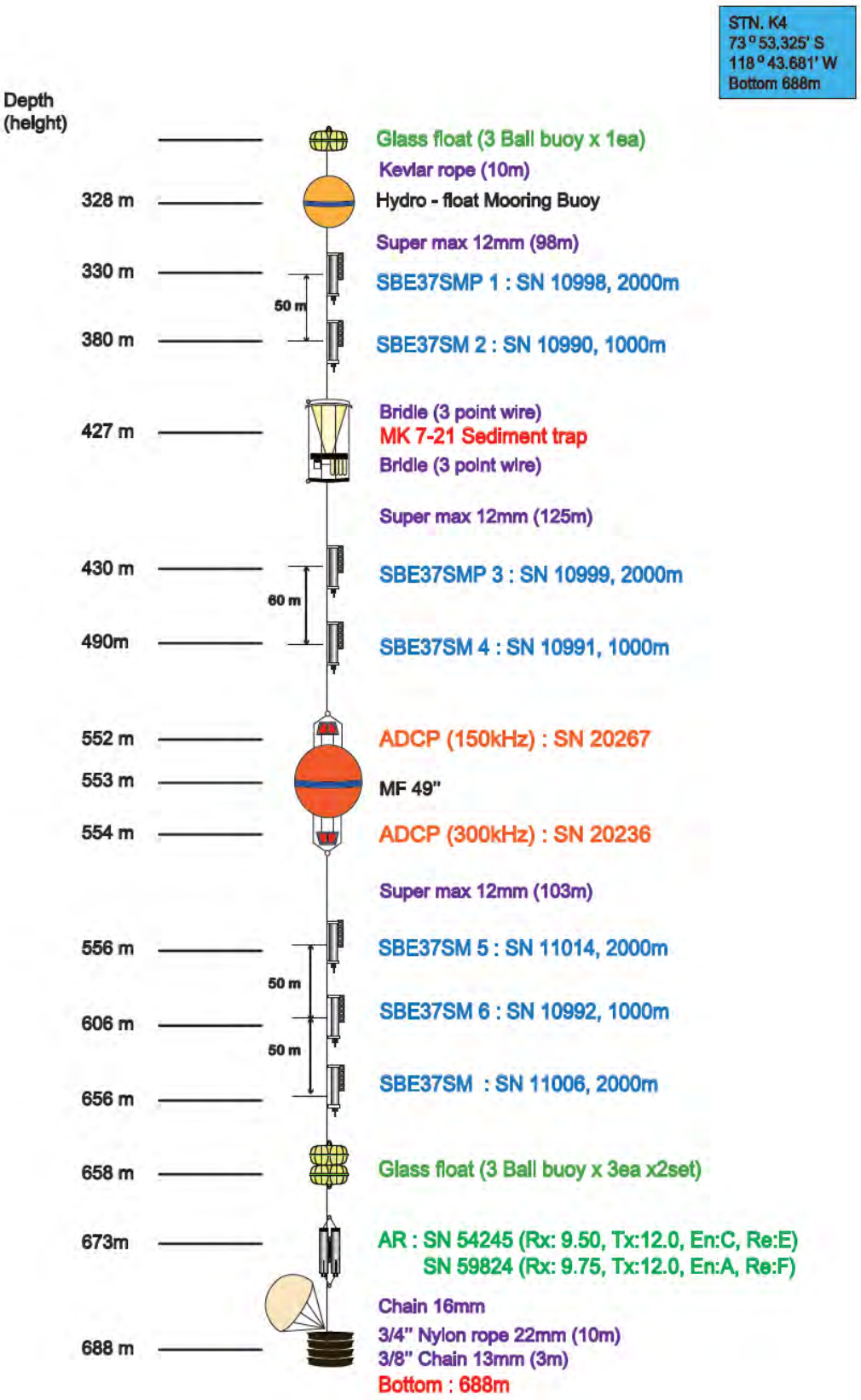

AP2 04 Mooring design K5

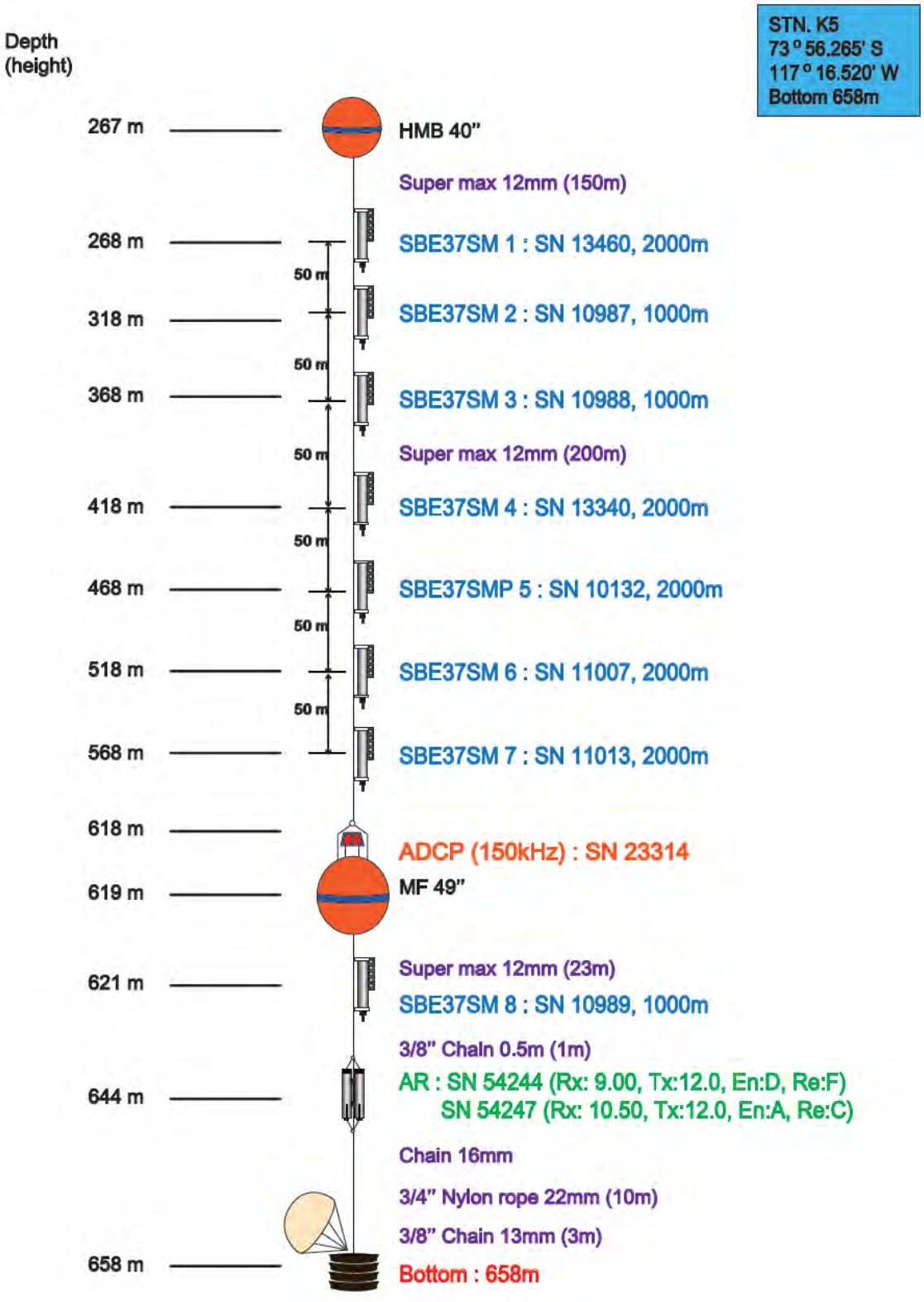

AP2 05 Mooring design K6

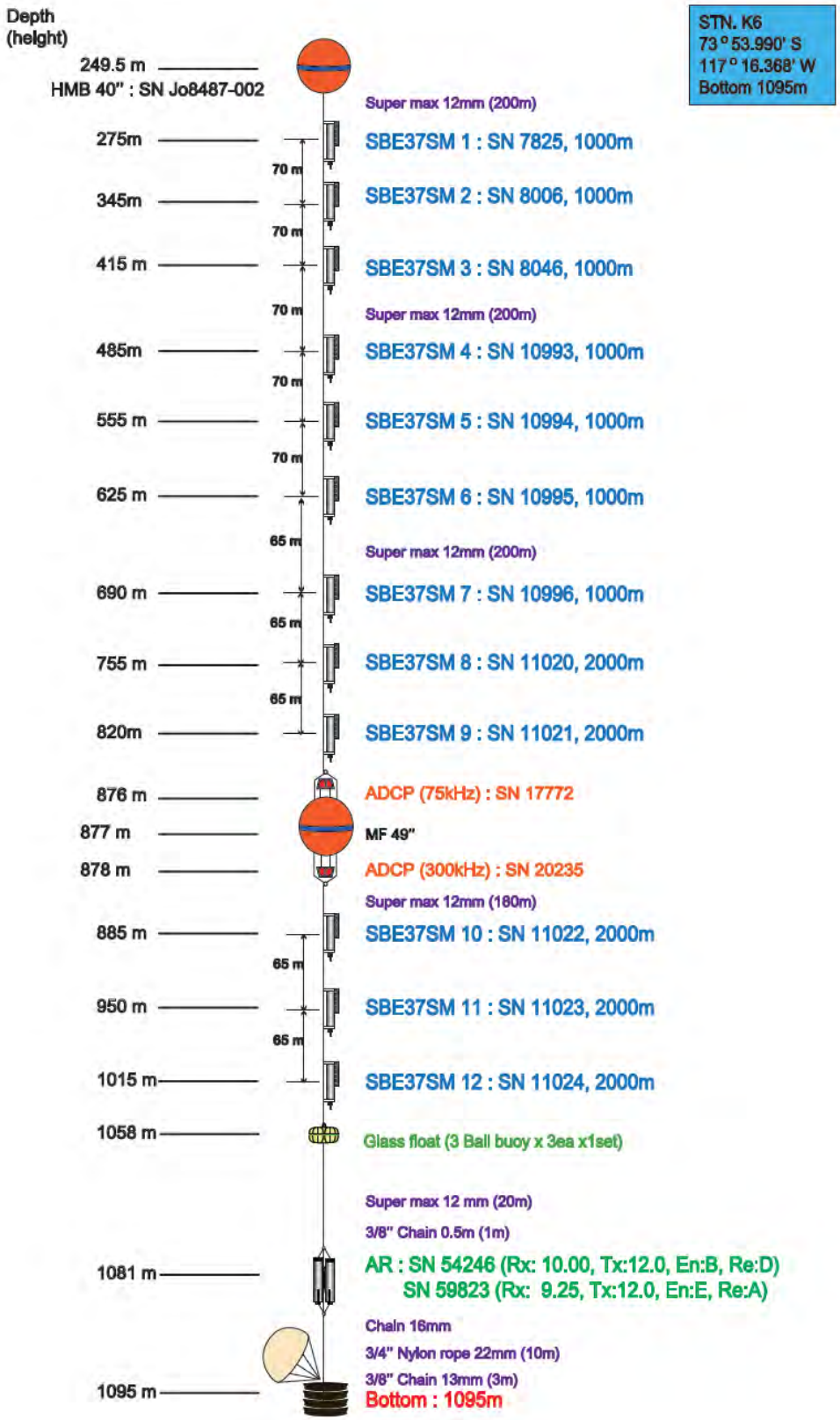

AP2 06 Mooring design S1

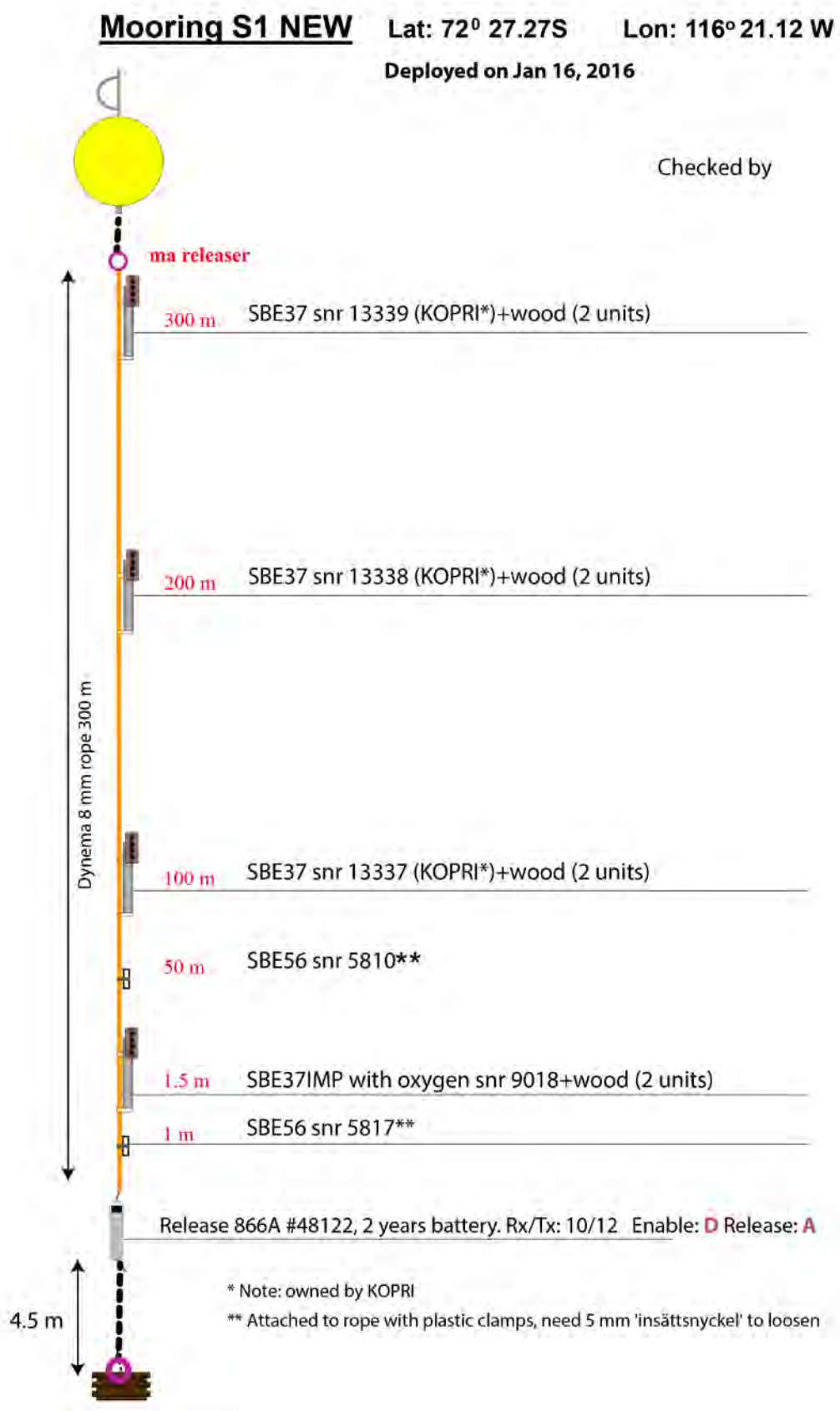

AP2 07 Mooring design S6

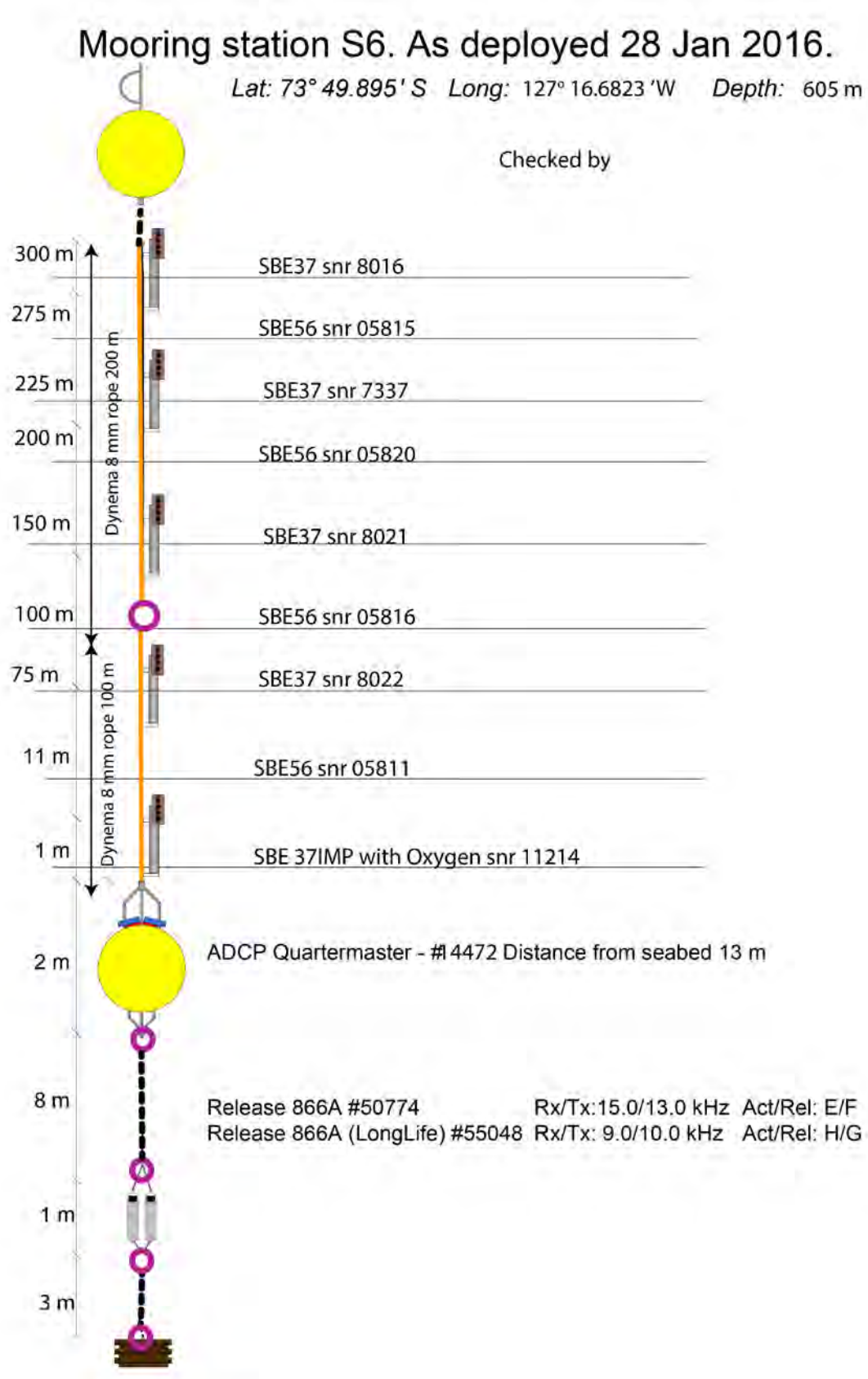

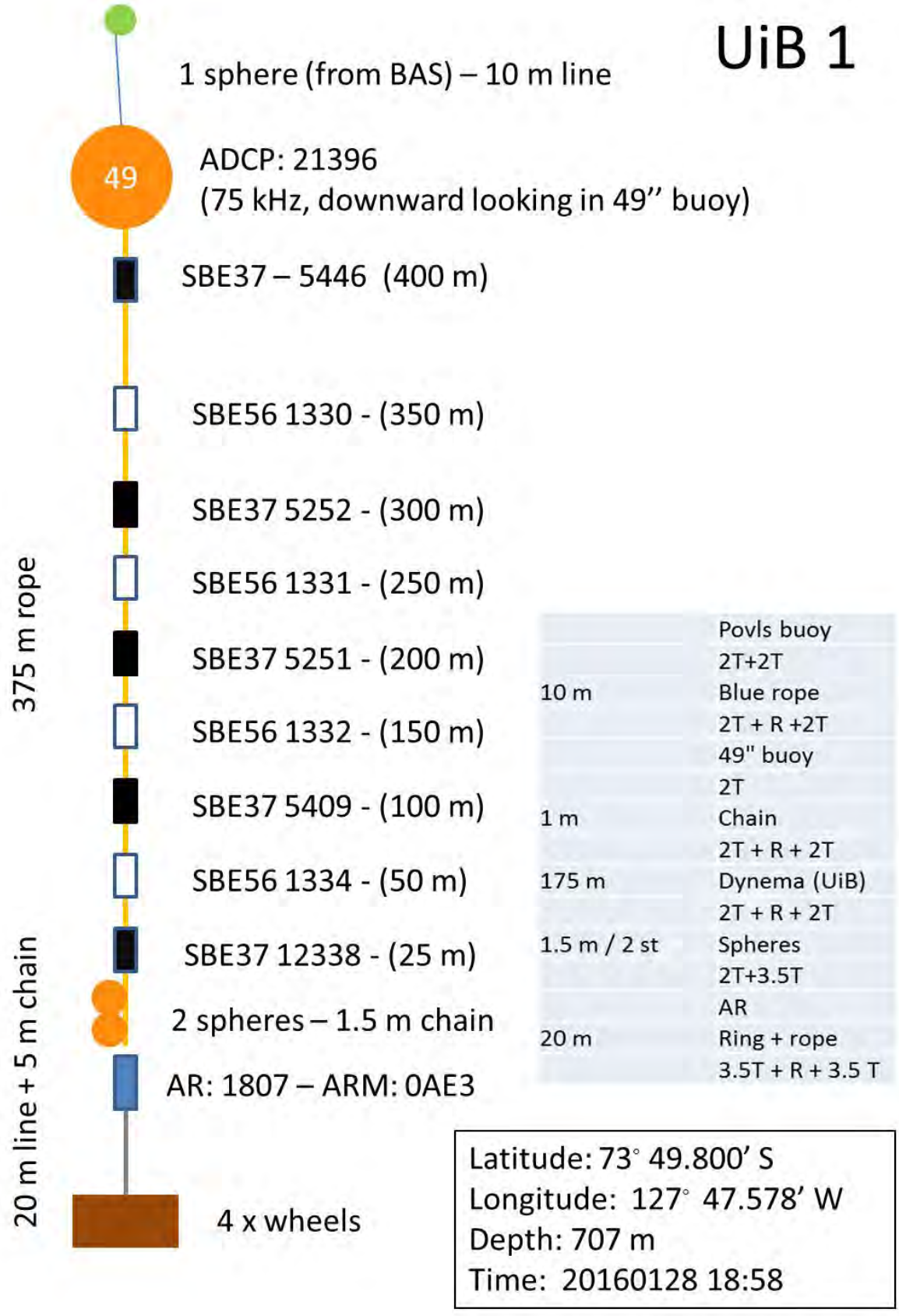
UiB 1
1 sphere (from BAS) – 10 m line
49
ADCP: 21396
(75 kHz, downward looking in 49'' buoy)
SBE37 – 5446 (400 m)
SBE56 1330 - (350 m)
SBE37 5252 - (300 m)
SBE56 1331 - (250 m)
SBE37 5251 - (200 m)
SBE56 1332 - (150 m)
SBE37 5409 - (100 m)
SBE56 1334 - (50 m)
SBE37 12338 - (25 m)
2 spheres – 1.5 m chain
AR: 1807 – ARM: 0AE3
4 x wheels
375 m rope
20 m line + 5 m chain
Povls buoy
2T+2T
10 m
Blue rope
2T + R +2T
49" buoy
2T
1 m
Chain
2T + R + 2T
175 m
Dynema (UiB)
2T + R + 2T
1.5 m / 2 st
Spheres
2T+3.5T
AR
20 m
Ring + rope
3.5T + R + 3.5 T
Latitude: 73° 49.800' S
Longitude: 127° 47.578' W
Depth: 707 m
Time: 20160128 18:58

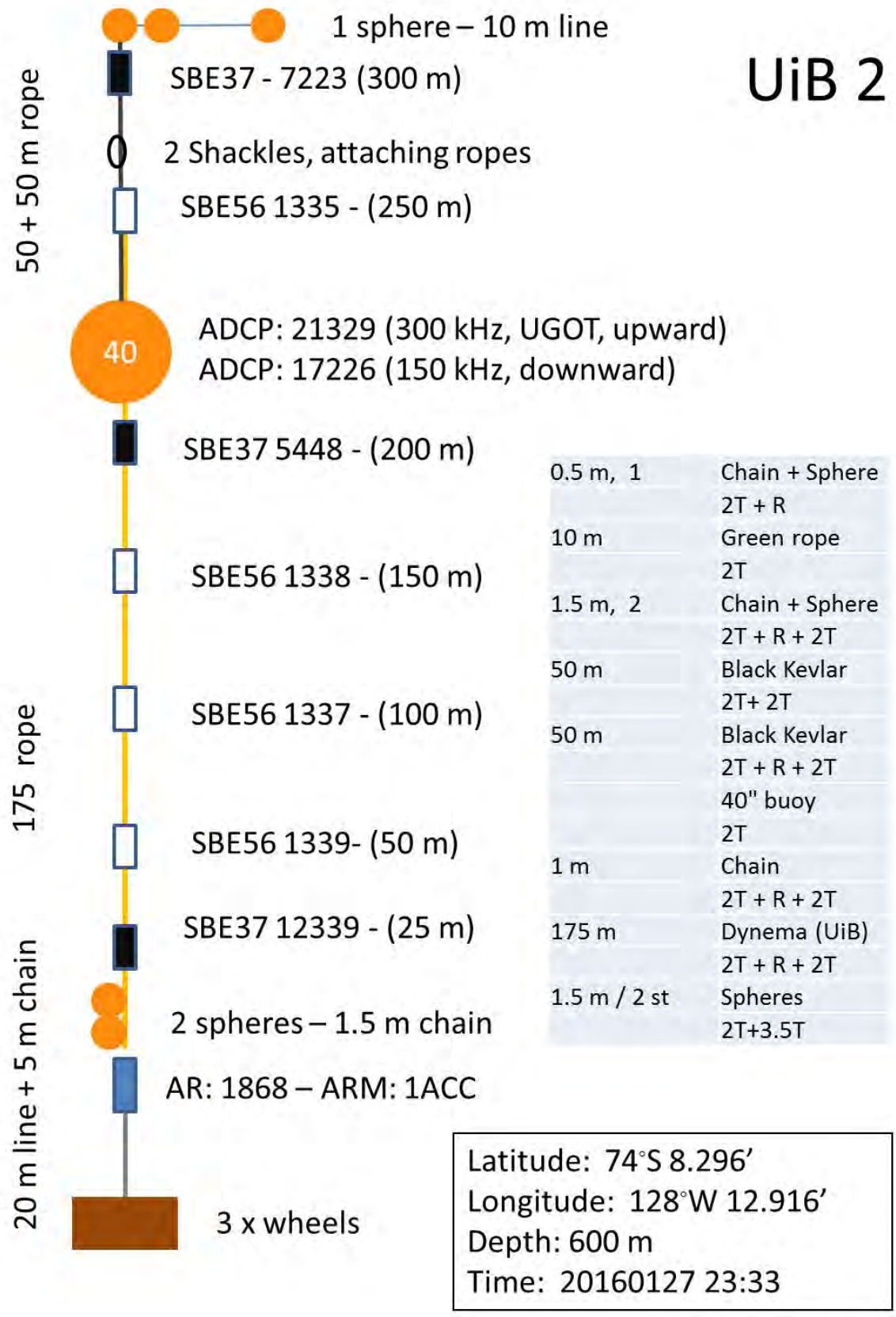
UiB 2
1 sphere – 10 m line
SBE37 - 7223 (300 m)
2 Shackles, attaching ropes
SBE56 1335 - (250 m)
50 + 50 m rope
40
ADCP: 21329 (300 kHz, UGOT, upward)
ADCP: 17226 (150 kHz, downward)
SBE37 5448 - (200 m)
SBE56 1338 - (150 m)
SBE56 1337 - (100 m)
175 rope
SBE56 1339- (50 m)
SBE37 12339 - (25 m)
2 spheres – 1.5 m chain
20 m line + 5 m chain
AR: 1868 – ARM: 1ACC
3 x wheels
0.5 m, 1 Chain + Sphere
2T + R
10 m Green rope
2T
1.5 m, 2 Chain + Sphere
2T + R + 2T
50 m Black Kevlar
2T+ 2T
50 m Black Kevlar
2T + R + 2T
40" buoy
2T
1 m Chain
2T + R + 2T
175 m Dynema (UiB)
2T + R + 2T
1.5 m / 2 st Spheres
2T+3.5T
Latitude: 74°S 8.296'
Longitude: 128°W 12.916'
Depth: 600 m
Time: 20160127 23:33

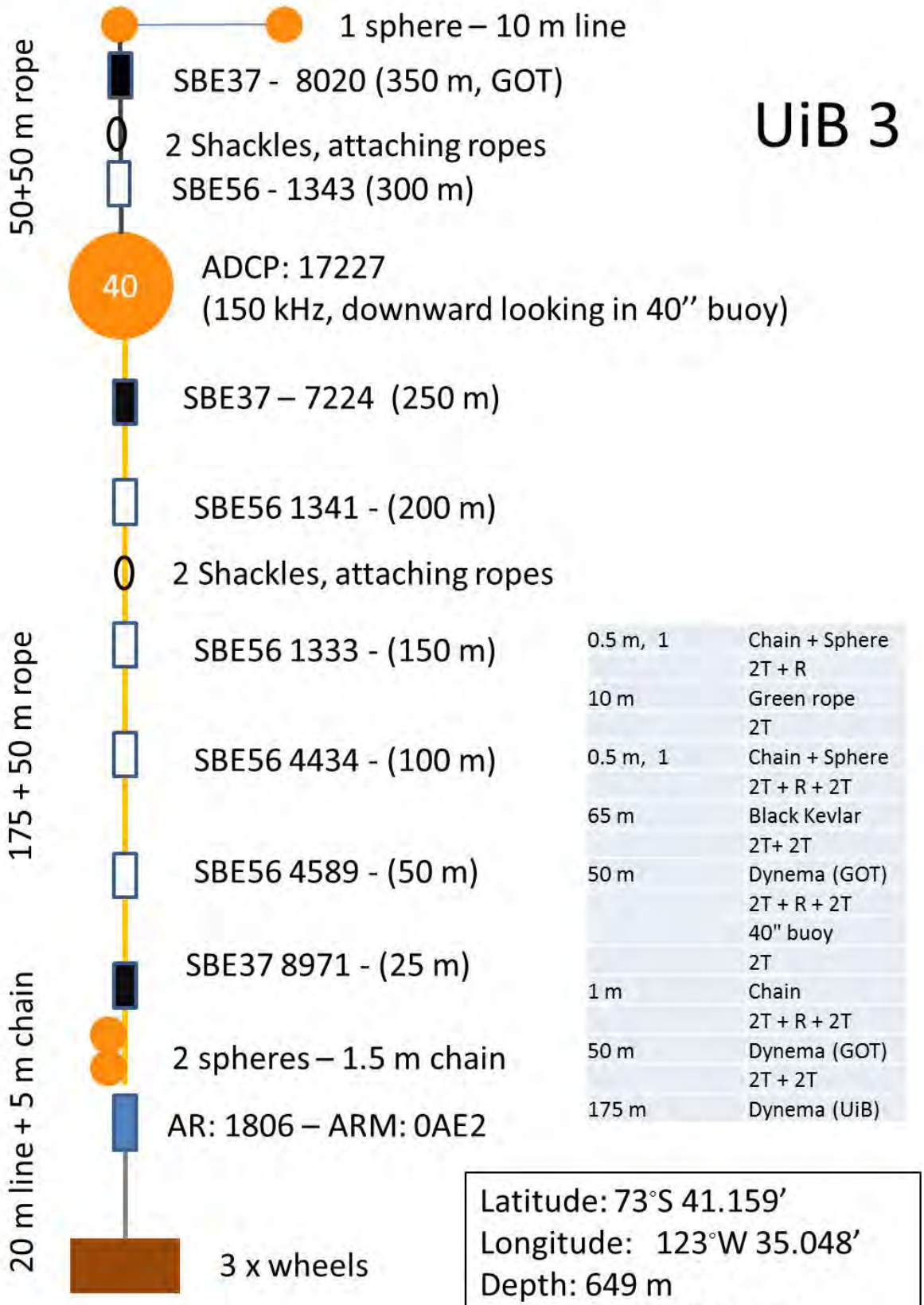


| | |
|---|---|
| 0.5 m, 1 | Chain + Sphere |
| | 2T + R |
| 10 m | Green rope |
| | 2T |
| 0.5 m, 1 | Chain + Sphere |
| | 2T + R + 2T |
| 65 m | Black Kevlar |
| | 2T+ 2T |
| 50 m | Dynema (GOT) |
| | 2T + R + 2T |
| | 40" buoy |
| | 2T |
| 1 m | Chain |
| | 2T + R + 2T |
| 50 m | Dynema (GOT) |
| | 2T + 2T |
| 175 m | Dynema (UiB) |

Latitude: 73°S 41.159'
Longitude: 123°W 35.048'
Depth: 649 m
Time: 20160130 01:44

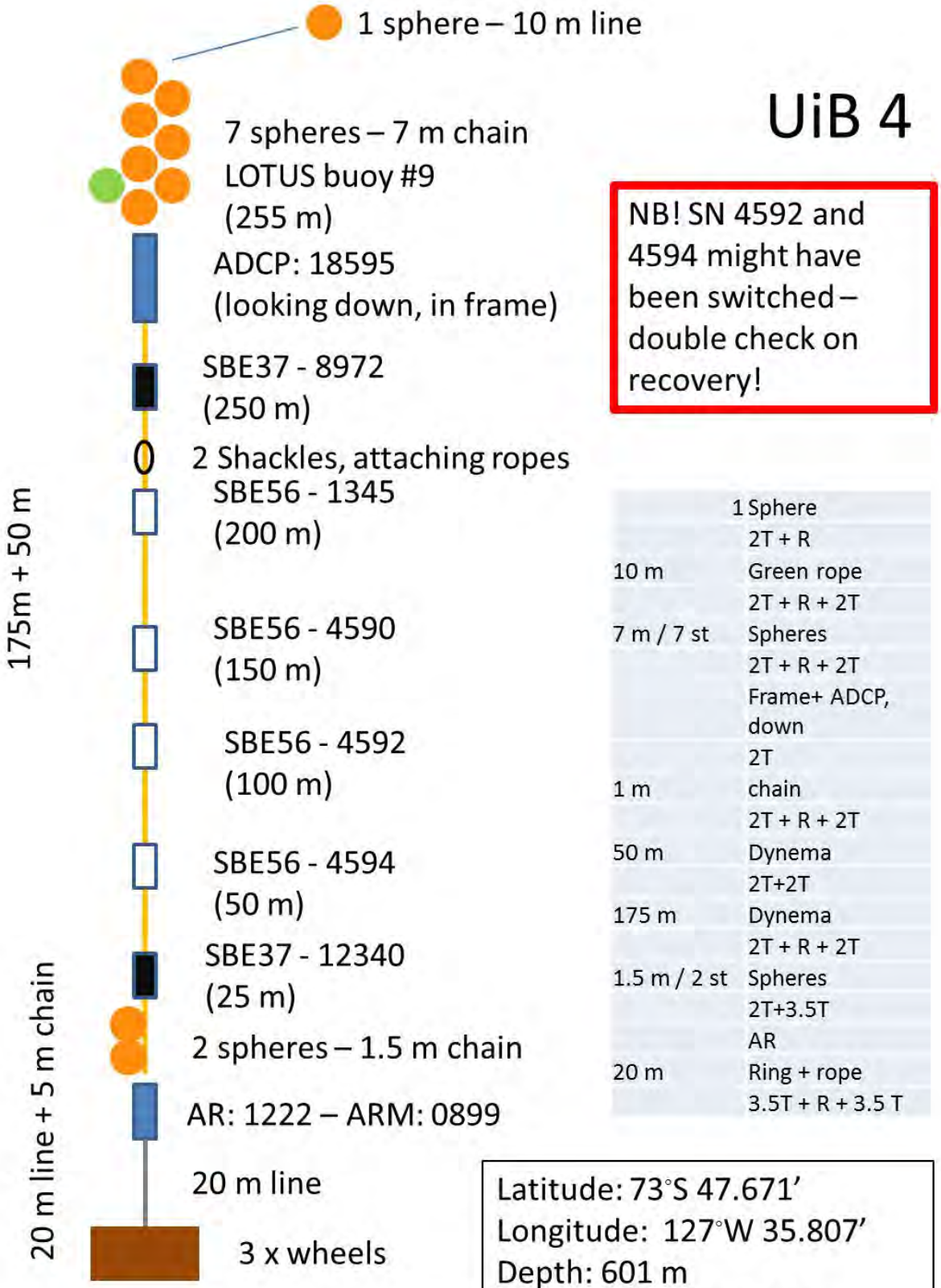


# UiB 4

NB! SN 4592 and 4594 might have been switched – double check on recovery!

| | |
|---|---|
| | 1 Sphere |
| | 2T + R |
| 10 m | Green rope |
| | 2T + R + 2T |
| 7 m / 7 st | Spheres |
| | 2T + R + 2T |
| | Frame+ ADCP, down |
| | 2T |
| 1 m | chain |
| | 2T + R + 2T |
| 50 m | Dynema |
| | 2T+2T |
| 175 m | Dynema |
| | 2T + R + 2T |
| 1.5 m / 2 st | Spheres |
| | 2T+3.5T |
| | AR |
| 20 m | Ring + rope |
| | 3.5T + R + 3.5 T |

Latitude: 73°S 47.671'
Longitude: 127°W 35.807'
Depth: 601 m
Time: 20160128 22:38

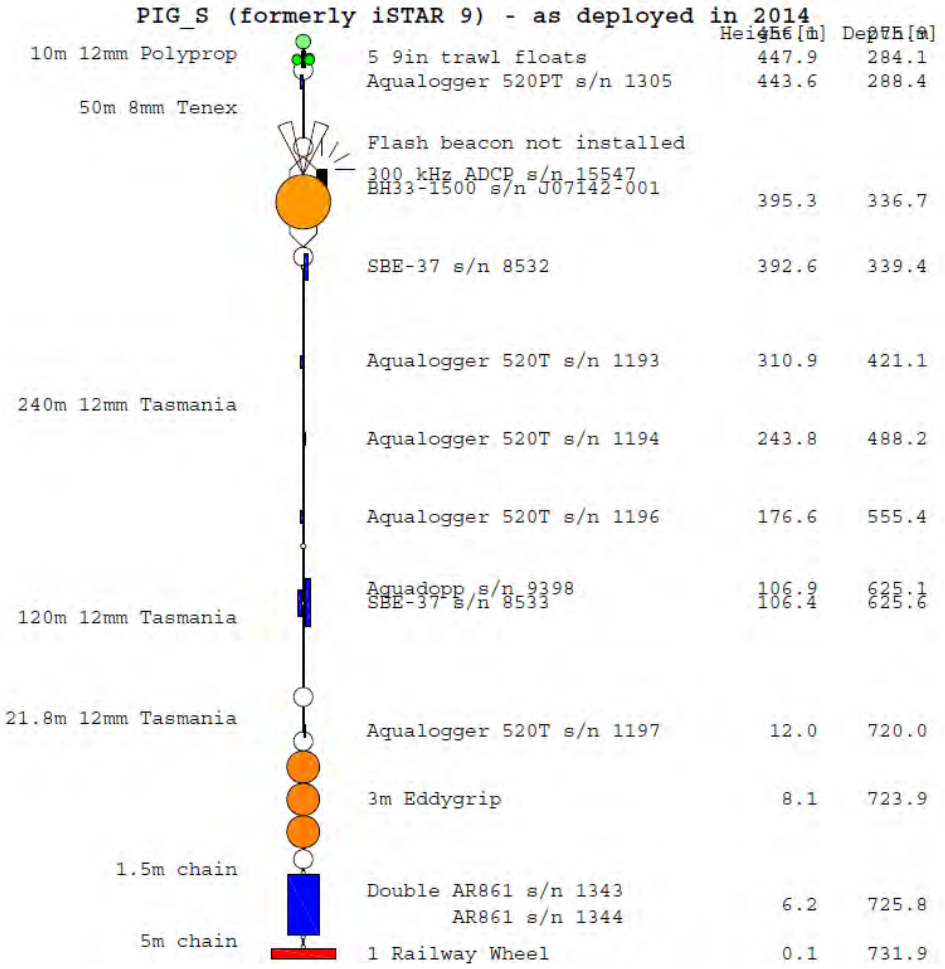
PIG_S (formerly iSTAR 9) - as deployed in 2014
Height [m]
Depth [m]
10m 12mm Polyprop
5 9in trawl floats 447.9 284.1
Aqualogger 520PT s/n 1305 443.6 288.4
50m 8mm Tenex
Flash beacon not installed
300 kHz ADCP s/n 15547
BH33-1500 s/n J07142-001 395.3 336.7
SBE-37 s/n 8532 392.6 339.4
Aqualogger 520T s/n 1193 310.9 421.1
240m 12mm Tasmania
Aqualogger 520T s/n 1194 243.8 488.2
Aqualogger 520T s/n 1196 176.6 555.4
Aquadopp s/n 9398 106.9 625.1
SBE-37 s/n 8533 106.4 625.6
120m 12mm Tasmania
21.8m 12mm Tasmania
Aqualogger 520T s/n 1197 12.0 720.0
3m Eddygrip 8.1 723.9
1.5m chain
Double AR861 s/n 1343
AR861 s/n 1344 6.2 725.8
5m chain
1 Railway Wheel 0.1 731.9

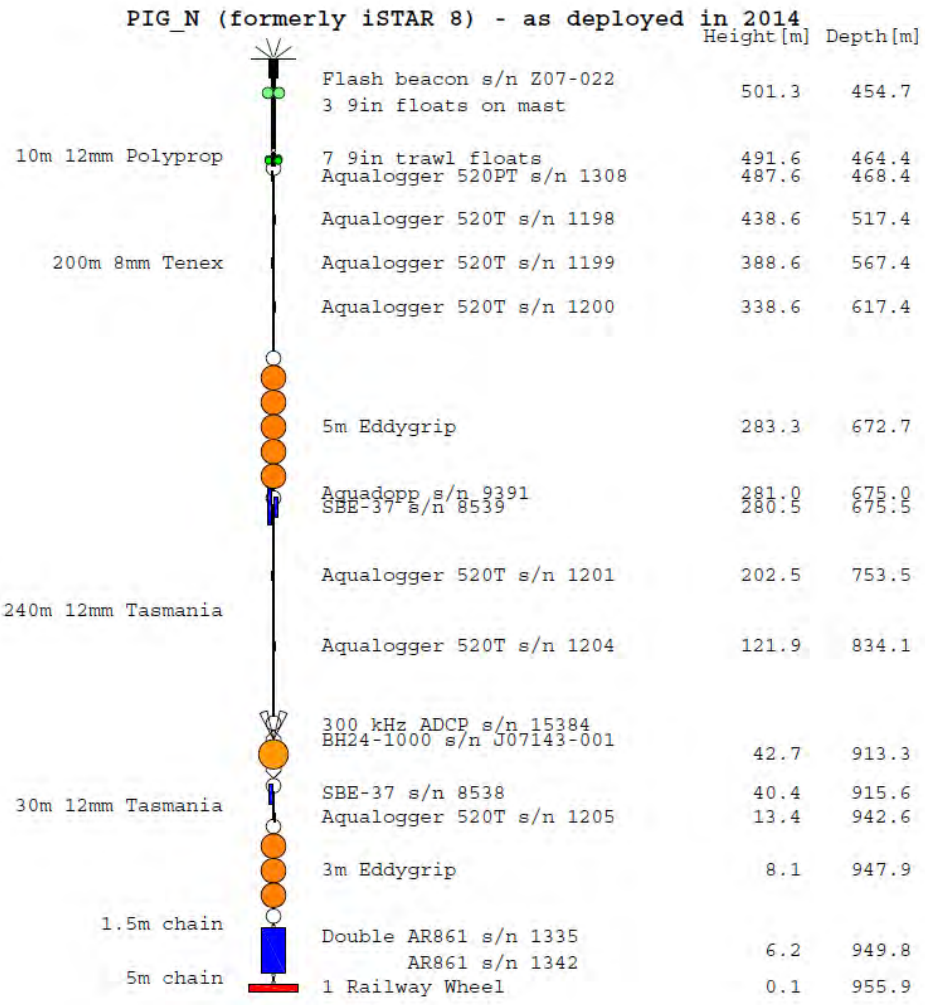
PIG_N (formerly iSTAR 8) - as deployed in 2014
Height[m] Depth[m]
Flash beacon s/n Z07-022
3 9in floats on mast
501.3 454.7
10m 12mm Polyprop
7 9in trawl floats
Aqualogger 520PT s/n 1308
491.6 464.4
487.6 468.4
Aqualogger 520T s/n 1198
438.6 517.4
200m 8mm Tenex
Aqualogger 520T s/n 1199
388.6 567.4
Aqualogger 520T s/n 1200
338.6 617.4
5m Eddygrip
283.3 672.7
Aquadopp s/n 9391
SBE-37 s/n 8539
281.0 675.0
280.5 675.5
Aqualogger 520T s/n 1201
202.5 753.5
240m 12mm Tasmania
Aqualogger 520T s/n 1204
121.9 834.1
300 kHz ADCP s/n 15384
BH24-1000 s/n J07143-001
42.7 913.3
SBE-37 s/n 8538
Aqualogger 520T s/n 1205
30m 12mm Tasmania
40.4 915.6
13.4 942.6
3m Eddygrip
8.1 947.9
1.5m chain
Double AR861 s/n 1335
AR861 s/n 1342
6.2 949.8
5m chain
1 Railway Wheel
0.1 955.9

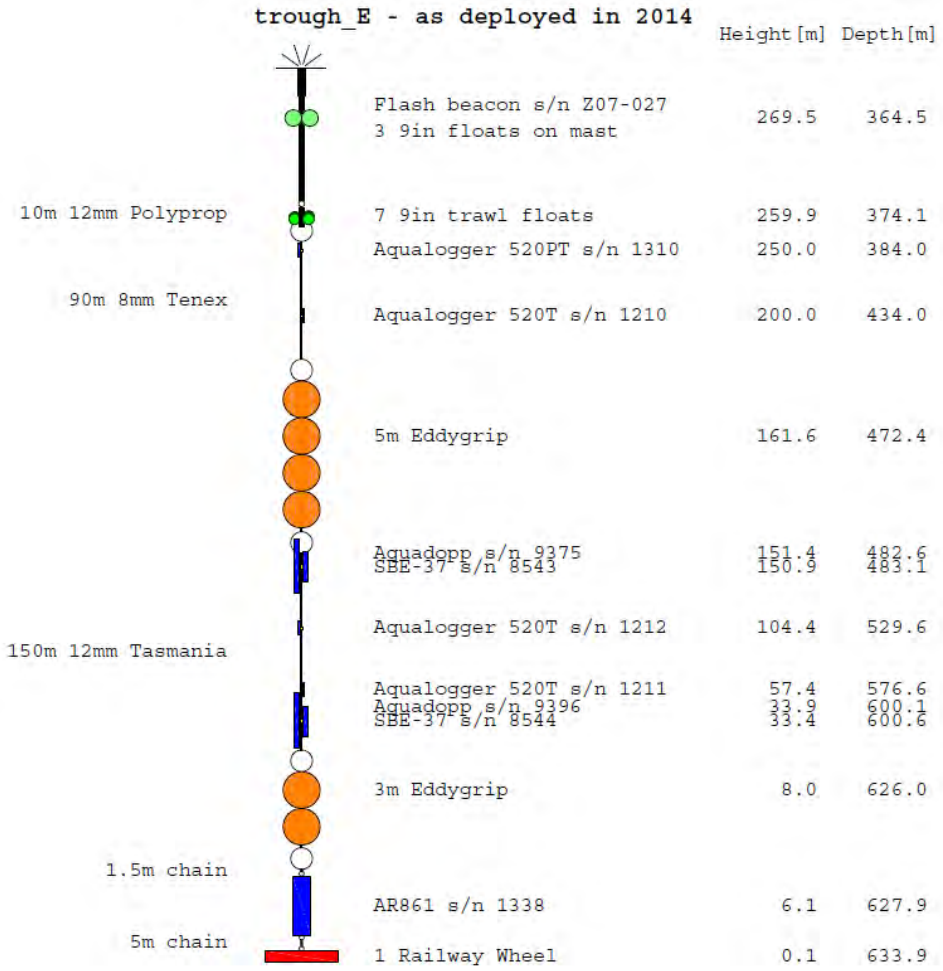
trough_E - as deployed in 2014
Height [m]
Depth [m]
Flash beacon s/n Z07-027
3 9in floats on mast
269.5
364.5
10m 12mm Polyprop
7 9in trawl floats
259.9
374.1
Aqualogger 520PT s/n 1310
250.0
384.0
90m 8mm Tenex
Aqualogger 520T s/n 1210
200.0
434.0
5m Eddygrip
161.6
472.4
Aquadopp s/n 9375
151.4
482.6
SBE-37 s/n 8543
150.9
483.1
Aqualogger 520T s/n 1212
104.4
529.6
150m 12mm Tasmania
Aqualogger 520T s/n 1211
57.4
576.6
Aquadopp s/n 9396
33.9
600.1
SBE-37 s/n 8544
33.4
600.6
3m Eddygrip
8.0
626.0
1.5m chain
AR861 s/n 1338
6.1
627.9
5m chain
1 Railway Wheel
0.1
633.9

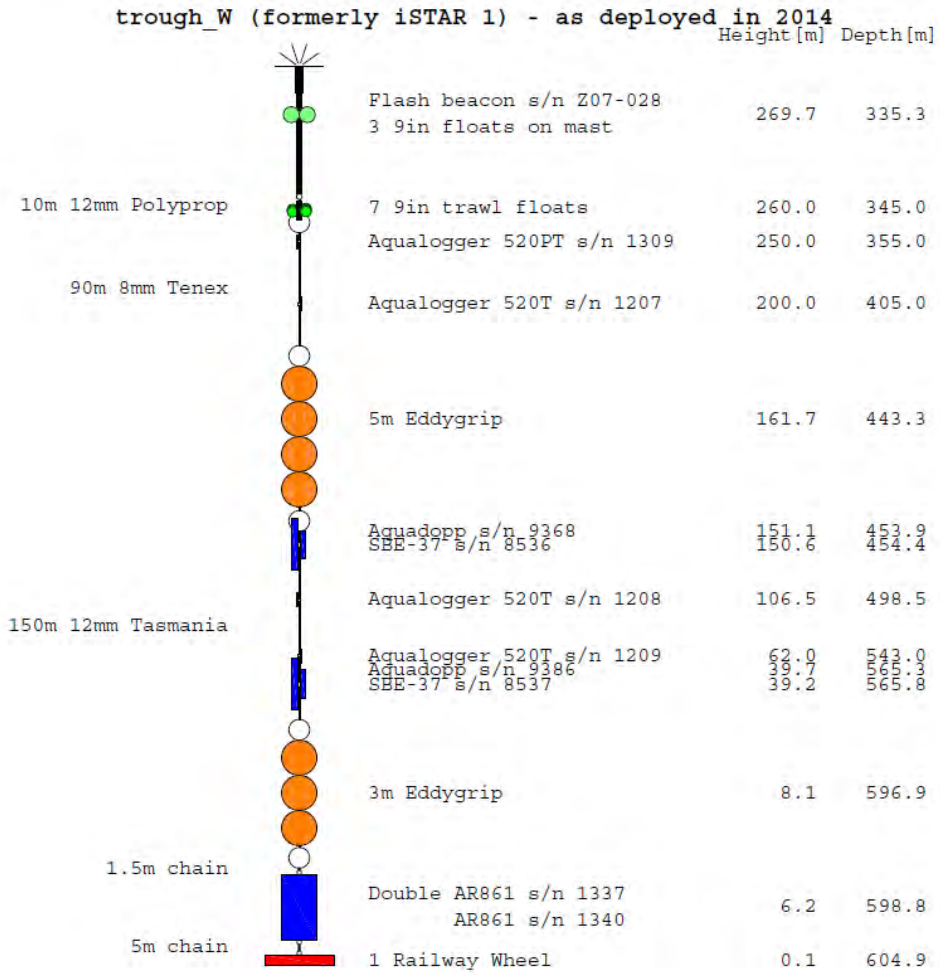
trough_W (formerly iSTAR 1) - as deployed in 2014
Height [m]
Depth [m]
Flash beacon s/n Z07-028
3 9in floats on mast
269.7
335.3
10m 12mm Polyprop
7 9in trawl floats
260.0
345.0
Aqualogger 520PT s/n 1309
250.0
355.0
90m 8mm Tenex
Aqualogger 520T s/n 1207
200.0
405.0
5m Eddygrip
161.7
443.3
Aquadopp s/n 9368
SBE-37 s/n 8536
151.1
150.6
453.9
454.4
Aqualogger 520T s/n 1208
106.5
498.5
150m 12mm Tasmania
Aqualogger 520T s/n 1209
Aquadopp s/n 9386
SBE-37 s/n 8537
62.0
39.7
39.2
543.0
565.3
565.8
3m Eddygrip
8.1
596.9
1.5m chain
Double AR861 s/n 1337
AR861 s/n 1340
6.2
598.8
5m chain
1 Railway Wheel
0.1
604.9

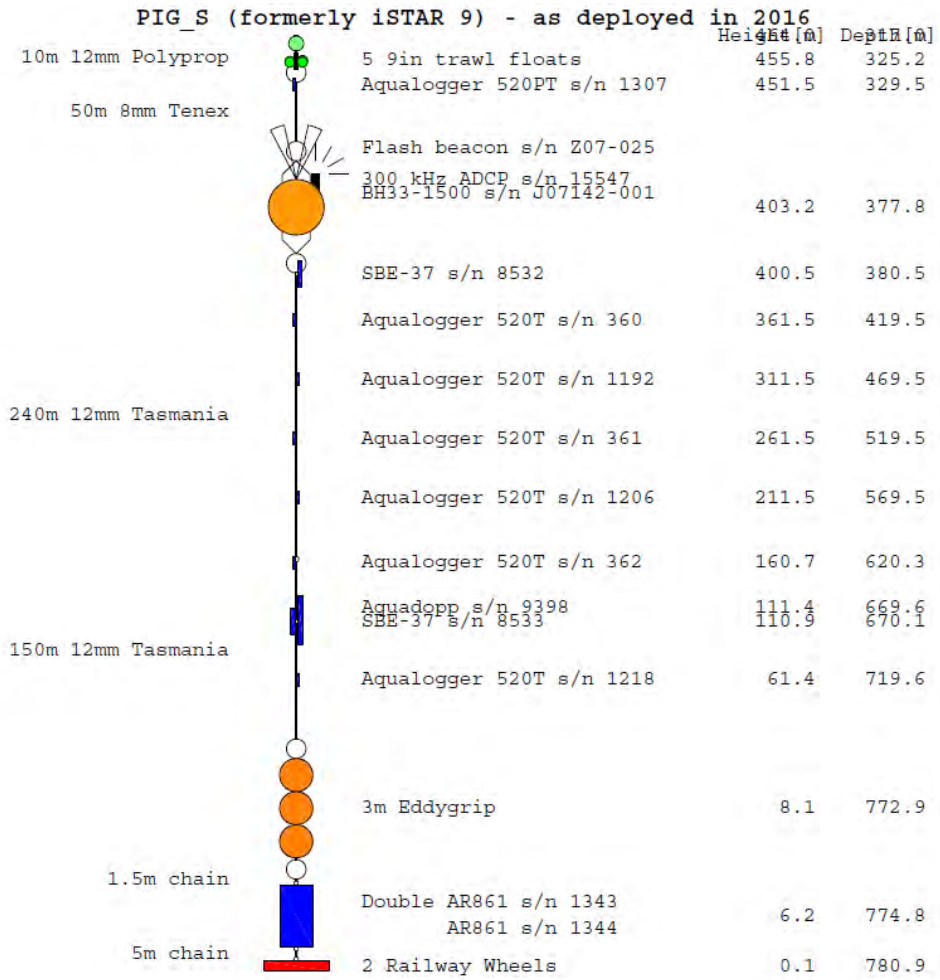
PIG_S (formerly iSTAR 9) - as deployed in 2016
Height [m]
Depth [m]
10m 12mm Polyprop
5 9in trawl floats 455.8 325.2
Aqualogger 520PT s/n 1307 451.5 329.5
50m 8mm Tenex
Flash beacon s/n Z07-025
300 kHz ADCP s/n 15547
BH33-1500 s/n J07142-001 403.2 377.8
SBE-37 s/n 8532 400.5 380.5
Aqualogger 520T s/n 360 361.5 419.5
Aqualogger 520T s/n 1192 311.5 469.5
240m 12mm Tasmania
Aqualogger 520T s/n 361 261.5 519.5
Aqualogger 520T s/n 1206 211.5 569.5
Aqualogger 520T s/n 362 160.7 620.3
Aquadopp s/n 9398 111.4 669.6
SBE-37 s/n 8533 110.9 670.1
150m 12mm Tasmania
Aqualogger 520T s/n 1218 61.4 719.6
3m Eddygrip 8.1 772.9
1.5m chain
Double AR861 s/n 1343
AR861 s/n 1344 6.2 774.8
5m chain
2 Railway Wheels 0.1 780.9

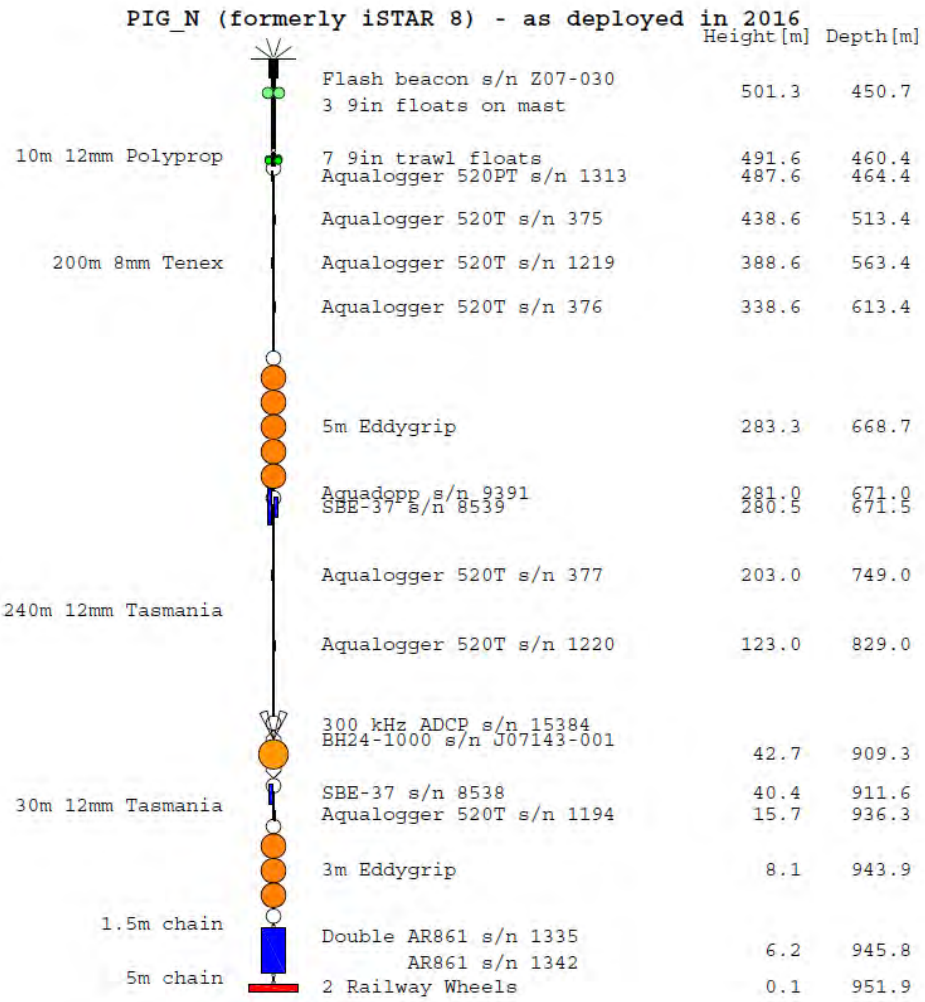
PIG_N (formerly iSTAR 8) - as deployed in 2016
Height[m] Depth[m]
Flash beacon s/n Z07-030
3 9in floats on mast
501.3 450.7
10m 12mm Polyprop
7 9in trawl floats
Aqualogger 520PT s/n 1313
491.6 460.4
487.6 464.4
Aqualogger 520T s/n 375
438.6 513.4
200m 8mm Tenex
Aqualogger 520T s/n 1219
388.6 563.4
Aqualogger 520T s/n 376
338.6 613.4
5m Eddygrip
283.3 668.7
Aquadopp s/n 9391
SBE-37 s/n 8539
281.0 671.0
280.5 671.5
Aqualogger 520T s/n 377
203.0 749.0
240m 12mm Tasmania
Aqualogger 520T s/n 1220
123.0 829.0
300 kHz ADCP s/n 15384
BH24-1000 s/n J07143-001
42.7 909.3
SBE-37 s/n 8538
Aqualogger 520T s/n 1194
40.4 911.6
15.7 936.3
30m 12mm Tasmania
3m Eddygrip
8.1 943.9
1.5m chain
Double AR861 s/n 1335
AR861 s/n 1342
6.2 945.8
5m chain
2 Railway Wheels
0.1 951.9

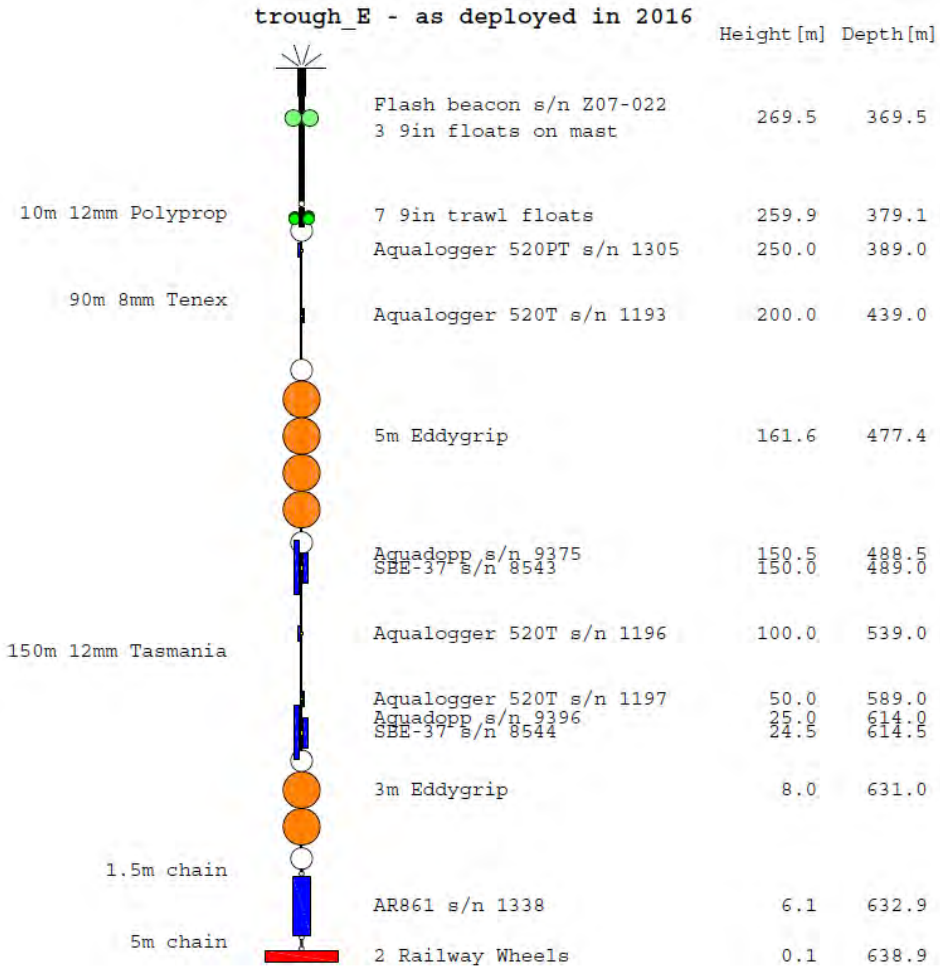
trough_E - as deployed in 2016
Height [m]
Depth [m]
Flash beacon s/n Z07-022
3 9in floats on mast
269.5
369.5
10m 12mm Polyprop
7 9in trawl floats
259.9
379.1
Aqualogger 520PT s/n 1305
250.0
389.0
90m 8mm Tenex
Aqualogger 520T s/n 1193
200.0
439.0
5m Eddygrip
161.6
477.4
Aquadopp s/n 9375
SBE-37 s/n 8543
150.5
150.0
488.5
489.0
150m 12mm Tasmania
Aqualogger 520T s/n 1196
100.0
539.0
Aqualogger 520T s/n 1197
Aquadopp s/n 9396
SBE-37 s/n 8544
50.0
25.0
24.5
589.0
614.0
614.5
3m Eddygrip
8.0
631.0
1.5m chain
AR861 s/n 1338
6.1
632.9
5m chain
2 Railway Wheels
0.1
638.9

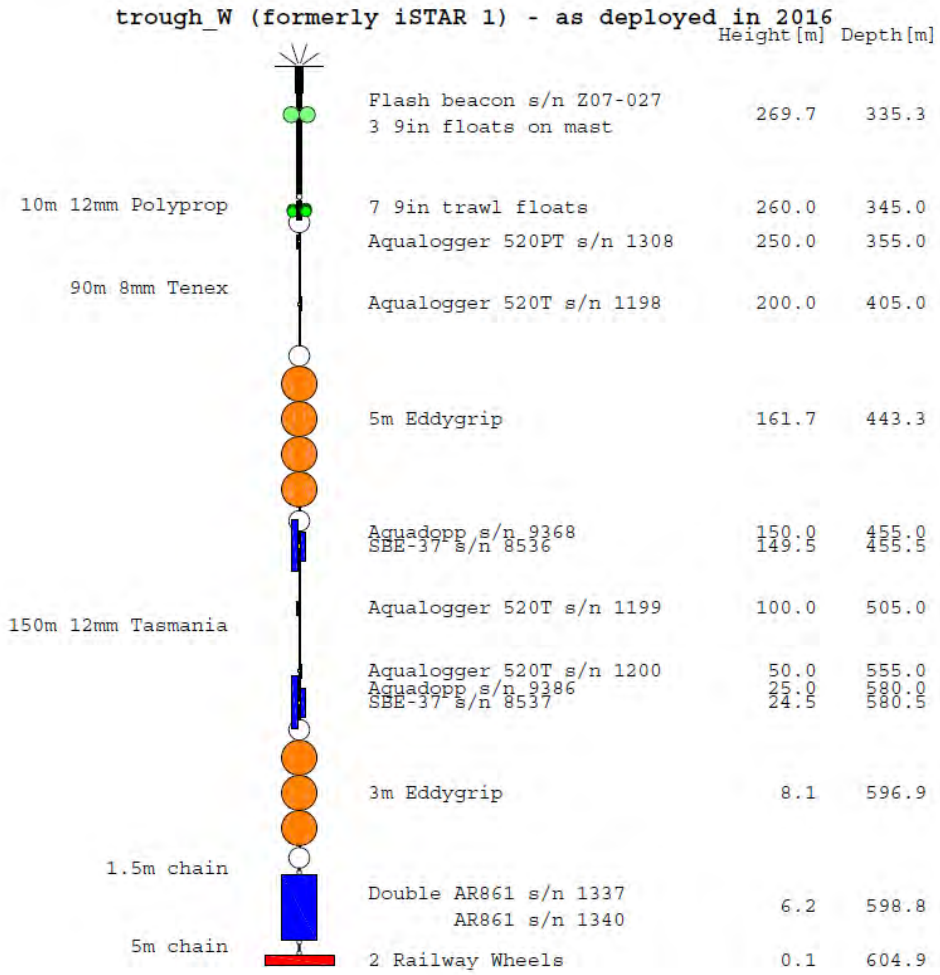
trough_W (formerly iSTAR 1) - as deployed in 2016
Height [m]
Depth [m]
Flash beacon s/n Z07-027
3 9in floats on mast
269.7
335.3
10m 12mm Polyprop
7 9in trawl floats
260.0
345.0
Aqualogger 520PT s/n 1308
250.0
355.0
90m 8mm Tenex
Aqualogger 520T s/n 1198
200.0
405.0
5m Eddygrip
161.7
443.3
Aquadopp s/n 9368
SBE-37 s/n 8536
150.0
149.5
455.0
455.5
Aqualogger 520T s/n 1199
100.0
505.0
150m 12mm Tasmania
Aqualogger 520T s/n 1200
Aquadopp s/n 9386
SBE-37 s/n 8537
50.0
25.0
24.5
555.0
580.0
580.5
3m Eddygrip
8.1
596.9
1.5m chain
Double AR861 s/n 1337
AR861 s/n 1340
6.2
598.8
5m chain
2 Railway Wheels
0.1
604.9

## Appendix 1.3. Multibeam survey results

AP3 1 Multibeam Survey K3

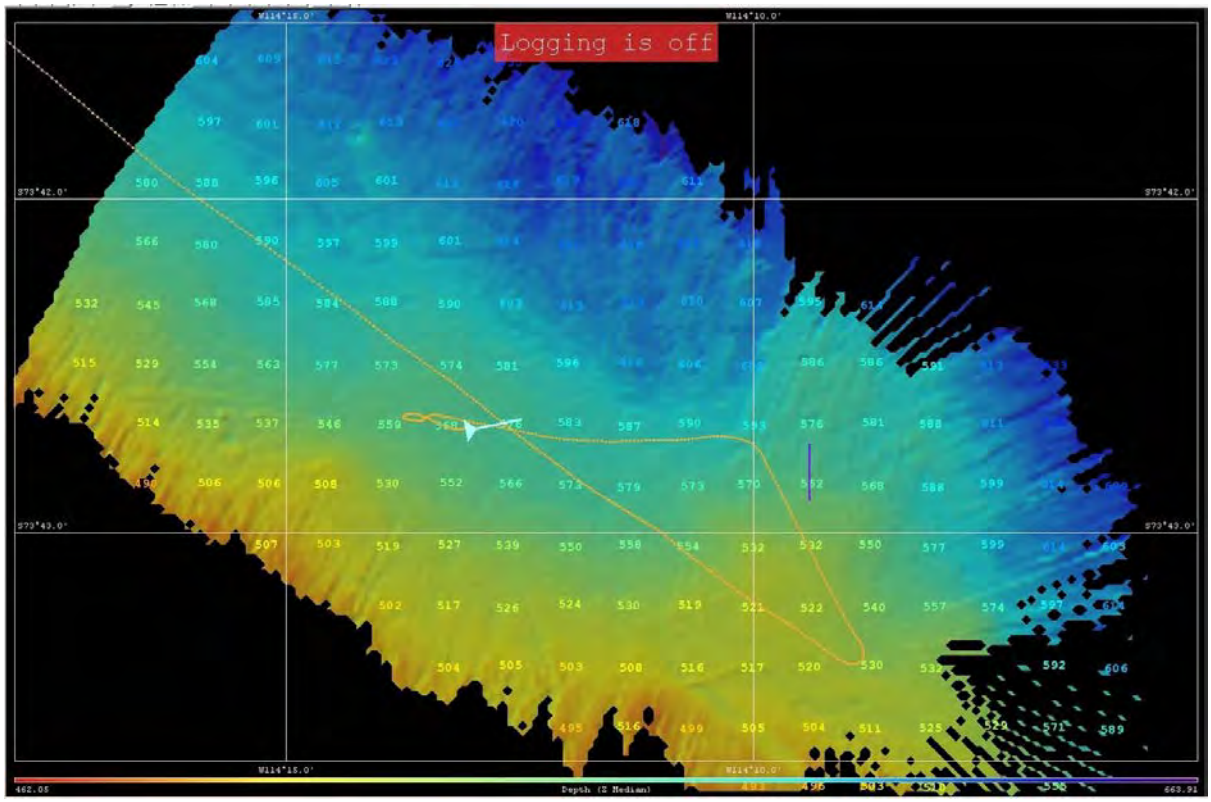

AP3 2 Multibeam Survey K4

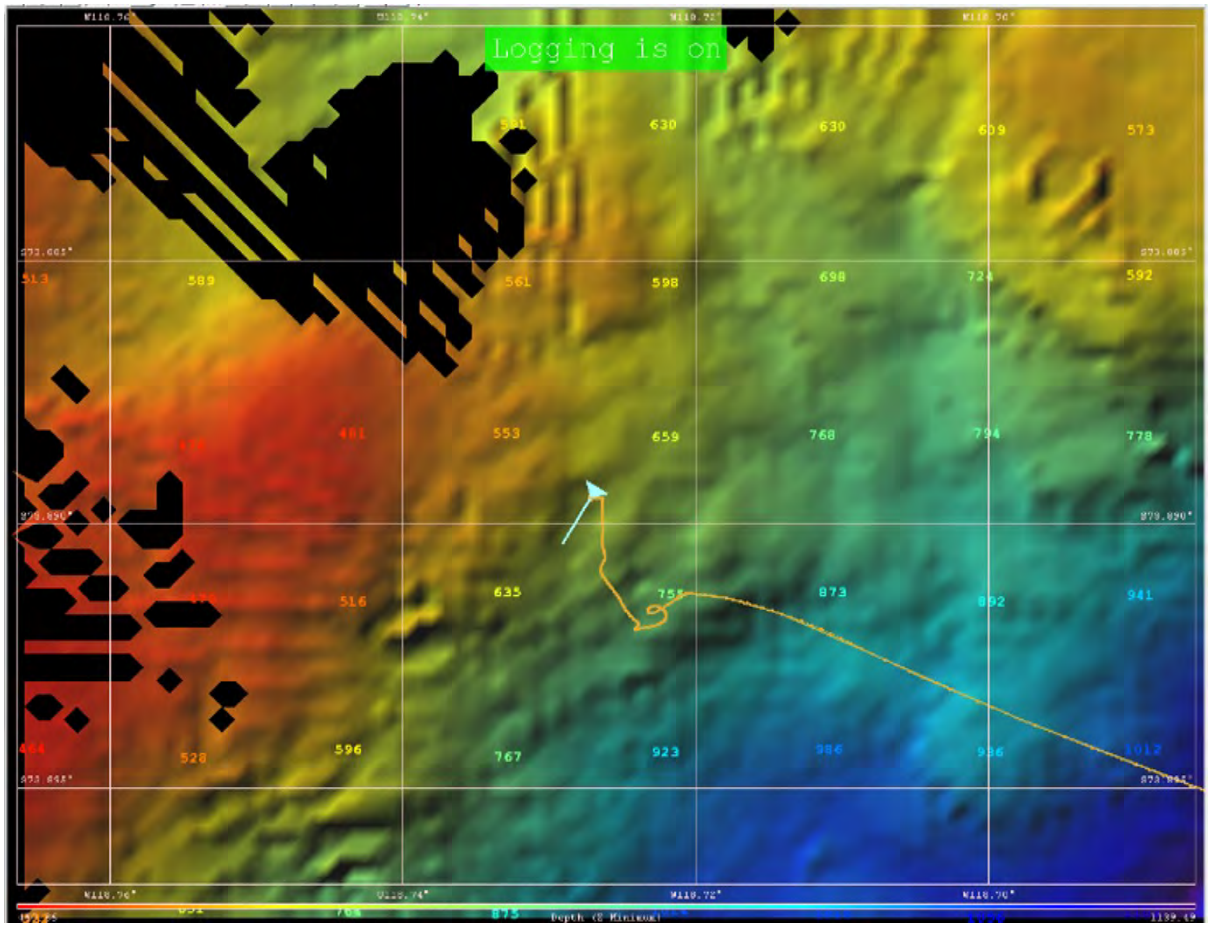

AP3 3 Multibeam Survey K5

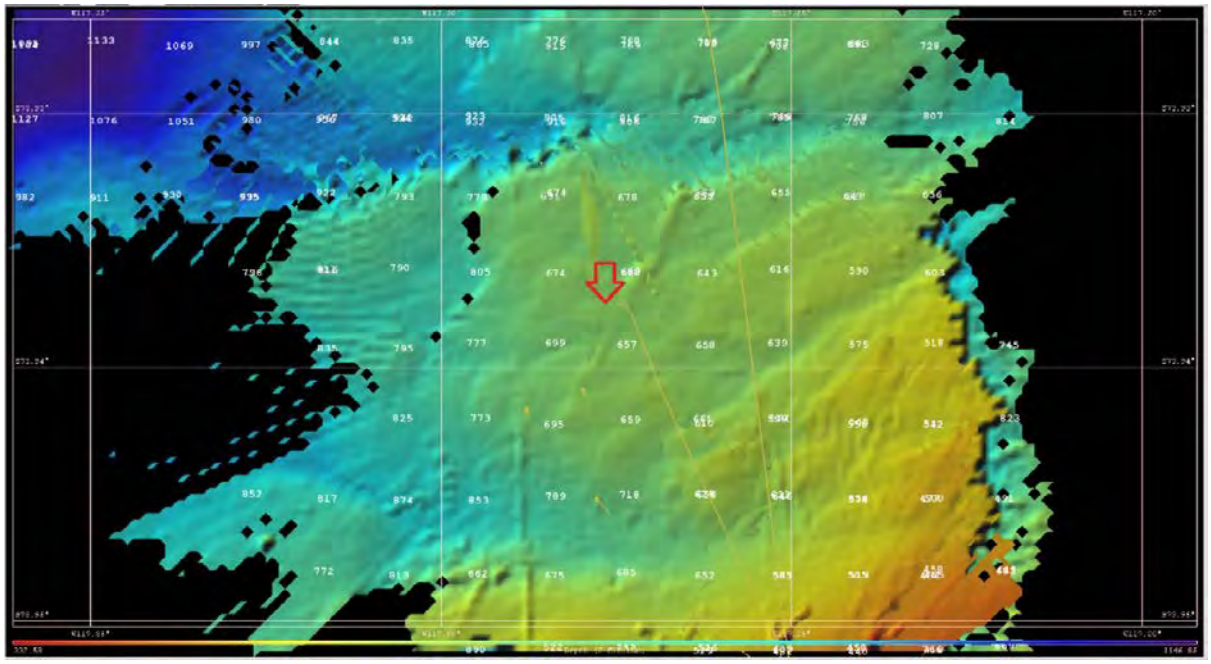

AP3 4 Multibeam Survey K6

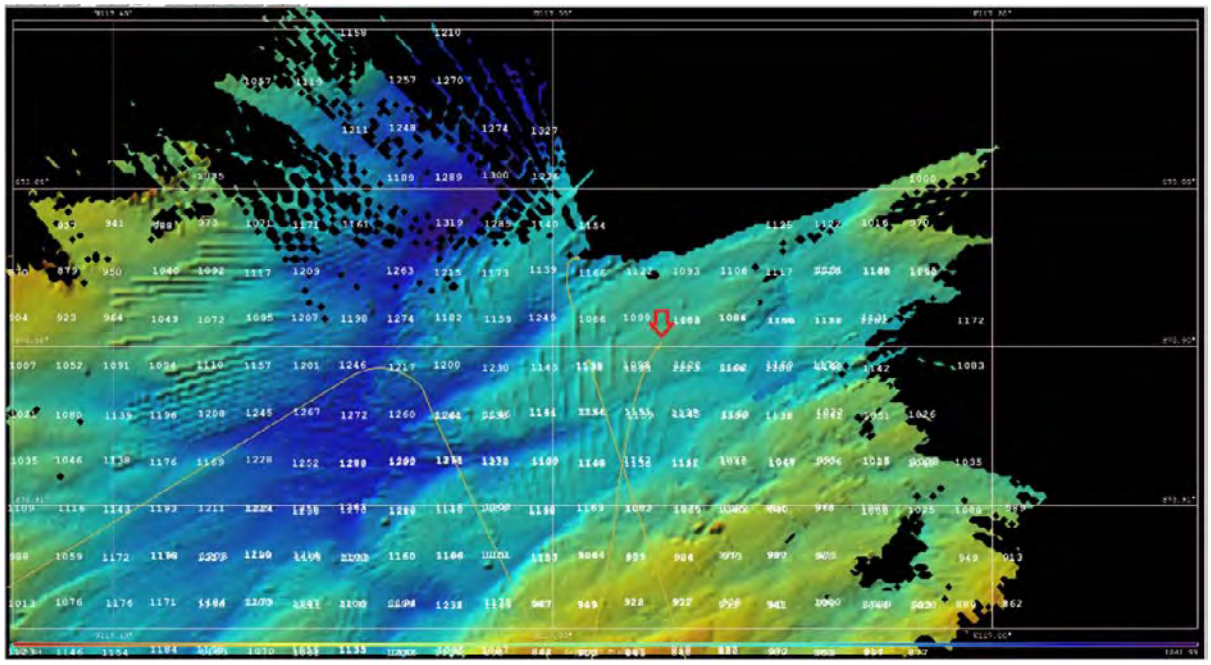

## Appendix 1.4. Triangulation results

AP4 01 mooring range K2

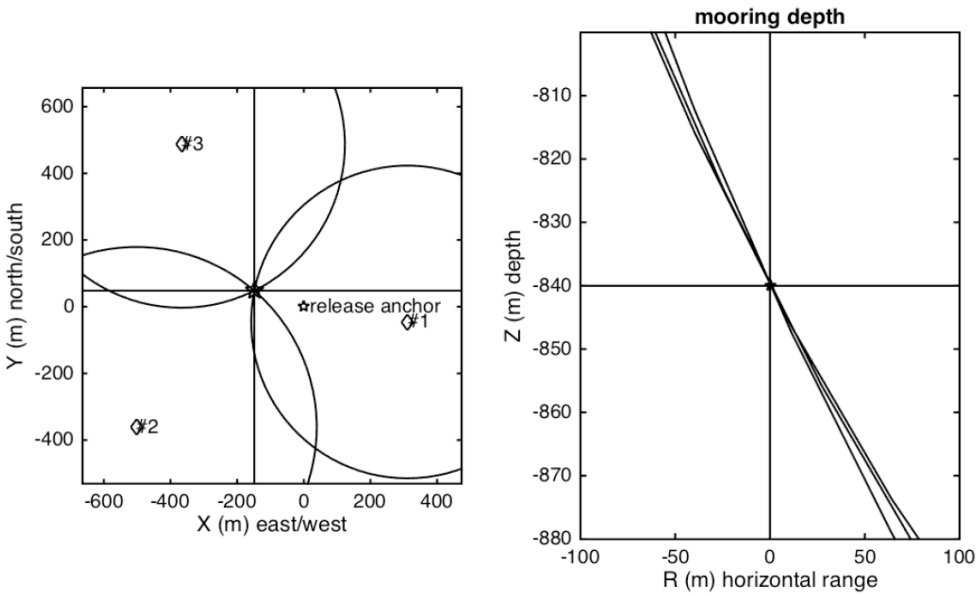


anchor release position: 73°S 16.802' 114°W 56.680'; depth: 831 m
3D mooring position: 73°S 16.776' 114°W 56.959'
drift: 156 m; direction: 288°
mooring depth: 840 m; slant error: 0 m
2D mooring position: 73°S 16.775' 114°W 56.956'
drift: 155 m; direction: 288°
horizontal error: 8 m
sound speed at site: 1445 m/s

#1 pos: 73°S 16.827' 114°W 56.097' range: 941 m range soundspeed 1500
#2 pos: 73°S 16.997' 114°W 57.622' range: 979 m range soundspeed 1500
#3 pos: 73°S 16.539' 114°W 57.368' range: 952 m range soundspeed 1500

AP4 02 mooring range K3

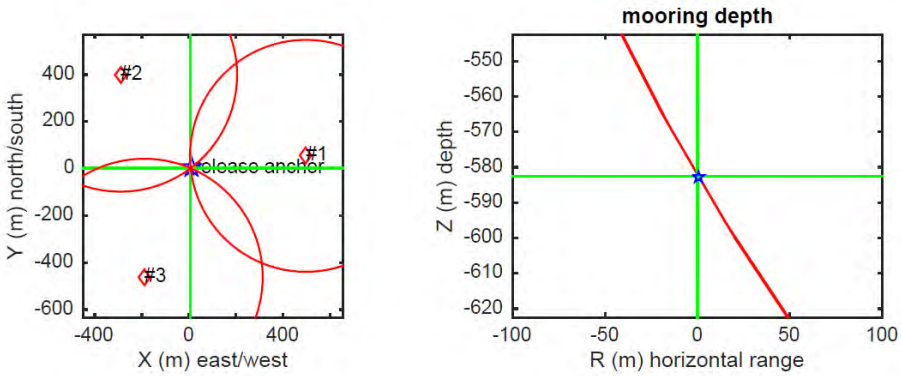


anchor release position: 73°S 42.681' 114°W 12.931'; depth: 593 m
3D mooring position: 73°S 42.680' 114°W 12.916'
drift: 8 m; direction: 78°
mooring depth: 583 m; slant error: 0 m
2D mooring position: 73°S 42.680' 114°W 12.916'
drift: 8 m; direction: 79°
horizontal error: 8 m
sound speed at site: 1445 m/s
#1 pos: 73°S 42.652' 114°W 11.971' range: 745 m range soundspeed 1500
#2 pos: 73°S 42.466' 114°W 13.492' range: 747 m range soundspeed 1500
#3 pos: 73°S 42.931' 114°W 13.296' range: 751 m range soundspeed 1500

AP4 03 mooring range K4

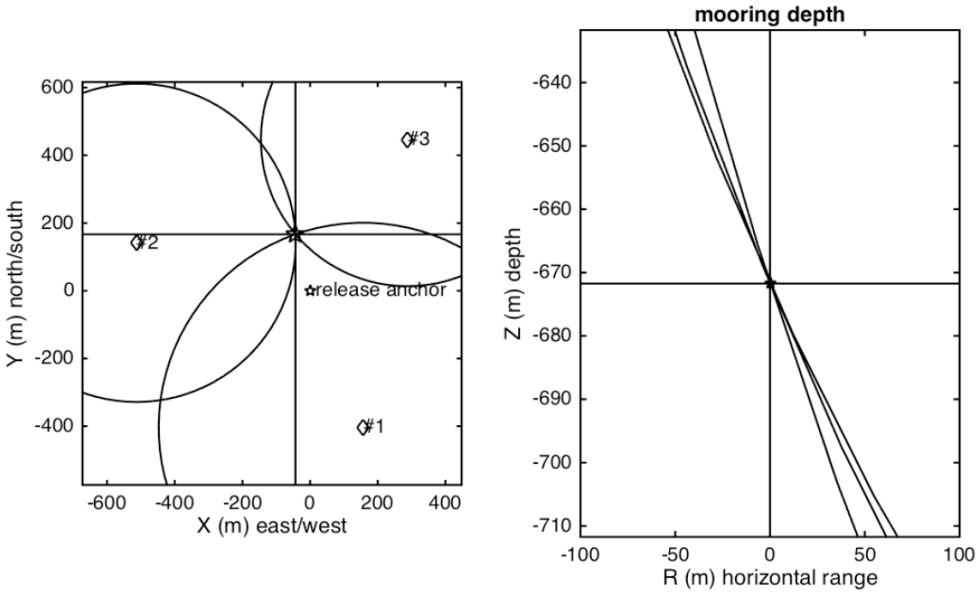


anchor release position: 73°S 53.412' 118°W 43.600'; depth: 688 m
3D mooring position: 73°S 53.322' 118°W 43.684'
drift: 172 m; direction: 345°
mooring depth: 672 m; slant error: 0 m
2D mooring position: 73°S 53.325' 118°W 43.681'
drift: 167 m; direction: 345°
horizontal error: 12 m
sound speed at site: 1445 m/s

#1 pos: 73°S 53.630' 118°W 43.295' range: 885 m range soundspeed 1500
#2 pos: 73°S 53.336' 118°W 44.598' range: 800 m range soundspeed 1500
#3 pos: 73°S 53.171' 118°W 43.040' range: 778 m range soundspeed 1500

AP4 04 mooring range K5

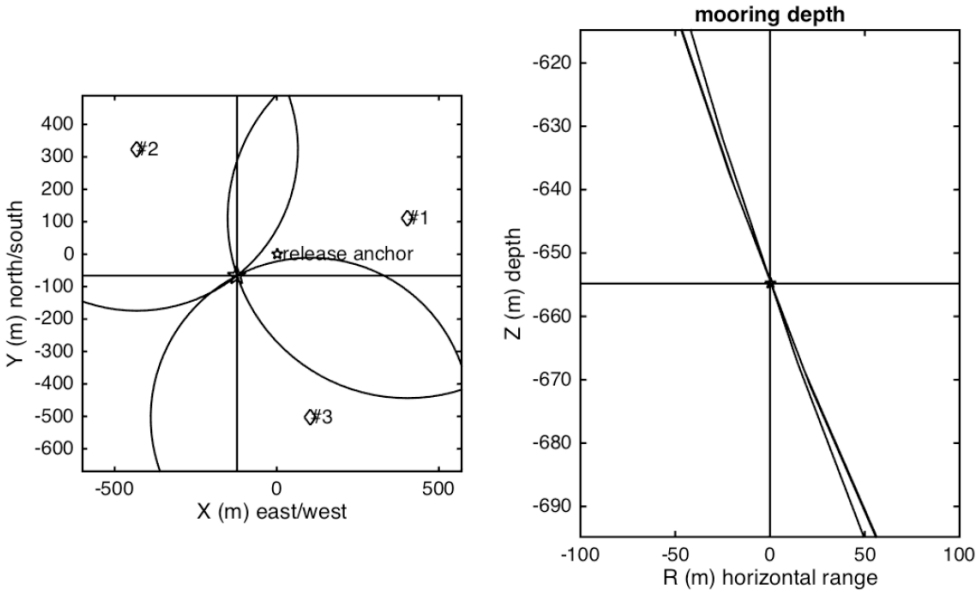


anchor release position: 73°S 56.230' 117°W 16.286'; depth: 658 m
3D mooring position: 73°S 56.266' 117°W 16.525'
drift: 139 m; direction: 242°
mooring depth: 655 m; slant error: 0 m
2D mooring position: 73°S 56.265' 117°W 16.520'
drift: 136 m; direction: 242°
horizontal error: 2 m
sound speed at site: 1445 m/s

#1 pos: 73°S 56.170' 117°W 15.499' range: 840 m range soundspeed 1500
#2 pos: 73°S 56.056' 117°W 17.129' range: 803 m range soundspeed 1500
#3 pos: 73°S 56.502' 117°W 16.083' range: 801 m range soundspeed 1500

AP4 05 mooring range K6

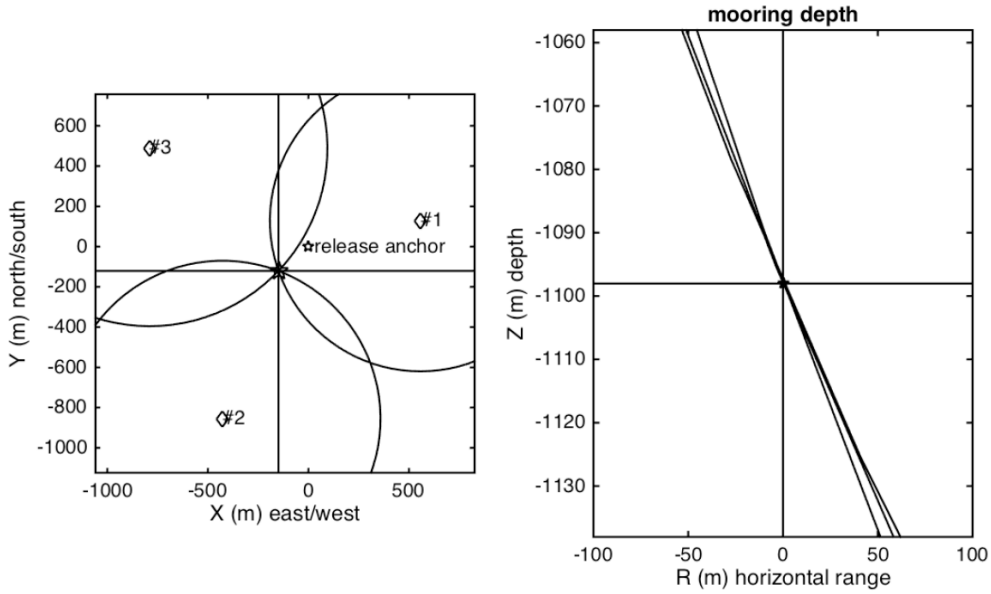


anchor release position: 73°S 53.925' 117°W 16.079'; depth: 1095 m
3D mooring position: 73°S 53.990' 117°W 16.369'
drift: 192 m; direction: 231°
mooring depth: 1098 m; slant error: 0 m
2D mooring position: 73°S 53.990' 117°W 16.368'
drift: 192 m; direction: 231°
horizontal error: 2 m
sound speed at site: 1445 m/s

#1 pos: 73°S 53.856' 117°W 14.995' range: 1309 m range soundspeed 1500
#2 pos: 73°S 54.387' 117°W 16.910' range: 1330 m range soundspeed 1500
#3 pos: 73°S 53.661' 117°W 17.616' range: 1391 m range soundspeed 1500

AP4 06 mooring range S1

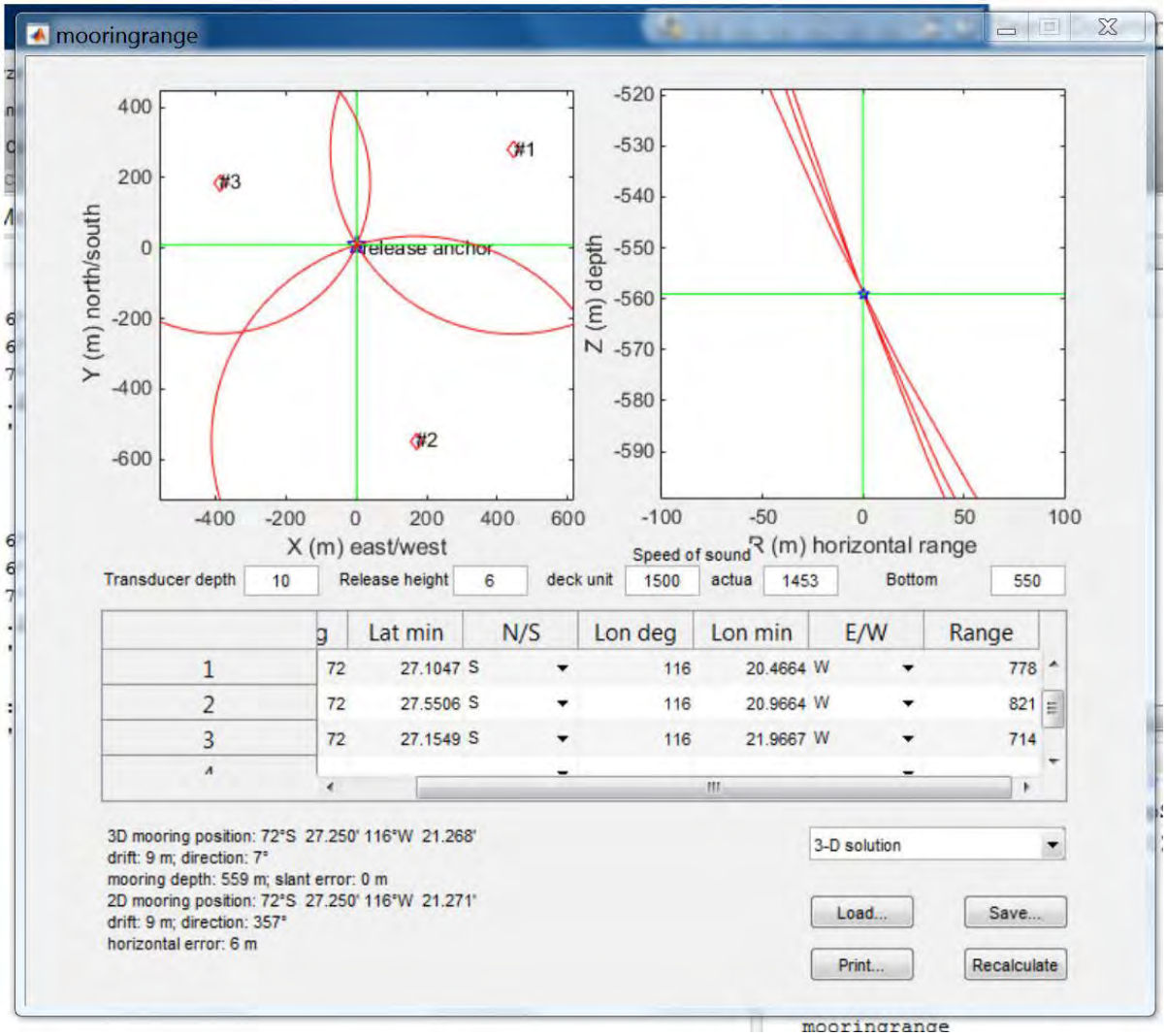

AP4 07 mooring range S5

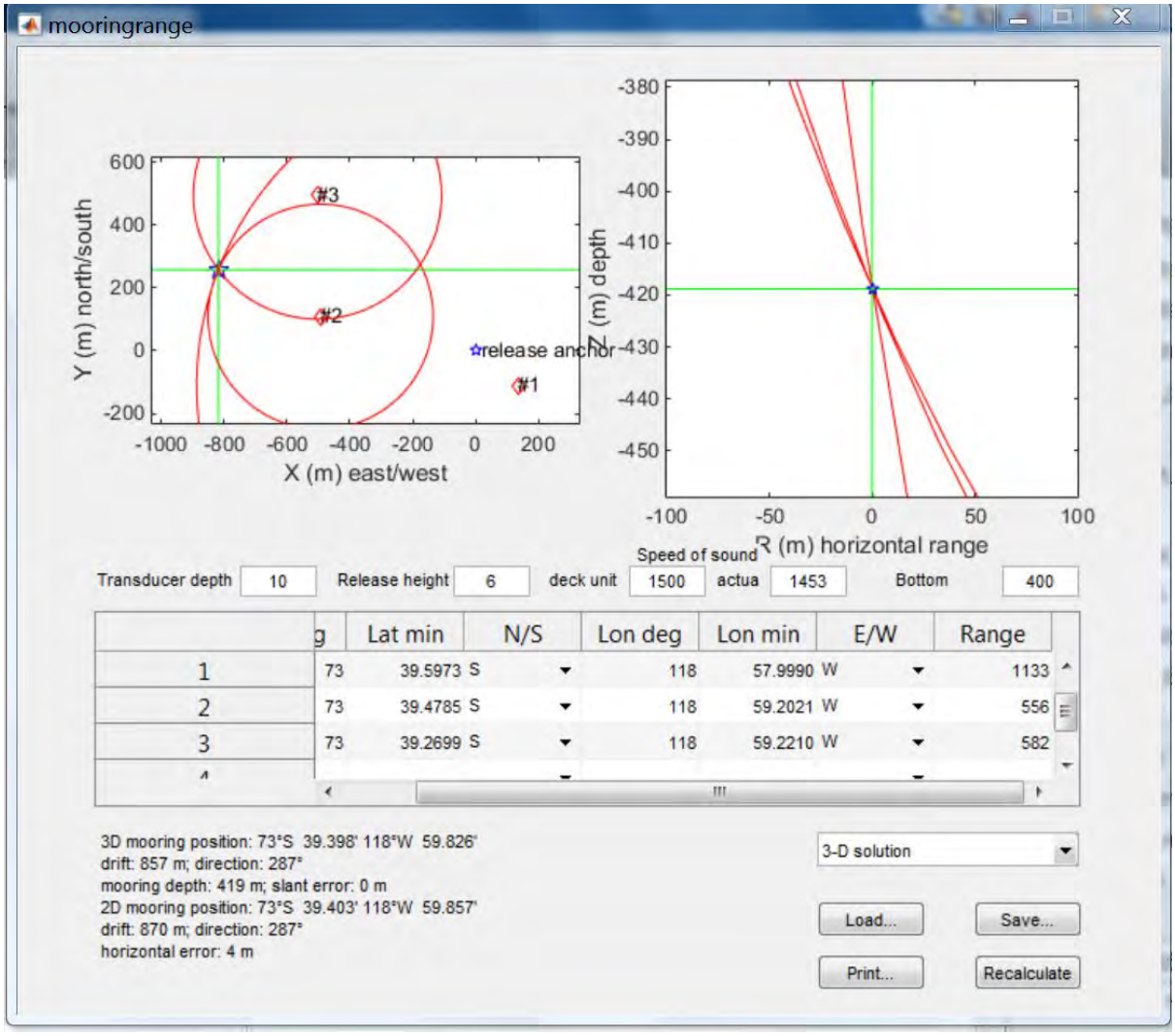

AP4 08 mooring range S6

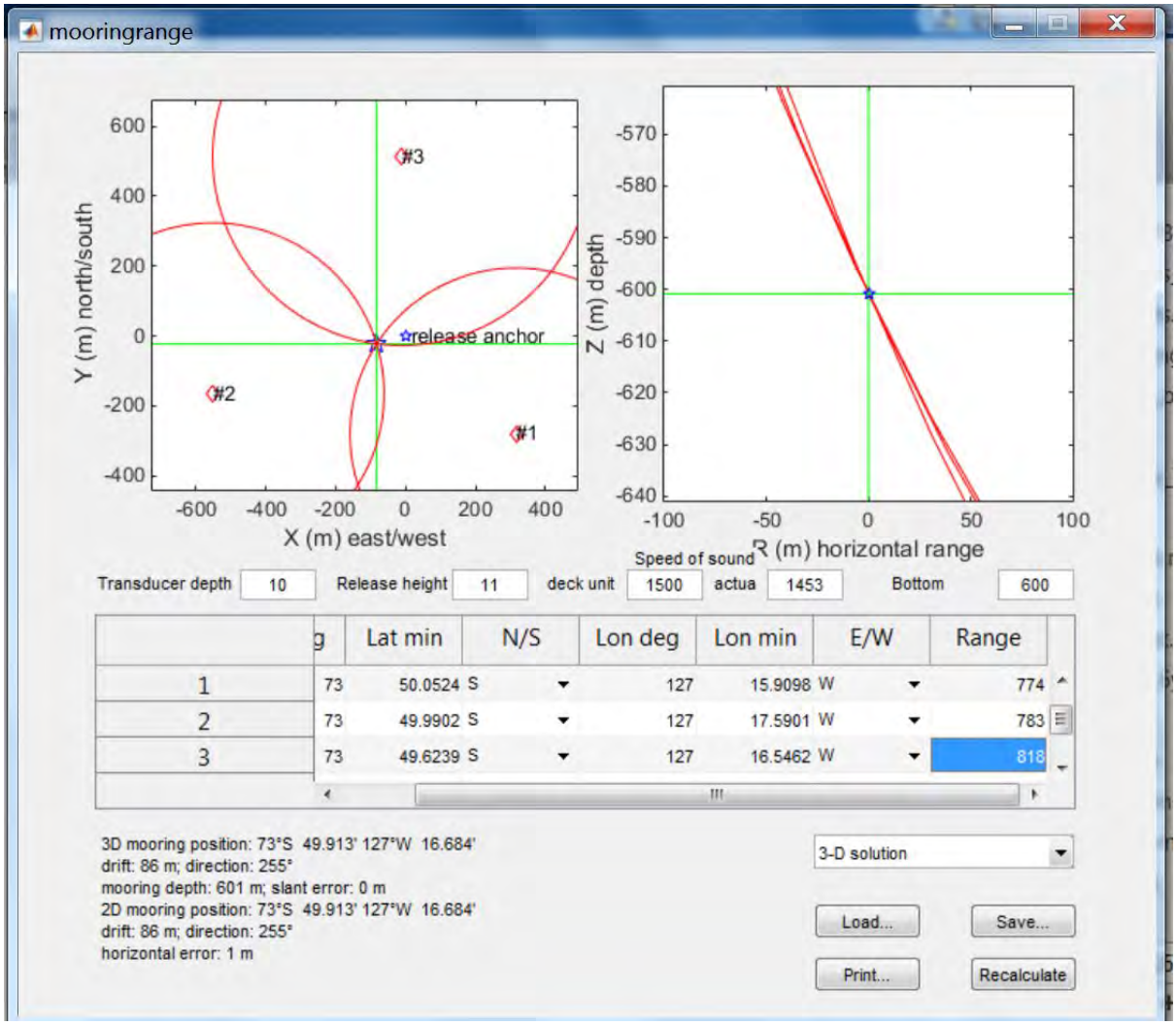

AP4 09 mooring range UiB1

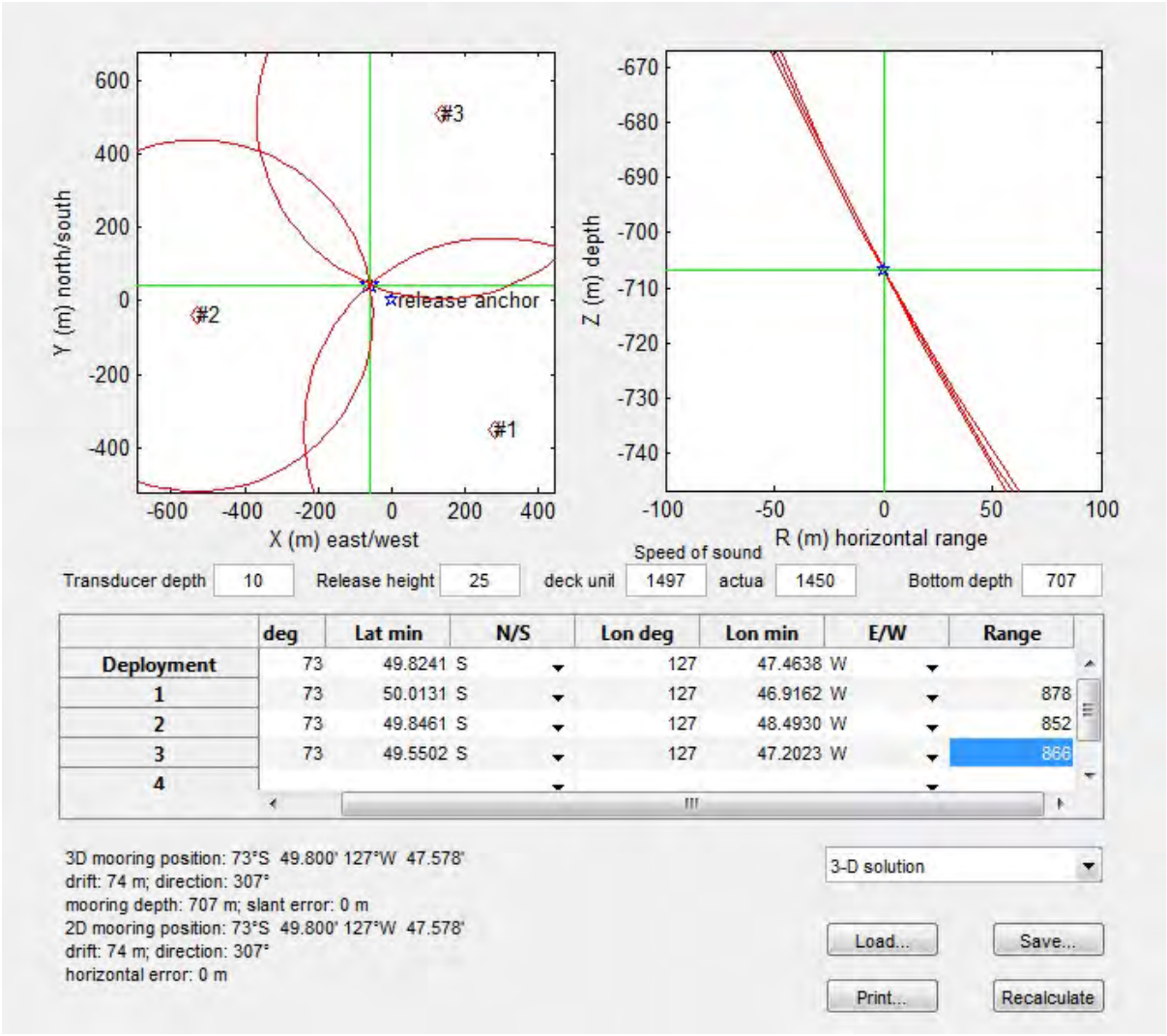

AP4 10 mooring range UiB2

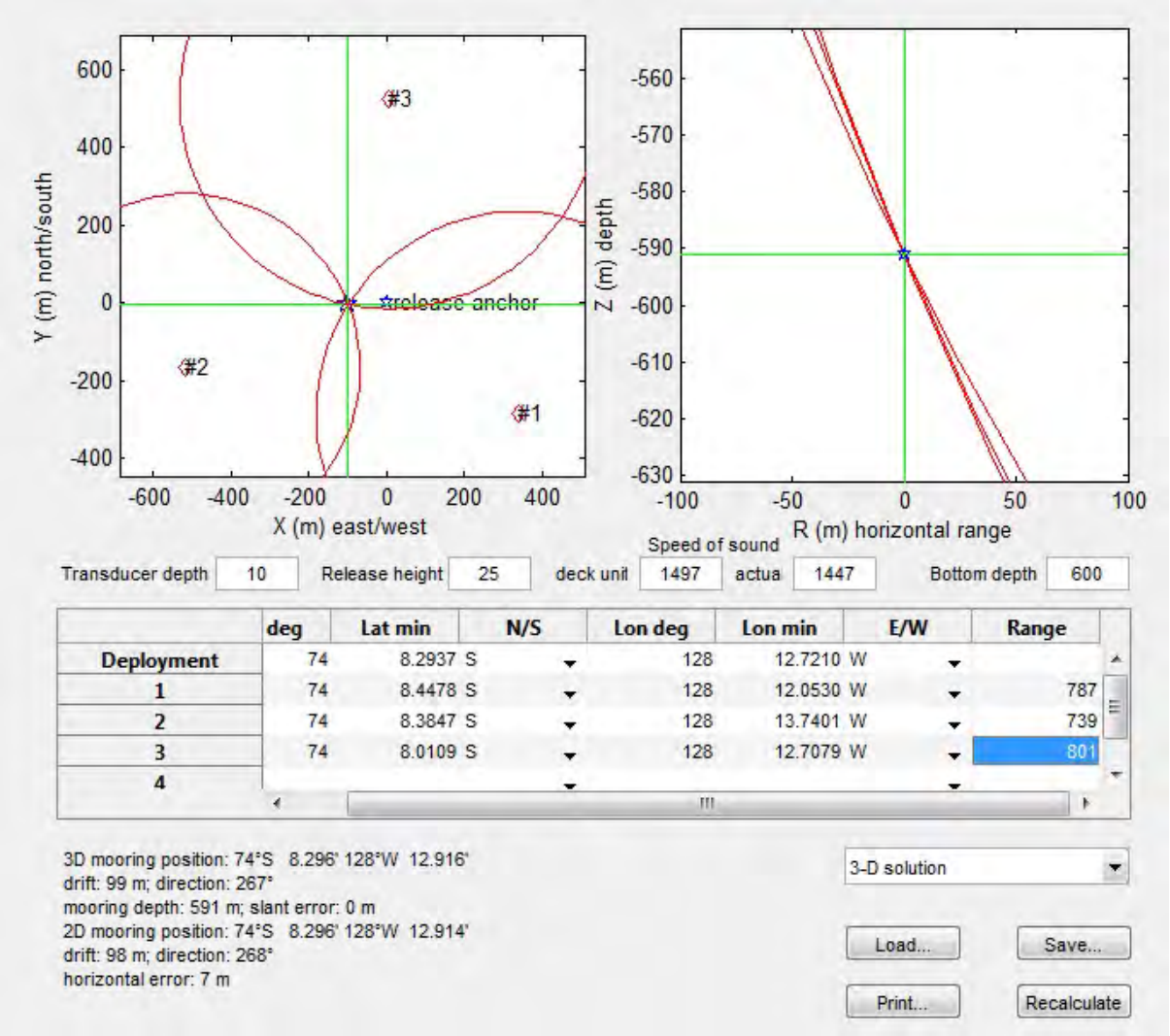

AP4 11 mooring range UiB3

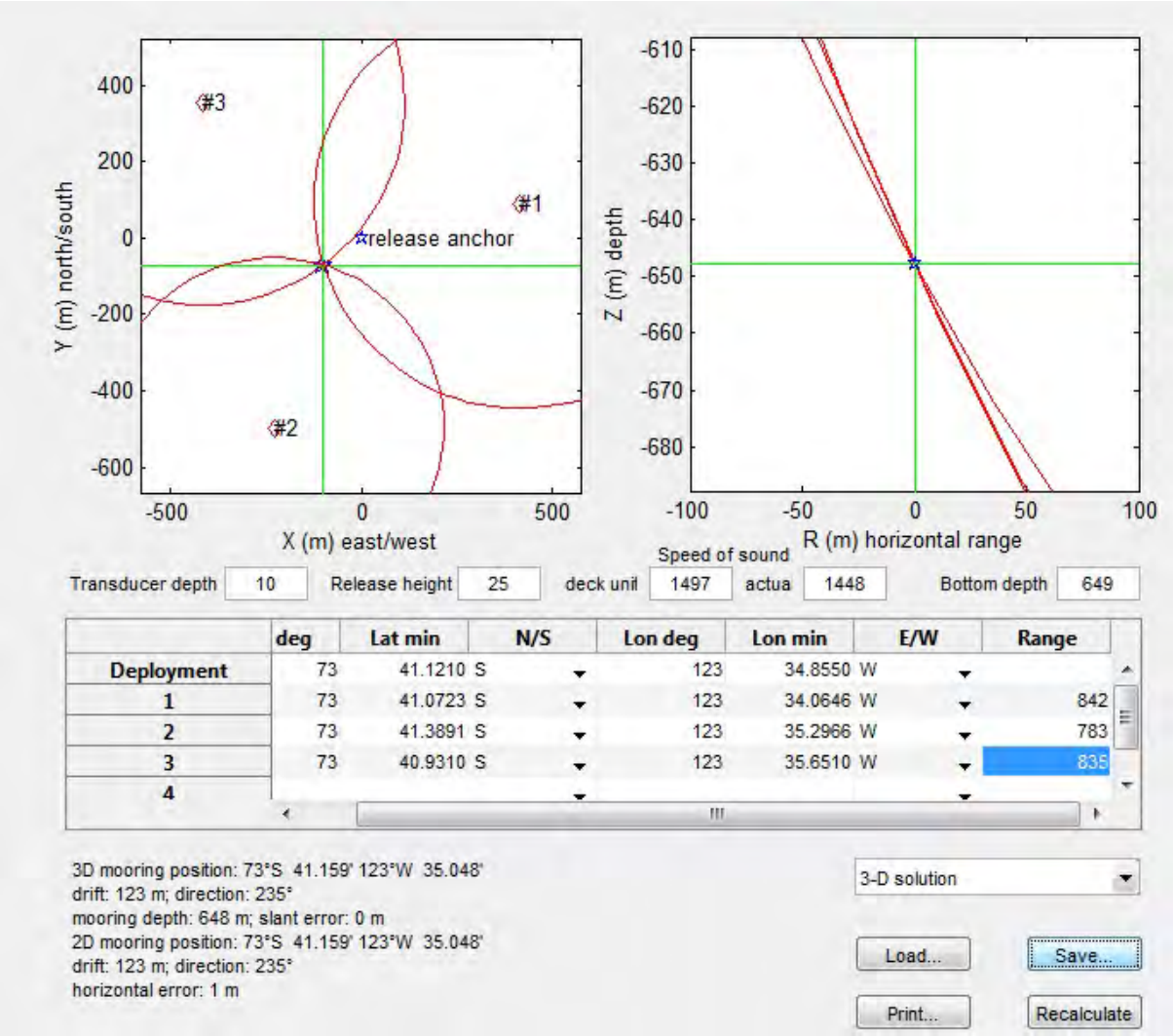

AP4 12 mooring range UiB4

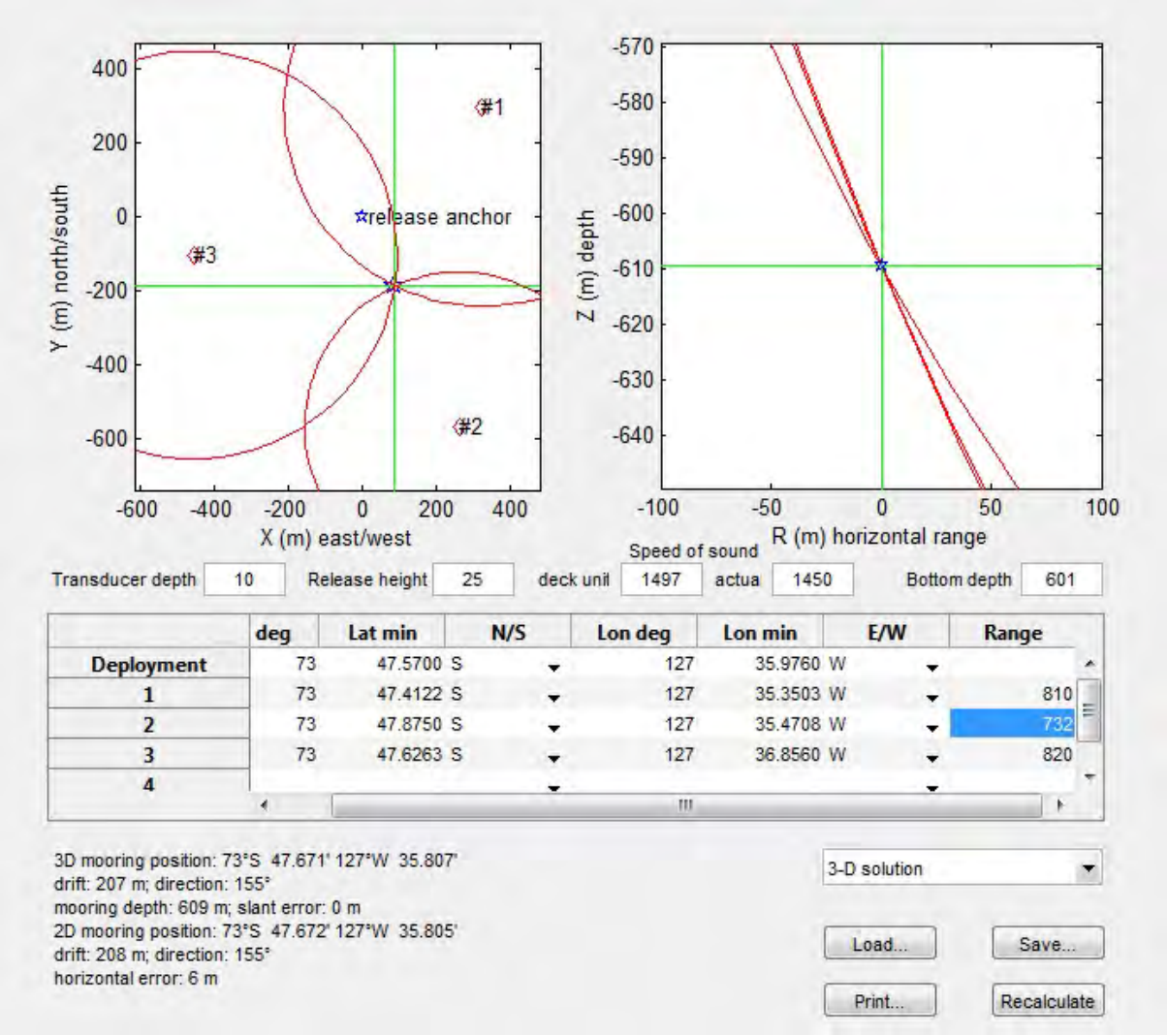

## Appendix 1.5. ADCP deployment files

AP5 01 ADCP Setup S6 150kHz

[BREAK Wakeup A]

WorkHorse Broadband ADCP Version 50.38
Teledyne RD Instruments (c) 1996-2010
All Rights Reserved.
>CR1
[Parameters set to FACTORY defaults]
>CF11101
>EA0
>EB0
>ED0
>ES35
>EX11111
>EZ1111101
>WA50
>WB1
>WD111100000
>WF352
>WN44
>WP25
>WS800
>WV175
>TE00:30:00.00
>TP01:12.00
>CK
[Parameters saved as USER defaults]
>The command CS is not allowed in this command file.  It has been ignored.
>The following commands are generated by this program:
>CF?
CF = 11101 ---------- Flow Ctrl (EnsCyc;PngCyc;Binry;Ser;Rec)
>CF11101
>RN 16S06
>cs

## AP5 02 ADCP Setup UiB1 75kHz

```
WorkHorse Broadband ADCP Version 50.40
Teledyne RD Instruments (c) 1996-2010
All Rights Reserved.
>CR1
[Parameters set to FACTORY defaults]
>CQ255
>CF11101
>EA0
>EB0
>ED3000
>ES35
>EX11111
>EZ1111101
>WA50
>WB0
>WD111100000
>WF704
>WN25
>WP15
>WS1600
>WV175
>TE02:00:00.00
>TP00:05.00
>TF16/01/27 00:00:00
>CK
[Parameters saved as USER defaults]
>The command CS is not allowed in this command file.  It has been ignored.
>The following commands are generated by this program:
>CF?
CF = 11101 ---------- Flow Ctrl (EnsCyc;PngCyc;Binry;Ser;Rec)
>CF11101
>RN 21396
>cs
```

## AP5 03 ADCP Setup UiB2 150kHz

SN 17226 has 2 battery packs

[BREAK Wakeup A]
WorkHorse Broadband ADCP Version 50.40
Teledyne RD Instruments (c) 1996-2010
All Rights Reserved.
>CR1
[Parameters set to FACTORY defaults]
>CF11101
>EA0
>EB0
>ED3000
>ES35
>EX11111
>EZ1111101
>WA50
>WB0
>WD111100000
>WF352
>WN26
>WP34
>WS800
>WV175
>TE01:00:00.00
>TP00:02.00
>TF16/01/27 00:00:00
>CK
[Parameters saved as USER defaults]
>The command CS is not allowed in this command file.  It has been ignored.
>The following commands are generated by this program:
>CF?
CF = 11101 ---------- Flow Ctrl (EnsCyc;PngCyc;Binry;Ser;Rec)
>CF11101
>RN 17226
>cs

AP5 04 ADCP Setup UiB2 300kHz

```
CR1
CF11111
EA0
EB0
ED4000
ES35
EX11111
EZ1111101
WA50
WB0
WD111100000
WF176
WN26
WP60
WS400
WV175
TE01:00:00.00
TF16/01/27 02:05:00
TP00:02.00
CK
CS
;
;Instrument         = Workhorse Monitor
;Frequency          = 307200
;Water Profile      = YES
;Bottom Track       = NO
;High Res. Modes    = NO
;High Rate Pinging  = NO
;Shallow Bottom Mode= NO
;Wave Gauge         = NO
;Lowered ADCP       = NO
;Ice Track          = NO
;Surface Track      = NO
;Beam angle         = 20
;Temperature        = -2.00
;Deployment hours   = 26400.00
;Battery packs      = 2
;Automatic TP       = NO
;Memory size [MB]   = 3900
;Saved Screen       = 2
;
;Consequences generated by PlanADCP version 2.06:
;First cell range   = 6.17 m
;Last cell range    = 106.17 m
;Max range          = 103.71 m
;Standard deviation = 0.46 cm/s
;Ensemble size      = 674 bytes
;Storage required   = 16.97 MB (17793600 bytes)
;Power usage        = 745.58 Wh
;Battery usage      = 1.7
;
; WARNINGS AND CAUTIONS:
; Advanced settings have been changed.
```

## AP5 05 ADCP Setup UiB3 300kHz

SN 17227 has 2 battery packs

```
[BREAK Wakeup A]
WorkHorse Broadband ADCP Version 50.40
Teledyne RD Instruments (c) 1996-2010
All Rights Reserved.
>CR1
[Parameters set to FACTORY defaults]
>CF11101
>EA0
>EB0
>ED3000
>ES35
>EX11111
>EZ1111101
>WA50
>WB0
>WD111100000
>WF352
>WN32
>WP32
>WS800
>WV175
>TE01:00:00.00
>TP00:02.00
>TF16/01/27 00:00:00
>CK
[Parameters saved as USER defaults]
>The command CS is not allowed in this command file.  It has been ignored.
>The following commands are generated by this program:
>CF?
CF = 11101 ---------- Flow Ctrl (EnsCyc;PngCyc;Binry;Ser;Rec)
>CF11101
>RN 17227
>cs
```

## AP5 06 ADCP Setup UiB4 150kHz

Sn 18595 has 4 battery packs

```
[BREAK Wakeup A]
WorkHorse Broadband ADCP Version 50.40
Teledyne RD Instruments (c) 1996-2010
All Rights Reserved.
>CR1
[Parameters set to FACTORY defaults]
>CF11101
>EA0
>EB0
>ED4000
>ES35
>EX11111
>EZ1111101
>WA50
>WB1
>WD111100000
>WF352
>WN34
>WP67
>WS800
>WV175
>TE01:00:00.00
>TP00:05.00
>TF16/01/27 00:00:00
>CK
[Parameters saved as USER defaults]
>The command CS is not allowed in this command file.  It has been ignored.
>The following commands are generated by this program:
>CF?
CF = 11101 ---------- Flow Ctrl (EnsCyc;PngCyc;Binry;Ser;Rec)
>CF11101
>RN 18595
>cs
```

# Chapter 2
# Chemical Oceanography

## 2.1 Nutrient measurements

Jinyoung Jung

Korea Polar Research Institute, Incheon 21990, South Korea

### 요약문

아문젠 폴리냐는 남극에서 생물생산력이 가장 높은 폴리냐로 알려져 있으며, 동시에 남극순환류 (Circumpolar Deep Water)의 유입으로 인해 빙붕이 빠르게 녹고 있는 지역이다. 급격한 환경변화를 겪고 있는 아문젠 폴리냐 내의 영양염 성분의 공간분포 및 생물종조성에 따른 질산염과 인산염의 소모율 변화를 조사하기 위해 아문젠해 탐사기간 동안 64개의 정점에서 영양염(아질산염+질산염, 인산염, 암모늄, 규산염)시료를 채취하여 선상에서 분석하였다. 영양염의 농도는 외양에서 높았고, 아문젠 폴리냐에서 급격히 감소하는 경향을 보여 폴리냐 내의 활발한 해양생물활동으로 인해 영양염의 소비가 증가하는 것을 알 수 있었으며, 암모늄의 농도 관측을 통해 아문젠해 폴리냐 내에서 유기물질의 분해가 활발히 일어나고 있음이 시사되었다.

### Introduction

The Amundsen Sea Polynya (ASP) is the most biologically productive polynya in Antarctica. At the same time, the ice-shelves of the Amundsen Sea are experiencing basal melt by intrusions of warm circumpolar deep water (CDW) onto the continental shelf down deep troughs. These features make the Amundsen Sea an ideal region to monitor the influence of environmental changes on marine biogeochemical cycles. To improve our understanding of roles of nutrients in biological processes such as variations of N/P ratio in water column and N and P uptake ratio by different phytoplankton species, we investigated spatial and temporal variations of nutrients ($PO_4^{3-}$, $NO_3^-$+$NO_2^-$, $NH_4^+$, and $SiO_2$) in seawater collected in the Amundsen Sea. The results for nutrients would be valuable for filling the data gap, and useful to understand biogeochemical cycles of C, N, and P as well as carbon sequestration by biological carbon pump in the Amundsen Sea.

### Methodology and preliminary results

Seawater sampling for nutrients was carried out at 64 stations (58 stations + 6 revisit stations) over the Amundsen Sea using a CTD/rosette sampler holding 24-10L Niskin bottles (OceanTest Equipment Inc., FL, USA) during Korea research Ice Breaker R/V Araon cruise (ANA06B, December 28, 2015–February 27, 2016) (Figure 2.1). Samples for nutrients were collected from the Niskin rosette into 50 ml conical tubes and immediately stored in a refrigerator at 4°C prior to chemical analyses. All nutrients samples were analyzed within 3 days. Concentrations of nutrients were measured using standard colorimetric methods adapted for use on a 4-channel continuous Auto-Analyzer (QuAAtro, Seal Analytical). The channel configurations and reagents were prepared according to the ‘QuAAtro

Applications'. Standard curves were run with each batch of samples using freshly prepared standards that spanned the range of concentrations in the samples. The $r^2$ values of all the standard curves were greater than or equal to 0.99. Surface $NO_2^-$+$NO_3^-$ and $PO_4^{3-}$ concentrations in the open ocean stations were higher than those observed in the polynya owing to low biological activity in these two stations. The surface $NO_2^-$+$NO_3^-$ and $PO_4^{3-}$ concentrations gradually decreased with increasing fluorescence, indicating that $NO_2^-$+$NO_3^-$ and $PO_4^{3-}$ were utilized by phytoplankton.

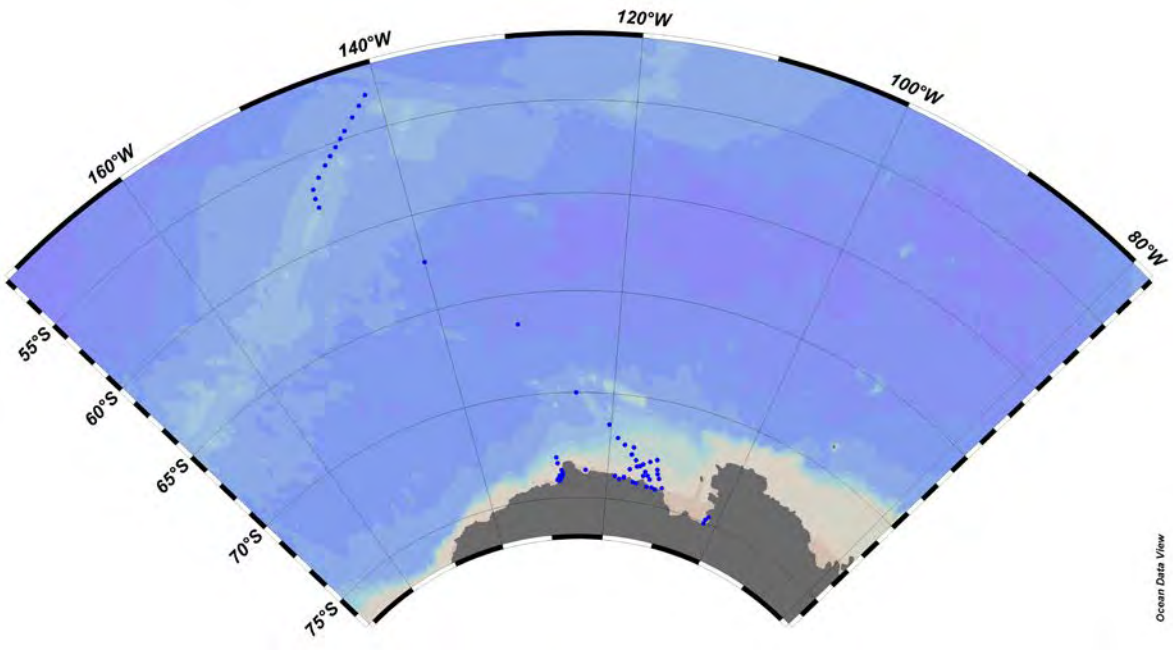


Figure 2.1. Map of study area. Blue dots show the CTD stations during the expedition.

## 2.2. Dissolved and particulate matters

Jinyoung Jung, and Sun Yong Ha

Korea Polar Research Institute, Incheon 21990, South Korea

### 요약문

유기물의 해양 심층으로의 저장은 해양생태계에서의 탄소균형을 조절하는 중요한 생지화학적 과정이다. 용존 및 입자상 유기탄소는 생물학적 펌프를 결정하는 주요 화합물임에도 불구하고, 아문젠 해역에서의 이들 화합물의 거동에 대한 이해는 아직 부족한 실정이다. 게다가 아문젠 해역에서의 주요 식물플랑크톤인 *Phaeocystis antarctica*와 *diatom*은 질산염과 인산염의 흡수율이 다르므로 식물플랑크톤의 종조성에 따른 탄소순환 및 격리 효율의 변화가 예상된다. 하지만 현재까지 아문젠해에서 입자상, 용존 유기물질들을 연구한 예는 극히 적은 실정으로 이번 아문젠해 탐사를 통하여 입자상, 용존 유기물질의 생지화학적 특성을 이해하고자 한다.

## Introduction

Export of organic matter is an important biogeochemical processes contributing to the carbon balance in marine ecosystem (Ducklow et al., 2015). In the ocean, export is defined as the transport, by sinking, advection or migration, of dissolved and particulate organic carbon (DOC and POC). Together the processes of export and its consumption in the upper 1000 m determine the amount of carbon ultimately stored in the deeper ocean, isolated from exchange with the atmosphere over time scales of centuries to millennia. The processes governing the export and the efficiency of its transfer to deep sea are poorly understood, especially in the Amundsen Sea, an important ocean carbon dioxide ($CO_2$) sink. In the Amundsen Sea, *Phaeocystis antarctica* and *diatom* are the dominant phytoplankton taxa. Because of the different N:P uptake ratios between these two taxa (Arrigo et al., 1999), potential shift in plankton community composition can influence the biological pump efficiency in the Amundsen Sea. Until now, few studies have been carried out to investigate the distribution and dynamics of dissolved and particulate organic matter in the Amundsen Sea. Our objective of this study therefore is to examine the biogeochemical characteristics of dissolved organic matter (DOM) and particulate organic matter (POM) and their C:N ratios during the expedition.

## Methodology

Seawater sampling for dissolved organic matter was carried out at 52 stations (46 stations + 6 revisit stations) over the Amundsen Sea using a CTD/rosette sampler holding 24-10L Niskin bottles. For dissolved organic matter measurements, a pre-cleaned (soaked in 10% HCl and rinsed with ultrapure water) Teflon tube was used to connect between spigot and pre-cleaned 47 mm filtration holder made of PP (PP-47, ADVANTEC) (Figure 2.2 (a)). About 200 ml of seawater was filtered through a pre-combusted (at 550°C for 6 hours) Whatman GF/F filter (47 mm in diameter) under gravity. The filtered samples were collected directly into pre-cleaned glass bottles. The filtrate was distributed into two pre-combusted 20 ml glass ampoules with a sterilized serological pipette. Each ampoule was sealed with a torch, quick-frozen, and preserved at approximately -24°C until the analysis in our land laboratory. Simultaneous dissolved organic carbon/total dissolved nitrogen analyses will be basically made with an HTCO system consisting of a commercial unit, the Shimadzu TOC-L system (Shimadzu Co.), fitted with a chemiluminescence (CLS) detector that was incorporated into the total nitrogen micro analyzer. The concentration of dissolved organic nitrogen (DON) will be obtained by the difference between total dissolved nitrogen and dissolved inorganic nitrogen (i.e., $NO_2^-$+$NO_3^-$ and $NH_4^+$) concentrations.

A 1 L of seawater for analysis of POC was drained from the Niskin bottles into a pre-cleaned amber polyethylene bottle, as was the particulate organic nitrogen (PON) sample. POC and PON samples were filtered with pre-combusted (at 550°C for 6 hours) GF/F filters (25 mm in diameter) using a nitrogen gas purging system under low (< 1.0 atm) pressure (Figure 2.2 (b)). The GF/F filters for POC and PON measurements were stored at -24°C in hinged-lid and airtight PP containers. Prior to analysis of POC sample, particulate inorganic carbon should be removed using acid. The filters for POC and PON measurements will be analyzed using a CHN analyzer in our land laboratory.

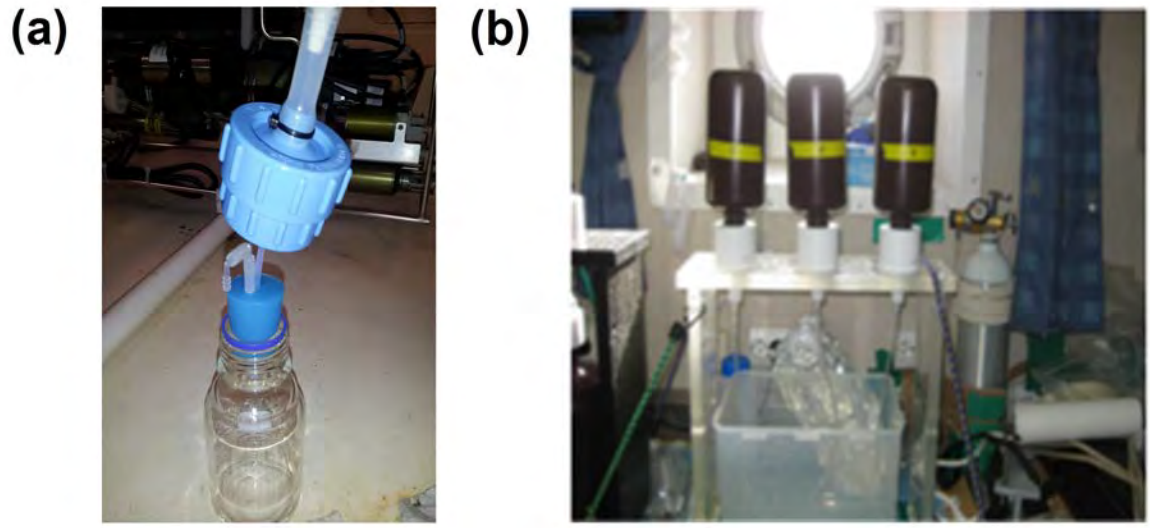


Figure 2.2. Instruments for sampling of dissolved (a) and particulate (b) organic matters.

## References

Arrigo, K.R., Robinson, D.H., Worthen, D.L., Dunbar, R.B., DiTullio, G.R., VanWoert, M., Lizzotte, M.P., (1999) Phytoplankton community structure and the drawdown of nutrients and $CO_2$ in the Southern Ocean. Science, 283, 365–367.

Ducklow, H.W., Wilson, S.E., Post, A.F., Stammerjohn, S.E., Erickson, M., Lee, S., Lowry, K.E., Sherrell, R.M., Yager, P.L., (2015) Particle flux on the continental shelf in the Amundsen Sea Polynya and Western Antarctic Peninsula. Elementa: Science of the Anthropocene, 3, 1–20.

# 2.3. Sulfur species in marine aerosols

Jinyoung Jung

Korea Polar Research Institute, Incheon 21990, South Korea

## 요약문

해양에서 가장 주요한 황화합물은 dimethylsulfide (DMS)이며, 이는 식물플랑크톤의 물질대사 작용에 의해 생성된다. 대부분의 DMS는 해양에서 박테이라에 의해 분해되지만 일부는 대기중으로 배출된다. 대기중으로 배출된 DMS는 산화되며 입자상 물질인 비해염성 황산염 (nss-$SO_4^{2-}$)과 메탄술폰산 (MSA)으로 존재하게 된다. 이들 황화합물은 구름의 응결핵으로 작용하여 구름을 형성, 태양복사광 균형에 영향을 미쳐 지구냉각 효과를 일으킨다고 알려져 있다. 아문젠 폴리냐는 남극에서 생물학적 생산이 가장 높고 인위적 오염발생원이 극히 적은 지역이므로 DMS기원의 비해염성 황산염과 메탄술폰산의 연구에 적합한 장소이다. 뿐만 아니라 지금까지 아문젠 해역에서 이들 황화합물에 대한 연구예는 전무한 실정이므로 이번 아문젠항해를 통해 황화합물의 생지화학적 순환을 이해하고자 한다.

## Introduction

The biogeochemical cycle of sulfur between the marine atmosphere and the ocean has received considerable attention in the last two decades due to its potential for climate regulation. Dimethylsulfide (DMS), the most dominant sulfur species throughout the ocean, is a metabolic byproduct of the production of dimethylsulfoniopropionate (DMSP), which is produced primarily by phytoplankton. Although most DMS is consumed by bacteria, sea surface layers are always supersaturated with it, which implies a net flux of DMS to the atmosphere. As a result, about 1% of the DMSP produced in seawater is transported to the atmosphere in the form of DMS through sea-to-air flux. Atmospheric non-sea-salt sulfate (nss-$SO_4^{2-}$) and methanesulfonic acid (MSA) derived from DMS oxidation could affect the Earth's radiation balance through the formation of cloud condensation nuclei and, thereby, exert a cooling effect by increasing planetary albedo (Quinn and Bates, 2011). Although considerable effort has been devoted to estimating the contribution of biogenic source through the investigation of spatial and temporal characteristics of nss-$SO_4^{2-}$ and MSA in aerosols collected over various regions and during different periods, no data has been reported for the Amundsen Sea. The results for sulfur compounds obtained from the expedition would be valuable for filling the data gap, and useful to understand biogeochemical cycles of sulfur in the Amundsen Sea.

## Methodology

Two high-volume (1000 LPM) air samplers (Sibata Co., Ltd.) were used to collect fine (D < 2.5 μm) and coarse (D > 2.5 μm) marine aerosols on a quartz filter (8X10 inch, Sibata), respectively. The aerosol samplers were put on the front of the compass deck of the ship (Figure 2.3). A wind-sector controller was used to avoid contamination from ship's exhaust during the cruise. The wind-sector controller was set to collect marine aerosol samples only when the relative wind directions were within plus or minus 100º relative to the ship's bow and the relative wind speeds were over 1 m $s^{-1}$ during the cruise. The total aerosol sampling intervals varied between 3–4 days. After sampling, the filter was stored frozen at –24°C prior to chemical analysis in our land laboratory. A total of 14 samples were collected during the cruises. In the land laboratory, aerosol samples will be ultrasonically extracted using 50 ml of Milli-Q water. The extraction solution was then filtered through a 13-mm diameter, 0.45-mm pore-size membrane filter (PTFE syringe filter, Millipore Co.). The filtrates were analyzed by ion chromatography (IC; Dionex-320, Thermo Scientific Dionex) for anions including $SO_4^{2-}$and MSA and for cations including $Na^+$. The concentrations of nss- $SO_4^{2-}$ were calculated as total $SO_4^{2-}$ minus the $Na^+$ concentration times 0.2516, the $SO_4^{2-}/Na^+$ mass ratio in bulk seawater.

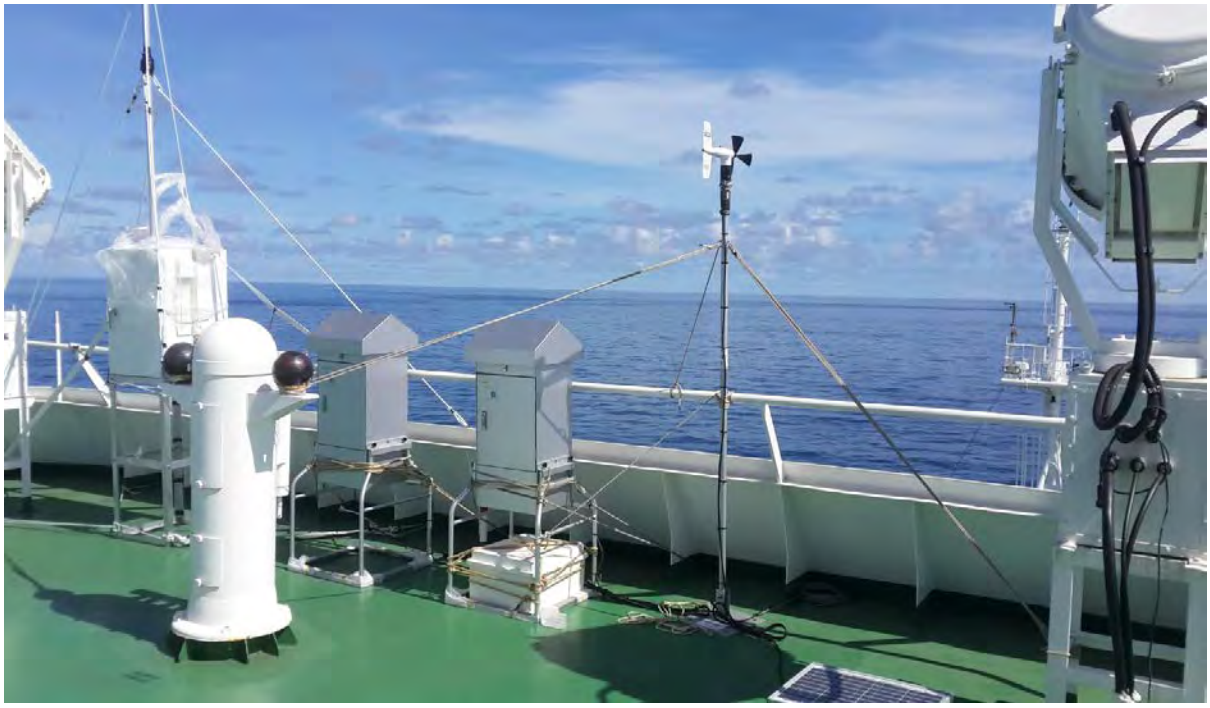

Figure 2.3. The high volume air samplers and the wind-sector controller set in the compass deck.

## References

Quinn, P.K., Bates, T.S., (2011) The case against climate regulation via oceanic phytoplankton sulfur emissions. Nature, 480, 51–56.

# 2.4 Dissolved oxygen determined by automated amperometric titrator

Jung-Ok Choi and Doshik Hahm
Korea Polar Research Institute, Korea

## 요약문

용존산소 농도는 해양의 일차 생산과 생물활동 연관 산화환원 반응에 직접적으로 연관될 뿐 아니라, 물리적인 수괴의 특성을 직접적으로 반영하기 때문에 전통적으로 해양에서 중요한 화학인자로 여겨져 왔다. 본 관측에서는 용존 산소 측정 기법 중 가장 널리 알려진 Winkler 적정법을 응용한 전류 측정기 (amperometer)를 이용하여 용존 산소 농도를 12개 정점에서 측정하였다. 반복 측정 결과 측정 오차는 중간값과 평균값이 각각 0.12%, 0.28%로 나타났으며, 이는 본 연구에서 적용한 방법을 통해 해수 중 용존산소의 매우 정밀한 측정이 가능함을 시사한다. 이 결과는 CTD에 장착된 용존 산소 센서(SBE-43) 자료와의 상호 비교 및 검정에 쓰일 예정이다.

## Introduction

Due to its central role in biological redox reactions and the availability of reliable sensors, dissolved oxygen is one of the most commonly measured chemical parameters in sea-going observations. In the cruise, along with the oxygen sensor (SBE–43) attached to the CTD-rosette system, we determined oxygen concentration by amperometric Winkler titration method (Langdon, 2010). The method involves applying a potential to electrodes placed in a solution and adding thiosulfate to react with $I_2$ to form $2I^-$. The gradual decrease of $I_2$ during the reaction results in the decrease of the current measured at the electrodes. The endpoint is determinded as the point at which the current does not decrease further. The bottle oxygen measurements will be used to check wether SBE–43 oxygen sensor shows any drift or malfunctioning.

## Work at sea

The water samples were taken in flared neck Pyrex bottles following the guidelines of WHP Reference Manual (Dickson, 1995) and kept the flared neck of the sample bottles topped with deionized water until analysis (<1 day) to prevent gas exchange with the ambient water. No bubble formation or sample degradation was observed during the storage. Bottle samples were measured in duplicate at the 12 CTD stations (Figure 2.4). The median and mean values of the measurement errors, based on duplicate measurements, were 0.12% and 0.28%, respectively. There was a linear correlation between the sensor and the bottle values with a mean difference of –11.3 +- 3.6 umol/kg (~ –0.26 +- 0.08 mL/L) (Figure 2.5). The mean difference is significantly larger than our measurement accuracy and it is advised that the sensor values should be corrected with the bottle measurements. Comparison between the sensor and bottle values further indicated that Niskin bottle 10 became leaky since Station 70 (remember the Baltic room event?) and water samples collected afterward from the bottle were contaminated by surface waters with high $O_2$.

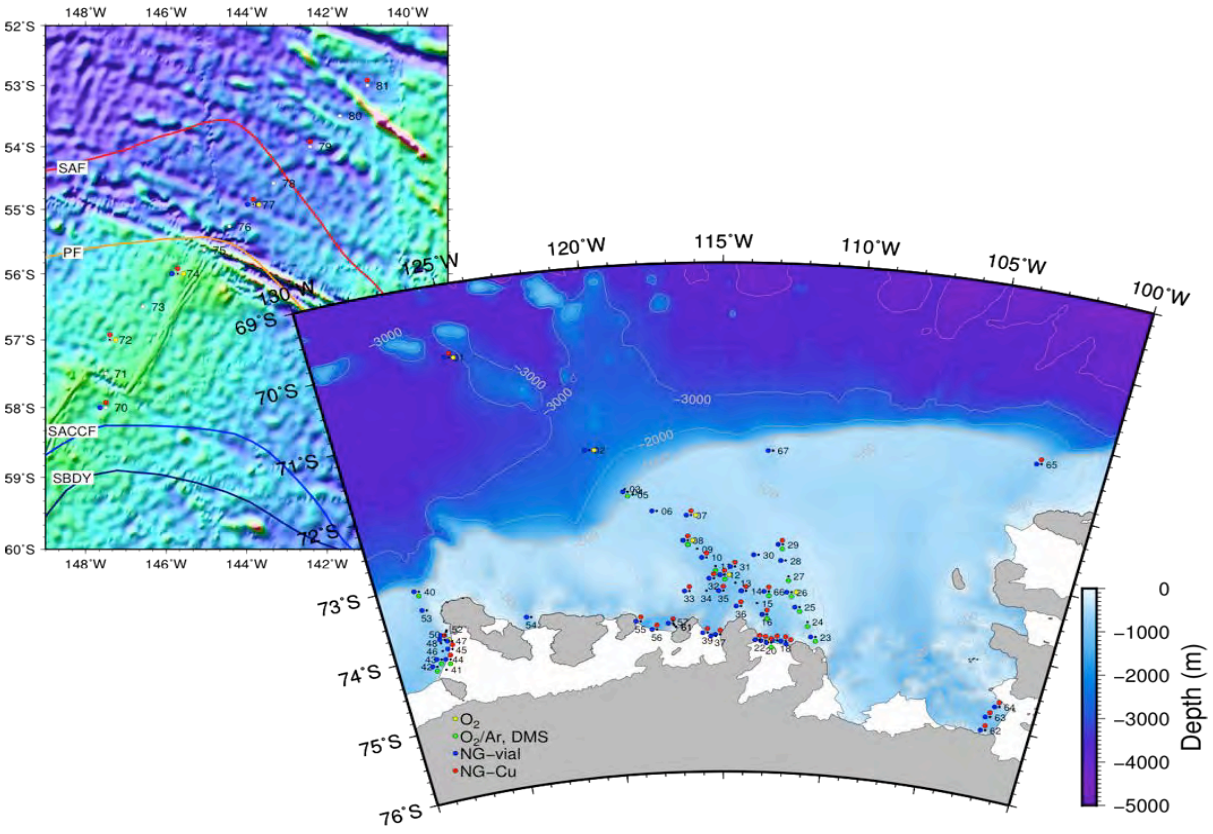


Figure 2.4. Stations where water samples of dissolved oxygen (yellow) were collected. Blue and red circles stand for the stations where water samples collected for on-board and onshore measurement of noble gases, respectively. Green circles show the locations where water samples for $O_2$/Ar and DMS measurement were collected. The left and right show the stations in the Udintsev Fracture Zone and Amundsen Sea.

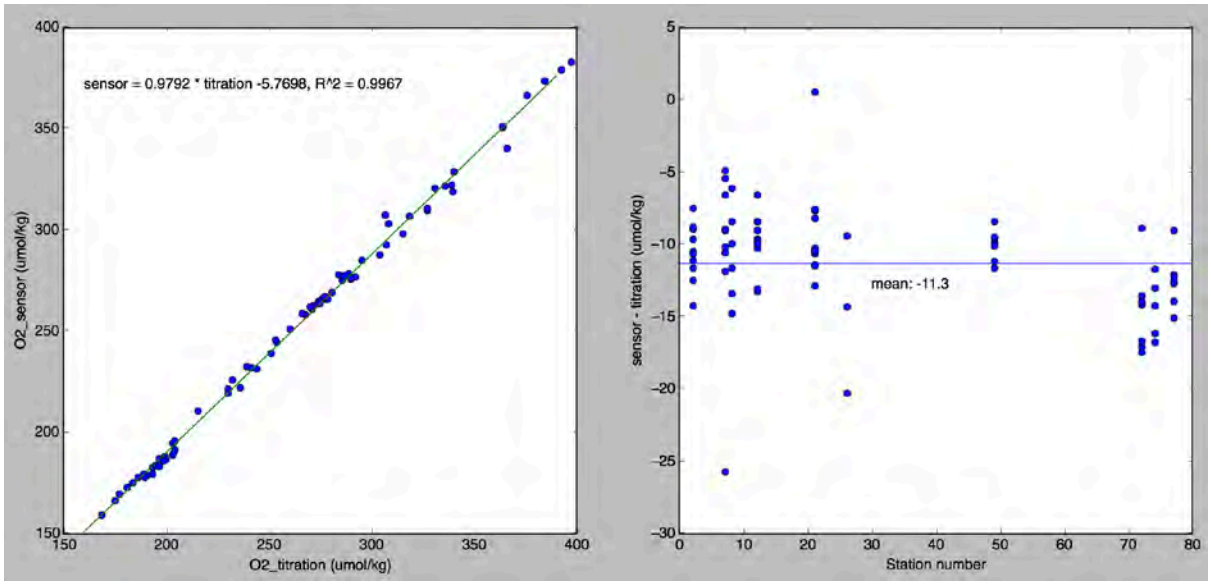


Figure 2.5. Correlation between the CTD sensor and the titration values (left). The mean difference between the sensor and bottle measurement values were –11.3 umol/kg (right).

## References

Dickson, A. G. (1995) Determination of dissolved oxygen in seawater by Winkler titration. WOCE Operations Manual. WHP Office Report WHPO 91–1, 1995.

Langdon, C. (2010) Determination of dissolved oxygen in seawater by Winkler titration using the amperometric technique. GO-SHIP Repeat Hydrography Manual. IOCCP Report No. 14, ICPO Publication Series No. 134.

# 2.5 Continuous $O_2$/Ar measurement as a proxy of net community production

Jung-Ok Choi, Intae Kim and Doshik Hahm
Korea Polar Research Institute, Korea

### 요약문

해양에서 순군집 생산량(Net community production, NCP)은 광합성을 통한 일차 생산과 호흡량의 차이로 정의된다. 본 연구에서는 표층에서의 순군집 생산량(산소 생산량)을 평형 주입식 질량분석기를 이용하여 이동 중에 측정하였다. 생물생산과 관련없이 수온, 기압, 물의 혼합 등으로 변동하는 산소양을 보정하기 위하여 생물화학적으로 안정한 불활성기체인 아르(Ar)을 함께 측정하였고, 산소/아르곤의 비 값을 이용하여 군집생산량을 계산하였다. 본 연구결과를 수온, 염분, 형광, 용존 산소 농도 등의 다양한 인자들과 함께 자료 해석을 함으로써, 아문젠 해 해양 일차 생산에 대하여 보다 자세히 알아 낼 수 있을 것으로 기대된다.

## Objectives

Net community production (NCP), defined as the difference between autotrophic photosynthesis and (autotrophic and heterotrophic) respiration, produces $O_2$ proportional to the amount of net carbon. By measuring chemically and biologically inert Ar together with $O_2$, it is possible to remove $O_2$ variation by physical processes (e.g., air temperature and pressure change and mixing of water masses) and deduce $O_2$ variation by biological processes (Craig and Hayward, 1987).
To determine the net community (oxygen) production underway, we adopted a continuous $O_2$/Ar measurement system developed by Cassar et al. (2009). The so called `equilibrator inlet mass spectrometer (EIMS)' is centered around a quadrupole mass spectrometer that measures dissolved gas molecules equilibrated with air in and supplied by an equilibrator. Water temperature, salinity, oxygen and fluorescence were also obtained to help the interpretation of temporal and spatial variation of $O_2$/Ar.

## Preliminary results

The preliminary results were summarized in Figure 2.6 and 2.7. The highest values of $\Delta O_2$/Ar ($=[(\Delta O_2/Ar)_{sample}/(\Delta O_2/Ar)_{air} - 1]*100$), reaching over 30%, were found eastern part of the Amundsen Sea Polynya (ASP). Similarly high values were also found along the coast of Siple Island (SI). It is

interesting to note that those two areas with high biological production exhibited contrasting environmental parameters. The high production area in ASP had high sea surface temperature and salinity, consistent with previous observations in 2011, 2012, and 2014 (Hahm et al., 2014); In contrast, the high production area along the coast of SI had significantly lower sea surface temperature and salinity than those in ASP area. This discrepancy might be explained by different bloom stages in the two areas. That is, the ASP area has been exposed to solar irradiation longer than the coast of SI and is in a mature bloom stage. The lower temperature and salinity in the coast of SI indicates a recent sea-ice melting, which is likely to provide a stable surface layer and higher photosynthetically available radiation to phytoplankton. Overall, the $\Delta O_2/Ar$ values within the polynya were in a range similar to those January of 2011 and 2014.

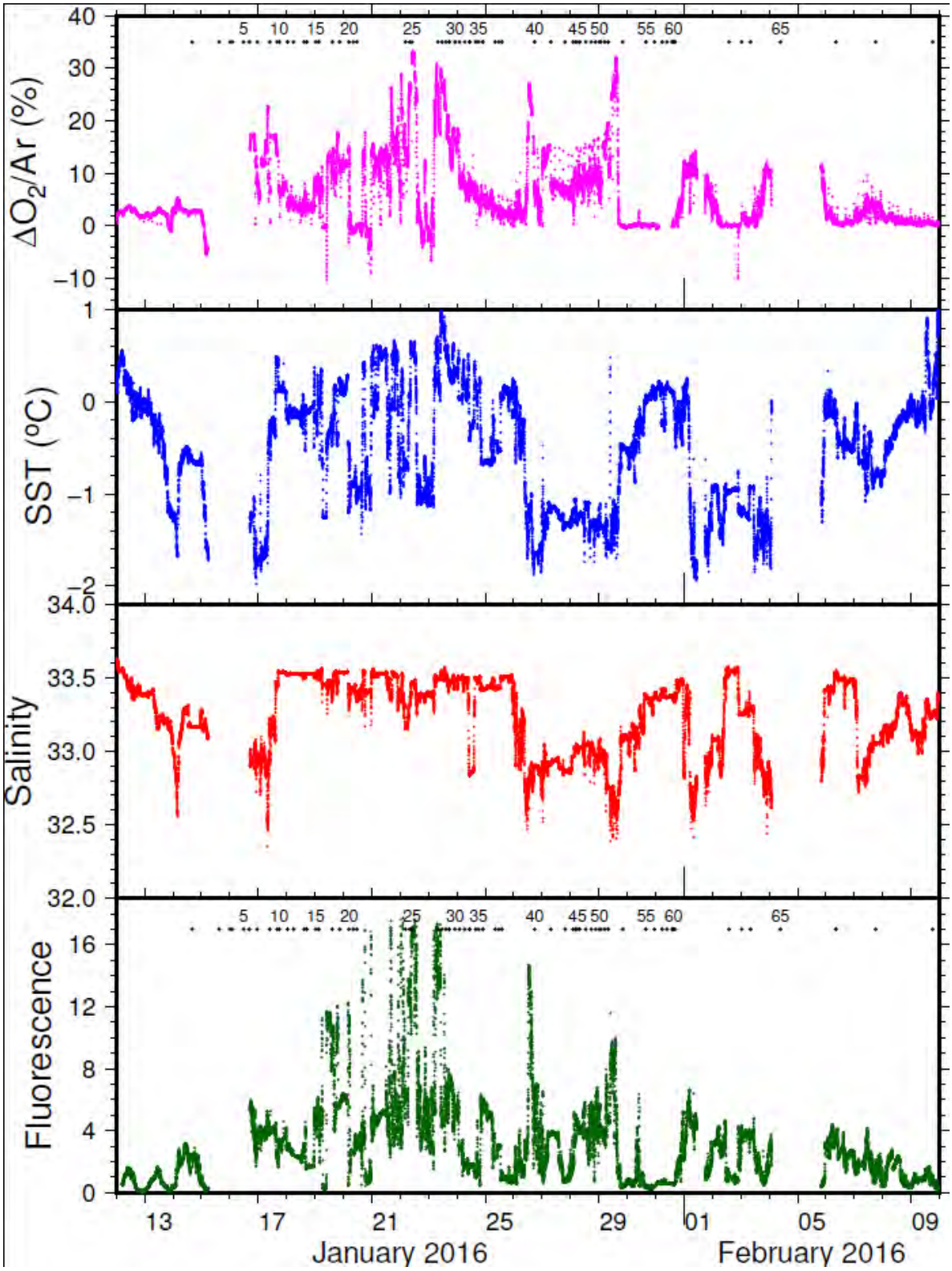


Figure 2.6. Time-series of the underway measurements of $\Delta O_2/Ar$, SST, SSS, and fluorescence. SST, SSS, and fluorescence have not been calibrated yet.

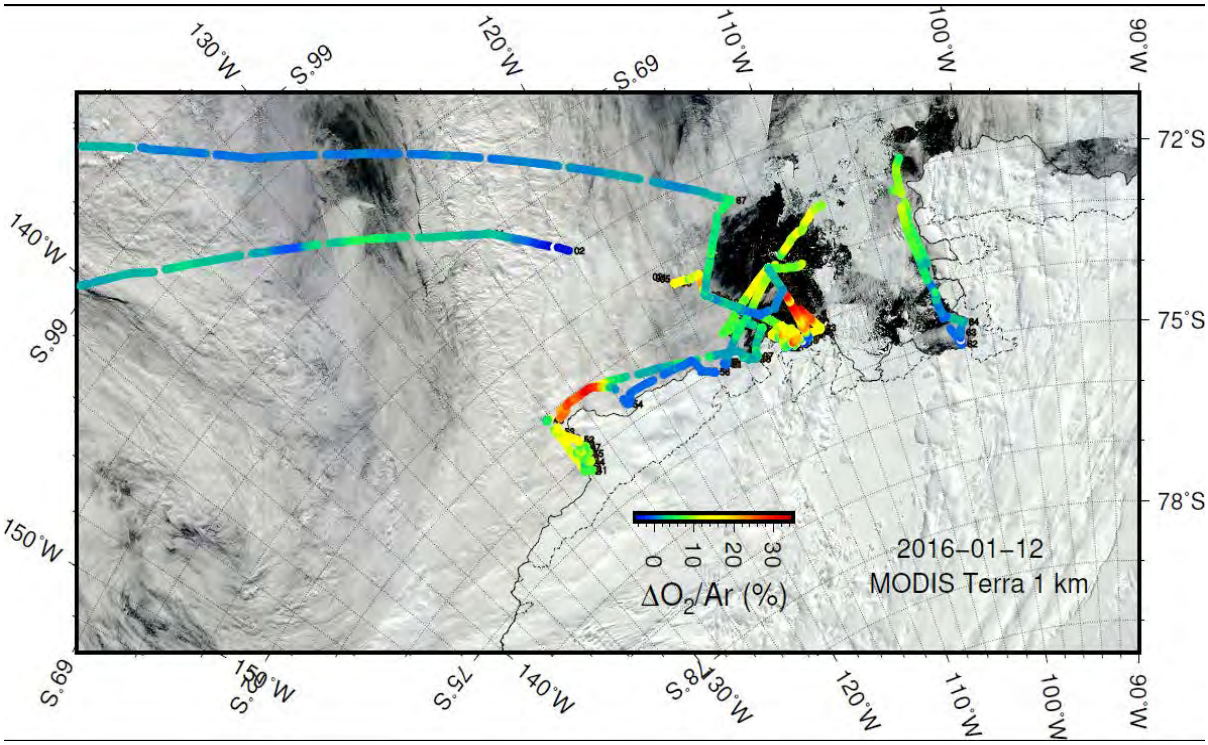


Figure 2.7. Spatial distribution of DO2/Ar in the Amundsen Sea superimposed on MODIS-Terra image on 12 February 2016.

## References

Cassar, N., Barnett, B. A., Bender, M. L. , Kaiser, J. , Hamme, R. C., Tilbrook, B. 2009. Continuous high-frequency dissolved O$_2$/Ar measurements by equilibrator inlet mass spectrometry. Analytical Chemistry, 81, 1855–1864.

Craig, H., Hayward, T., 1987. Oxygen supersaturation in the ocean: Biological versus physical contributions. Science 235, 199–202.

Hahm, D., T. S. Rhee, H.-C. Kim, J. Park, Y. N. Kim, H. C. Shin, and S. Lee (2014), Spatial and temporal variation of net community production and its regulating factors in the Amundsen Sea, Antarctica, Journal of Geophysical Research, 119(5), 2815–2826, doi:10.1002/2013JC009762.

# 2.6 Underway measurement of DMS using MIMS system

Jung-Ok Choi, Intae Kim, and Doshik Hahm

Korea Polar Research Institute, Korea

## 요약문

Dimethyl sulfide(DMS)는 구름의 응결핵으로 작용하는 물질로 기후변화 관련 인자로 잘 알려져 있으며, 남빙양은 전지구적인 DMS의 생산량의 62%를 공급하는 것으로 잘 알려져 있다.

아문젠해 폴리냐에서 여름철 *Phaeocystis*의 번성이 DMS생산에 직접적으로 연관되어 있다는 사전 연구 결과를 토대로, 본 연구에서는 표층에서 DMS의 분포를 연막 주입식 질량분석기를 이용하여 이동 중에 측정하고자 하였다. 측정된 DMS 농도는 공간적으로 큰 차이를 보이고 있었으며, 이러한 분포는 의 시공간적 변동성이 산소/아르곤 비값으로 계산된 신군집생산량과 엽록소 농도와 좋은 상관관계를 보이는 것으로 나타났다.

## Introduction

It is known that the Southern Ocean is responsible for ~62% of the global DMS flux (Lana et al, 2011), which is often ascribed to recurring bloom of efficient DMS producer - *Phaeocystis*. Given the fact that the large primary production in the Amundsen Sea Polynya (ASP) is supported by enormous bloom of *Phaeocystis* in austral summer, the ASP, along with other coastal polynyas around the Antarctica, is likely to be a hot spot of DMS flux. In order to investigate the spatial and temporal variations of DMS in the surface waters of the ASP and the its proposed correlation with net community production (NCP), we observed the horizontal and vertical (upper 100 m) distriubtions of DMS and $\Delta O_2/Ar$, a proxy of NCP, in the ASP using a membrane inlet mass spectrometer (MIMS; Tortell, 2005).

## Preliminary results

As we shared the MIMS for the measurements of DMS and noble gases, our DMS measurements was made only during the time when the instrument was not being used for noble gas measurements. In this report we present, as an example, the measurements made from noon of February 4 to midnight of February 7 (Figure 2.8 and 2.9). The DMS concentrations during the period showed a strong spatial variability (35 +- 27 nM) and some of them were as high as 100 nM. It was also noted that the vertical distributions of DMS largely resembled those of chl-a fluorescence measured with a sensor on CTD package.

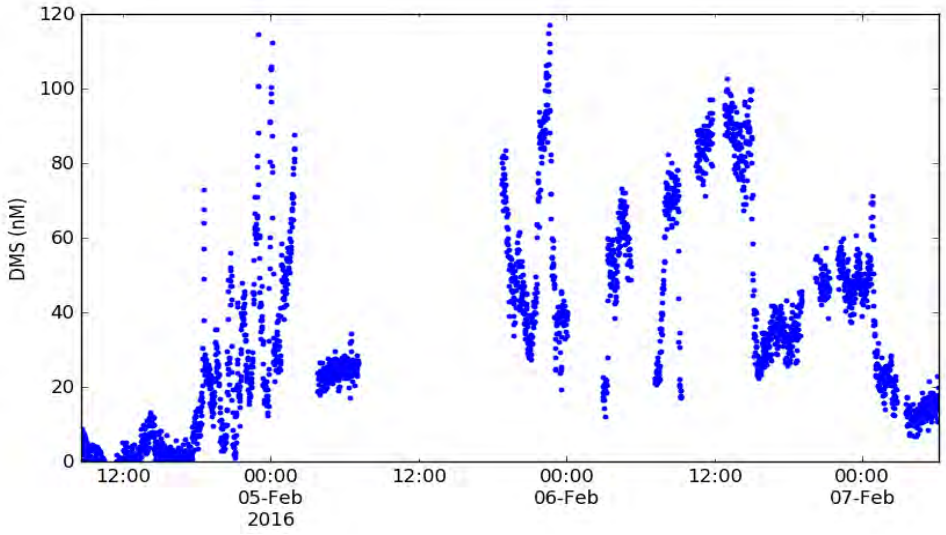


Figure 2.8. DMS concentrations in surface waters from noon of February 4 to midnight of

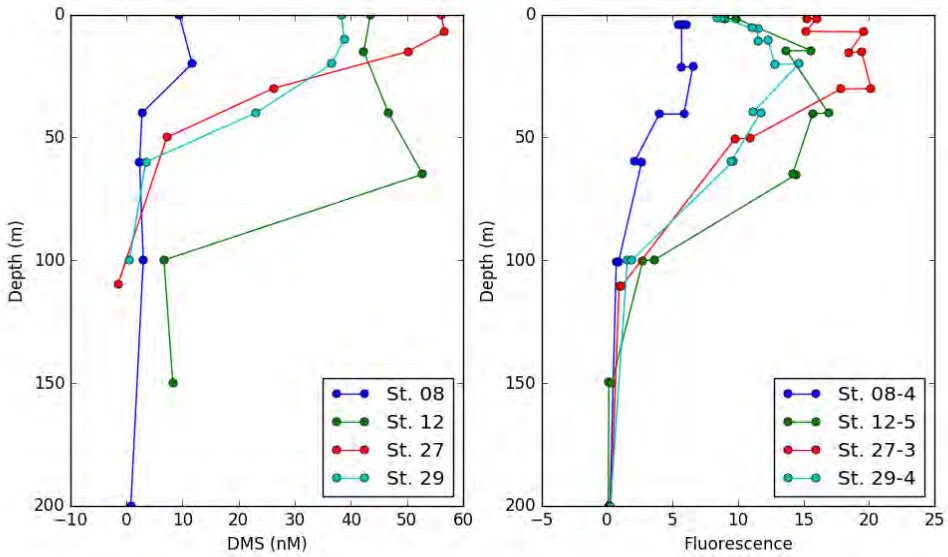


Figure 2.9. Example vertical profiles of DMS (left) and fluorescence (right).

## References

Lana, A. et al. (2011), An updated climatology of surface dimethlysulfide concentrations and emission fluxes in the global ocean, Global Biogeochemical Cycles, 25(1), doi:10.1029/2010GB003850.

Tortell, P. D. (2005), Dissolved gas measurements in oceanic waters made by membrane inlet mass spectrometry, Limnology and Oceanography - Methods, 3, 24–37.

# 2.7 Water sampling for the measurement of noble gases

Intae Kim and Doshik Hahm

Korea Polar Research Institute, Korea

## 요약문

헬륨(He)을 포함한 불활성 기체들은 해수 중 매우 안정한 거동을 보이며, 이를 이용하여 해양에서 매우 유용한 물리/생물학적 현상을 밝히는 추적자로 이용되어왔다. 또 하나의 예로, 얼음/물 간의 고유의 분배계수를 통해 이는 해수 중 빙하 또는 해빙의 분포를 알아내는 추적자로 이용 될 수 있다. 본 연구에서는 빙하가 가장 빨리 녹는 것으로 알려진 서남극해 아문젠해에서, 해수 중 빙하 용융수의 분포를 알아내기 위하여 해수 중 불활성 기체를 측정하고자 시료를 채취하였다. 38개 정점에서 (아문젠 대륙붕의 가로, 세로 단면을 포함한)기체 손실 방지를 위해 해수를 구리관에 담아 밀봉, 보관하였으며 이 시료들은 차후 측정을 위해 보관될 예정이다.

## Objectives

The noble gases, especially helium isotopes ($^3$He and $^4$He) in conjunction with tritium ($^3$H), have been widely used to trace water mass movement due to their conservative behavior in the environment and to give time constraints (i.e., $^3$H–$^3$He age) on physical and biological processes in the ocean. Another interesting application is to detect ice-related processes using their different partitioning behavior in water, sea-ice and glacier (e.g., Hohmann et al. 2002; Kim et al., 2016). The hydrography of the Amundsen Sea is in substantial change due to rapid loss of glacier ice sheet and sea ice, occurring around the west Antarctica. Given the high resolving power of noble gases for ice-related processes, they will provide invaluable information on the influence of glacier and sea ice loss of this area on the changes of its hydrography and, in turn, biological processes.

## Work at sea

Water samples for noble gases were collected at 38 stations, including 6 in the Udintsev Fracture Zone, among the 81 CTD stations covered in the cruise (Figure 2.4). The sampling locations were selected to constitute sections of (1) along the Amundsen Trough, (2) across the trough, (3) along the ice shelves of Pine Island, Dotson, and Getz (the station with red circles in Figure 1).

## References

Hohmann, R., Schlosser, P., Jacobs, S., Ludin, A., Weppernig, R., 2002. Excess helium and neon in the southeast Pacific: Tracers for glacial meltwater. Journal of Geophysical Research-Oceans, 107, doi:10.1029/2000JC000378.

Kim, I., D. Hahm, T.S. Rhee, T.W. Kim, C.S. Kim and S.H. Lee (in press), The distribution of glacial meltwater in the Amundsen Sea, Antarctica, revealed by dissolved helium and neon, J. Geophys. Res. Oceans.

# 2.8 On-board measurements of noble gases using a membrane inlet mass spectrometer

Intae Kim, Jung-Ok Choi, and Doshik Hahm
Korea Polar Research Institute, Korea

## 요약문

일반적으로 남극 빙하 후퇴 연구는 인공위성 기반 원격탐사 관측에 의존하여 이루어졌으나, 이 방법은 주로 표면 관측에 집중할 뿐 해양 내부에서 해수 중 빙하 용융수가 어떻게 분포하는지에 대한 정보를 주지 못한다. 최근 해수 중 불활성 기체(헬륨과 네온)을 추적자로 이용하여 아문젠해 빙하 용융수의 분포를 알아내는 연구 결과가 발표되었으나, 불활성기체의 측정 방법이 매우 까다로운 탓에 이 방법이 넓은 연구 지역에서 활용되기엔 어려움이 있었다. 따라서 본 관측에서는 연막 주입식 질량분석기를 응용해 자체 제작한 전처리 라인을 부착하여 해수 중 불활성 기체를 현장에서의 실시간 측정을 전세계적으로 처음으로 시도하였다. 총 56개

정점에서 모든 깊이에서 5개의 불활성 기체들을 측정하였다. 예비결과에 의하면 측정 기기는 좋은 선형성을 보였으며, 현재 자료 검증과 자료 처리, 자료 해석 중에 있다.

## Background & Research Goal

Remote sensing approaches based on satellite observations have been widely conducted to investigate the retreat of Antarctic ice sheets. However, most of the satellite-based studies have following limitations; i) they cannot capture the short-term variability of basal melting rate due to the relatively lower temporal resolutions from several years to decades, and ii) they cannot give an insights to pathways or distributions of glacial meltwater (GMW) in the water columns.

Recently, Kim et al. (2016) presented the distributions of GMW in the water column of Amundsen Sea revealed by light noble gas tracers, helium (He) and neon (Ne). The study shows that there were significant spatio-temporal variations between each ice shelves and (inter-annual) sampling periods. However, the conventional method to determine noble gases is dependent on shore-based mass spectrometric system and very time-consuming processes. The main objective of our study is i) to make on-board measurements of 5 noble gases ($^{4}$He, $^{22}$Ne, $^{38}$Ar, $^{84}$Kr, and $^{132,136}$Xe) in seawater, for the first time, ii) to get a broader understandings of meltwater distribution in the Amundsen Sea. The detailed method and onboard works were presented in the following sections.

## Analytical Methods and Water Sampling

Recently, Visser et al. (2013) developed a quicker and more efficient noble gas analysis for laboratory experiments using a semi permeable membrane. This, so-called noble gas membrane inlet mass spectrometer (NG-MIMS) system has a simplified version of traditional gas extraction lines. The noble gas extraction line used in this study consists of a membrane inlet, water vapor trap immersed into MeOH, cooled in a deep freezer (~ –65 $^{o}$C), carbon-dioxide trap (Carbosorb), 400$^{o}$C of hot getter (Zr-alloy), and 250 $^{o}$C of Sorb AC. Two syringe pumps were used to deliver samples and a set of calibration standards to the membrane (Figure 2.10). The high vacuum of the extraction line (~$10^{-7}$ torr) allows the dissolved trace gases to pass through the membrane from the water samples.

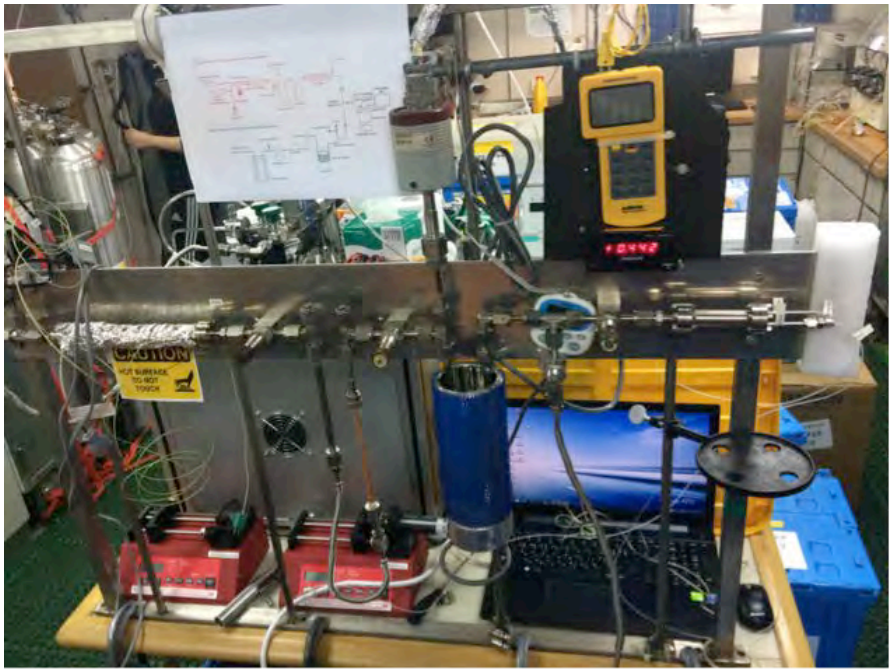

Figure 2.10. The on-board noble gases extraction line used in this study.

Water samples for noble gase measurements were collected at 56 stations, including those in the UFZ (Figure 1). The sampling activities were concentrated on the stations close to Dotson- and Getz ice shelves (DIS and GIS) and DT. The samples were collected in glass vials and stored in refrigerator until analyses. Most of the samples were measured within 40 hrs after sampling to minimize degassing of light noble gases from the sample bottles. At 38 stations we also collected water samples in Cu-tubes (Figure 1, red circles). The Cu-tube samples will be used to make precise measurements of noble gases and He isotopic ratios at the laboratory and compare them with the on-board measurements using MIMS.

## Preliminary results

Data processing of the measured samples is stil in its early stage. In this report we only present an example measurement that was carried out to test the linearity of the NG-MIMS system. We prepared a range of binary mixtures of air equilibrated seawater (AEW) and degassed (boiled) water by changing the flow rate of the syringe pump which was used to inject degassed water into the sample stream. The AEW was prepared by gently bubbling ambient air through seawater kept in a water bath at 2 $^{o}$C. The 2 end-members (degassed water and AEW) and their mixtures showed good linearity (n=7 trials) with $R^2$ value of 0.97 – 0.99 for $^{4}$He, $^{38}$Ar, and $^{84}$Kr (Figure 2.11). $^{22}$Ne and $^{132}$Xe values are excluded in this stage due to $CO_2$ interference and low intensities, respectively. These elements will be re-calibrated in the data handling stages.

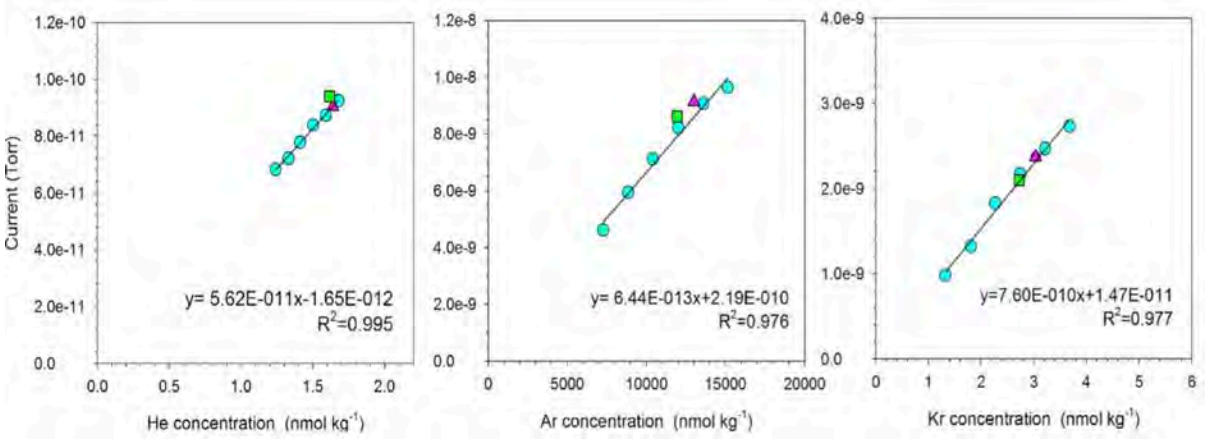


Figure 2.11. Results of linearity test of He, Ar, and Kr. To check the validity of this method, we also analyzed two AEW samples with different temperatures (Red triangle and green square symbols).

## Remarks and Implications

The shipboard GMW observations using noble gases in this study have advantages not only i) to capture short-term variability of basal melting rate but also ii) to offer insights into GMW pathways in water columns. Our group has collected the samples from 2011 to 2016 during 4 cruises. For now, therefore, we can present the short-term (i.e., inter-annual) variations of GMW in recent 5 years. This will enhance the understanding of GMW variations over short temporal and spatial scales together with other isotope studies such as 18O.

Previously, only He and Ne have been used to trace the GMW. However, recently, Loose and Jenkins (2014) suggested that the uses of all 5 noble gases to trace the origins of GMW in the polar oceans based on optimum mutiparameter analysis (OMP). The NG-MIMS system has also advantage to apply these approaches of GMW study because it can measure the 5 noble gases at the same time. With settlements and further improvements of NG-MIMS system (although it is proto-type at present) used in this work, we can observe GMW distributions with a larger spatial coverage of polar oceans in future.

## Reference

Kim, I., D. Hahm, T.S. Rhee, T.W. Kim, C.S. Kim and S.H. Lee (in press), The distribution of glacial meltwater in the Amundsen Sea, Antarctica, revealed by dissolved helium and neon, J. Geophys. Res. Oceans.

Visser, A. et al. (2013), A membrane inlet mass spectrometry system for noble gases at natural abundances in gas and water samples, Rapid Commun. Mass Spectrom. 2013, 27, 2472–2482, DOI: 10.1002/rcm.6704.

Loose, B., and W. J. Jenkins (2014), The five stable noble gases are sensitive unambiguous tracers of glacial melt- water, Geophys. Res. Lett., 41, doi:10.1002/2013GL058804.

# 2.9 Inorganic Carbon System and Dissolved Trace Gases

Rhee, Tae Siek and Hur, Nakwon

Korea Polar Research Institute, Korea

## 요약문

아문젠해 무기탄소 시스템을 분석하였다. 총용존무기탄소 (Dissolved Inorganic Carbon; DIC), 총알칼리도 (Total Alkalinity; TA), 용존이산화탄소 ($pCO_2$) 농도를 86개 정점의 수층에서 채수한 700여개 시료에서 분석하였다. DIC는 인산을 이용하여 모두 이산화탄소로 산화시킨 후 이들 이산화탄소를 적정하는 쿨로메트릭 방법을 이용하였으며 TA는 알고 있는 농도의 염산을 해수에 적정하여 적정점을 찾아 농도를 계산하였다. 용존 이산화탄소는 니켈 촉매를 이용하여 메탄으로 환원시킨후 FID로 분석하는 가스크로마토그래프를 이용하였다. 이들 자료를 이용하여 아문젠해 폴리냐와 해빙역, 외양을 중심으로한 무탄소 시스템의 차이를 알아보고자 한다. 표층 CO2 농도를 항해기간동안 연속 관측하였다. 아문젠 연안에서 100 ppb 에 이르는 매우 낮은 용존 CO2 농도가 관측되었으며 전반적으로 불포화 상태였으며 외해에서는 포화또는 과포화 상태였다.

## Objectives

The Amundsen Sea is renowned for rapid melting of Pine Island Glacier (Rignot et al., 2008). The Upper Circumpolar Deep Water (UCDW) upwelled to the continental shelf drives melting of the glaciers, which will influence ecosystem in the Amundsen Sea with changing carbon storage compartments. To understand the impact of glacier melt to the carbon flux in the water column of the Amundsen Sea, we investigated inorganic carbon system in the polynyas of Dotson, Getz, and Pine Island Glaciers, sea-ice zone, and the offshore. In addition, we had opportunity taking seawater samples in the Undintsev Fracture Zone of the Southern Ocean. As the hydrographic stations were crossed the core of the Antarctic Circumpolar Current (ACC), we anticipate to see the difference of inorganic carbon systems in the water masses crossing the ACC.

## Work at sea

Hydrographic survey was conducted in the Amundsen Sea by casting CTD/Rosette at 81 stations, and among them 4 stations were replicated to investigate short-term variation of ecosystem parameters (Figure 2.12). The survey area covers the Amundsen and Pine Island polynyas, sea-ice zone, and the open see off the shelf break. We met far narrower band of sea-ice zone this year then before when entering the Amundsen Polynya (AP) and found that the sea-ice zone disappeared almost completely when leaving the AP. To investigate inorganic carbon system, dissolved $CO_2$ ($pCO_2$), dissolved inorganic carbon (DIC), and total alkalinity (TA) were measured underway along the ship track and at the hydro-casting stations. $pCO_2$ was measured using two different instruments: a non-dispersive infrared (NDIR) detecting system and a gas chromatographic system. The former was dedicated for measuring $pCO_2$ underway whereas the latter was both for underway measurement and for analyzing discrete samples collected at the hydro-casting stations. Underway measurement of $pCO_2$ was carried out by supplying uncontaminated seawater to a small Weiss-type equilibrator from which headspace air was delivered to the analytical system. To determine DIC and TA underway, uncontaminated

seawater samples were collected at 2 hours interval along the ship track. For analyzing $pCO_2$ in the seawater samples collected at the station, a specially designed glass bottle was used to avoid any contamination from the air during sampling and storage. Atmospheric $CO_2$ in the marine boundary layer was also analyzed in a regular interval using the same instruments by pumping the ambient air. The $pCO_2$ analyzing systems were calibrated using a series of standard gases and zero air. Dissolved inorganic carbon (DIC) was analyzed by coulometric titration using a system similar to SOMMA analyzer (Johnson et al., 1993). Total alkalinity (TA) was measured by potentiometric titration with HCl in an open cell. DIC and TA analyzer are combined in one analytical system, which saves seawater samples and analytical duration. The analytical systems for DIC and TA were calibrated using a certified reference material (CRM) provided by Prof. Andrew Dickson at Scripps Institution of Oceanography. The inventory of samples collected and analyzed at the hydro-casting stations is listed in Table 2.1.

## Preliminary results

The NDIR detecting system for $pCO_2$ equips a streamline of software that provides the values in situ, while the gas chromatographic technique requires computation to determine $pCO_2$ based on the calibration runs which were carried out between sample runs. We use preliminary data logged in the NDIR detecting system. In Figure 1.1, $pCO_2$ in seawater drawn by uncontaminated seawater supply system is shown along the ship track. $pCO_2$ in seawater was supersaturated in the open ocean, in particular in the core of Antarctic Circumpolar Current, while that was undersaturated in the continental shelf area including polynyas. $pCO_2$ in the Pine Island polynya and in front of the eastern Getz ice-shelf were in general larger than in front of the Dotson ice-shelf and western Getz ice-shelf. In particular the lowest $pCO_2$ was observed near Siple Dome of the western Getz ice-shelf.

## References

Johnson, K. M., Wills, K. D., Butler, D. B., Johnson, W. K., Wong, C. S., 1993, Coulometric total carbon dioxide analysis for marine studies: maximizing the performance of an automated continuous gas extraction system and coulometric detector, Mar. Chem. 44, 167-187.

Rignot, E., Bamber, J.L., Van den Broeke, M.R., Davis, C., Li, Y., Van de Berg, W.J., and Van Meijgaard, E., 2008, Recent Antarctic ice mass loss from radar interferometery and regional climate modeling, Nature Geosci. 1, 106-110

Table 2.1. Number of samples collected at the station for analyses of inorganic carbon system parameters

| Station No. | Cast No. | Sampling Date | $CO_2$ | DIC/TA |
|---|---|---|---|---|
| 1 | 1 | 2016-01-14 | 12 | 11 |
| 2 | 1 | 2016-01-15 | 12 | 10 |
| 3 | 1 | 2016-01-15 | 12 | 12 |
| 4 | 1 | 2016-01-16 | 12 | 12 |
| 5 | 1 | 2016-01-16 | 0 | 0 |
| 6 | 1 | 2016-01-16 | 10 | 10 |
| 7 | 1 | 2016-01-16 | 10 | 7 |
| 8 | 1 | 2016-01-17 | 10 | 9 |
| 8R | 4 | 2016-02-07 | 8 | 8 |
| 9 | 1 | 2016-01-17 | 3 | 3 |
| 10 | 1 | 2016-01-17 | 9 | 9 |
| 12 | 1 | 2016-01-18 | 9 | 9 |
| 12R | 5 | 2016-02-06 | 7 | 7 |
| 13 | 1 | 2016-01-18 | 4 | 4 |
| 14 | 1 | 2016-01-18 | 10 | 11 |
| 14R | 3 | 2016-02-06 | 7 | 7 |
| 15 | 1 | 2016-01-19 | 11 | 11 |
| 16 | 1 | 2016-01-19 | 4 | 4 |
| 16R | 2 | 2016-01-21 | 10 | 10 |
| 17 | 2 | 2016-01-19 | 8 | 9 |
| 18 | 1 | 2016-01-19 | 7 | 8 |
| 19 | 1 | 2016-01-19 | 8 | 8 |
| 20 | 1 | 2016-01-20 | 7 | 7 |
| 21 | 1 | 2016-01-20 | 8 | 8 |
| 22 | 1 | 2016-01-20 | 12 | 12 |
| 23 | 1 | 2016-01-22 | 8 | 8 |
| 24 | 1 | 2016-01-22 | 5 | 5 |
| 25 | 1 | 2016-01-22 | 9 | 10 |
| 26 | 1 | 2016-01-23 | 9 | 10 |
| 27 | 1 | 2016-01-23 | 8 | 8 |
| 27R | 3 | 2016-02-06 | 8 | 8 |
| 28 | 1 | 2016-01-23 | 5 | 5 |
| 29 | 1 | 2016-01-23 | 7 | 7 |
| 29R | 4 | 2016-02-05 | 7 | 7 |
| 30 | 1 | 2016-01-23 | 5 | 6 |
| 31 | 1 | 2016-01-24 | 10 | 10 |
| 32 | 1 | 2016-01-24 | 8 | 8 |
| 33 | 1 | 2016-01-24 | 9 | 9 |
| 34 | 1 | 2016-01-24 | 8 | 8 |
| 35 | 1 | 2016-01-24 | 12 | 12 |
| 36 | 1 | 2016-01-24 | 8 | 8 |
| 37 | 1 | 2016-01-25 | 10 | 9 |
| 38 | 1 | 2016-01-25 | 9 | 9 |
| 39 | 1 | 2016-01-25 | 9 | 9 |
| 40 | 1 | 2016-01-26 | 10 | 11 |
| 41 | 1 | 2016-01-27 | 8 | 8 |
| 42 | 1 | 2016-01-27 | 7 | 7 |
| 43 | 1 | 2016-01-28 | 8 | 8 |
| 44 | 1 | 2016-01-28 | 8 | 8 |
| 45 | 1 | 2016-01-28 | 8 | 8 |
| 46 | 1 | 2016-01-28 | 7 | 7 |
| 47 | 1 | 2016-01-28 | 7 | 7 |
| 48 | 1 | 2016-01-28 | 6 | 6 |

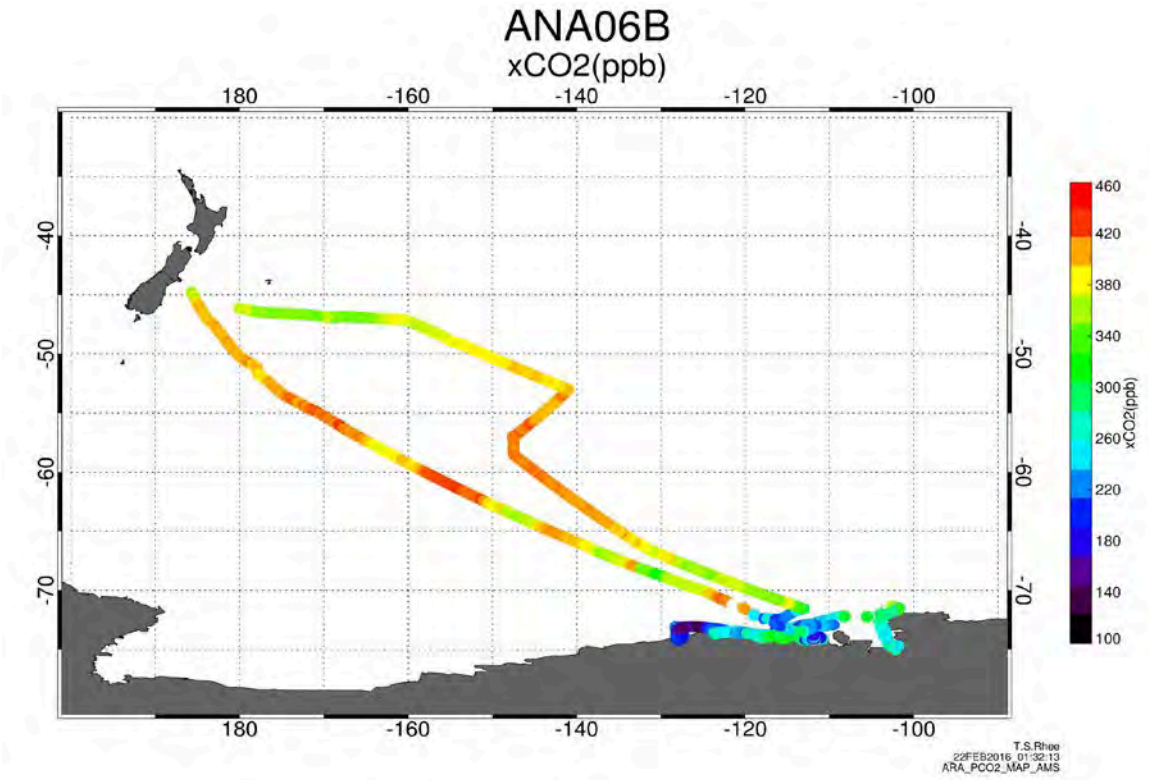


Figure 2.12. Distribution of $CO_2$ mole fractions in the surface waters along the cruise track.

## 2.10 Greenhouse gases other than $CO_2$

Rhee, Tae Siek and Ku, Ah-Young

Korea Polar Research Institute, Korea

### 요약문

이산화탄소 이외에 메탄과 아산화질소는 지구 기후 변화의 주요 원인으로 지목되는 온실기체이다. 일산화탄소와 수소는 직접적인 온실효과를 가져오지 않지만 대기에서 화학반응에 의해 간접적으로 온실효과를 가져온다. 아문젠해 탐사기간 동안 이들 기체의 해수표층과 해양경계층, 해양 내부의 수직구조 분포를 관측하였으며 일산화탄소와 수소의 광화학 반응과 생물활동으로 인한 농도변화 실험을 26개 정점에서 실행하였다. 이들 용존기체들은 가스크로마토그래프를 이용하여 분석하였으며 표준기체를 이용하여 기기를 보정하였다. 모든 기체 분석 결과를 최종 농도값으로 정량화하는 작업은 탐사후 연구소에 돌아가서 수행할 계획이다.

### Objectives

The ocean acts as a source for $CH_4$, $N_2O$, $H_2$, and CO. Microbes produce $CH_4$ and $N_2O$ in water column while photochemical degradation of organic matters is a major source of CO and likely for $H_2$ in the ocean. However, oceanic source strengths of these gases to the atmospheric budget are not well

quantified due mainly to insufficient observations in the ocean. In particular, sea-ice region and continental shelf of the Amundsen Sea is a void of these data. Following the same goal in the previous expeditions, we aim to quantify the emission rates of these gases in the southern ocean and in the Amundsen Sea.

## Work at sea

Non-$CO_2$ greenhouse gases ($N_2O$, $CH_4$, $H_2$, and CO) were monitored along the cruise track in the marine boundary layer and in the surface seawater at ~1 hour interval. An air sampling inlet was mounted on the top of foremast, ~29 m above the sea surface. The air sampling inlet was positioned to avoid the flow of contaminated air from ship's exhaust. Air samples were withdrawn through the polyethylene inner-coated aluminum tubing (Dekabon) using a membrane pump. The total length of tubing was ~100 m. The inlet was capped with a funnel to prevent rainwater or sea spray from entering the tubing and a filter pack was mounted at the tip of the inlet to protect the tubing and analyzing system from inhaling solidified sea salts. Uncontaminated surface seawater was supplied at a depth of ~6 m into two Weiss-type equilibrators in which the headspace air equilibrates with dissolved gases in seawater. The headspace air was introduced to gas chromatographic analyzers every hour to determine the dissolved gas concentrations. To keep the analyzing system from being wet, sample and calibration gases were forced to flow through a drying agent ($P_2O_5$).

To investigate the distribution of these gases in the water column, aliquots of seawater samples were drawn into a specially designed glass containers from the Niskin bottles mounted on CTD/Rosette. In the laboratory a precisely known volume of pure Ar (99.9999%) was injected into the glass containers to make headspace. After equilibration with dissolved gases, the headspace air was taken using a syringe and injected into sample loops equipped in the gas chromatographs. $CH_4$ and $N_2O$ were separated in packed columns, detected by flame ionization detector (FID) and electron capture detector (ECD), respectively, and quantified by calibrating the gas chromatographic system using a series of calibration gases (Rhee et al., 2009). CO and $H_2$ were separated in a molecular sieve packed column and detected by Hg vapour which was quantitatively produced by the reaction of CO and $H_2$ with HgO in a hot bed at ~250°C (Park and Rhee, 2016). Gas chromatograph for CO and $H_2$ measurements was calibrated for every sample from the equilibrator or from the marine boundary layer. Total 705 samples were analyzed for $CH_4$ and $N_2O$ and 309 samples for CO and $H_2$ in the water columns during the expedition (Table 2.2). These results are under process to obtain the final concentrations. In addition, a series of culture experiments was carried out to estimate the microbial oxidation of CO at the surface waters. An aliquot of seawater was subsampled from a Niskin in an amber glass jar overflowing for a certain period to make sure the water exposed to the headspace air was completely flown out. In the laboratory a given volume (80 – 90 mL) of pure Ar (99.9999%) past CO scrubber (Hokalite) was injected into the bottle to take an aliquot (ca. 60 mL) of the seawater in a glass syringe. Then, pure Ar was added into the glass syringe to make headspace with which the dissolved CO in the seawater was equilibrated. The syringe was immersed in an isothermal water bath at ~20°C. After equilibrium, the headspace air was sampled and injected into the analyser.

## References

Park, K., Rhee, T.S., 2016, Ocean source strength of carbon monoxide on the basis of basin-wide observations in the Atlantic, Environ. Sci. Processes and Impacts, DOI:10.1039/C5EM00546A.

Rhee, T.S., Kettle, A.J., Andreae, M.O., 2009, Methane and nitrous oxide emissions from the ocean: A reassessment using basin-wide observations in the Atlantic, J. Geophysic. Res. 114, D12304.

Table 2.2. Number of samples collected at the stations to analyze $CH_4$, $N_2O$, CO and $H_2$

| Station No. | Cast No. | Sampling Date | $CH_4/N_2O$ | $CO/H_2$ |
|---|---|---|---|---|
| 1 | 1 | 2016-01-14 | 11 | 8 |
| 2 | 1 | 2016-01-15 | 10 | 8 |
| 3 | 1 | 2016-01-15 | 12 | 7 |
| 4 | 1 | 2016-01-16 | 12 | 5 |
| 5 | 1 | 2016-01-16 | 0 | 0 |
| 6 | 1 | 2016-01-16 | 10 | 6 |
| 7 | 1 | 2016-01-16 | 7 | 6 |
| 8 | 1 | 2016-01-17 | 9 | 5 |
| 8R | 4 | 2016-02-07 | 8 | 0 |
| 9 | 1 | 2016-01-17 | 3 | 0 |
| 10 | 1 | 2016-01-17 | 9 | 5 |
| 12 | 1 | 2016-01-18 | 9 | 5 |
| 12R | 5 | 2016-02-06 | 7 | 6 |
| 13 | 1 | 2016-01-18 | 4 | 0 |
| 14 | 1 | 2016-01-18 | 11 | 5 |
| 14R | 3 | 2016-02-06 | 7 | 0 |
| 15 | 1 | 2016-01-19 | 11 | 0 |
| 16 | 1 | 2016-01-19 | 4 | 5 |
| 16R | 2 | 2016-01-21 | 10 | 5 |
| 17 | 2 | 2016-01-19 | 9 | 5 |
| 18 | 1 | 2016-01-19 | 8 | 0 |
| 19 | 1 | 2016-01-19 | 8 | 5 |
| 20 | 1 | 2016-01-20 | 7 | 0 |
| 21 | 1 | 2016-01-20 | 8 | 0 |
| 22 | 1 | 2016-01-20 | 12 | 5 |
| 23 | 1 | 2016-01-22 | 8 | 5 |
| 24 | 1 | 2016-01-22 | 5 | 0 |
| 25 | 1 | 2016-01-22 | 10 | 6 |
| 26 | 1 | 2016-01-23 | 10 | 0 |
| 27 | 1 | 2016-01-23 | 8 | 6 |
| 27R | 3 | 2016-02-06 | 8 | 6 |
| 28 | 1 | 2016-01-23 | 5 | 0 |
| 29 | 1 | 2016-01-23 | 7 | 6 |
| 29R | 4 | 2016-02-05 | 7 | 8 |
| 30 | 1 | 2016-01-23 | 6 | 6 |
| 31 | 1 | 2016-01-24 | 10 | 6 |
| 32 | 1 | 2016-01-24 | 8 | 0 |
| 33 | 1 | 2016-01-24 | 9 | 7 |
| 34 | 1 | 2016-01-24 | 8 | 0 |
| 35 | 1 | 2016-01-24 | 12 | 0 |
| 36 | 1 | 2016-01-24 | 8 | 5 |
| 37 | 1 | 2016-01-25 | 9 | 5 |
| 38 | 1 | 2016-01-25 | 9 | 0 |
| 39 | 1 | 2016-01-25 | 9 | 5 |
| 40 | 1 | 2016-01-26 | 11 | 6 |
| 41 | 1 | 2016-01-27 | 8 | 0 |
| 42 | 1 | 2016-01-27 | 7 | 6 |
| 43 | 1 | 2016-01-28 | 8 | 0 |
| 44 | 1 | 2016-01-28 | 8 | 0 |
| 45 | 1 | 2016-01-28 | 8 | 0 |
| 46 | 1 | 2016-01-28 | 7 | 5 |
| 47 | 1 | 2016-01-28 | 7 | 0 |
| 48 | 1 | 2016-01-28 | 6 | 0 |

# 2.11 Clean sampling for trace metals (Fe, Cd)

D. J. Jang, K. K. Park, M. S. Choi

Div. Oceanography, Chungnam National University, Korea

## 요약문

해양에서 철은 생물제한 원소로 알려져 있으며, 카드뮴도 영양염 형태의 거동을 보인다. 따라서 철과 카드뮴 같은 미량원소의 생지화학적 조절요인을 이해하고 이들의 기원과 어떠한 경로를 통하여 이동되는지에 대하여 이해하는 것이 매우 중요하다. 일반적으로 남빙양의 미량금속 농도는 매우 낮은 수준으로 보고되어있어 배에서 채수 장비를 이용하여 채수 시 다양한 오염원에 의한 오염이 발생할 위험이 있다. 그러므로 이러한 오염을 예방하기 위하여 케블라 와이어가 장착된 윈치, 플라스틱 시브, 티타늄 재질의 로젯에 고무로 코팅된 추를 부착하였으며 GO-FLO 채수 병을 사용하였다. 그리고 로젯 프레임에 압력 센서 외에 다른 수온 염분 측정 센서들을 장착하지 않아 금속 처리된 센서들로부터 나올 수 있는 오염을 줄였다. 위와 같은 방법으로 아문젠해에서 총 12개의 정점에서 수심에 따라서 깊이를 달리하여 채수하였다. 채수한 채수 병은 곧바로 청정 실험실로 옮겨 실험실 내에서 전부 처리하였으며, 샘플은 받는 순서에 따라서 필터를 하지 않은 0.25L, 필터 한 두 개의 0.25L 그리고 1L의 샘플을 받아 정제질산을 넣어 산성화하였다. 샘플분석은 입자상과 용존상을 모두 분석할 예정이다.

## Objectives

Fe is known as a bio-limiting element in the ocean and Cd exhibits a nutrient type behavior. Therefore, understanding the processes controlling the trace elements (Fe, Cd) biogeochemistry in the Amundsen Sea and identification of Fe, Cd sources and transport using isotope ratios are important. Generally, the Southern Ocean is known to lower concentration of trace elements. The extremely low natural concentration of many trace elements in seawater and the ubiquity of these materials in the sampling platforms (ships and sampling equipment such as bottles and frames) results in samples being highly susceptible to contamination during the sampling and subsampling process. Therefore, we adopt several methods to prevent contamination. First, to avoid the problem of potential cable contamination for Cu, Cd, Zn and Ni by using non-metallic Kevlar wire with plastic sheave. Second, we used GO-FLO bottles for sampling, which contain no internal spring s and could be deployed in the closed position, thus avoiding surface water slicks that are believed by many to be potential sources of contamination. Last, we used rosette. We placed 12 GO-FLO bottles (5L) on a Titanium rosette frame with rubber coated weights. The rosette frame, however, did not include a CTD or other sensor except pressure sensor, as it was believed that the metal casings of these instruments could contaminate the water surrounding the rosette and thus the samples when the bottles were closed. And we also process the sample handling and filtration in the clean cell.

## Work at sea

Following above methods, seawater samples were collected at different depths of 12 stations (Table. 2.3). Handling of samples was performed in a clean cell. Our GO-FLO bottles have been modified slightly from the original manufacturer's design. The modifications consist of drilling out the receptacles to accept the air vent fixtures and sampling valves. After racking the bottles and removing

the hair cab from the subsampling cocks. The vent cabs are then removed, and initial unfiltered samples (0.25 L) are drawn from the cocks. The bottles must be drained slightly at this stage to lower the sample level below the air vent cabs. Bottles are then connected to clean hose (equipped air filter) fittings and pressurized with compressed air that has been passed through an In-line filter (0.45 ㎛ membrane filter, 1.5L). All the samples were acidified using concentric nitric acid. We plan to analysis both dissolved metals and particulate metals to reveal the source of metals.

Table 2.3. Fe, Cd sampling location and sampling depth during ANA06B

| Station | Lat. (S) | Long. (W) | Depth (m) |
|---|---|---|---|
| **4** | 72° 06.00’ | 118° 52.80’ | 20, 40, 60, 100, 150, 200, 300, 350, 400, 500, 600, 700, |
| **6** | 72° 23.19’ | 117° 42.76’ | 10, 40, 60, 100, 150, 200, 250, 300, 350, 400, 450, 500 |
| **8** | 72° 48.00’ | 116° 30.00’ | 20, 60, 100, 150, 200, 250, 300, 350, 400, 450, 500, 600 |
| **10** | 73° 02.39’ | 115° 43.51’ | 20, 60, 100, 150, 200, 250, 300, 350, 400, 450, 550, 650, |
| **14** | 73° 30.00’ | 114° 00.00’ | 20, 40, 60, 100, 150, 200, 250, 300, 350, 400, 500, 650 |
| **19** | 74° 10.29’ | 112° 31.70’ | 15, 40, 60, 100, 200, 250, 300, 350, 400, 500, 650, 800 |
| **16 revisit** | 73° 49.18’ | 111° 02.71’ | 10, 20, 50, 100, 200, 250, 300, 350, 400, 500, 600 |
| **54** | 73° 40.80’ | 123° 42.00’ | 10, 30, 60, 100, 150, 200, 250, 300, 350, 400, 500, 600 |
| **56** | 73° 59.80’ | 118° 01.93’ | 40, 80, 100, 150, 200, 250, 30, 350, 450, 500, 600, 700 |
| **62** | 75° 03.53’ | 102° 09.15’ | 50, 100, 150, 200, 300, 350, 400, 450, 600, 700 |
| **65** | 71° 19.76’ | 102° 33.02’ | 20, 50, 100, 150, 200, 250, 300, 380, 400, 500, 600 |
| **67** | 71° 33.73’ | 113° 02.78’ | 10, 30, 60, 100, 150, 200, 250, 300, 400, 500, 550 |

## 2.12 Carbon Cycling on the Amundsen Shelf: Insights from radiocarbon analysis

Bumsoo Kim, Jeomshik Hwang

Seoul National University (SNU), Korea

### 요약문

빙상과 빙붕의 급격한 감소를 보이는 서남극 아문젠 해는 지구 온난화의 영향을 크게 받고 있는 해역 중 한 곳이다. 기후 변화와 상대적으로 고온고염의 Circumpolar Deep Water의 유입의 결과 이는 해양 일차 생산자인 식물 플랑크톤에 의한 일차 생산을 비롯한 아문젠 해의 탄소순환 양상에 영향을 미칠 것으로 예상된다. 본 연구에서는 나이와 기원 추적에 대한 정보를 제공하는 방사성탄소 동위원소를 이용하여 용존무기탄소, 용존유기탄소, 부유성 입자유기탄소 그리고 퇴적물로부터 아문젠 해의 무기 및 유기탄소 순환을 이해하려 하였다.

## Introduction

The Amundsen Sea in the west Antarctic is experiencing rapid decline in sea-ice cover and glacial melting. Climate change and intrusion of the warm Circumpolar Deep Water may affect the biogeochemical processes in the Amundsen Sea including primary production. To understand the carbon budget and carbon cycling based on radiocarbon analysis, we have sampled dissolved inorganic/organic carbon, suspended particulate organic carbon and sediment in the Amundsen Sea. Understanding the cause of the change in carbon cycling of this region will provide information to interpret the future climate change through feedback mechanisms and to enhance the model performance for future climate projection.

## Work at Sea

Various samples to understand the carbon cycling based on radiocarbon analysis were collected including dissolved inorganic carbon (DIC), dissolved organic carbon (DOC), suspended particulate organic carbon (POC) in the surface water and sediment on the Amundsen Shelf, Antarctica, during the ANA06B cruise on the IBRV ARAON (Table 2.4 and Table 2.5).

Seawater samples for DIC were collected in 3 stations: the outer shelf (St. 1) for reference, eastern and western station along the Doston Ice Shelf (St. 18 and St. 22, respectively). The purpose of sampling was to complement the previous radiocarbon analysis and to trace the glacial meltwater based on radiocarbon. Each depths of seawater were collected into 500 mL pyrex glass bottle (Duran) which was pre-combusted in 450 °C for 4 hours. To prevent any bubbles being trapped, every sample were filled from the bottom of the bottle by a silicon tube and overflowed by half of the bottle's volume. After sampling, 100 μl of saturated $HgCl_2$ was injected to each sample to prevent any biological processes of organic matter. Bottles were closed with greased stopper, bind by rubber band and stored in room temperature until further analysis.

DOC samples were sampled mainly along the Doston Trough: one station in the outer shelf (St. 1), two in the sea-ice zone (St. 6, 8), two inside the polynya (St. 12, 14) and one in the middle of Doston Ice Shelf (St. 19) and Getz Ice Shelf (St. 39). Each depths of seawater were collected into 500 mL Boston amber glass bottle (Wheaton) which was previously combusted in 450 °C for 4 hours. Each sample was filtered on pre-baked 47 mm GF/F filter with nominal pore size of 0.7 μm (Whatman). Then, the filtered seawater sample was moved into a new pre-combusted bottle and stored frozen until further analysis.

Suspended POC in the surface water was collected by filteration of seawater from the ship's uncontaminated seawater intake on pre-baked 47 mm GFF filter (pore size: 0.7 μm; Whatman) without any pre-filteration. Depending on the amount of particles 1.5 – 5 L of surface water was filtered under low vacuum (~500 mmHg). Each filter was folded and stored frozen in a pre-combusted aluminum foil pouch until further analysis. Total sampling was conducted at 20 stations (including revisited stations) with duplicate filtering for most of the stations.

Sediment samples were collected using box-core (Marine Tech, Korea) at six stations to supplement the spatial distribution of the sedimentation process on the Amundsen Shelf (Kim et al, 2015) – St. 4, 10, 16, 19, 26 and 33. Upon detachment of the canister, acryl cores of 8cm diameter and 30 – 60 cm length were gently pushed in for sub-cores. Each sediment core was sliced into 1 – 2 cm thick subsamples on board and stored in pre-baked 4 oz glass jar (Wheaton) and kept frozen until further analysis.

## References

Kim, M., et al., Sedimentation of particulate organic carbon on the Amundsen Shelf, Antarctica. Deep-Sea Res. II (2015), http://dx.doi.org/10.1016/j.dsr2.2015.07.018i

Table 2.4. DIC, DOC, susp POC sampling location and sampling depth during ANA06B

| Sample | Station[b] | Lat. (S) | Long. (W) | Depth (m) |
|---|---|---|---|---|
| **DIC** | 1 | 69° 59.99’ | 125° 00.01’ | 3415, 1000, 600, 250, 100, 30, 0 |
| | 18 | 74° 10.51’ | 112° 08.32’ | 938, 700, 700, 500, 360, 260, 260, 100, 20, 0, 0 |
| | 22 | 74° 10.31’ | 113° 19.71’ | 625, 600, 480, 400, 400, 240, 200, 100, 20, 20, 0 |
| **DOC** | 1 | 69° 59.99’ | 125° 00.01’ | 3415, 1000, 600, 250, 100, 30, 0 |
| | 6 | 72° 22.90’ | 117° 44.93’ | 510, 400, 300, 100, 40, 10, 0, 0 |
| | 8 | 72° 48.01’ | 116° 30.05’ | 615, 500, 380, 380, 200, 100, 100, 60, 20, 0 |
| | 12 | 73° 16.79’ | 114° 57.05’ | 820, 820, 750, 500, 350, 350, 200, 65, 65, 15, 0 |
| | 14 | 73° 30.00’ | 113° 59.94’ | 700, 700, 550, 400, 320, 200, 60, 60, 20, 0 |
| | 19 | 74° 10.29’ | 112° 31.70’ | 600, 440, 440, 200, 100, 75, 50, 25, 25, 0, 0 |
| | 39 | 74° 04.80’ | 115° 43.49’ | 1045, 1045, 800, 420, 300, 300, 220, 120, 80, 40, 20, 20, 0, 0 |
| **Susp POC[a]** | 1 | 69° 59.99’ | 125° 00.01’ | 0 (4.8L), 0 (3.0L) |
| | 4 | 72° 06.15’ | 118° 52.75’ | 0 (4.1L), 0 (4.1L) |
| | 6 | 72° 22.90’ | 117° 44.93’ | 0 (3.0L), 0 (3.0L) |
| | 8 | 72° 48.01’ | 116° 30.05’ | 0 (3.5L), 0 (3.0L) |
| | 10 | 73° 02.40’ | 115° 43.50’ | 0 (3.5L), 0 (3.0L), 0 (4.0L) |
| | 12 | 73° 16.79’ | 114° 57.05’ | 0 (4.0L), 0 (3.5L) |
| | 14 | 73° 30.00’ | 113° 59.94’ | 0 (4.0L), 0 (3.5L), 0 (8.0L) |
| | 17 | 74° 12.90’ | 111° 53.54’ | 0 (5.1L), 0 (5.1L) |
| | 19 | 74° 10.29’ | 112° 31.70’ | 0 (2.5L), 0 (2.5L) |
| | 24 | 73° 53.92’ | 111° 11.73’ | 0 (1.5L), 0 (1.5L) |
| | 26 | 73° 30.00’ | 111° 59.97’ | 0 (1.8L), 0 (1.8L) |
| | 31 | 73° 09.99’ | 114° 29.98’ | 0 (2.5L), 0 (2,5L) |
| | 32 | 73° 19.70’ | 115° 25.24’ | 0 (4.5L), 0 (4.5L) |
| | 33 | 73° 30.00’ | 116° 29.98’ | 0 (5.0L), 0 (5.0L) |
| | 39 | 74° 04.80’ | 115° 43.49’ | 0 (5.0L), 0 (5.0L) |
| | 63 | 74° 52.03’ | 102° 04.80’ | 0 (4.6L), 0 (4.6L) |
| | 14 re | 73° 29.97’ | 114° 00.05’ | 0 (4.2L), 0 (4.0L) |
| | 12 re | 73° 16.79’ | 114° 57.03’ | 0 (2.6L), 0 (2.4L) |
| | 8 re | 72° 48.00’ | 116° 30.00’ | 0 (3.7L), 0 (4.0L) |

a. In column ‘Depth (m)’, the amount of filtered seawater is in the parenthesis
b. re : revisited station

Table 2.5. Sediment Core sampling location and sub-core ID (core length)

| Box Core Station | Lat. (S) | Lon. (W) | Sub-Core ID (Core Length) |
|---|---|---|---|
| 4 | 72° 06.15’ | 118° 52.75’ | St 4-1 (25cm)<br>St 4-2 (20cm) |
| 10 | 73° 02.40’ | 115° 43.50’ | St 10-1 (30cm)<br>St 10-2 (29cm) |
| 16 | 73° 49.18’ | 113° 02.71’ | St 16-1 (37cm) |
| 19 | 74° 10.29’ | 112° 31.70’ | DIS 1 (30cm) |
| 26 | 73° 30.00’ | 111° 59.97’ | St 26-1 (37cm)<br>St 26-2 (36cm) |
| 33 | 73° 30.00’ | 116° 29.98’ | St 33-1 (31cm)<br>St 33-2 (24cm) |

# 2.13 Sediment trap

Jin Hyun Jeong and Dong Seon Kim

Korea Institute of Ocean and Science Technology (KIOST), Korea

## 요약문

남극 아문젠해에서 생물학적 펌프에 의해 해양 내부로 유입되는 이산화탄소의 양을 추정하기 위한 목적으로, 퇴적물포집기를 이용하여 아문젠해에서의 침강입자 플럭스(유기탄소와 탄산칼슘, 생물기원 규소, 육상기원 쇄설물)의 시공간적 변화를 알아보고자 한다. 2016년 2월, 2014년 1월에 계류한 폴리냐 외부 대륙사면 지역 (K1; 설치수심 414m)과 폴리냐 지역 (K2; 설치수심 430m), 폴리냐 연안 지역 (K3; 설치수심 400m와 K6; 설치수심 400m)에 각각 설치한 퇴적물 포집기를 회수하였다. K1과 K2 정점에서 퇴적물 트랩 포집기의 유실로 인하여 샘플 채취에 실패하였다. K6에 설치한 퇴적물 포집기는 배터리 전압 부족으로 인하여 일부 샘플만 채취하였다. 회수한 퇴적물 포집기는 정비 후 K2와 K3, K4 정점에서 재계류 하였다 (Fig. 1). K2 정점에서 퇴적물 포집기는 약 1년 동안 여름은 9일 간격, 봄/가을은 15일 간격, 겨울은 1~2달 간격으로 샘플을 채집하도록 설정하였다. K3와 K4 정점에서 퇴적물 포집기는 약 2년 동안 여름은 15일 간격, 봄/가을은 1달 간격, 겨울은 2달 간격으로 샘플을 채집하도록 설정하였다 (Table 1). 채집한 2014년 1월부터 약 1년간의 샘플들은 모두 사진으로 기록한 뒤 밀봉하여 냉장보관 하였으며, 실험실로 이동 후 분석할 계획이다.

## Objectives

The flux of the sinking particles is a major control on the inventory of carbon and the chemical composition of deep sea in the ocean. This process, therefore, has an important influence on global biogeochemical cycle and then important in understanding the global carbon cycle.

The objective of this survey is to investigate the seasonal variations in the sinking fluxes of biogenic

elements such as particulate organic carbon (POC), $CaCO_3$ and biogenic silica using sediment trap and to estimate the amounts of $CO_2$ removed into the ocean from atmosphere by "Biological pump" in the Amundsen sea.

## Work at sea

To understand the temporal and spatial variations of the sinking particle fluxes in the Amundsen sea, sediment traps (Mark 78G) were deployed. In February 2016, sediment traps deployed at continental slope outer polynya (K1), polynya center (K2) and polynya coastal (K3 and K6) were recovered and then three sediment traps were separately deployed about 400 m depth at center (K2) and coastal (K3, K4) in the ploynya (Figure 2.13). At K2, operating time interval of the each bottles was 9, 15, and 30 days during summer, spring/autumn, and winter seasons, respectively (Table 2.6). At K3 and K4 stations, operating time interval of the each bottles was 15, 30, and 60 days during summer, spring/autumn, and winter seasons, respectively (Table 2.6). Samples collected at sediment trap were stored in refrigerator in sealed (Figure 2.13), will be analyzed in the laboratory to understand temporal and spatial variations of sinking particle fluxes in the Amundsen Sea.

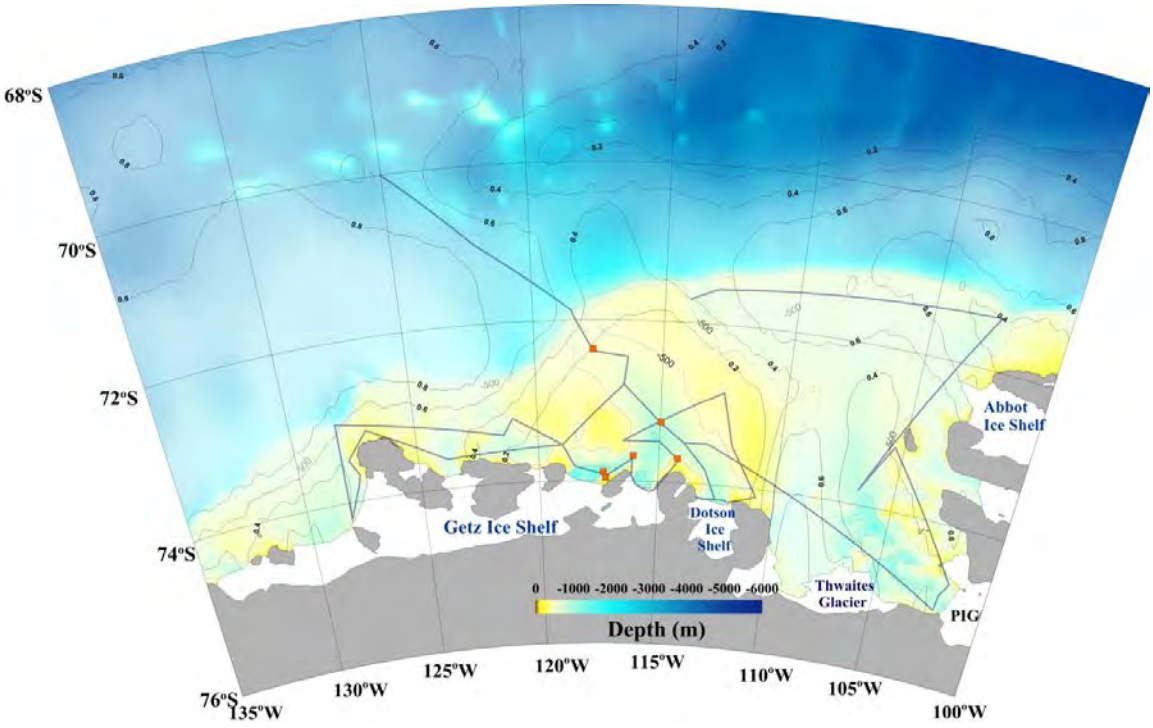


Figure 2.13. Sediment trap deployment station.

Table. 2.6. Sediment trap time schedules

| Bottle Number | K2 | K3 | K4 |
|---|---|---|---|
| 1 | 2016.02.10 | 2016.02.01 | 2016.02.01 |
| 2 | 2016.03.01 | 2016.02.16 | 2016.02.16 |
| 3 | 2016.03.16 | 2016.03.10 | 2016.03.10 |
| 4 | 2016.04.01 | 2016.04.01 | 2016.04.01 |
| 5 | 2016.05.01 | 2016.06.01 | 2016.06.01 |
| 6 | 2016.06.01 | 2016.08.01 | 2016.08.01 |
| 7 | 2016.07.01 | 2016.10.01 | 2016.10.01 |
| 8 | 2016.08.01 | 2016.12.01 | 2016.12.01 |
| 9 | 2016.09.01 | 2016.12.21 | 2016.12.21 |
| 10 | 2016.10.01 | 2017.01.17 | 2017.01.17 |
| 11 | 2016.11.01 | 2017.01.30 | 2017.01.30 |
| 12 | 2016.11.16 | 2017.02.19 | 2017.02.19 |
| 13 | 2016.12.01 | 2017.03.11 | 2017.03.11 |
| 14 | 2016.12.10 | 2017.04.01 | 2017.04.01 |
| 15 | 2016.12.19 | 2017.06.01 | 2017.06.01 |
| 16 | 2017.01.01 | 2017.08.01 | 2017.08.01 |
| 17 | 2017.01.10 | 2017.10.01 | 2017.10.01 |
| 18 | 2017.01.19 | 2017.12.01 | 2017.12.01 |
| 19 | 2017.02.01 | 2017.12.21 | 2017.12.21 |
| 20 | 2017.02.10 | 2018.01.11 | 2018.01.11 |
| 21 | 2017.02.19 | 2018.02.01 | 2018.02.01 |
| close | 2017.03.01 | 2018.02.28 | 2018.02.28 |

## 2.14 Sediment samples by Box-core

Sun-Yong Ha, Youngju Lee, Eric Potvin

Korea Polar Research Institute, Korea

### 요약문

남극 아문젠해 폴리냐 및 ice shelf, marginal sea ice zone에서 총 9정점에서 박스형 퇴적물 채취기를 이용하여 현장 퇴적물 시료를 채취하였다. 표층 퇴적물의 색소 분석 및 총유기탄소 및 질소, DNA 시료를 각각 확보하였다. 아문젠해 marginal sea ice zone에서 1정점, 아문젠 폴리냐에서 5정점, ice shelf (Dotson, Getz 그리고 Pine island)에서 각각 1정점씩 3개의 정점의 시료를 확보하였다. 식물플랑크톤 대발생에 의해 생성된 유기물이 저층으로 퇴적되는 총유기탄소 및 질

소, 퇴적된 식물플랑크톤의 잔류 색소 분석을 통하여 저층 생태계 내로 공급되는 에너지 흐름을 파악하고자 한다.

## Introduction

Sediment work is conducted in combination with biogeochemistry and microbiology during the ARAON Amundsen Expedition in 2016. Overall goal of sediment sampling for the ARAON Amundsen cruise is to take sediment cores from the selected research target areas including the Amundsen Sea Polynya (ASP), Dotson ice shelf, Getz ice shelf, and Pine island polynya (Figure 2.14). To retrieve the sediment cores at selected geological and oceanographic stations we used coring gears such as box corer. Undisturbed surface sediments are taken by using box corer.

The Amundsen Sea polynya (ASP) was found the most productive region among the 37 coastal polynyas around Antarctica (Arrigo and van Dijken 2003). The Amundsen Sea polynya (ASP) center region represented the higher sedimentation rate (0.2 cm $y^{-1}$) then ice shelf (0.12 cm $y^{-1}$) and sea ice marginal zone (0.13 cm $y^{-1}$). Organic matter (POC and PON) in the sediment also showed the higher value than other region; because phytoplankton bloom (dominated *phaeocysts* sp.) occurred on the polynya center region (Kim et al. in press). Primary production in the ASP during the early and late bloom was measured 28 to 357 mmol $Cm^{-2}$ $d^{-1}$ in the polynya (Lee et al. 2012).

Resting stages of phytoplankton can fossilize within the sediment. Applications to resting stages are broad. They can be used as bioindicator, reconstruct past climate, etc. The diversity of resting stages in the ASP and marginal sea are increasingly being known. However, unknown morphotypes are often being observed putting forward that further works to address the diversity still remain. Furthermore, the species producing these resting stages are often unknown. Surface sediment samples were collected in various regions or the ASP. Live resting stages of phytoplankton contained in the sediment will be observed and unknown species will be characterized. Trials to establish the life cycle of relevant species through cyst incubation will be convened.

The aim of this study is to understand the effects of environmental factors on the spatial distribution of phytoplankton pigment and resting stages of phytoplankton in the ASP. Furthermore, to understand the distribution of phytoplankton as an important primary producer on the sea floor, the community composition was studied in four stations using box core during this cruise.

## Material and methods

Box Coring

The Box corer equipped with weights of ca. 350 kg that are attached to the top of a rectangular steel tube (30*40*60 cm) have been used 10 times at 9 stations (Table 2.7). From the Box corer, surface sediments were taken. If necessary, box core sediments are for the following investigations.

Surface sediment samples were collected from box core sediment surface 0-2 cm. Thess samples are collected for qualitative study.

The CHEMTAX program based on photosynthetic pigments data has potential benefits for the estimation of phytoplankton composition, including small and fragile forms. For photosynthetic pigments analysis, subsamples from the box core were collected in the conical tube and stored at -80 ºC. The pigments will be analyzed with high performance liquid chromatography (HPLC) in the laboratory.

In order to determine relevant species, potential resting stages will be firstly characterized based on DNA using single-cell PCR focusing on the genes coding for the small subunit ribosomal RNA (18S) and the large subunit ribosomal RNA (28S). The sequences obtained will be compared with others through the NCBI database. Individuals with high divergence with known species will be further studied based on optical and scanning electron microscopy. Relevant specimens will also be isolated by micromanipulation in algal medium and incubated in various conditions in order to tentatively germinate them and establish cultures of motile forms in order to establish their life cycles. Thereafter, the motile form will be further studied based also on optical and scanning electron microscopy.

## Reference

Arrigo KR, van Dijken GL (2003) Phytoplankton dynamics within 37 Antarctic coastal polynyas. J Geophy Res 108: doi:10.1029/2002JC001739.

Kim, S., Choi, A., Yang, E.J., Lee, S., Hyun, J., Low benthic respiration and nutrient flux at the highly productive Amundsen Sea Polynya, Antarctica. In press.

Lee,S.H., Kim,B.K., Yon,M.S., Joo,H., Yang,E.J., Kim,Y.N., Shin,H.C., Lee,S., (2012) Spatial distribution of phytoplankton productivity in the Amundsen Sea, Antarctica. Polar Biol. 35,1721–1733.

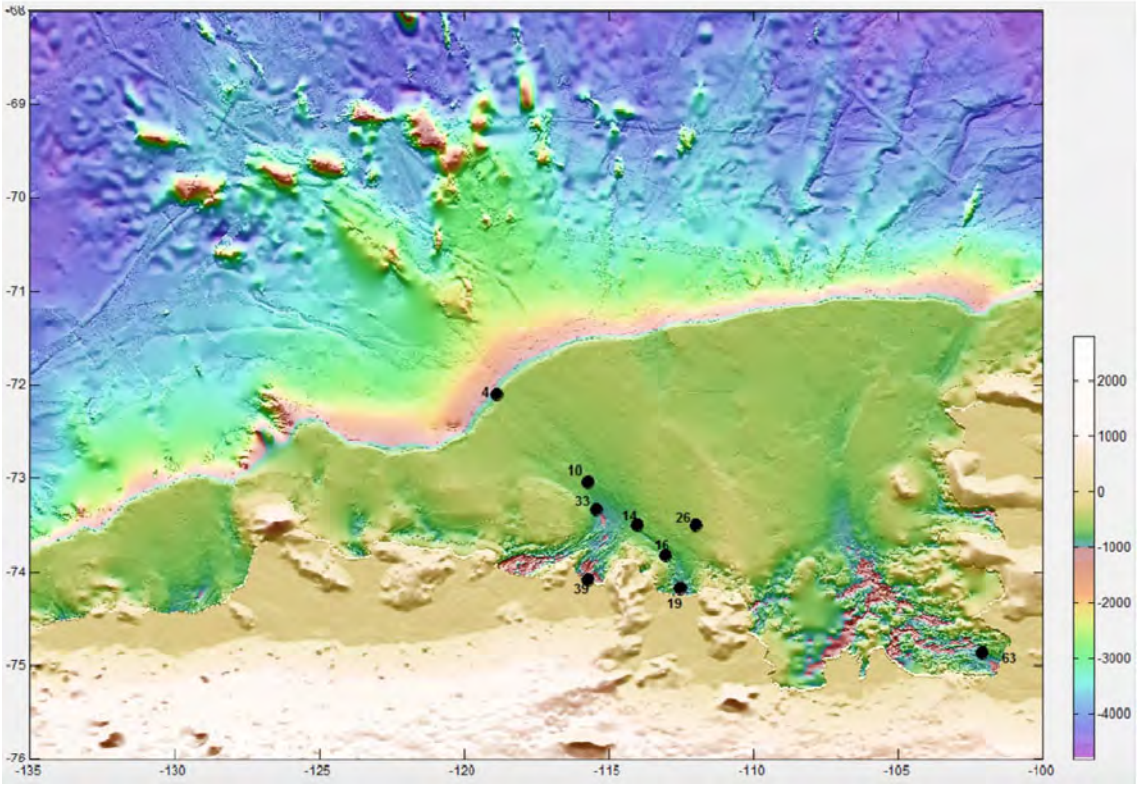


Figure 2.14. Sediment recovered with a box corer.

Table 2.7. Box core sampling list

| Data | Station | Corer type | Location | | Water depth (m) | |
|---|---|---|---|---|---|---|
| | | | Latitude | Longitude | | |
| 2016.01.16 | 4 | Box (BC-1) | 72°5.03314S | 118°53.0507W | 745 | |
| 2016.01.18 | 10 | Box (BC-2) | 73°02.4011S | 115°43.5043W | 710 | |
| 2016.01.18 | 14 | Box (BC-3) | 73°29.9923S | 114°00.0052W | 720 | Fail |
| 2016.01.20 | 19 | Box (BC-4) | 74°10.2902S | 112°31.7884W | 1036 | |
| 2016.01.21 | 16 | Box (BC-5) | 73°49.1636S | 113°02.7278W | 788 | |
| 2016.01.23 | 26 | Box (BC-6) | 73°29.9966S | 111°59.9773W | 420 | |
| 2016.01.24 | 33 | Box (BC-7) | 73°29.9989S | 116°29.9838W | 374 | |
| 2016.01.25 | 39 | Box (BC-8) | 74°04.8120S | 115°43.5032W | 1064 | |
| 2016.02.03 | 63 | Box (BC-9) | 74°52.0324S | 102°04.7986W | 945 | |
| 2016.02.06 | 14 | Box (BC-3) | 73°29.9923S | 114°00.0052W | 720 | |

# Chapter 3
# Biological Oceanography

## 3.1 Phytoplankton community

Youngju Lee and Seungjun Lee

Korea Polar Research Institute, Incheon, 21990, Korea (yjulee@kopri.re.kr)

### 요약문

아문젠해와 Udintsev fracture zone (UFZ) 해역에서 식물플랑크톤 군집의 분포와 이를 조절하는 주요 환경요인을 파악하기 위하여 현장조사가 수행되었다. 2016년 1월 15일부터 2월 16일까지 33일간 51개 정점 (revisit 포함)에서 수심에 따른 엽록소-a, 크기별 엽록소-a 농도가 측정되었으며 현미경과 광합성색소 기반의 군집연구를 위한 시료를 확보하였다. 엽록소 농도와 초미소식물플랑크톤 현존량 중 일부는 현장에서 측정되었다. 현미경 시료는 해수를 고정 후 필터하여 슬라이드를 제작하였고 광합성 색소는 해수를 필터한 후 냉동보관 하였으며 추후 실험실에서 분석될 예정이다. 식물플랑크톤 정성분석을 위하여 26개 정점 (revisit 포함)에서 네트 시료를 채집하였으며 실험실에서 분석 예정이다.

### Introduction

The Southern Ocean is a net sink for atmospheric $CO_2$ on annual timescales, accounting for 20% of global ocean (Takahashi et al., 2009) due to high primary productivity (Arrigo et al., 2008). Phytoplankton bloom appeared in austral summer in the coastal Polynya which is local areas of reduced ice cover that generally form due to offshore katabatic winds and seasonal ice melt (Tremblay and Smith, 2007). In the growing season, higher insolation and thinner sea ice allow sufficient irradiance to penetrate and drive photosynthesis in this continental shelf area. Seasonal variation of phytoplankton biomass and primary production in the Antarctic shelf waters plays an important role in the biogeochemical cycle in the southern ocean.

Several researches have been intensively studied the dynamics of phytoplankton in the Antarctic coastal waters and revealed that diatoms and prymnesiophyte *Phaeocystis antarctica* formed massive bloom in different season and area in the coastal waters (Arrigo et al., 1999). However, variations occur among years not only in the dominant rate of these two major groups, but also in the controlling mechanisms, and it is hard to predict their distribution (Smith Jr et al., 2006). Moreover, most studies were mainly concerned with regions in the Ross Sea, Weddell Sea, and eastern Antarctica (Arrigo et al., 1999; Lancelot et al., 1993; Wright et al., 2010).

Amundsen Sea Polynya (ASP) is the most productive area per unit area of the 37 identified coastal polynya systems in the Antarctic (Arrigo and van Dijken, 2003). It is also well known that Amundsen Sea is the highest melting area in the Antarctica by the global warming (Rignot et al., 2013). Modified Circumpolar Deep Water (mCDW) intruded onto the continental shelf and accelerate the basal melting of ice shelves in the ASP (Rignot et al., 2013). The changes in water column stratification, water circulation, coastal upwelling and Fe supply could also be caused by mCDW extending in the

ASP (Gerringa et al., 2012). Therefore, the distribution and response of whole phytoplankton groups in the rapidly melted Amundsen Sea need to be understood for prediction of phytoplankton response under climate change.

## Materials and methods

### Field survey

Field survey was conducted onboard the Korean Research IBRV Araon in the ASP and the seas around ASP during austral summer from 15 January to 16 February 2016 (Figure 3.1). Water samples for chlorophyll *a* (Chl-a) concentration, microscopic analysis, picophytoplankton, and pigments were collected from 4 ~ 7 depths in the upper 100m using a 10-L PVC Niskin water sampler attached to a CTD rosette system.

### Size-fractionated Chl a concentration

Subsamples from the Niskin bottles were filtered through a cascade connection of 20-μm nylon mesh, Nuclepore filter (Whatman International) with pore size of 3 μm, and a Whatman GF/F filter to determine size-fractionated Chl a (Sieburth 1978). Thus, micro-Chl a (>20 μm), nano-Chl a (3-20 μm), and pico-Chl a (<3 μm) could be measured directly. Subsamples for total Chl a were filtered onto 47 mm GF/F Whatman filters. Each filter was extracted in 90% acetone, and Chl a concentrations were measured with a fluorometer (model Trilogy, Turner Designs, USA; method: Parson et al., 1984).

### Phytoplankton community

To estimate the phytoplankton abundance, water samples from Niskin bottles were collected in 200-mL high density polyethylene bottles, preserved with glutaraldehyde (final concentration 1%), and stored at 4℃ until analysis. Sample volumes of 50 - 150 mL were filtered through nuclepore filters (0.8 μm pore size, black, 25 mm diameter). During filtration, the samples were drawn down until 5 mL remained in the filtration tower. Concentrated DAPI (50 μg $mL^{-1}$ final concentration) was then added and allowed to sit briefly (5 seconds) before filtering the remaining sample until dry (Taylor et al., 2011). The total 300 slides were made for identifying species compositions of phytoplankton.

Phytoplankton was sampled with 20 μm mesh plankton net hauled vertically from 100 m to the surface. The samples were preserved with Lugol's solution (final concentration 1%) and will be transported to the laboratory for further analysis.

### Heterotrophic bacteria and picophytoplankton abundance

Water samples for flow cytometry analysis were fixed for 15 min with paraformaldehyde (final concentration: 1%) and stored at -80 ºC. Since fixation with added chemical reagents may result in loss of cells, natural samples were also analyzed on a Accuri C6 flow cytometer (Becton Dickinson) equipped with an air-cooled argon laser (488 nm, 15 mW), placed on-board so that after sample collection the analyses could immediately be performed. Picophytoplankton groups were identified and their abundance enumerated using the characteristics of 90°-angle light scatter, orange fluorescence from phycoerythrin, and red fluorescence from chlorophyll (Marie et al., 1997). For the enumeration of heterotrophic bacteria, seawater samples were stained with SYBR green I (Molecular

Probes), and incubated in the dark at room temperature for 15 min before analysis. Bacteria were identified for their side light scatter and green fluorescence signals. Raw data from the flow cytometer will be processed using the FlowJo program (Tree Star, www.flowjo.com).

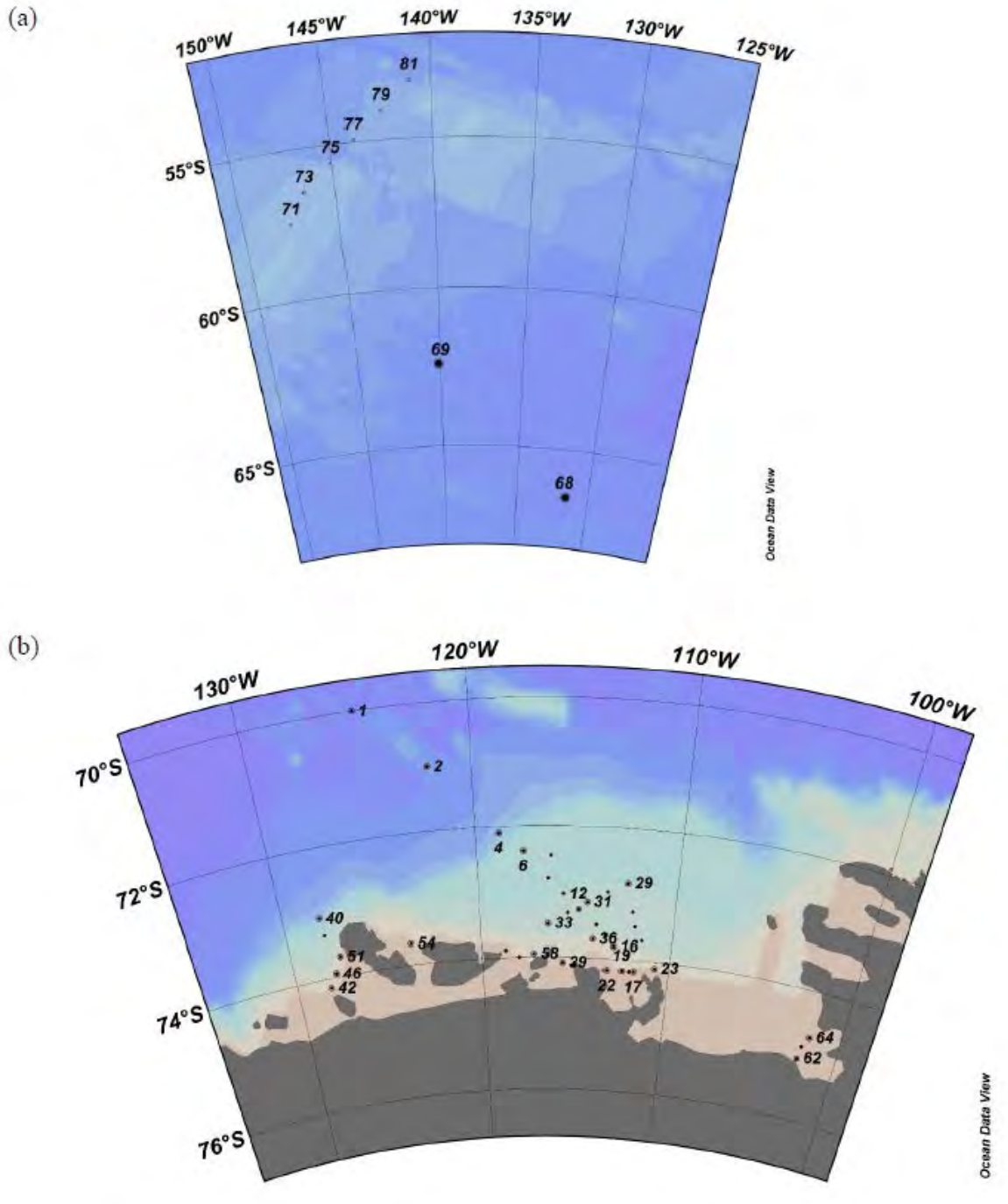


Figure 3.1. Sampling stations of plankton net and phytoplankton community in (a) the UFZ and (b) the Amundsen Sea during the Amundsen 2016 cruise. Large dots indicate the stations of plankton net.

Photosynthetic pigments

The CHEMTAX program based on photosynthetic pigments data has potential benefits for the estimation of phytoplankton composition, including small and fragile forms. For photosynthetic pigments analysis, 1~4 L subsamples from the Niskin bottles were filtered onto 47 mm GF/F Whatman filters and stored at -80 ºC. The pigments will be analyzed with high performance liquid chromatography (HPLC) in the laboratory.

# References


Arrigo, K.R., van Dijken, G., Long, M., 2008. Coastal Southern Ocean: A strong anthropogenic CO2 sink. Geophysical Research Letters 35 (21).

Takahashi, T., Sutherland, S.C., Wanninkhof, R., Sweeney, C., Feely, R.A., Chipman, D.W., Hales, B., Friederich, G., Chavez, F., Sabine, C., 2009. Climatological mean and decadal change in surface ocean pCO 2, and net sea–air CO 2 flux over the global oceans. Deep Sea Research Part II: Topical Studies in Oceanography 56 (8), 554-577.

Tremblay, J.-É., Smith, W., 2007. Primary production and nutrient dynamics in polynyas. Elsevier Oceanography Series 74, 239-269.

Arrigo, K.R., Robinson, D.H., Worthen, D.L., Dunbar, R.B., DiTullio, G.R., VanWoert, M., Lizotte, M.P., 1999. Phytoplankton community structure and the drawdown of nutrients and CO2 in the Southern Ocean. Science 283 (5400), 365-367.

Smith Jr, W.O., Shields, A.R., Peloquin, J.A., Catalano, G., Tozzi, S., Dinniman, M.S., Asper, V.A., 2006. Interannual variations in nutrients, net community production, and biogeochemical cycles in the Ross Sea. Deep-Sea Research Part II: Topical Studies in Oceanography 53 (8-10), 815-833.

Lancelot, C., Mathot, S., Veth, C., de Baar, H., 1993. Factors controlling phytoplankton ice-edge blooms in the marginal ice-zone of the northwestern Weddell Sea during sea ice retreat 1988: field observations and mathematical modelling. Polar Biology 13 (6), 377-387.

Wright, S.W., van den Enden, R.L., Pearce, I., Davidson, A.T., Scott, F.J., Westwood, K.J., 2010. Phytoplankton community structure and stocks in the Southern Ocean (30-80°E) determined by CHEMTAX analysis of HPLC pigment signatures. Deep-Sea Research Part II: Topical Studies in Oceanography 57 (9-10), 758-778.

Arrigo, K.R., van Dijken, G.L., 2003. Phytoplankton dynamics within 37 Antarctic coastal polynya systems. Journal of Geophysical Research: Oceans (1978–2012) 108 (C8).

Rignot, E., Jacobs, S., Mouginot, J., Scheuchl, B., 2013. Ice-shelf melting around Antarctica. Science 341 (6143), 266-270.

Gerringa, L.J.A., Alderkamp, A.C., Laan, P., Thuróczy, C.E., De Baar, H.J.W., Mills, M.M., van Dijken, G.L., Haren, H.V., Arrigo, K.R., 2012. Iron from melting glaciers fuels the phytoplankton blooms in Amundsen Sea (Southern Ocean): Iron biogeochemistry. Deep-Sea Research Part II: Topical Studies in Oceanography 71-76, 16-31.

Taylor, A.G., Landry, M.R., Selph, K.E., Yang, E.J., 2011. Biomass, size structure and depth distributions of the microbial community in the eastern equatorial Pacific. Deep Sea Research Part II: Topical Studies in Oceanography 58 (3), 342-357.

Marie, D., Partensky, F., Jacquet, S., Vaulot, D., 1997. Enumeration and cell cycle analysis of natural

populations of marine picoplankton by flow cytometry using the nucleic acid stain SYBR Green I. Appl. Environ. Microbiol. 63 (1), 186-193.

Sieburth, J.McN., 1978. Pelagic ecosystem structure: Heterotrophic compartments of the plankton and their relationship to plankton size fractions. Limnology and Oceanography, 23: 1256-1263.

# 3.2 Primary production and macromolecular composition of phytoplankton

Dabin Lee and Sang H. Lee

Pusan National University, Korea

## 요약문

식물플랑크톤의 탄소와 질소 섭취율을 알아보기 위해 아문젠해의 18개 정점 (revisit 2정점 포함)에서 13C-15N dual isotope tracer를 이용한 방법을 통해 6개의 light depths (표층 광도의 100, 50, 30, 12, 5, 1%)에서 CTD rosette water sampler를 이용해 얻어진 해수를 자연광 아래에서 4-6시간 배양하였다. 배양이 끝난 즉시 실험실로 옮겨와 25mm GF/F 필터에 여과한 후 냉동보관 (-80℃)하였다. 현장조사가 끝난 후, 시료는 알래스카 대학교 안정동위원소 실험실에 있는 Finnigan Delta+XL mass spectrometer를 이용하여 탄소와 질소 동위원소를 동시에 측정할 예정이다.

## Introduction

The Southern Ocean has low chlorophyll-*a* (chl-*a*) despite high concentration of nutrients in ambient water (Minas et al., 1986), where is low primary production compared to other regions (upwelling, coastal and estuary) on an annual basis. On the other hand, this region is crucial role in air - heat exchange, global deep seawater (such as Antarctic Bottom Water) formation, and efficient biological pump in world's ocean (Siegenthaler and Sarmiento, 1993). The Amundsen Sea is located in the West Antarctic, which is known as one of the most productive polynya with Ross Sea and Ronne Ice Shelf, Prydz Bay and sum of these regions were accounting for over 75 % of total primary production in the Antarctic (Arrigo and van Dijken, 2003). Recently, the West Antarctic was issued region, covered by West Antarctic Ice sheet (WAIS) which has been declining in extent and thinning unlike East Antarctic (Rignot et al., 2008). The primary production has been estimated by satellite observations in the Amundsen Sea (Arrigo et al., 2008; Arrigo et al., 2012), but in situ field data are scarce due to a difficult accessibility caused by sea ice cover (Lee et al., 2012). Therefore, in this study we measured in situ carbon and nitrogen uptake rates to investigate seasonal variations in primary and new productions of phytoplankton in the Amundsen Sea.

## Methods and Materials

To estimate carbon and nitrogen uptake of phytoplankton at different locations, productivity experiments were executed by incubating phytoplankton in the incubators on the deck for 4-6 hours

(Figure 3.2) after stable isotopes ($^{13}C$, $^{15}NO_3$, and $^{15}NH_4$) as tracers were inoculated into each bottle. Total 18 productivity experiments were completed at water column (revisit : 2) station during this cruise (Figure 3.3 and Table 3.1), respectively. At every CTD station, the productivity waters were collected by CTD rosette water samplers at 6 different light depths (100, 50, 30, 12, 5, and 1%). After the incubation, all productivity sample waters were filtered on GF/F (ø = 25 mm) filters for laboratory isotope analysis at University of Alaska Fairbanks after this cruise. For the background data for the productivity stations, water samples were collected for alkalinity, total and size-fractionated (only for 100, 30 and 1% of light depth) chlorophyll-*a* concentrations. In addition, water samples for macromolecular composition of phytoplankton obtained from 3 light depths (100, 30 and 1%) to study the physiological status and nutritional conditions of phytoplankton at selected 19 stations (revisit : 2) in the Amundsen Sea (Fig. 2 and Table. 1).

## References


Arrigo, K.R., Lowry, K.E., and van Dijken, G.L. (2012) Annual changes in sea ice and phytoplankton in polynyas of the Amundsen Sea, Antarctica. Deep Sea Res., Part II, 5: 71-76.

Arrigo, K.R., van Dijken, G.L.(2003) Phytoplankton dynamics within37 Antarctic coastal polynya systems. J. Geophys. Res. 108.doi:10.1029/2002JC001739.

Arrigo, K. R., van Dijken, G. L., and Bushinsky, S. (2008) Primary production in the Southern Ocean, 1997–2006. J. Geophys., Res., 113: DOI: 10.1029/2007JC004551.

Arrigo, K. R., Worthen, D. L. and Robinson, D. H. (2003) A coupled ocean -ecosystem model of the Ross Sea: 2. Iron regulation of phytoplankton taxonomic variability and primary production. J. Geophys. Res., 108 (C7): 3231, doi:10.1029/2001JC000856.

Lee, S.H., Kim, B.K., Yun, M.S., Joo, H.T., Yang, E.J., Kim, Y.N., Shin, H.C., and Lee, S.H. (2012) Spatial distribution of phytoplankton productivity in the Amundsen Sea, Antarctica. Polar Biol., 35: 1721-1733.

Minas, H. J., Minas, M. and Packard, T. T. (1986) Productivity in upwelling areas deduced from hydrographic and chemical fields. Limnol. Oceanogr., 31:71 1182-1206.

Rignot, E., Bamber, J. L., Van den Broeke, M. R., Davis, C., Li, Y. H., van de Berg, W. J. and van Meijgaard, E. (2008) Recent Antarctic ice mass loss from radar interferometry and regional climate modelling. Nat.Geosci., 1 (2): 106-110.

Siegenthaler, U. and Sarmiento, J. L. (1993) Atmospheric carbon dioxide and the ocean. Nature, 365: 119-125.\

Figure 3.2. In situ incubation on deck for 4-6 hours.

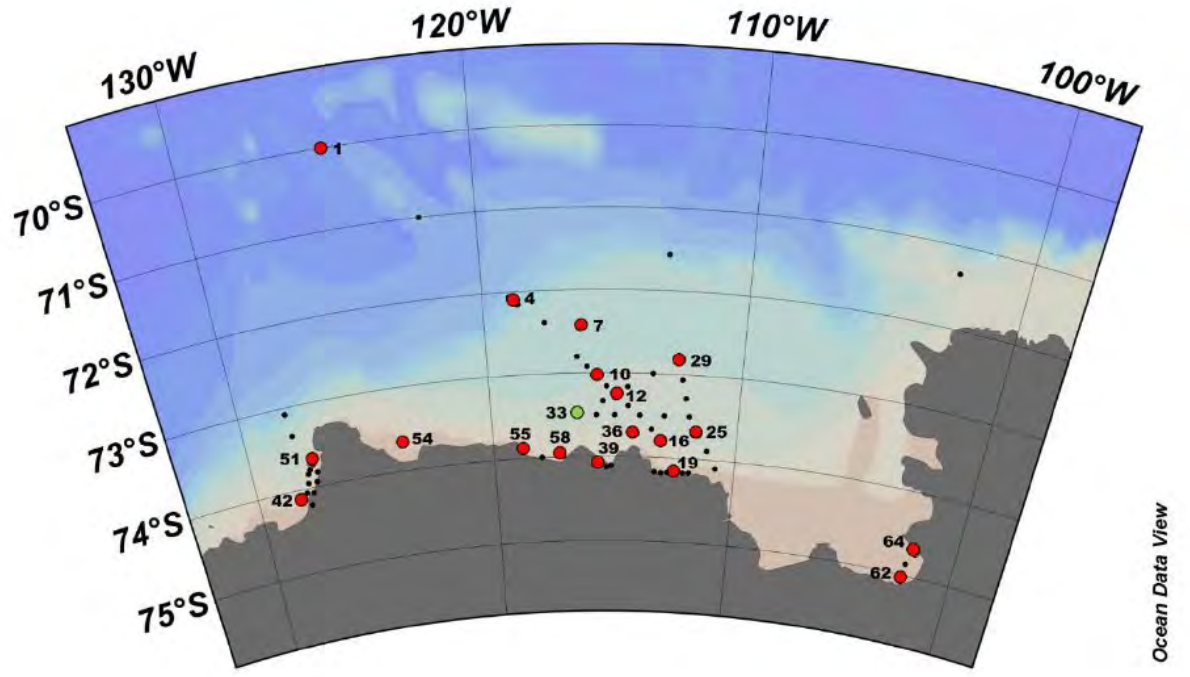


Figure 3.3. Stations for primary production (red circles) and macromolecular composition (green circle) during the 2016 Antarctic cruise.

Table 3.1. Sampling station for primary production and macromolecular composition of phytoplankton during the 2015/2016 Antarctic cruise

| Station | Primary Production | Macromolecular composition | Station | Primary Production | Macromolecular composition |
|---|---|---|---|---|---|
| 1 | o | o | 45 | x | x |
| 2 | x | x | 46 | x | x |
| 3 | x | x | 47 | x | x |
| 4 | o | o | 48 | x | x |
| 5 | x | x | 49 | x | x |
| 6 | x | x | 50 | x | x |
| 7 | o | o | 51 | o | o |
| 8 | x | x | 52 | x | x |
| 9 | x | x | 53 | x | x |
| 10 | o | o | 54 | o | o |
| 11 | x | x | 55 | o | o |
| 12 | o | o | 56 | x | x |
| 13 | x | x | 57 | x | x |
| 14 | x | x | 58 | o | o |
| 15 | x | x | 59 | x | x |
| 16 | o | o | 60 | x | x |
| 17 | x | x | 61 | x | x |
| 18 | x | x | 62 | o | o |
| 19 | o | o | 63 | x | x |
| 20 | x | x | 64 | o | o |
| 21 | x | x | 65 | x | x |
| 22 | x | x | 29 (revisit) | o | o |
| 23 | x | x | 27 (revisit) | x | x |
| 24 | x | x | 66 | x | x |
| 25 | o | o | 14 (revisit) | x | x |
| 26 | x | x | 12 (revisit) | o | o |
| 27 | x | x | 10 (revisit) | x | x |
| 28 | x | x | 8 (revisit) | x | x |
| 29 | o | o | 67 | x | x |
| 30 | x | x | 68 | x | x |
| 31 | x | x | 69 | x | x |
| 32 | x | x | 70 | x | x |
| 33 | x | o | 71 | x | x |
| 34 | x | x | 72 | x | x |
| 35 | x | x | 73 | x | x |
| 36 | o | o | 74 | x | x |
| 37 | x | x | 75 | x | x |
| 38 | x | x | 76 | x | x |
| 39 | o | o | 77 | x | x |
| 40 | x | x | 78 | x | x |
| 41 | x | x | 79 | x | x |
| 42 | o | o | 80 | x | x |
| 43 | x | x | 81 | x | x |
| 44 | x | x | 82 | x | x |

# 3.3 Phytoplankton physiology by photochemistry

Jisoo Park and Eunho Ko

Korea Polar Research Institute, Korea

## 요약문

본 연구항차에서는 식물플랑크톤의 광합성 중 명반응(light reaction)에서 광 에너지를 광화학에너지로 전환하는 양자수율을 측정하기 위해서 Fluorescence Induction and Relaxation system (mini-FIRe)을 사용하였으며, 동시에 선상에서 직접 바다로 In-situ FIRe (Fluorescence Induction and Relaxation)를 수직 투입하여 유광층 내의 식물플랑크톤 전자전달률을 측정하기도 하였다. 또한, 각 수층에서 채수한 해수를 25mm GF/F 여과지에 걸러 식물플랑크톤색소 및 부유물의 흡광계수를 측정하였다. 총 52개 정점 중 아문젠 해역이 44개 정점 (5정점 재방문), Udintsev fracture zone (UFZ) 해역 8개 정점에서 관측을 수행하였다. 식물플랑크톤의 광화학 반응의 양자수율은 모든 정점(수직적으로 6개 수층), 식물플랑크톤 흡광계수는 38개 정점(3개 수층)에서 채수한 해수를 활용하여 분석하였다. In-situ FIRe는 20개 정점 (2정점 재방문)에서 A-frame을 이용하여 자료를 확보하였다. 그리고 또 하나의 mini-FIRe를 활용하여 연구항차 중 선저 펌프로부터 공급되는 표층해수를 이용한 표층 연속관측도 동시에 실시하였다.

## Introduction

To investigate photosynthetic and physiological characteristics of phytoplankton in the Amundsen Sea, we measured photochemical efficiency (quantum yield), electron transport rate (through Photosystem II) by using mini-FIRe and In-situ FIRe (Fiugre 3.4). The basic principle for assessment of active fluorometry relies on the measurement and analysis of chlorophyll “variable fluorescence” profiles (Falkowski et al, 2004). The advantage of this method is sensitive, fast and non-destructive, and it has been used to monitor variations in the photochemistry (Kolber and Falkowski 1993; Falkowski and Kolber 1995). Through the FIRe technology, we can understand physiological condition of phytoplankton affected on nutrient limitation (ex. iron) and estimate primary production in the Amundsen Sea (polynya center, front of ice shelf).

## Work at sea

We collected water sample (6 depths) by Niskin bottles at total 52 stations (revisited 5 stations) that included ice margin, Amundsen polynya, and UFZ (Udintsev fracture zone). Before we measured water samples, the lab were kept under *in situ* temperature. After 30 minutes deem light adaptation, we measured chlorophyll *a* fluorescence by mini-FIRe. Chlorophyll a fluorescence mainly arises from PSII reaction centers are in the open state (with Qa oxidized), the fluorescence yield is minimal, Fo. When the Qa is reduced, the reaction centers are closed and the fluorescence yield increases to its maximum level, Fm. Quantum efficiency of photochemistry in PSII (Fv/Fm) was calculated as a ratio of variable fluorescence (Fv=Fm-Fo) to the maximum one (Fm). The rate of fluorescence induction is proportional to the functional absorption cross section of PSII, $\sigma_{PSII}$. Because of background fluorescence (Dissolved organic matter and dissolved degradation products in water), water sample was corrected from blank sample that was filtered by 0.2 μm syringe filter set. In the FIRe instrument, fluorescence is basically excited by radiation from blue (450nm) light-emitting diodes and recorded in

the red spectral region (680nm). However, in this cruise, we added new program (FCOLOR.exe) to mini-FIRe. By using this program, we measured fluorescence excited by radiation from five spectrums (450, 470, 500, 530, 590nm). Consequently, we estimated phytoplankton absorption from water samples at total 38 stations. Water samples (200 ~ 2000 mL) were filtered by 25mm GF/F. After filtering water sample, we measured phytoplankton absorption from filter paper by spectrophotometer (Cary-100, Agilent Technologies). As comparing primary production with electron transfer rate in the euphotic depth, we have casted In-situ FIRe at total 20 stations (revisited 2 stations). We also observed photosynthetic parameters using pumped seawater through a flow-through cuvette of the fluorometer (another mini-FIRe) in the laboratory during the cruise and ARAON transit from Incheon to the Amundsen Sea.

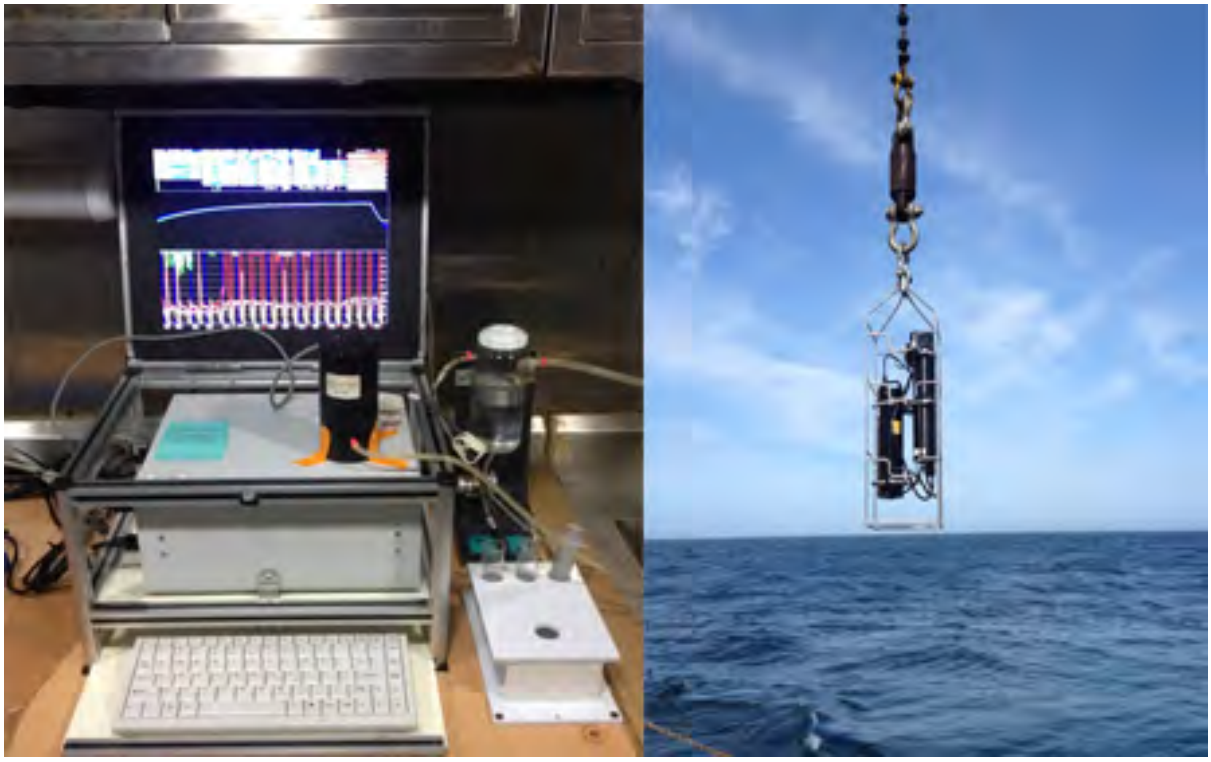

Figure 3.4. Mini-Fluorescence Induction and Relaxation System (Left), In-situ FIRe (Right).

## Preliminary results

The Amundsen polynya is usually surrounded by sea ice in summer. However, it was widely extended and connects with open sea in this year. Quantum efficiency of photochemistry (Fv/Fm) was higher in the center of polynya, in front of Dotson ice shelf than in the edge of polynya and Getz ice shelf (Figure 3.5). This is comparable from the last cruise (13/14 Amundsen cruise). As the previous study, minimum florescence (Fo) was significantly correlated with chlorophyll *a* concentration. Minimum florescence was high around 23 – 29 stations because the phytoplankton biomass was higher than other stations (Figure 3.6). Figure 3.7 shows the absorption coefficients of phytoplankton (Aph) at 470 nm in the station 12 and station 29, respectively. This represents accessory pigments were different (probably dominant species were different) between the stations. The implications are discussed after looking at other environmental parameters such as nutrient concentrations, iron concentrations, and DOC with chlorophyll *a* concentrations. The Fv/Fm values were higher in the Amundsen Sea than in the regions from New Zealand to Amundsen Sea transit (Figure 3.8).

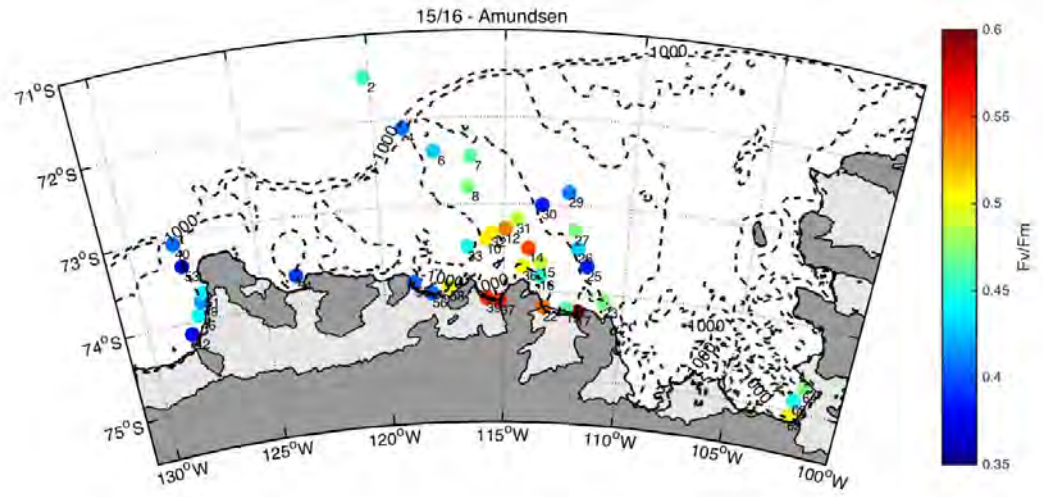


Figure 3.5. Quantum efficiency of photochemistry (Fv/Fm) in the Amundsen Sea.

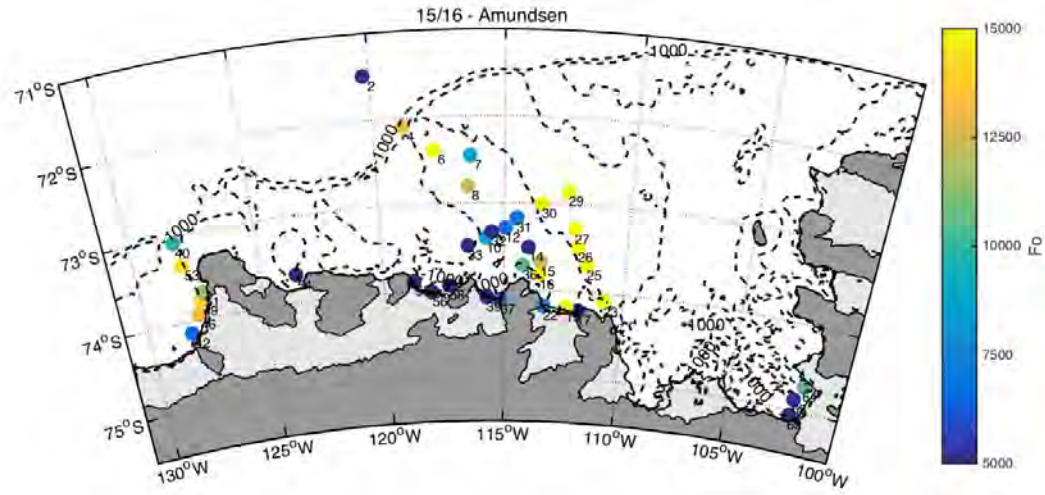


Figure 3.6. Minimal fluorescence (Fo) in the Amundsen Sea.

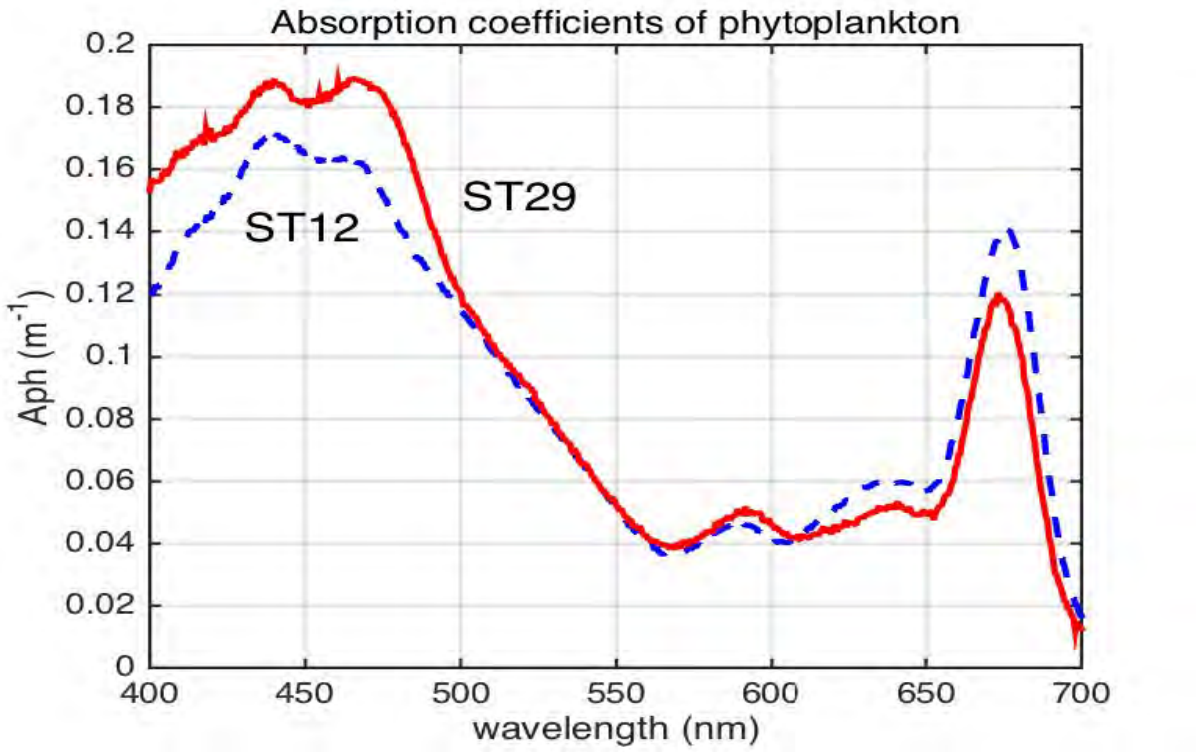


Figure 3.7. Surface absorption coefficients of phytoplankton at 12, 29 stations.

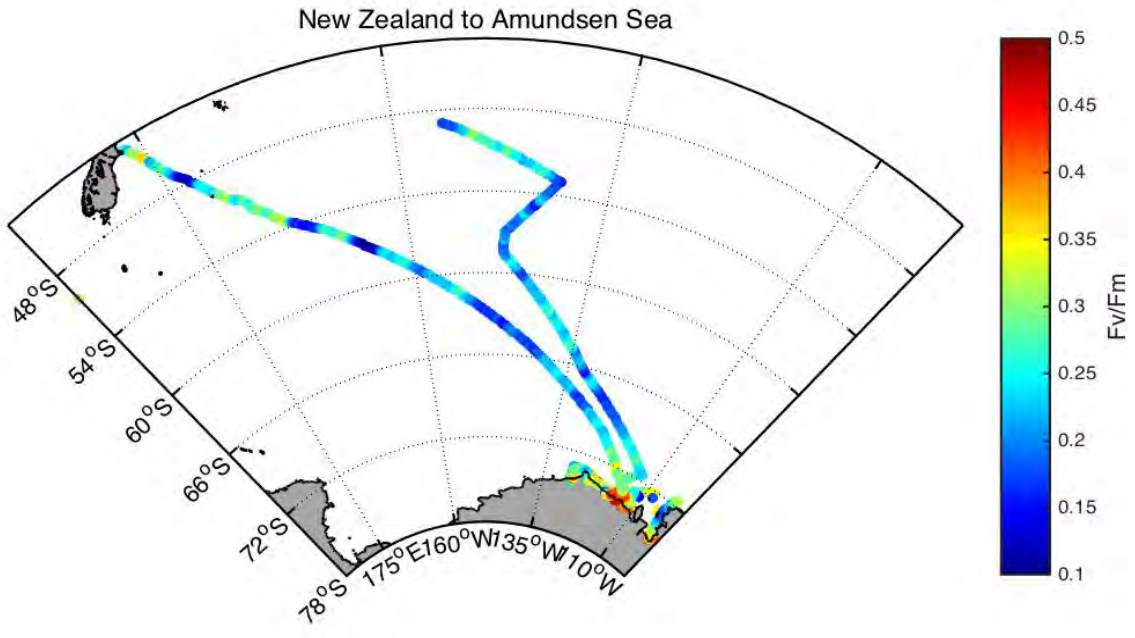


Figure 3.8. Underway measured surface quantum efficiencies of photochemistry (Fv/Fm) by mini-FIRe.

## References

Falkowski, P. G. and Z. Kolber (1995). "Variations in chlorophyll fluorescence yields in phytoplankton in the world oceans." Aust. J. Plant Physiol. 22(2): 341-355.

Falkowski, P. G. and Kobizek M., Gorbunov M, and Kolber Z., (2004) “Development and application of variable chlorophyll fluorescence techniques in marine ecosystems : chlorophyll a fluorescence: A signature of photosynthesis” Springer. 757-778.

Kolber, Z. and P. G. Falkowski (1993). "Use of active fluorescence to estimate phytoplankton photosynthesis in situ." Limnol. Oceanogr. 38(8): 1646-1665.

# 3.4 Abundance and distribution of mesozooplankton

Hyoung Sul La

Korea Polar Research Institute, Korea

## 요약문

중형동물플랑크톤은 남극 해양생태계의 하위 영양단계와 상위 영양단계를 연결하는 주요 연결 고리이다. 이에 아문젠해역에 서식하는 중형동물플랑크톤의 공간 분포를 정량적으로 파악하고 해양환경 인자 (수온, 염분, 엽록소, 해빙 등)와의 비교를 통해서 중형동물플랑크톤의 생태계 특성을 이해하는 것이 필수적이다. 본 연구에서는 중형동물플랑크톤 분포를 파악하기 위해서 35개 정점에서 봉고네트와 사각네트를 이용하여 샘플을 채집하였다. 향후 중형동물플랑크톤의 지역별 군집 특성과 군집 분포에 영향을 미치는 주요 해양환경 인자를 파악할 예정이다.

## Introduction

Coastal Polynya, an area of open water surrounded by sea ice, is an important part of the coastal system in the Southern Ocean. Mesozooplankton taxon in Southern Ocean believed to play key roles in the planktonic food web consuming organic energy produced by primary producers and as energy linker to the higher trophic levels.The Amundsen Seas is one of the most productive areas of the Southern Ocean (Fragoso and Smith, 2012), with annual primary production reaching up to 160 g C $m^{-2}$ and chlorophyll concentrations exceeding >10 μg $l^{-1}$ (Arrigo and van Djiken, 2003). Little is known about the abundance and community of zooplankton throughout the Amundsen Sea, because most biological investigations have focused on other trophic levels. Also, despite the numerical importance of mesozooplankton community, little studies have been conducted on their feeding ecology in the Amundsen Sea.

In this study the main goals are to quantify the mesozooplankton community and understand interactions among the environmental factors (i.e. seawater temperature, salinity and chlorophyll a concentration), protozoa and mesozooplankton community in the polynya and non-polynya area according to different water masses.

## Materials and methods

Zooplankton samples were collected with a Bongo net (330 and 505 μm mesh) and rectangular net with a 1 $m^{-2}$ opening (330 μm mesh) at 35 selected stations (Figure 3.9 and Table 3.2). Twenty-three Bongo net was towed vertically within the upper 200 m of water column. 330 μm mesh samples were immediately fixed and preserved with buffered formaldehyde (pH 8, final concentration ca. 5%) for quantitative analyses while the samples from 505 μm mesh was preserved in alcohol and frozen in -80ºC.

The thirteen rectangular nets in 400m oblique trawls were used to characterise the mesozooplankton community around Amundsen Sea. The wire-up speed was 30 m $min^{-1}$ and ship speed was about 1.5-2 knots for about 1 hours. The some of copepod and ice krill were taken and frozen in -80 ºC for separate analysis. The remaining samples were split using a Folsom plankton splitter as follows: 1/2 of each tow was split and preserved in alcohol and archived in -80ºC and ½ was preserved in 10% buffered formalin for taxonomic identification.

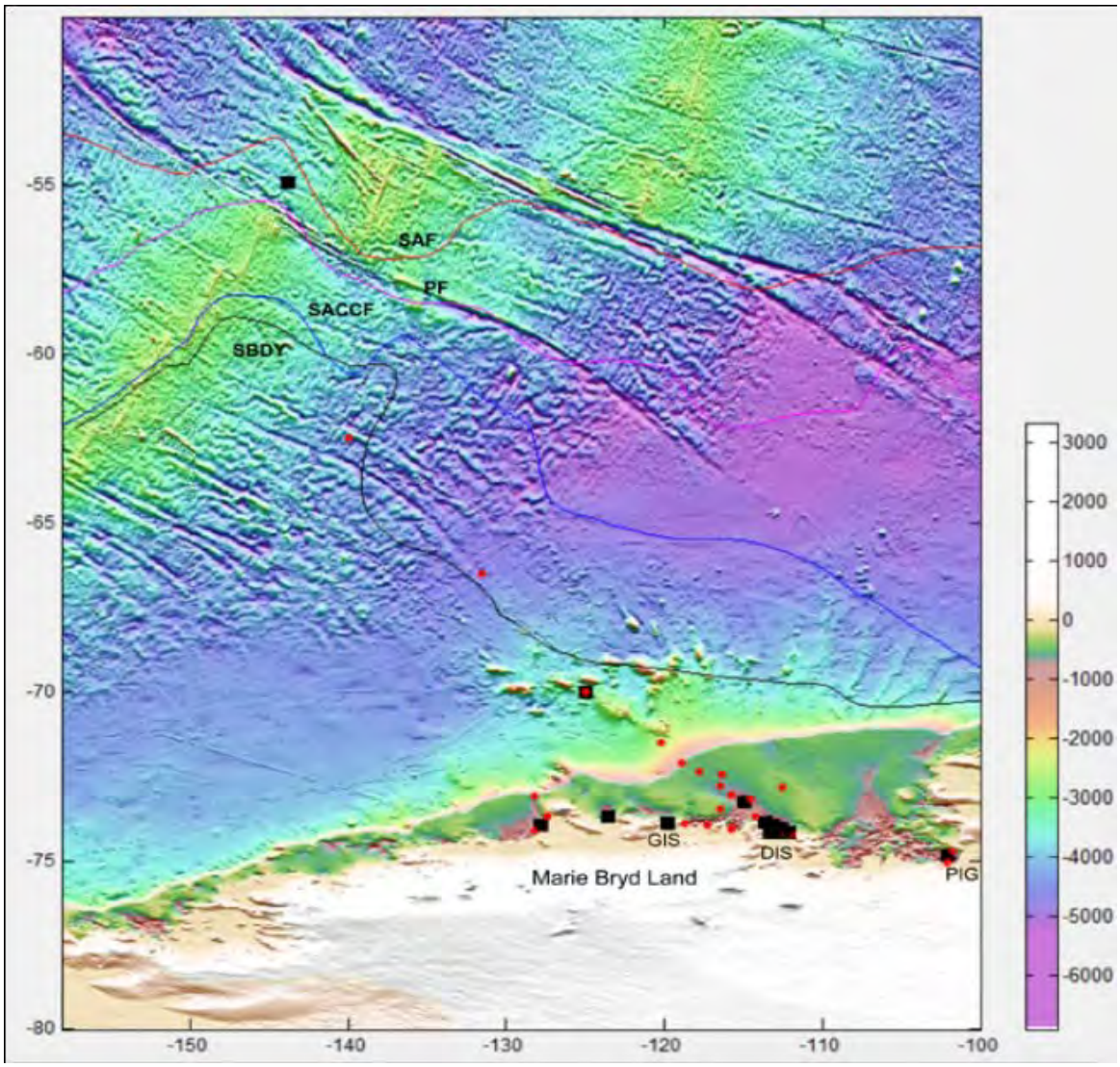


Figure 3.9. Mesozooplankton stations during ANA06B. Red dots and black squares represent Bongo and rectangular net sampling stations, respectively.

Table 3.2. Net information

| Station number | Date (yyyymmdd) | Time Start (UTC) | Event number | Latitude (S) | Longitude (W) |
|---|---|---|---|---|---|
| 1 | 20160114 | 19:00 | B1 | 70.0000 | 125.0000 |
| 2 | 20160115 | 13:50 | B2 | 71.4900 | 120.2500 |
| 4 | 20160115 | 4:30 | B3 | 72.1004 | 118.8783 |
| 6 | 20160116 | 16:15 | B4 | 72.3800 | 117.7500 |
| 6 | 20160116 | 16:30 | B4 | 72.3800 | 117.7500 |
| 7 | 20160117 | 5:00 | B5 | 72.4548 | 116.3523 |
| 10 | 20160117 | 18:50 | B6 | 73.0400 | 115.7250 |
| 12 | 20160118 | 7:50 | B7 | 73.2798 | 114.9504 |
| 12 | 20160118 | 12:55 | R1 | 73.2806 | 114.9281 |
| 17 | 20160119 | 7:50 | B8 | 74.2150 | 111.8923 |
| 18 | 20160119 | 15:34 | R2 | 74.1750 | 112.1454 |
| 19 | 20160119 | 23:00 | B9 | 74.1715 | 112.5283 |
| 21 | 20160120 | 9:15 | R3 | 74.1799 | 113.0688 |
| 22 | 20160121 | 2:14 | B10 | 74.1718 | 113.3285 |
| T1 | 20160121 | 16:48 | R4 | 74.1409 | 112.6502 |
| T2 | 20160121 | 13:30 | R5 | 73.8749 | 113.6576 |
| T3 | 20160121 | 16:17 | R6 | 73.9610 | 113.1717 |
| T4 | 20160121 | 20:43 | R7 | 74.0398 | 112.6658 |
| 29 | 20160123 | 8:22 | B11 | 72.8500 | 112.5000 |
| 31 | 20160124 | 3:00 | B12 | 73.1666 | 114.4996 |
| 33 | 20160124 | 12:20 | B13 | 73.5000 | 116.5000 |
| 36 | 20160125 | 0:05 | B14 | 73.7114 | 114.2155 |
| 39 | 20160125 | 15:20 | B15 | 74.0794 | 115.7230 |
| 40 | 20160126 | 20:00 | B16 | 73.0769 | 128.1838 |
| 42 | 20160127 | 21:20 | B17 | 74.1380 | 128.2140 |
| 46 | 20160128 | 8:55 | B18 | 73.9401 | 127.7995 |
| 46 | 20160128 | 9:52 | R8 | 73.9401 | 127.7995 |
| 51 | 20160129 | 3:30 | B19 | 73.6901 | 127.4496 |
| 54 | 20160129 | 22:00 | B20 | 73.6855 | 123.5841 |
| 54 | 20160130 | 3:46 | R9 | 73.6812 | 123.5964 |
| 55 | 20160130 | 17:45 | B21 | 73.8895 | 118.7272 |
| 56 | 20160131 | 2:22 | R10 | 74.0137 | 118.0179 |
| 58 | 20160131 | 12:35 | B22 | 73.9417 | 117.2875 |
| 62 | 20160202 | 16:05 | B23 | 75.0589 | 102.1190 |
| 62 | 20160202 | 16:25 | B23-2 | 75.0589 | 102.1190 |
| 63 | 20160203 | 6:09 | R11 | 74.8536 | 102.0998 |
| 64 | 20160203 | 9:45 | B24 | 74.7067 | 101.7619 |
| 29-Re | 20160206 | 1:45 | B25 | 72.8500 | 112.5000 |
| 12-Re | 20160206 | 20:45 | B26 | 73.2798 | 114.9504 |
| 12-Re | 20160206 | 23:39 | R12 | 74.2757 | 114.9558 |
| 8-Re | 20160207 | 5:45 | B27 | 72.8000 | 116.5000 |
| 68 | 20160209 | 22:35 | B28 | 66.5000 | 131.5997 |
| 69 | 20160211 | 13:35 | B29 | 62.5000 | 140.0000 |
| 77 | 20160215 | 8:07 | R13 | 54.9204 | 143.8354 |

## References

Arrigo KR, van Dijken GL (2003) Phytoplankton dynamics within 37 Antarctic coastal polynyas. J Geophy Res 108: doi:10.1029/2002JC001739.

Fragoso GM, Smith WO (2012) Influence of hydrography on phytoplankton distribution in the Amundsen and Ross Seas, Antarctica. J Mar Syst 89:19-29.

# 3.5 Acoustics

Hyoung Sul La

Korea Polar Research Institute, Korea

### 요약문

남극 아문젠해 도슨 빙붕 (Dotson ice shelf) 주위에 서식하는 중대형 동물플랑크톤의 분포를 파악하기 위해서 음향조사를 실시하였다. 음향시스템은 아라온에 설치된 과학 음향탐지기 (scientific echo sounder) EK60을 사용하였으며 3개의 주파수 (38, 120, and 200 kHz)를 이용하여 표층에서 수심 1000 m 까지 데이터를 수신하였다. 선속은 음향자료의 안정성을 고려하여 7-10 노트로 일정하게 유지하였다. 사각네트를 이용한 사선채집을 통해 음향 산란층 내의 중대형 동물플랑크톤을 채집하였으며 채집된 샘플은 현정에서 길이 (body length) 분포를 측정하였다. 채집된 아이이스 크릴은 최소 7 mm 에서 최대 29 mm 의 범위에서 평균길이 16.4 mm (표준편차: 4.34) 로 측정되었다.

## Introduction

The coastal polynya in the Southern Ocean is noted for sustaining enhanced levels of biological production and biogeochemical activity during because they are the first polar marine systems to be exposed to the increasing solar radiation during spring and summer (Arrigo, 2003). The coastal polynya is considered significant regions not only for the primary production but also zooplankton because highly deformed ice with many ridges provides a favorable habitat for zooplankton.

The Amundsen Sea coastal polynya is also well known for the rapid sea ice retreat (Jacobs and Comiso, 1997), as well as one of the most productive areas among 37 coastal polynyas in the Southern Ocean. It is responsible for >75% of total production in Antarctica (Arrigo, 2003). While a few biological investigations have conducted, little is known about the abundance and distribution of zooplankton throughout the Amundsen Sea because it is one of the most remote and least known continental shelf regions of the Southern Ocean (Jones, 1982).

The EK60 was run throughout ANA06B to collect information on the horizontal and vertical distribution of zooplankton and to derive estimates of zooplankton distribution in the Amundsen Sea. The overall purposes of acoustic observation are to collect acoustic data to accompany all stations and transects, acoustic surveys, and net tows during the Amundsen Sea survey.

## Acoustic transects

Simrad ER60 v.2.2.0 was used for ER60.raw data files, which were logged to extra hard drive using a USB cable. All raw data were collected to 1000 m and Echolog was run on the EK60 workstation. All raw data were saved in a general folder ANA06B/raw, all echolog data were saved in the folder ANA06B/data/EK60. All files were prefixed with ana06b. Calibration data were not additionally saved because calibration was not properly conducted during the cruise. The EK60 was run initially using default settings, although the environmental settings were updated at the start of the cruise to a temperature of and salinity of these resulted in new settings for c and alpha. The transducer settings were reset to default and the gain settings setup with the last measured values during ANA02B. The EK60 was calibrated on the January 2012, and the calibration variables were applied to the all transducers (Table 3.3).

Acoustic data were collected using a multi-frequency echo sounder (EK60, Simrad) configured with down-looking 38, 120, and 200 kHz split-beam transducers mounted in the hull of the IBRV Araon. Because of stability of the acoustic data, confined data with ship speed below 10 knots were used. In order to avoid any signal interference with other acoustic systems, other acoustic equipment such as ADCP and EM122 were turned off during the entire running time.

Post processing will be followed using virtual echogram (Myriax, Echoview software). The raw acoustic data will convert to raw volume backscattering strengths (SV) binned into mean SV cells with an interval of 0.1 nautical mile (nmi) horizontal distance and a width of 1-m depth. The data will threshold to 85 dB at three frequencies. The contribution of other zooplankton such as copepod and amphipod could be negligible because of their low densities and low mean target strength. For example, target strength is about 103 dB for a 2-3 mm long copepod at 120 kHz (Stanton and Chu, 2000). During the cruse the acoustic survey was run in a north to south direction starting at the Northern end around Dotson Ice Shelf (Figure 3.10 and Table 3.4).

Table 3.3. System parameters of transceiver for acoustic survey

| Variable | 38 kHz | 120 kHz | 200 kHz |
|---|---|---|---|
| Ping interval (per sec) | 1.2 | 1.2 | 1.2 |
| Sound velocity (m/s) | 1450 | 1450 | 1450 |
| Mode | Active | Active | Active |
| Transducer type | ES38B | ES120-7C | ES200-7C |
| Transceiver Serial no. | 00907205b607 | 00907205f07a | 00907205f085 |
| Transducer depth (m) | 7 | 7 | 7 |
| Absorption coef. (dB/km) | 9.70 | 24.80 | 38.60 |
| Pulse length (ms) | 1.024 | 1.024 | 1.024 |
| Max Power (W) | 2000 | 500 | 300 |
| 2-way beam angle (dB) | -20.70 | -21.00 | -20.70 |
| Sv transducer gain (dB) | 22.48 | 26.63 | 25.37 |
| Sa correction (dB) | -0.41 | -0.33 | -0.29 |
| Angle sensitivity along | 21.90 | 23 | 23 |
| Angle sensitivity athwart | 21.90 | 23 | 23 |
| 3 dB Beam along | 7.03 | 6.51 | 6.57 |
| 3 dB Beam athwart | 7.05 | 6.58 | 6.45 |
| Along offset | 0.01 | 0.00 | -0.05 |
| Athwart offset | 0.06 | 0.01 | -0.02 |

Table 3.4. Acoustics transect date, time, and distance

| Transect | Date (MM/DD/YYY) | Start time (UTC) | End time (UTC) | Distance (nmile) |
|---|---|---|---|---|
| AT.1 | 01/21/2016 | 11:53 | 14:23 | 13.3 |
| AT.2 | 01/21/2016 | 14:23 | 15:27 | 8.0 |
| AT.3 | 01/21/2016 | 15:27 | 18:24 | 14.6 |
| AT.4 | 01/21/2016 | 18:24 | 19:30 | 7.0 |
| AT.5 | 01/21/2016 | 19:30 | 22:55 | 16.3 |
| AT.6 | 01/21/2016 | 22:55 | 23:42 | 5.8 |
| AT.7 | 01/22/2016 | 23:42 | 02:10 | 18.6 |

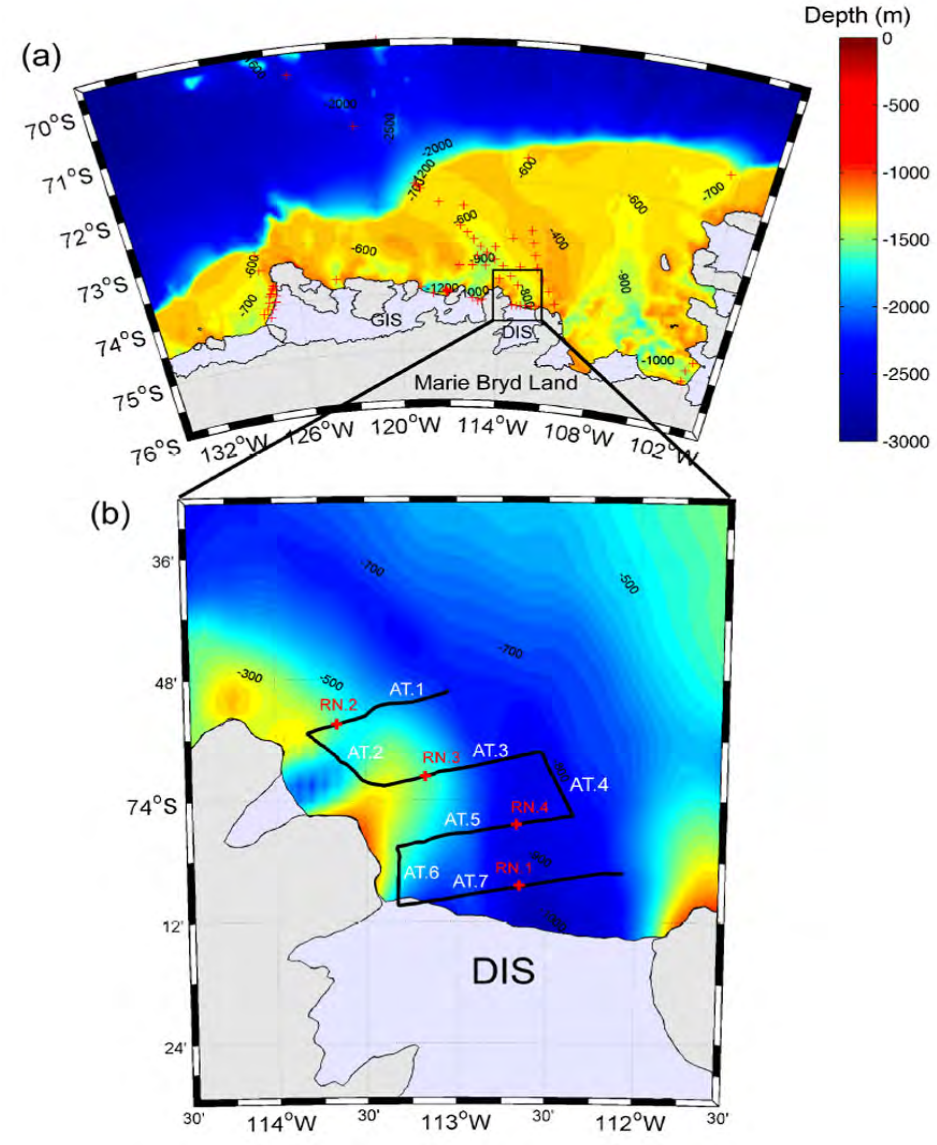


Figure 3.10. (a) Study area on the bathymetry of Amundsen Sea showing the locations of conductivity-temperature-depth (CTD) (red cross) (b) Study area on the bathymetry around Dotson ice shelf showing the acoustic transects (black line) and the locations of oblique tow with rectangular net (red cross).

## Krill length frequency

Ice krill (*Euphausia crystallorophias*) were sampled to determine the variation in the structure of the population around Dotson ice shelf and to provide parameters required in the target strength model for krill biomass estimation.

Ice krill samples were taken from oblique tow (surface to 400 m) samples using a rectangular net (1 $m^{-2}$ mouth area, 330 μm mesh) where there were sufficient numbers of krill to select 100 decent state specimens for length frequency (Figure 3.10 and Table 3.5). Four times tows were conducted at a speed of 2-3 knots for about 1-h period. Weather conditions were good during the all sets of transects and the four times oblique tows. Krill total length was measured from the anterior edge of the eye to the tip of the telson, with measurements rounded down to the nearest millimetre. The ice krill length frequency for the whole net tows are shown in Figure 3.11. The mean length of ice krill was 16.4 mm (SD=4.34 mm) and varied from 7 to 29 mm.

Table 3.5. Rectangular nets date, time, and location

| Nets | Date (MM/DD/YYY) | Start time (UTC) | Latitude (S) | Longitude (W) |
|---|---|---|---|---|
| RN.1 | 01/21/2016 | 16:48 | -74.140267 | -112.593778 |
| RN.2 | 01/21/2016 | 13:30 | -73.876268 | -113.673788 |
| RN.3 | 01/21/2016 | 16:17 | -73.961280 | -113.171648 |
| RN.4 | 01/21/2016 | 20:43 | -74.038622 | -112.667312 |

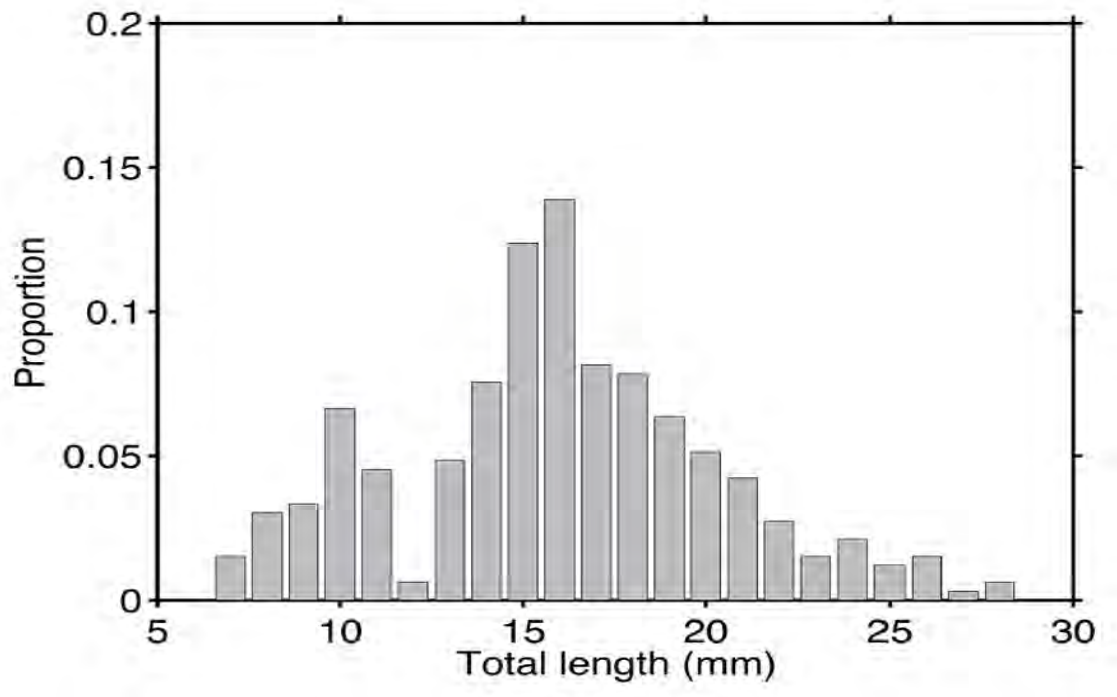


Figure 3.11. Length-frequency distribution of ice krill (Mean length: 16.4 (SD:4.34), N=400).

## Problems encountered

Interference from other acoustic instruments was continuously generated as the sync unit was not properly working to synchronise the ADCP and EM122. The sync unit has kept instruments (ADCP and EM122) into standby even if it does give the signals to work on them. As a result, we disable to use the sync unit to minimize the interference from other scientific instruments all triggering.

## References

Arrigo, K.R., and van Dijken, G.L., 2003. Phytoplnkton dynamics within 37 Antarctic coastal polynya systems. Journal of Geophysical Research 108: 3271

Jacobs, S.S., and Comiso, J.C. 1997. A climate anomaly in the Amundsen and Bellingshausen Seas. J. Climate, 10: 697-711.

Jones, A.G.E. 1982. Antarctica Observed. Caedmon of Whitby, Yorkshire, UK. 118 pp.

Stanton, T.K. and Chu, D. 2000. Review and recommendations for the modelling of acoustic scattering by fluid-like elongated zooplankton: euphausiids and copepods. ICES J. Mar. Sci., 57 (4): 793-807.

# 3.6 Grazing impacts and community structure of heterotrophic protists

Eun-Jin Yang and Seungjun Lee

Korea Polar Research Institute, Incheon, 21990, Korea (ejyang@kopri.re.kr)

### 요약문

아문젠해와 Udintsev fracture zone (UFZ) 해역에서 2016년 1월에 원생동물의 생물량, 군집구조, 식물플랑크톤 및 박테리아에 대한 섭식률 실험을 총 35개 정점에서 수행하였다. 원생동물의 생물량 분포 및 군집구조 분석은 현장에서 고정하여 실험실로 가져간 후 분석될 예정이다. 또한 해수희석법을 이용하여 측정한 식물플랑크톤과 박테리아에 대한 섭식률 측정은 2010/11년 자료와 비교하여 분석될 예정이다.

## Background study

Heterotrophic protists ingest a broad size spectrum of prey, from bacteria to microphytoplankton, and are themselves important prey items for mesozooplankton. Many researches suggest that heterotrophic protists contribute to the trophic linkage between phytoplankton and mesozooplankton and are important in the pelagic food webs of many oceanic waters. The importance of heterotrophic protists in pelagic ecosystems has become increasingly evident in the past two decades, and trophic interaction between heterotrophic protists and phytoplankton has been reported in various marine. Studies of protozooplankton in the Southern Ocean have emphasized the importance of protozooplankton in microbial communities and their role as major consumers of phytoplankton (Burkill et al., 1995; Froneman and Perissinotto, 1996; Landry et al., 2001; Pearce et al., 2011; Safi et

al., 2007; Selph et al., 2001). Overall, previous research has suggested that knowledge of the structure of the microbial community and protozoan grazing impacts, is central to developing an understanding of carbon flux in the Southern Ocean. However, comprehensive studies on protozooplankton assemblages have been generally limited to the Weddell Sea, Bellingshausen Sea, and the Atlantic and Indian sectors of the Southern Ocean, particularly the marginal ice-edge zone (Froneman et al., 2004; Klass, 1997; Safi et al., 2007). There is no information on the relative importance of heterotrophic protists in the pelagic ecosystem of the Amundsen Sea. The Amundsen Sea, which is historically known as a region of heavy ice, is undergoing sea ice recession within the last decades (Jacobs and Comiso, 1993), and extensive phytoplankton blooms near the coast have been observed (Smith and Comiso,2008). In this study area, we investigated the meso-scale variations and structure of heterotrophic protist communities and grazing rates on phytoplankton in the various environmental conditions such as sea ice zone, polynya, and ice shelves. During this cruise, we investigated protozoa abundance, biomass and grazing rate in total 35 stations. This data will be compared to ANA01 data set.

## Work at Sea

Abundance and community composition of heterotrophic protists

This study was conducted total 35 stations (Figure 3.12). To determine the abundance of heterotrophic protists, a CTD-Niskin rosette sampler was used to take water samples from 4 depths in the upper 100m and 3~6 depths in the deeper 100m. For ciliates and sarcodina, 1,000 ml water from the vertical profiles was preserved with 1% acid Lugol's iodine solution these samples were then stored in darkness. For heterotrophic nanoflagellates and heterotrophic dinoflagellates smaller than 20 $\mu$m, 500 ml of water was preserved with glutaraldehyde (0.5% final concentration) and stored at 4° C.

Grazing experiments

Grazing rates of heterotrophic protists were determined by the dilution method (Landry and Hassett 1982). Water for grazing experiments was collected from 3~5 depth of each station, and gently filtered through a 200-$\mu$m mesh. At each station, 50L seawater were collected in a Niskin bottle and transferred to a polycarbonate carboy. Part of this water was filtered through the 0.22-$\mu$m filtration system. Dilution series were set up in ten 1.3-l PC bottles. Ten bottles were used to establish a nutrient-enriched dilution series consisting of replicate bottles with 11, 28, 50, 75, and 100% natural seawater. The bottles were incubated on deck for 24 – 48 h at ambient sea surface temperatures and screened to the ambient light level with neutral density screening. Subsamples were collected from replicate bottles at 0 and 24-48h to determine chlorophyll-a concentrations and bacterial abundance.

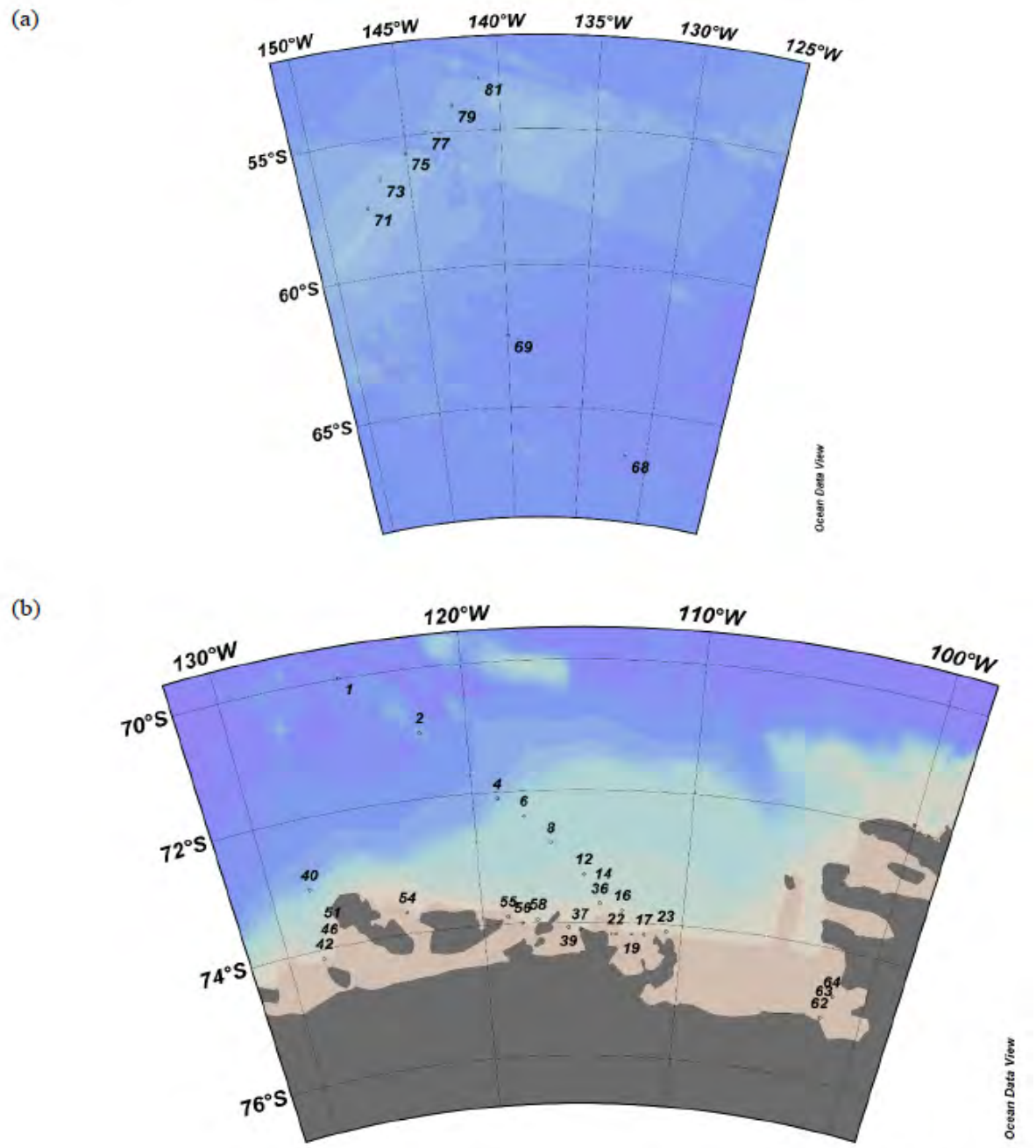


Figure 3.12. The sampling stations of protozoa community and grazing rate in (a) the UFZ and (b) the Amundsen Sea.

## References

Jacobs, S. S., Comiso, J. C. 1993. A recent sea-ice retreat west of the Antarctic Peninsula. Geophysical Research Letters 20: 1171-1174.

Smith, W. O. Jr., Comiso, J. C. 2008. Influence of sea ice on primary production in the Southern Ocean: a satellite perspective. Journal of Geophysical Research 113 doi:10.1029/2007JC004251.

Pearce, I., Davidson, A.T., Thomson, P.G., Wright, S., van den Enden, R., 2011. Marine microbial

ecology in the sub-Antarctic Zone: Rate of bacterial and phytoplankton growth and grazing by heterotrophic protists. Deep-Sea Res. Part II. 58, 2248-2259.

Safi, K.A., Griffiths, F.B., Hall, J.A., 2007. Microzooplankton composition, biomass and grazing rates along the WOCE SR3 line between Tasmania and Antarctica. Deep-Sea Res. Part I. 54, 1025-1041.

Selph, K.E., Landry, M.R., Allen, C.B., Calbet, A., Christiansen, S., Bidigare, R.R., 2001. Microbial community composition and growth dynamics in the Antarctic Polar Front and seasonal ice zone during late spring 1997. Deep-Sea Res. Part II. 48, 4059-4080.

Landry, M.R., Brown, S.L., Selph, K.E., Abbott, M.R., Letelier, R.M., Christensen, S., Bidigare, R.R., Casciotti, K., 2001. Initiation of the spring phytoplankton increase in the Antarctic Polar Front Zone at 170°W. J. Geophys. Res. 106(C7), 13,903-13,915.

Froneman, P.W., 2004. Protozooplankton community structure and grazing impact in the eastern Atlantic sector of the Southern Ocean in austral summer 1998. Deep-Sea Res. Part II. 51, 2633-2643.

Landry, M.R., Hassett, R.P., 1982. Estimating the grazing impact of marine microzooplankton. Mar. Biol. 67, 283-288. Froneman, P.W., Perissinotto, R., 1996. Structure and grazing of the microzooplankton communities of the subtropical convergence and a warm core eddy in the Atlantic sector of the Southern Ocean. Mar. Ecol. Prog. Ser. 135, 237-245.

Burkill, P.H., Edwards, E.S., Sleigh, M.A., 1995. Microzooplankton and their role in controlling phytoplankton growth in the marginal ice zone of the Bellingshausen Sea. Deep-Sea Res. Part II. 42, 1277-1299.

# 3.7 Bacterial respiration

Jung-Ho Hyun, Sung-Han Kim, Jun-Oh Min, and Euo-Jung Jung

Department of Marine Sciences and Convergent Technology, Hanyang University, Korea

## 요약문

남극 아문젠해의 아문젠 polynya(AP)의 open sea, marginal sea ice zone, polynya 및 ice-shelf에 위치한 연구정점들에서, 수층의 물리-화학-생물 요인의 변화에 따른 박테리아의 생체량 및 미생물 호흡율 변화양상을 규명하기 위한 연구를 수행하였다. 호흡율은 polynya (3.6-30.2 mmol $m^{-3}d^{-1}$)가 open sea (1.4-2.6 mmol $m^{-3}d^{-1}$), marginal sea ice zone (1.7–11.3 mmol $m^{-3}d^{-1}$) 및 ice shelf (2.2–10.1 mmol $m^{-3}d^{-1}$)에 비해 높은 값을 나타냈다. 이는 아문젠 폴리냐에서 미생물의 호흡이 탄소순환을 조절하는 중요한 생물요인임을 나타내는 것이다. 향후 식물플랑크톤 bloom의 시기에 따른 미생물 요인의 시 계열 분석을 통해, 미생물 호흡이 아문젠 폴리냐의 탄소순환에 미치는 영향 및 아문젠 폴리냐가 남극해의 해양-대기간 탄소순환을 조절하는 역할에 대한 정보가 획득 될 수 있을 것으로 전망된다. 한편, 미생물 생체량 분포 및 미생물 생장조절 요인을 파악하기 위한 다양한 실험들(UV 효과, 생장제한 영양요인 등)을 선택된 연구 정점들에서 추가적으로 실시하였으며, 추후 연구실에서의 분석을 위해 확보된 시료들을 냉장 또는 냉동상태로 보관하였다.

## Background

Respiration represents the transfer of carbon from organic pool to inorganic pool, and reflects the rate of organic matter supply that is available to the biota within the system (Jahnke and Craven, 1995). Long-term shifts in respiration have a potential to provide the best warning system for global change (del Giorgio and Williams, 2005). Therefore, it is particularly important to measure the respiration in polar ocean to better understand any shifts in biogeochemical carbon cycles associated with large-scale climate changes.

## Work at sea

During this cruise, we measured the plankton community respiration rates and bacterial abundance at 4 different sites, polynya, outer shelf, ice-shelf and offshore. Water samples were collected using a Sea-bird Electronics CTD system equipped with specific sensors such as photosynthetically active radiation (PAR) sensor, fluorometer, transmissometer and dissolved oxygen meter. Water samples for bacterial abundance were fixed with glutaraldehyde (final concentration, 1%) and kept in the freezer for cell enumeration in the lab. Respiration rates were measured onboard from the decrease of dissolved oxygen concentration during incubation using a spectrophotometeric-Winkler method (Labasque et al. 2004). Briefly, water samples were taken using 20-l Niskin bottles at 3 – 5 different water depth in the surface layer, and were then transferred into six 300ml BOD bottles (Wheaton Co.) that were washed and rinsed with acid (10% HCl) and distilled water, respectively. The BOD bottles were filled using a silicon tubing inserted almost to the bottom, and overflowed by at least one bottle volume. The BOD bottles were then wrapped with aluminum foil, and incubated for 20 – 25 hours in the dark in incubator through which in situ seawater continuously flowed. At the end of incubation, BOD bottles were immediately fixed by adding 2 ml of manganese chloride solution (3 M) and 2 ml of alkaline iodide reagents (NaOH, 8 M; NaI, 4 M). After being vigorously shaken for about 1 min, the BOD bottles were stored in the dark. When most of the flocculation had settled, the bottles were reopened and 2 ml of sulfuric acid solution (10 M) was added. The mixture was then gently stirred with a magnetic stirrer until all the precipitate had dissolved. Absorbance was measured onboard within 3 min using a Shimadzu UV-1700 spectrophotometer. The spectrophotometric Winkler method has a precision of 0.1% for the onboard measurement. Respiration rates were calculated from the linear regression of time-course measurement of dissolved oxygen concentration with time.

## Preliminary results

Vertical profiles of microbial community respiration measured at offshore, outer shelf (i.e., polynya margin), polynya center and ice shelf sites are presented in Figure 3.13. Respiration rates at polynya (3.6 – 30.2 mmol $m^{-3}$ $d^{-1}$) were higher than those measured at marginal sea ice zone (1.7 – 11.3 mmol $m^{-3}$ $d^{-1}$), iceshelf (2.2 – 10.1 mmol $m^{-3}$ $d^{-1}$) and offshore sites (1.4 – 2.6 mmol $m^{-3}$ $d^{-1}$). Highest community respiration observed at the center of the polynya (30 mmol $m^{-3}$ $d^{-1}$ at St. 12R) at late stage of the bloom. The results indicated that time series investigation on the community respiration according to the bloom stage may provide certain information on the biogeochemical C cycles associated with microbiological process and on the role of the Amundsen polynya as either C sink or source for atmospheric $CO_2$. Other parameters associated with the community respiration such as bacterial abundance, DOC and cDOM will be presented after completing further analyses in the lab.

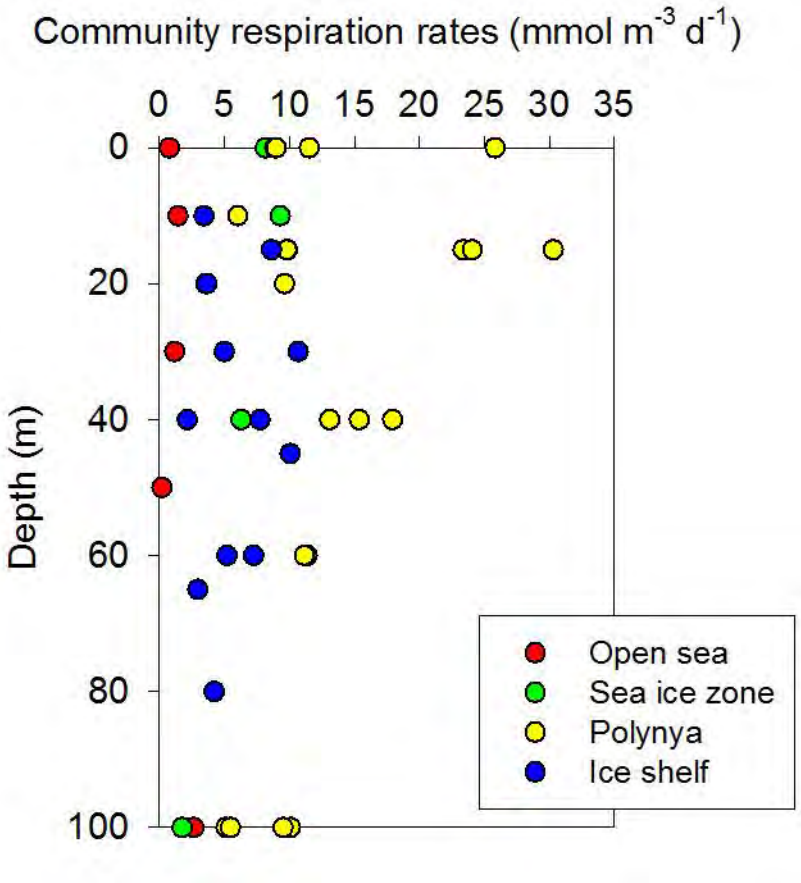


Figure 3.13. Vertical profiles of microbial community respiration rates measured at open sea, sea-ice zone, polynya and ice-shelf sites. Note that respiration rates were highest at polynya.

## References

del Giorgio, P. A. and Williams, P. J. le B., 2005. The global significance of respiration in aquatic ecosystems: from single cells to the biosphere. In: P.A. del Giorgio and P. J. le B. Williams (eds) respiration in aquatic ecosystems. Oxford University Press, New York, pp. 267-303.

Jahnke, R. A. and Craven, D. B., 1995. Quantifying the role of heterotrophic bacteria in the carbon cycle: a need for respiration rate measurements. Limnology and Oceanography. 40: 436-441.

Labasque, T., Chaumery, C., Aminot, A., and Kergoat, G., 2004. Spectrophotometric Winkler determination of dissolved oxygen:re-examination of critical factors and reliability, Marine Chemistry, 88, 53-60

# 3.8 Metagenome and production of virus

Yeonju Hwang

Korea Polar Research Institute, Incheon 406-840, Korea

## 요약문

박테리아와 바이러스를 포함한 해양 미생물들은 전 지구상에 가장 풍부하게 존재하며, 해양환경의 생지화학적 순환에 중요한 역할을 하고 있다. 해양 미생물(본문에서는 박테리아와 바이러스를 지칭하는 말로 사용.)은 해수면의 microlayer 부터 시작해서 심해에 이르기까지 해양 생태의 도처에 존재한다. 본 탐사에서는 아문젠해 폴리냐 및 인근 해역에 출현하는 박테리아와 바이러스의 개체수와 바이러스의 생산력을 측정하여 연구 해역의 미생물 먹이망(microbial loop) 특성을 보다 자세하게 이해하고자 하였다. 또한 획득된 박테리아, 바이러스 메타게놈자료를 통해 높은 일차 생산력을 보이는 남극 폴리냐의 박테리아 및 바이러스의 군집 구조를 밝히고자 한다.

## Abstract

Marine microbes including bacteria and viruses are the most abundant organisms on the planet and play vital roles in the biogeochemical cycle in marine environments. Marine microbes also exist in diverse environments extending from sea surface microlayer to deep sea. In this cruise, abundances of total bacteria and viruses, and viral productions were investigated in the Amundsen polynya and its vicinity for better understanding the microbial loop of the study area. Bacteria and virus metagenomes will unveil the marine microbial community structure in a highly productive area of the Antarctic polynya.

# Introduction

Marine microbes also exist in diverse environments extending from sea surface microlayer to deep sea. Bacteria and viruses are at the bottom of the marine food web and play important roles in biogeochemical cycles of organic matters and nutrients. Bacteria are believed to be important in carbon, nitrogen and sulphur cycles by chemolithotrophic reactions. Particularly activity of bacteria is associated with remineralization of fixed carbon, and thus, contributes to the efficiency of carbon sequestration in high latitudes. Viruses are significantly influence the production of DOM and the recycling of nutrients by viral lysis of host organisms (Fuhrman, 1999). In addition, marine viruses play important roles in eco-evolution of virus-host dynamics by transferring ecologically critical genes such as photosynthesis-related and phosphate metabolism.

To find microbiological signature of Antarctic polynya, bacterial community analysis are going to be analyzed using metagenomic approaches and extensive data of microbial community structures using 16S rRNA genes were obtained for the ambient seawaters. Despite their abundance and ubiquity, the study of Antarctic viral ecology is still in its infancy with only a limited number of studies addressing either virus mediated mortality or virus production (Guixa-Boixereu et al.,2002; Evans et al., 2009) and no study on marine virus community to date. During the cruise, abundances of total bacteria and viruses, and viral productions were investigated in the Amundsen polynya. Bacteria metagenomes and DNA/RNA virus metagenomes will unveil the microbial community in a highly productive area of the Antarctic polynya.

# Material and Methods

Seawater samples for microbial community structures using 16S rRNA genes were collected from 3-7 depth from surface to near bottom with 10 L Niskin bottles mounted on CTD rosette. Sampling for

microbiological study was made at 22 stations (including 3 revisiting stations) during the icebreaker R/V Araon expedition (ANA06B) in the Amundsen Sea (Table 3.6). For measurements of viral (VA) and total bacterial (BA), seawater samples (10 ml) were fixed with 0.02 um filtered formalin (final conc. of 2%), and stored at -80 ℃. Bacteria and viruses will be counted by using an epifluorescence microscope (Olympus BX35) after staining them with SYBR Gold as described by Noble & Fuhrman (1998). Seawater (2-4 L) for bacterial community analysis were pre-filtered through 3.0 μm pore-sized Nuclepore filters (Millipore) and collected onto 0.2 μm pore-sized cellulose nitrate membrane filters (Millipore). Filters immediately transferred to cryovial tubes containing 1 ml RNAlater (Ambion) to avoid decomposition of nucleic acids, and stored at -80℃. All filtrates were concentrated by the $FeCl_3$-precipitation method (John et al., 2011). These filtrates were collected onto 0.8 μm pore-sized cellulose nitrate membrane filters (Millipore) for viral community analysis. Sampling for bacteria and virus metagenome was made at 19 stations (including 3 revisiting stations) (Table 3.7). Each sample, from 25-50 L of seawater, was pre-filtered by a 1.6 μm 150 mm GF/A filter followed by a 0.22 μm, 142 mm diameter nitrocellulose membrane filter (Merck Milipore Ltd) using a large volume seawater filtration system (Figure 3.14). All filtrates were concentrated by the $FeCl_3$-precipitation method. DNA and RNA virome analysis will be made according to the protocols of Duhaime et al. (2012) and Steward & Culley (2010), respectively. Sediment samples were collected by box core at station 8 (Table 3.7) to isolate bacteria and analyze of bacteria community at the study area. Samples were collected at surface and subsurface of box core, respectively. In a land-based laboratory, extraction of nucleic acids and pyrosequencing will be made.

## Preliminary results

Preliminary results of microbial ecology were not available on aboard since further analyses need to be made in a land-based laboratory. However, it is expected that microbial distribution and viral production in the study area may reveal spatial variability along with a hydrographical separation. DNA/RNA virus metagenomes are also expected to provide new insights into roles of viruses in a highly productive area of the Antarctic polynya. The analysis results of sediments bacteria community obtained from these studies will be crucial for understanding the biogeochemical cycles involved in the Antarctic area.

## References

Duhaime, M.B., Deng, L., Poulos, B.T. and Sullivan, M.B., (2012) Towards quantitative metagenomics of wild viruses and other ultra-low concentration DNA samples: a rigorous assessment and optimization of the linker amplification method. Environmental Microbiology, 14, 2526-2537.

Evans, C., Pearce, I. and Brussaard, C.P.D., (2009) Viral-mediated lysis of microbes and carbon release in the sub-Antarctic and Polar Frontal zones of the Australian Southern Ocean. Environmental Microbiology, 11, 2924-2934.

Fuhrman, J.A., (1999) Marine viruses and their biogeochemical and ecological effects. Nature, 399, 541-548.

Guixa-Boixereu, N., Vaqué, D., Gasol, J.M., Sánchez-Cámara, J. and Pedrós-Alió, C., (2002) Viral distribution and activity in Antarctic waters. Deep Sea Res Part II, 49, 827-845.

John, S.G., Mendez, C.B., Deng, L., Poulos, B., Kauffman, A.K.M., et al. (2011) A simple and efficient method for concentration of ocean viruses by chemical flocculation. Environmental Microbiology Reports, 3, 195-202.

Noble, R.T., and Fuhrman, J.A., (1998) Use of SYBR Green I for rapid epifluorescence counts of marine viruses and bacteria. Aquat Microb Ecol, 14, 113-118.

Steward, G.F. and Culley, A.I., (2010) Extraction and purification of nucleic acids from viruses.Manual of Aquatic Viral Ecology, 16, 154-165.

Table 3.6. Summary of seawater sampling information

| Sampling Site Information | | | | | | | | |
|---|---|---|---|---|---|---|---|---|
| Sample | Numbering | | Navigation | | Sampling Time (UTC) | | Sampling Depth (m) | |
| | Station No. | CTD No. | Latitude | Longitude | Date | Time | Depth | Depth of CTD water sampling |
| Sea water (2 L- 4L) | ANA06B01 | CTD01 | 69°59.9971S | 125°00.0000W | 16/1/14 | 18:51:00 | 3451 | 0, 30, 100, 250. 1000. 3000 |
| | ANA06B02 | CTD02 | 71°24.4138S | 120°15.0514W | 16/1/15 | 16:26:00 | 2550 | 0, 30, 100, 270, 1000, 2000 |
| | ANA06B06 | CTD06 | 77°41.5966S | 120°15.0514W | 16/1/16 | 9:30:00 | 517 | 0, 10, 40, 100, 180, 300, 480 |
| | ANA06B10 | CTD10 | 73°02.4011S | 115°43.5065W | 16/1/17 | 17:12:00 | 710 | 0, 20, 100, 230, 370, 620 |
| | ANA06B12 | CTD12 | 73°16.7917S | 114°57.0519W | 16/1/18 | 7:37:00 | 837 | 0, 15, 100 |
| | ANA06B19 | CTD19 | 74°10.2920S | 112°35.6999W | 16/1/19 | 22:34:32 | 650 | 0, 15, 100, 300, 800, 1026 |
| | ANA06B22 | CTD22 | 74°10.3075S | 113°19.7099W | 16/1/20 | 12:51:33 | 633 | 0, 20, 100 |
| | ANA06B27 | CTD27 | 73°17.0000S | 112°10.003W | 16/1/23 | 11:43:00 | 445 | 0, 15, 100, 200, 330, 435 |
| | ANA06B33 | CTD33 | 73°29.999S | 116°29.982W | 16/1/24 | 11:02:00 | 375 | 0, 10, 80, 130, 200, 300 |
| | ANA06B37 | CTD37 | 74°06.3054S | 115°08.6008W | 16/1/25 | 8:49:00 | 647 | 0, 30, 150, 200, 400, 550 |
| | ANA06B40 | CTD40 | 73°04.6124S | 128°11.0330W | 16/1/26 | 18:02:35 | 561 | 0, 30, 100, 320, 450, 550 |
| | ANA06B42 | CTD42 | 74°08.2799S | 128°12.8386W | 16/1/27 | 19:54:30 | 596 | 0, 45, 100, 400, 440, 520 |
| | ANA06B46 | CTD46 | 73°56.4032S | 127°47.9728SW | 16/1/28 | 8:12:00 | 780 | 0, 38, 100, 310, 520, 700 |
| | ANA06B51 | CTD51 | 73°41.4311S | 127°26.8420W | 16/1/29 | 1:56:00 | 322 | 0, 15, 100, 200, 300 |
| | ANA06B54 | CTD54 | 73°41.1311S | 123°35.0243W | 16/1/29 | 20:30:36 | 640 | 0, 30, 100, 250, 420, 631 |
| | ANA06B58 | CTD58 | 73°56.2436S | 117°16.4467W | 16/1/31 | 9:57:54 | 658 | 0, 25, 100, 300, 450, 600 |
| | ANA06B62 | CTD62 | 75°03.5344S | 102°09.1377W | 16/2/2 | 14:37:43 | 743 | 0, 50, 150, 300, 400, 650 |
| | ANA06B64 | CTD64 | 74°42.4023S | 101°45.7129W | 16/2/3 | 8:31:00 | 559 | 0, 25, 100, 310, 400,580 |
| | ANA06B29R | CTD29 | 72°50.9974S | 112°29.9935W | 16/2/5 | 23:56:00 | 451 | 0, 40, 100, 200, 350, 441 |
| | ANA06B12R | CTD12 | 73°16.7931S | 114°57.0265W | 16/2/6 | 18:55:09 | 830 | 0, 65, 100, 265, 450, 700 |
| | ANA06B8R | CTD08 | 72°48.0008S | 116°30.0021W | 16/2/7 | 5:28:00 | 631 | 0, 20, 100, 200, 450, 550 |
| | ANA06B67 | CTD67 | 71°33.7271S | 113°02.7856W | 16/2/7 | 18:31:00 | 600 | 0, 30, 100, 300, 400, 590 |
| Sea water (25-50 L) | ANA06B01 | CTD01 | 69°59.9971S | 125°00.0000W | 16/1/14 | 18:51:00 | 3451 | 0 |
| | ANA06B02 | CTD02 | 71°24.4138S | 120°15.0514W | 16/1/15 | 16:26:00 | 2550 | 0 |
| | ANA06B06 | CTD06 | 77°41.5966S | 120°15.0514W | 16/1/16 | 9:30:00 | 517 | 0 |
| | ANA06B07 | CTD07 | 72°27.3137' S | 116°20.6612' W | 16/1/17 | 4:01:00 | 554 | 0 |
| | ANA06B08 | CTD08 | 72°48.1520' S | 116°30.8900' W | 16/1/17 | 12:58:00 | 627 | 0 |
| | ANA06B10 | CTD10 | 73°02.4011S | 115°43.5065W | 16/1/17 | 17:12:00 | 710 | 0 |
| | ANA06B12 | CTD12 | 73°16.7917S | 114°57.0519W | 16/1/18 | 7:37:00 | 837 | 0 |
| | ANA06B19 | CTD19 | 74°10.2920S | 112°35.6999W | 16/1/19 | 22:34:32 | 650 | 0 |
| | ANA06B22 | CTD22 | 74°10.3075S | 113°19.7099W | 16/1/20 | 12:51:33 | 633 | 0 |
| | ANA06B26 | CTD26 | 73°29.995 ' S | 111°59.976' W | 16/1/23 | 9:38:00 | 420 | 0 |
| | ANA06B31 | CTD31 | 73°09.9945' S | 114°29.9746' W | 16/1/24 | 4:11:00 | 708 | 0 |
| | ANA06B32 | CTD32 | 73°19.7017' S | 115°25.2444' W | 16/1/27 | 19:54:30 | 596 | 0 |
| | ANA06B37 | CTD37 | 74°06.3054S | 115°08.6008W | 16/1/25 | 8:49:00 | 647 | 0 |
| | ANA06B39 | CTD39 | 74°04.9666' S | 115°43.2029' W | 16/1/25 | 16:13:00 | 1060 | 0 |
| | ANA06B46 | CTD46 | 73°56.4032S | 127°47.9728SW | 16/1/28 | 8:12:00 | 780 | 0 |
| | ANA06B29R | CTD29 | 72°50.9974S | 112°29.9935W | 16/2/5 | 23:56:00 | 451 | 0 |
| | ANA06B12R | CTD12 | 73°16.7931S | 114°57.0265W | 16/2/6 | 18:55:09 | 830 | 0 |
| | ANA06B8R | CTD08 | 72°48.0008S | 116°30.0021W | 16/2/7 | 5:28:00 | 631 | 0 |
| | ANA06B67 | CTD67 | 71°33.7271S | 113°02.7856W | 16/2/7 | 18:31:00 | 600 | 0 |

Table 3.7. Summary of box core sediments sampling information

| Sampling Site Information | | | | | | |
|---|---|---|---|---|---|---|
| Numbering | | Navigation | | Sampling Time (UTC) | | Depth (m) |
| Station No. | box core No. | Latitude | Longitude | Date | Time | Depth |
| ANA06B04 | BC01 | 72°07.0995' S | 118°52.7228' W | 16/1/16 | 10:10:00 | 717 |
| ANA06B10 | BC02 | 73°02.4011S | 115°43.5065W | 16/1/17 | 17:12:00 | 710 |
| ANA06B19 | BC04 | 74°10.2920S | 112°35.6999W | 16/1/19 | 22:34:32 | 650 |
| ANA06B16R | BC05 | 73°49.1793' S | 113°02.7133' W | 16/1/21 | 11:56:00 | 788 |
| ANA06B26 | BC06 | 73°29.995 ' S | 111°59.976' W | 16/1/23 | 9:38:00 | 420 |
| ANA06B33 | BC07 | 73°29.999S | 116°29.982W | 16/1/24 | 11:02:00 | 375 |
| ANA06B39 | BC08 | 74°04.9666' S | 115°43.2029' W | 16/1/25 | 16:13:00 | 1060 |
| ANA06B63 | BC09 | 74°52.0320' S | 102°04.7984' W | 16/2/3 | 4:10:00 | 940 |

Figure 3.14. Photos of a large volume seawater filtration system used in the present study.

# 3.9 Transcriptome samples from phytoplankton

[1]Joo-Han Gwak, [1]Sung-Keun Rhee, [2]Éric Potvin, [2]Eun Jin Yang

[1]Chungbuk National University, Korea

[2]Korea Polar Research Institute, Korea

## 요약문

서남극해 아문젠해역의 폴리냐에서 일어나는 식물 플랑크톤 bloom은 주로 *Phaeocystis antarctica*가 우점한다. 2012-2014년 연구 탐사에서 얻은 미생물 시료를 통하여 식물 플랑크톤 bloom시기 중·후반간 미생물 메타지놈(metagenome)의 비교연구를 시도하여 우점종인 *Polaribacter*를 포함한 미생물들의 생물학적 및 무생물학적 환경 변인과 유전자 발현 정도에 대한 유전자 수준의 연구를 진행한바 있다. 2016년 연구 탐사에서는 *P. antartica*를 대상으로 식물 플랑크톤 bloom시기별 시료 채취를 하여 RNA-Seq을 진행함으로써 transcriptome 분석을 하고자 한다. *P. antartica*의 bloom시기별 유전자 발현을 비교 분석함으로써 생장 조절 인자와의 관계 등을 유전자 수준에서 연구하여 식물 플랑크톤 bloom의 기작을 구조적으로 밝힐 수 있기를 기대한다. 또한, 2012-2014년 연구 탐사의 연장으로 폴리냐의 식물 플랑크톤 bloom시기 미생물 우점종인 *Polaribacter*에 대한 바이러스 감수성 및 상호 작용을 연구 하기 위한 시료를 채취하였으며 해당 시료는 MDA(multiple displacement amplification)를 통해 다수의 SAG(single amplified genome)를 만들어 분석을 진행할 예정이다. 이외에 배양을 통한 생리 활성 관찰 및 신규 미생물 확보를 위하여 serial dilution method를 이용한 미생물 분리 배양을 시도하였으며, 자외선과 용존 유기물과의 광반응으로 생성되는 ROS(reactive oxygen species)의 일종인 Hydrogen peroxide의 측정을 위한 시료를 채취하였다.

## Objective

Phytoplankton bloom in the Amundsen Sea Polynya is dominated by *Phaeocystis antarctica*. The bloom of that species is recognized as one of the most productive in Antarctic (Yager et al., 2012). Abiotic environmental factors such as the availability of light and iron are thought to limit primary productivity in the polynya. On the other hand, the bacterioplankton community responds to phytoplankton bloom that produced different algal-derived organic matter. In this research, the shift of gene expression profile belonging to *P. antarctica* during and after the phytoplankton bloom will be investigated as well as how *P. antarctica* responded to biotic and abiotic environmental factors with seasonal variation. Seawater (50L) was filtered to accumulate large cell mass and to perform transcriptomic analyses that could provide understanding of bottom-up control involved in phytoplankton bloom.

Viruses are ubiquitous entities on earth, outnumbering the bacteria and modulating bacterial lifespan and evolution. To evaluate viral susceptibility and interactions with *Polaribacter*, the most abundant microbe in the late phytoplankton bloom, water samples were collected for single-cell genomic analyses and for preparation of MDA (multiple displacement amplification).

Additionally, incubation experiment for novel heterotroph isolation was performed with addition of dimethylthiourea (DMTU).

## Materials and methods

Collection of Phaeocystis for gene expression analysis

For collection of large phytoplanktonic cell, peristaltic pump-based high throughput filter system (Millipore) with 147 mm diameter filter was used. Fifty liters of seawater were used for filtration of biomass in surface water at key stations. Phytoplankton were collected with 1.6 um filters. In one hour, the process of sample collection was finished and the filters were stored at -80℃ in deep freezer with RNAlater until metagenomic DNA/RNA extraction.

Preparation bacterial cells for SAG (single amplicon genome)

For collection of bacterial cell for MDA, 1.6 μm filtrate water samples from surface and SCM zones were collected by vacuum filtration onto 47 mm filter housed in Millipore filter holders from which 1 ml aliquots were transferred to cryovials and 100 μl glyTE added (following Bigelow lab protocol). Subsequently, the cryovials were stored at -80℃ in deep freezer after ~1 minutes incubation at ambient temperature with gentle mixing.

Sampling for hydrogen peroxide measurement

For measurement of hydrogen peroxide, 0.1 μm filtrate water samples were collected at four depths above 100 m at key stations by syringe filtration.

Water sampling for heterotroph isolation

For isolation of novel heterotrophic bacteria, surface water samples (40 ml each) were collected at each station. The samples were stored at 4℃.

## References

Yager, P.L., R.M. Sherrell, S.E. Stammerjohn, A.-C. Alderkamp, O. Schofield, E.P. Abrahamsen, K.R. Arrigo, S. Bertilsson, D.L. Garay, R. Guerrero, K.E. Lowry, P.-O. Moksnes, K. Ndungu, A.F. Post, E. Randall-Goodwin, L. Riemann, S. Severmann, S. Thatje, G.L. van Dijken, and S. Wilson. 2012. ASPIRE: The Amundsen Sea Polynya International Research Expedition. Oceanography 25(3):40–53, http://dx.doi.org/10.5670/oceanog.2012.73.

# 3.10 Live/dead status of the heterotrophic prokaryote community

Éric Potvin and Eun Jin Yang

Korea Polar Research Institute (KOPRI), 406-840, Incheon, Korea

## 요약문

해양의 미세생물 먹이망에서 중요한 역할을 하는 종속영양 prokaryote 군집을 평가하는데 있어서그들의 생존 상태(dead or live)를 밝혀내는 것은 중요하다. 본 연구에서는 nucleic acid double-staining(NADS) 방법을 통하여 prokaryote 군집의 생존상태를 평가하고 서로 다른 환경에서 그들의 분포 특징을 파악하고자 아문젠 폴리니아와 파인아일랜드 폴리니아에서 해수를 채수하였다. 채수된 시료는 flow cytometry 와 형광현미경을 이용하여 prokaryote 군집의 생물량을 측정할 것이며, NADS 방법을 이용하여 그들의 생존 상태를 측정할 계획이다

## Objective

Heterotrophic prokaryotes play a relevant role in planktonic marine microbial food webs. As a relevant difference from other planktonic organisms, prokaryotes are known to sometimes be inactive or dead, but in the way that they are commonly enumerated (e.g. with 4′,6′-diamidino-2-phenylindole or DAPI), these cells are accounted for in budgets for prokaryote biomass since they are not distinguished from live and active cells.

The discrimination of active organisms among by others is done with consideration of some aspect of their physiological statuses, such as reproductive potential, respiratory activity, enzymatic activities, etc. Other aspects of the cell structure and physiology are used to discriminate dead cells from cells with at least potential for growth. Membrane integrity is one of the better-accepted criteria for distinguishing live cells from dead cells because of the assumption that cells with damaged membranes cannot sustain any electrochemical gradient and are not able to resume growth.

The nucleic acid double-staining (NADS) protocols have been applied in various areas of bacteriological research. The double-staining protocols are based on the simultaneous use of two stains targeting the nucleic acid, the first (Syto9, Sybr Green, etc.) being a membrane-permeable green dye and the second (Propidium iodide) being a membrane-impermeant dye. The principle of these protocols is based on energy transfer from an excited donor (the green stain) to an acceptor molecule (the red stain) according to the fluorescence resonance energy transfer (FRET) phenomenon; the green stain is quenched in the presence of the red stain, and energy is transferred to the latter one if present.

In this study, we collected samples to estimate the concentration of heterotrophic prokaryotes in the field by the use of DAPI and epifluorescence microscopy as well as flow cytometry. We also applied the NADS protocol using both SG1 (Sybr Green 1) and PI (Propidium iodide) to estimate the state of the bacteria.

## Material and methods

Sampling sites.

Sampling for all analyses was carried out in the Amundsen Sea and Pine Island polynya at a total of 24 stations. Seawater was collected at different depth at each of these stations and usually above 100 m during the upcast from a rosette.

Bacterial abundance.

Samples were preserved to determine the total concentration of prokaryotes. Seawater was fixed with formaldehyde (1% final concentration) for 20 min at room temperature and frozen at -80°C. The

samples will be stained with DAPI at a final concentration of 5 μg $mL^{-1}$for 5 min. Then, they will be filtered and the filters mounted on glass slides with cover slips to be counted by epifluorescence microscopy.

Samples were also analysed by flow cytometry for total prokaryote enumeration. The seawater was sometimes filtered with a 100-μm mesh net to prevent the clogging of the instrument. The samples were stained with SG1 at a final concentration of 1x for 20 min at room temperature and run through a C6 flow cytometer. All fluorescent filters and detectors used were the standard machine equipment, with green fluorescence collected in the FL1 channel, orange fluorescence collected in the FL2 channel, and red fluorescence collected in the FL3 channel. All parameters were collected as logarithmic signals. We generally acquired data at a low speed (ca. 14 μL $min^{-1}$). A calibrated fluorescent microsphere (yellow-green 0.92-μm Polysciences latex beads) solution was added to each sample as an internal reference. Heterotrophic prokaryotes were detected in a dot plot of side scatter versus green fluorescence (FL1).

NADS protocol.

PI was used at a final concentration of 10 μg $ml^{-1}$ and SG1 at a final concentration of 10x. After simultaneous addition of each stain, the samples were incubated for 20 min in the dark at room temperature and then analyzed flow cytometrically using a C6 flow cytometer. SG1 and PI fluorescence were detected in the green (FL1) and red (FL3) cytometric channels, respectively. A dot plot of red versus green fluorescence allowed distinction of the "live" cell cluster (i.e., cells with intact membranes and DNA present) from the "dead" cell one (i.e., with compromised membranes). We used a threshold in the green channel and ran the samples at a low speed (ca. 14 μL $min^{-1}$).

## Output

In collaboration with various PIs studying the Amundsen Sea and Pine Island polynya, insights to which factors are responsible for the different states of the heterotrophic prokaryote community as well as the effects it has on some processes will be investigated.

# 3.11 Mixotrophy and selectivity on bacteria *in situ* by CARD-FISH (catalyzed reporter deposition-fluorescent *in situ* hybridization)

Éric Potvin and Eun Jin Yang

Korea Polar Research Institute (KOPRI), 406-840, Incheon, Korea

## 요약문

해양먹이망의 에너지 흐름에서 박테리아 섭식자로서 혼합영양 원생동물의 중요한 역할에도 플랑크톤 생태계에서 혼합영양 원생동물의 기여도는 현재까지 잘 정의되지 않고 있으며, 특히 극지방에서 그들의 역할은 의문점으로 남아 있다. 본 연구에서는 CARD-FISH 방법을 활용하여 혼합영양 원생동물의 분포 특성, 박테리아에 대한 선택적 섭식률 특성을 파악하고자 아문제 폴리니아와 파인아일랜드 폴리니아에서 시료를 채집하였다.

## Objective

Planktonic protists are considered the main bacterivorous organisms in aquatic ecosystems. Besides controlling bacterial abundances in a wide range of aquatic ecosystem conditions, they also channel organic carbon to higher trophic levels and release inorganic nutrients that often limit primary production.

There is a very limited account of the composition of the bacterivorous community and few evidences of the occurrence of mixotrophy in the Southern Ocean. The lack of knowledge regarding the contribution of mixotrophic algae to the carbon flow in the microbial food web is in part due to the methodological approaches that have been commonly used to determine community bacterivory through dilution experiments, differential filtration, and disappearance of tracer particles over an extended time. These methods are generally ineffective for identifying ingestion by phagotrophic algae.

Selective feeding of bacterivorous protists is also not well understood in the Southern Ocean, while it is recognized as an important mechanism for the structuring of planktonic food webs. Size structured predator-prey interactions are of particular importance, and bacterial cell size must be considered a major feature that influences susceptibility towards different grazers. Different protists might have different prey preferences, being adapted to consume a specific part of the bacterial assemblage. However, prey features other than size and shape, such as motility, digestibility, cell surface, physiological state, and food quality can also mediate selective grazing.

In this study, we will evaluate mixotrophy *in situ* at the system level using the CARD-FISH (catalyzed reporter deposition-fluorescent *in situ* hybridization) technique using general probes in order to determine the abundances of mixotrophic organisms and there contributions to phototrophic and heterotrophic assemblages. We will also evaluate prey selectivity of different taxa within the natural community assemblage using CARD-FISH by estimating the relative proportions of different heterotrophic prokaryotes in the natural community compared with their proportions inside protistan digestive vacuoles.

## Material and methods

Sampling sites.

Sampling for all analyses was carried out in the Amundsen Sea and Pine Island polynya at a total of 24 stations. Seawater was collected at different depth at each of these stations and usually above 100 m during the upcast from a rosette.

CARD-FISH protocol.

Samples were collected in acid-washed plastic bottles pre-rinsed with seawater from various locations and depths.

Water samples were fixed with formaldehyde (2% final concentration). The volume of the aliquots was determined by a preliminary observation of DAPI stained samples with epifluorescence microscopy. The aliquots were filtered through 0.2-µm pore size (47 mm diameter) white polycarbonate filters, air-dried and kept frozen at -80°C until processed. The heterotrophic prokaryotes will be identified by applying the CARD-FISH technique.

Samples for the identification of heterotrophic prokaryotes within protist digestive vacuoles were processed in a similar way, except that the pore size of the filters used was 0.8-μm.

Section of the filters will be hybridized with various oligonucleotide probes with different degree of specificity. After hybridization, the signal will be amplified with Alexa 488-labeled tyramide, counter stained with DAPI, and observed by epifluorescence microscopy.

## Output

In collaboration with various PIs studying the Amundsen Sea and Pine Island polynya, insights to which factors triggering mixotrophy and selectivity will be investigated.

# 3.12 Bacterivory

Éric Potvin and Eun Jin Yang

Korea Polar Research Institute (KOPRI), 406-840, Incheon, Korea

### 요약문

종속영양 박테리아는 해양미세생물 먹이망의 중요한 구성자로서 해양의 생지화학적 순환에 중요한 역할을 하기 때문에 박테리아 군집에 영향을 미치는 요인을 파악하는 것은 중요하다. 본 연구에서는 박테리아 생물량을 조절하는 원인중에 하나로서 박테리아의 섭식률을 측정하고자 하였다. 아문젠해에서 박테리아의 섭식률을 파악하기 위하여 표층과 엽록소 최대층에서 해수를 채수하여 Fluorescent microspheres를 이용하여 선상배양을 수행하였다. 배양의 단계별로 얻어진 시료는 고정하여 냉동보관한 후에 실험실로 가져와 현광 현미경을 사용하여 분석될 예정이다.

## Objective

Bacterivory is often seen as an important link between the microbial loop and the higher trophic network. Knowing the importance of the bacterivory at the system level is highly relevant in our understanding of the transport of carbon in the system. No study on bacterivory has focused in the Amundsen Sea and Pine Island polynya.

## Material and methods

Sampling sites.

Sampling for all analyses was carried out in the Amundsen Sea and Pine Island polynya at a total of 13 stations. Seawater was collected at the surface and the subchlorophyll maximum (SCM) at each of the selected station.

Bacterivory protocol.

Subsamples from the surface and the SCM were collected for the establishment of various parameters including biological, physical, and chemical aspects.

Fluorescent tracers were used. Cultured *Polaribacter* sp. was brought aboard in order to produce fluorescent labeled bacteria (FLB). However, the size distribution of the FLB was not representative of the bacterial natural community. Fluorescent microspheres with a diameter of 0.5 μm were found to be more representative of the size of the bacterial community observed and thereafter used in the experiments.

For the bacterivory experiments, the water samples were collected in 4-L bottles. Metazooplankton was removed manually and the natural community put a few hours in deck incubators for recovery.

To determine the appropriate addition of tracer particles, bacterial abundances from each depth was initially assessed by epifluorescence microscopy from samples fixed with formaldehyde (1% final concentration) and filtered on 25-mm black polycarbonate filters (0.2 μm pore size). Filters were stained with DAPI at a final concentration of 5 μg $mL^{-1}$for 5 min. Filters were then mounted on glass slides with cover slips and the bacteria counted.

For feeding experiments, fluorescent microspheres were added to approximately 25% of natural bacterial abundance. The fluorescent microspheres were sonicated prior to addition to disperse the particle evenly. Then, the 4-L bottles were mixed gently and divided in three 1-L bottles that constituted the triplicate of the experiments. Each replicate was then subsampled to determine the actual initial concentration of bacteria by epifluorescence microscopy and fluorescent microspheres by flow cytometry. The replicate 1-L bottles were incubated in deck incubators. The deck incubators were shaded with neutral density filters in order to reproduce the light condition at the surface and at the SCM. The temperature of the incubators was maintained at *in situ* condition by pumping the water from the surface through the incubators. The temperature from the surface water was usually very similar to the temperature at the SCM.

To determine rates of bacterivory, 15 to 40 mL aliquots were taken from the 1-L bottles at several time points beginning immediately after particle addition and fixed using the Lugol-formaldehyde-sodium thiosulfate method to prevent egestion. After evaluation of the initial time course data indicated linear uptake for 90 minutes, samples were taken at the beginning of the experiment and after 30 minutes to determine ingestion. The aliquots were filtered on 0.8-μm pore size black polycarbonate filters (25 mm diameter), stained with DAPI at a final concentration of 5 μg $mL^{-1}$for 5 min, mounted between slides and coverslips, and stored at -20 °C until enumeration by epifluorescence microscopy onboard the ship.

## Output

The assessment of ingestion rates on bacteria will help to understand the flow of carbon at the system level. It will also help to determine if this process is able to control the production of bacteria in the region and its impact on the stock of bacteria.

# Chapter 4

# Physical Oceanography in Udintsev Fracture Zone

Y.H. Park[1], J.H. Lee[2], T.W. Kim[3], I. Durand[1], D.K. Kim[2], J.H. Jung[2], K.H. Cho[3], C.S. Kim[3], H.W. Yang[3]

[1]LOCEAN/USM 402, National Museum of Natural Histories, Paris, France

[2]Korea Institute of Ocean Science and Technology (KIOST), Ansan 425-600, Korea

[3]Korea Polar Research Institute (KOPRI), Incheon 406-840, Korea

## 요약문

남극해 태평양 해역에 위치한 Udintsev Fracture Zone (UFZ)은 남극순환류(Antarctic Circumpolar Current)가 통과하는 가장 좁은 길목의 하나이다. UFZ에서 흐름장을 가로질러 통과하는 열속의 물리적 과정 연구를 위하여 3정점, 극전선(Polar Front)과 남극순환류남부전선(Southern ACC Front) 사이 2정점 및 극전선 북쪽 1 정점)에서 해류계 계류와 12개 정점에서 전수심의 CTD 관측을 수행하였다.

## Abstract

The Udintsev Fracture Zone (UFZ) located in the South Pacific sector of the Southern Ocean is one of the narrowest pathway of the Antarctic Circumpolar Current (ACC). In order to study for physical processes for the cross-stream heat fluxes in the UFZ, the deployment of current meter moorings at three selected sites (two sites between the Polar Front and Southern ACC Front and one site at the area north of the Polar Front) and full-depth CTD castings at 12 stations are carried out.

## Objectives

Evaluation of cross-stream poleward heat flux across the Antarctic Circumpolar Current (ACC) in the Udintsev Fracture Zone, South Pacific sector of the Southern Ocean. Two processes have been proposed for the cross-stream heat fluxes in the Southern Ocean; one is caused by eddy activity and the other by time-mean flow. Although our major interest here is in the mean-flow contribution especially in the southern part of the ACC, the use of mooring current meter data may enable one to evaluate both eddy and mean-flow contributions.

## Current meter moorings

We moored 3 lines of current meters along a CTD section laid along a Jason satellite altimeter ground track across the ACC which is tightly channeled through the deep passage cut across the fractured Pacific Antarctic Ridge (Figure 4.1).

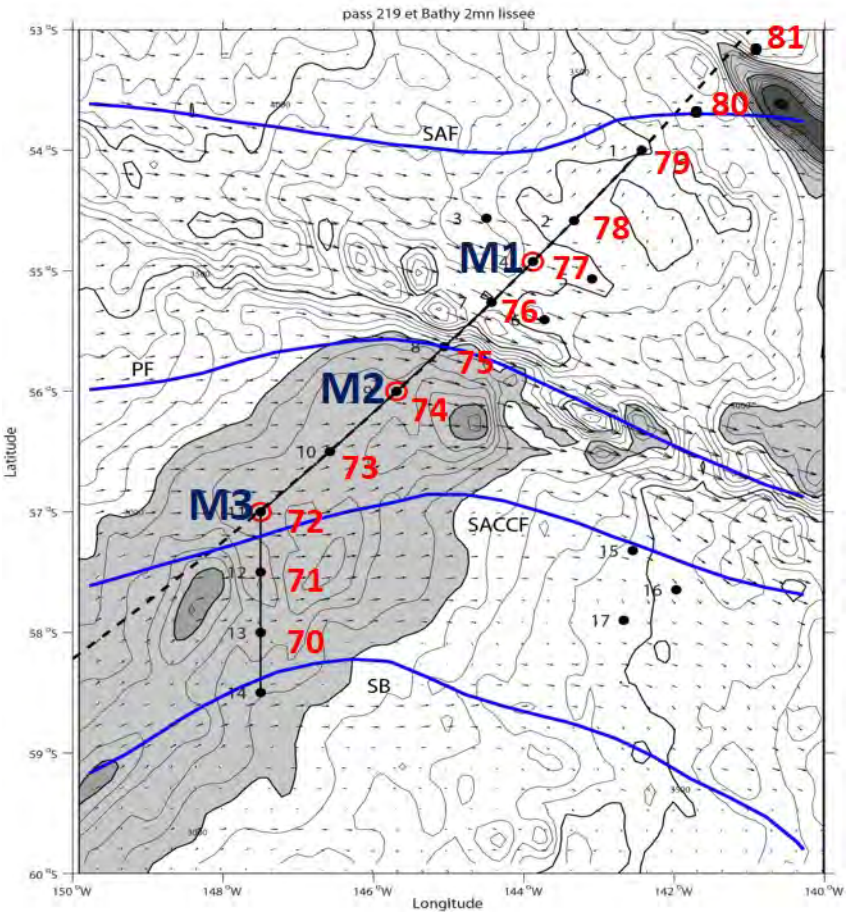


Figure 4.1 Current meter mooring points (red circles) superimposed on the CTD stations (black dots) and isobaths (black lines) from the ETOPO2 bathymetry. Isobaths of 3000 m and 4000 m are shown thickened and depths shallower than 3000 m and 2500 m are lightly and strongly stippled, respectively. Also indicated are four ACC fronts: SAF = Subantarctic Front, PF = Polar Front, SACCF = Southern ACC Front, SB = Southern Boundary of ACC.

Mooring M1: KIOST mooring at St. 77 north of the PF

Six current meters (5 Aquadopp + 1 Aanderaa) and six Microcat T/S sensors were installed between 300 m and bottom (Figure 4.2a). The mooring was done without any difficulty under calm sea state. However, some difficulties occurred with the triangulation because of the unexpected downstream drift of the mooring line over 1.4 km. This would have occurred due probably to strong NE flow of the region, together with excessive drag caused by 48 floats attached for maintaining the floatability of the mooring line. In fact, at the beginning of the triangulation at a radius of 2.5 km from the weight launch point, no return signals were detected probably because releasers were out of the acoustic detection limit. After several trials by changing the radius of the triangulation, we finally detected return signals at radius of 500 m from the release point. The final triangulation results indicate that the mooring line drifted to a point about 1.4 km NE of the weight launch point.

The 3D mooring position is: 54° 54.932'S, 143° 49.695'W over a bottom of 3766 m (Figure 4.2b).

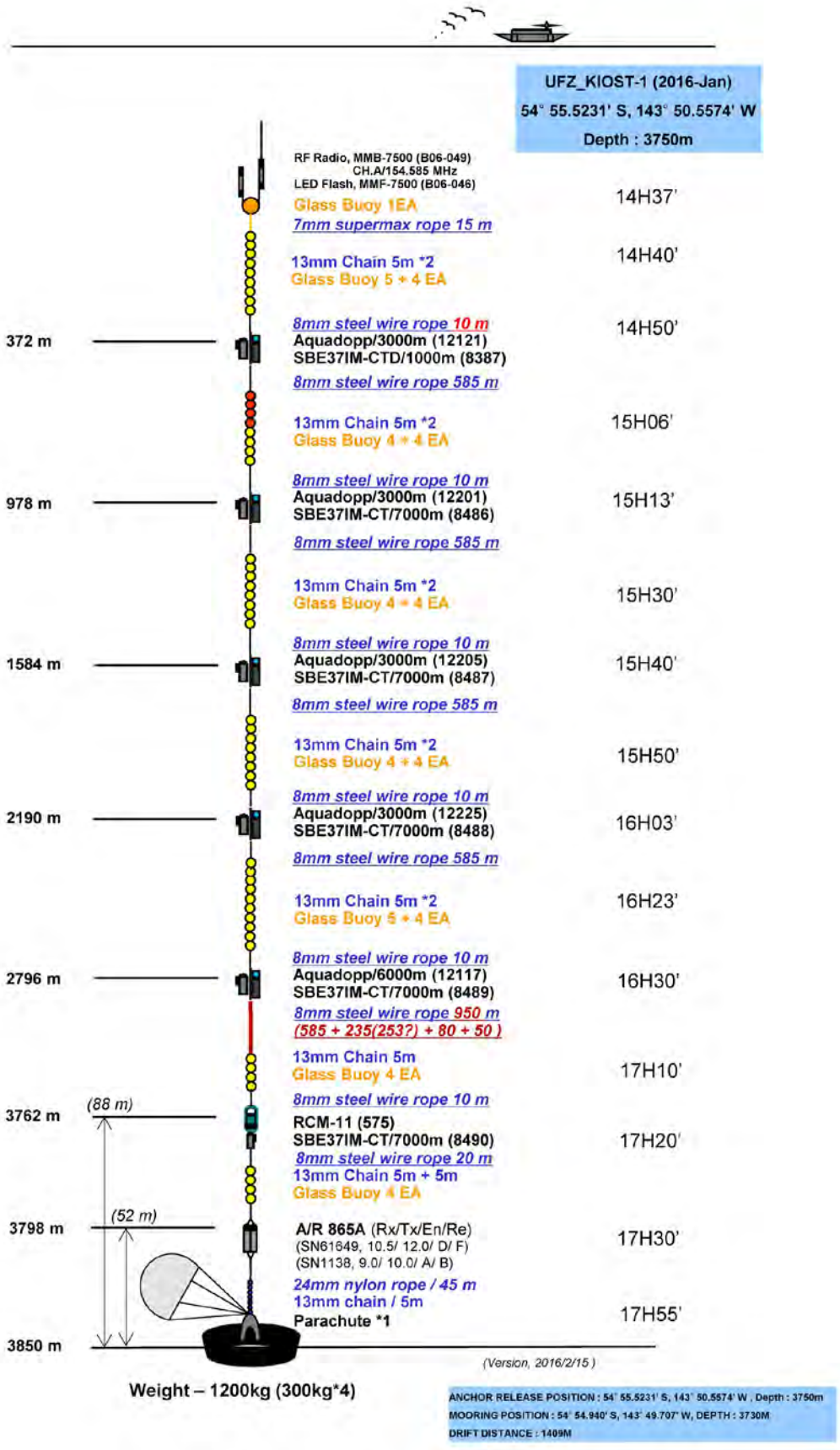


Figure 4.2a. Schematic view of the mooring line M1.

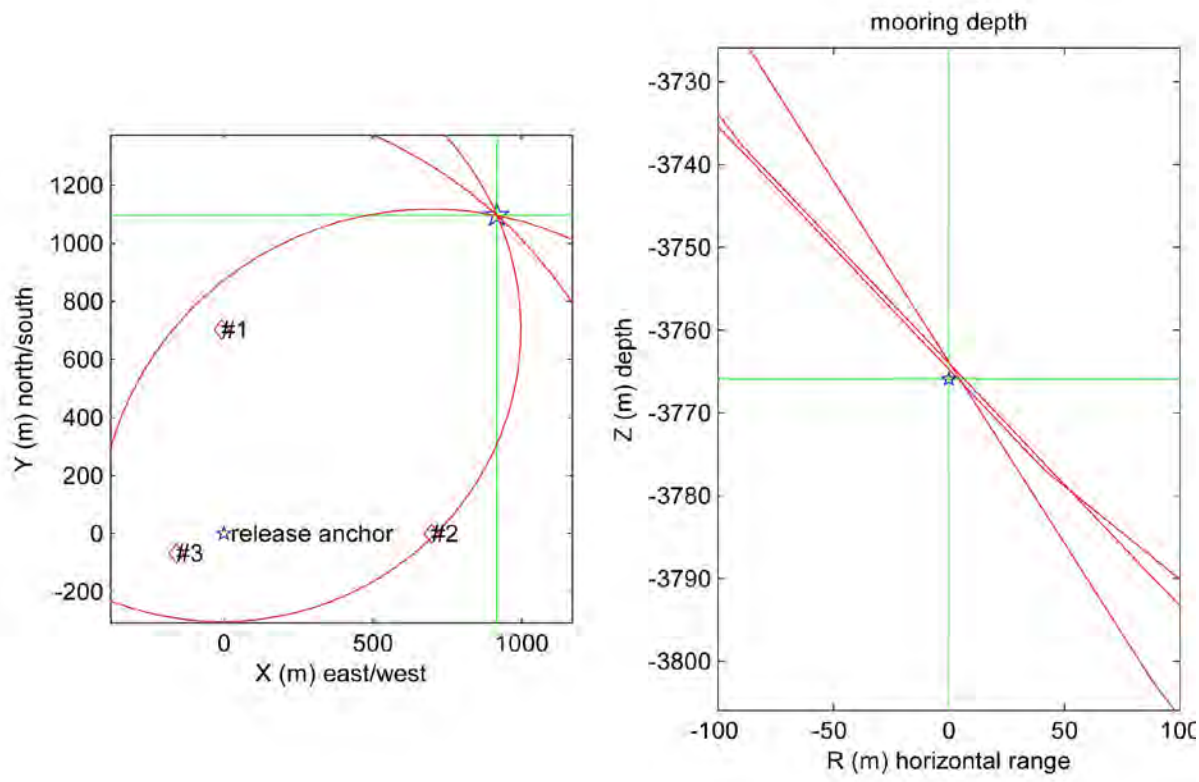


anchor release position: 54°S 55.523' 143°W 50.557'; depth: 3750 m
3D mooring position: 54°S 54.932' 143°W 49.695'
drift: 1429 m; direction: 40°
mooring depth: 3766 m; slant error: 0 m
2D mooring position: 54°S 54.912' 143°W 49.667'
drift: 1476 m; direction: 40°
horizontal error: 4 m
sound speed at site: 1490 m/s

#1 pos: 54°S 55.144' 143°W 50.565' range: 3840 m range soundspeed 1497
#2 pos: 54°S 55.523' 143°W 49.902' range: 3871 m range soundspeed 1497
#3 pos: 54°S 55.560' 143°W 50.708' range: 4031 m range soundspeed 1497

Figure 4.2b. Triangulation results of the mooring M1.

Mooring M2: LOCEAN mooring at St. 74 immediately south of the PF

Five current meters (5 Aquadopp) and five Microcat T/S sensors were installed between 400 m and bottom (Figure 4.3a). The mooring was done without any difficulty under calm sea state. The triangulation was also carried out in good condition without any difficulty with a search radius of 1.5 km from the weight launch point.

The 3D mooring position is: 56° 0.056'S, 145° 43.049'W over a bottom of 2920 m (Figure 4.3b).

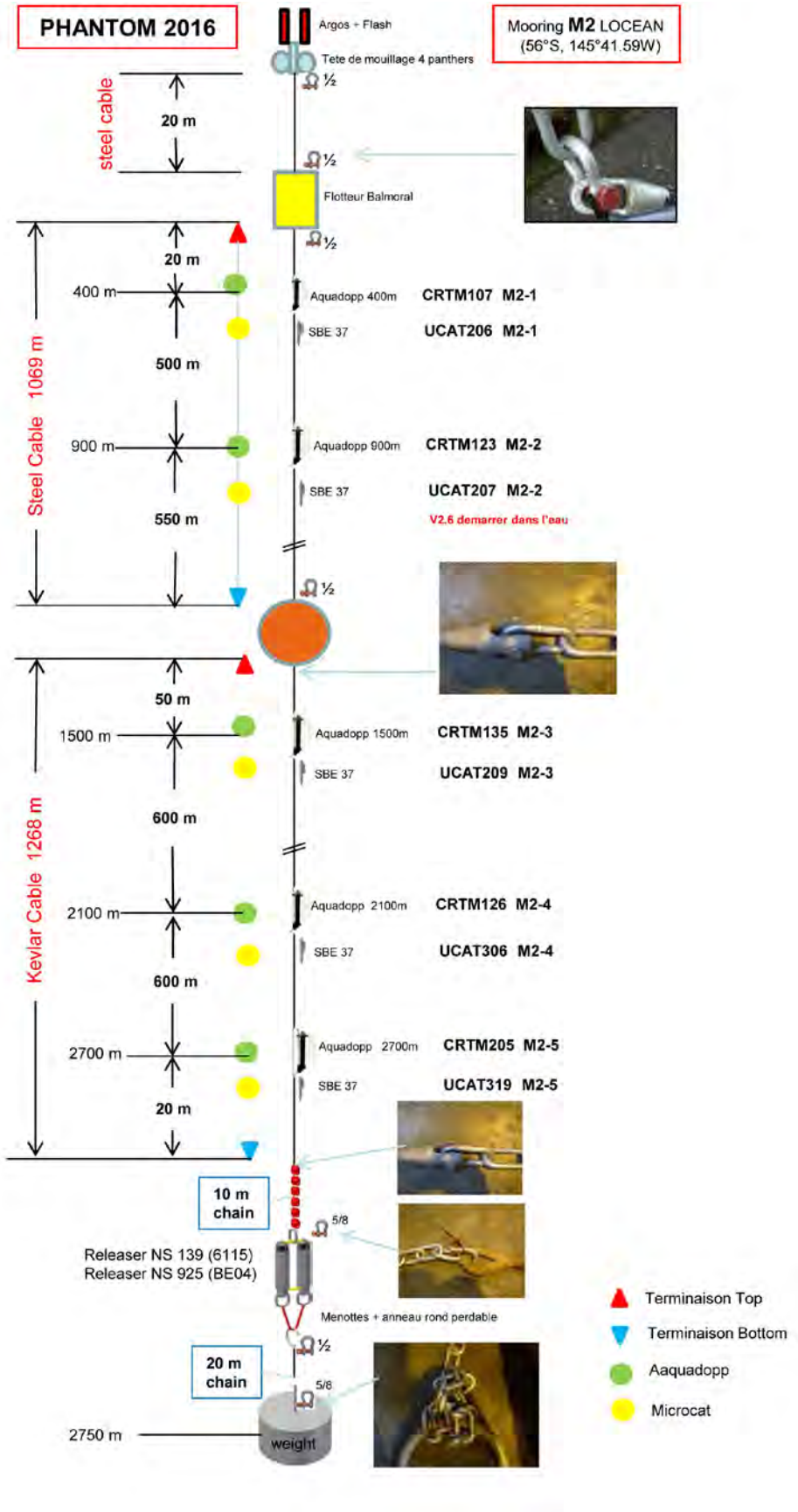


Figure 4.3a. Schematic view of the mooring line M2.

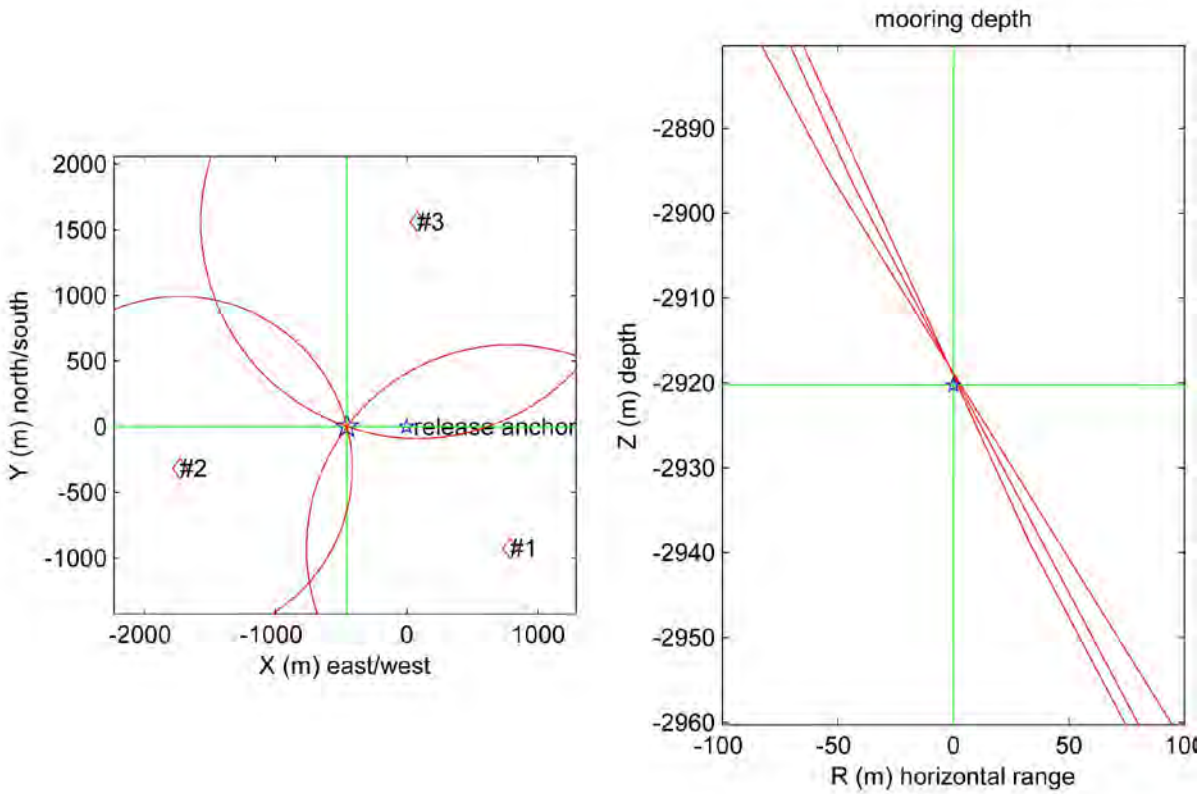


anchor release position: 56°S 0.056' 145°W 42.609'; depth: 2865 m
3D mooring position: 56°S 0.056' 145°W 43.049'
drift: 455 m; direction: 270°
mooring depth: 2920 m; slant error: 0 m
2D mooring position: 56°S 0.063' 145°W 43.068'
drift: 475 m; direction: 268°
horizontal error: 48 m
sound speed at site: 1497 m/s

#1 pos: 56°S 0.557' 145°W 41.848' range: 3280 m range soundspeed 1500
#2 pos: 56°S 0.228' 145°W 44.277' range: 3174 m range soundspeed 1500
#3 pos: 55°S 59.213' 145°W 42.530' range: 3328 m range soundspeed 1500

Figure 4.3b. Triangulation results of the mooring M2.

Mooring M3: LOCEAN mooring at St. 72 at the SACCF

Same as the M2 mooring except for the mooring position. Before mooring operations, a bathymetric search was conducted via a ship-borne multi-beam ecosounder, which showed a deeper bottom depth by about 150 m compared to the ETOPO2 bathymetry we used. We displaced therefore the mooring point to the east by about 13 km compared to the initial position.

The 3D mooring position is: 56° 59.721'S, 147° 23.510'W over a bottom of 2821 m (not shown).

## CTD section

A total of 12 full-depth stations were occupied using a SBE 9plus CTD unit. Most of these stations were laid on a NE-SW oriented ground track of the Jason altimeter, except for two southernmost stations at 137°30'W. These extend over the area (53°-58°S, 140°-148°W) and cover two fracture zones: Udintsev (central eastern part) and Eltanin (northeastern corner). A down-looking LADCP was mounted in the rosette frame. All CTD casts were made in favorable weather condition, with a negligible heaving effect of the vessel. Water samples for salinity calibration were taken at 10 levels at selected stations. The salinity of these water samples was measured using an Autosal salinometer. A rapid comparison indicates a slight overestimation by two salinity sensors of the CTD, although the sensor 1 is less positively biased (+0.001 PSU) than the sensor 2 (+0.003 PSU). This suggests that the use of the salinity sensor 1 is highly recommended. The oxygen content of water samples at different levels and stations was measured by a titration method by an onboard chemistry team, with the preliminary results suggesting a slight underestimation of CTD oxygen sensor by about 10% (personal communication of Dr. Do-Sik Ham). A precise post-cruise correction of CTD salinity and oxygen content waits to be determined.

A rapid analysis of the raw CTD data using the ODV software is shown below in maps of vertical property profiles, property-property relationships, and meridional sections of properties. As expected, the CTD section captures all water masses and fronts encountered within the whole breadth of the ACC of the region, although its northern limb (SAF) and southern limb (SB) are marginally covered. In conclusion, the ensemble of operations for current meter moorings and CTD stations in the Udintsev Fracture Zone has been carried out successfully, achieving 100% of our original planning.

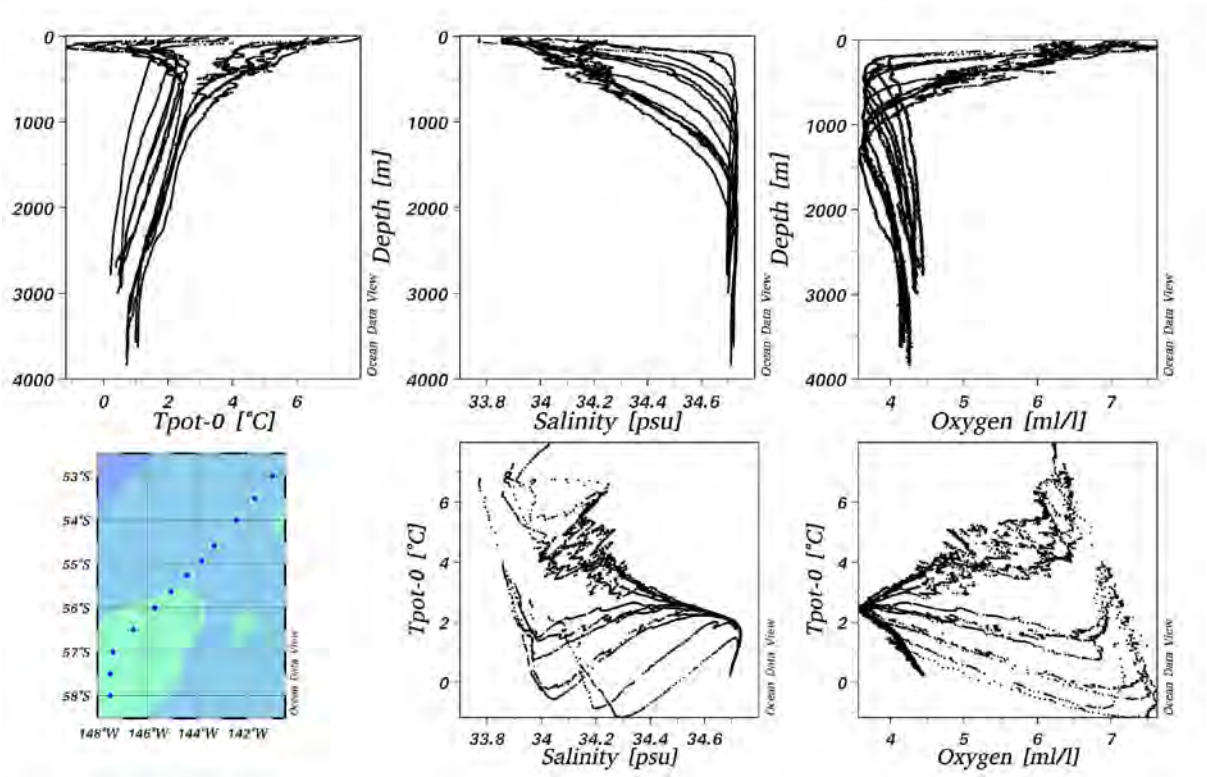


Figure 4.4a. Property profiles and property-property relationships in the Udintsev Fracture Zone.

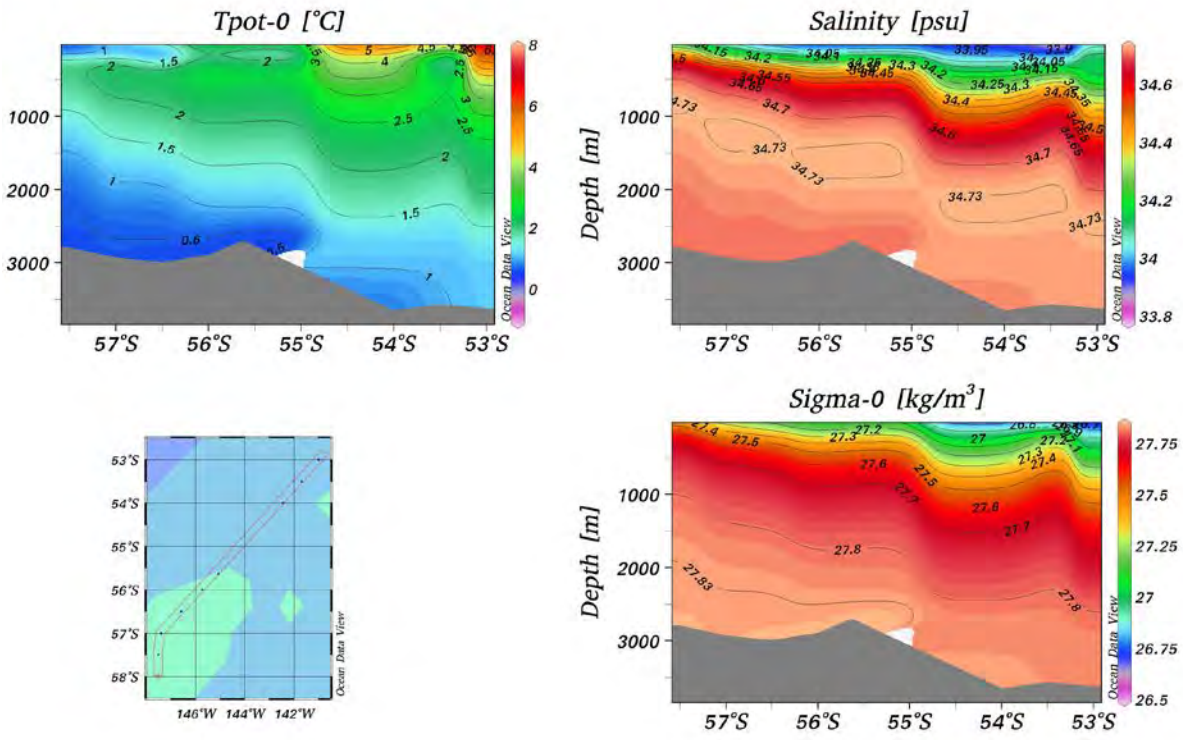


Figure 4.4b. Property sections in the Udintsev Fracture Zone.

# Chapter 5
# Geophysics on Getz Ice Shelf

Povl Abrahamsen[1], Karen Assmann[2], Elin Darelius Chiche[3], Kyoung-Ho Cho[4], Thomas Richter[5], Anna Wåhlin[2]

[1]British Antarctic Survey (BAS), Cambridge, UK

[2]University of Gothenburg (UGOT), Gothenburg, Sweden

[3]University of Bergen (UiB), Bergen, Norway

[4]Korea Polar Research Institute (KOPRI), Incheon, Korea

[5]University of Texas Institute for Geophysics (UTIG), Texas, USA

## 요약문

2016년 1월부터 2월까지의 남극 아문젠해 탐사 (ANA06B) 기간 동안, 겟즈빙붕 (Getz Ice Shelf: GIS)에서의 빙붕저면 용융률의 변화를 연구하기 위해 세 가지의 지구물리 관측이 수행되었다. 먼저 직접적인 빙붕저면 용융률을 관측하는 자동위상전파 음향측심기 (Autonomous phase-sensitive Radio Echo Sounder: ApRES)를 겟즈빙붕에 설치하였고, 같은 지점에서 지진파계측기 (geopebbles)를 사용하여 빙저면과 해저면의 수심을 측량하였다. 또한 중력계를 실은 헬리콥터를 이용하여 빙붕 아래의 전반적인 수심을 측량하는 항공 중력측량을 수행하였다. 자동위상전파음향측심기 설치와 지진파계측기는 겟즈빙붕 서쪽 네 지점에서 수행되었고 네 지점을 가로지르는 950 km정도의 항공중력측량을 3회 실시하였다. 이 세 가지 관측 자료는 겟즈빙붕에서의 더 정밀한 빙붕저면 용융율과 빙붕 아래 해저면과 빙붕 내의 경계면 및 구조를 파악하는데 상호보완적으로 사용될 것이다.

## Abstract

In order to investigate the response of ice-shelf basal melt rates to changes in the underlying ocean, we conducted geophysical surveys on the Getz Ice Shelf during the 2016 Amundsen Sea cruise (ANA06B). The surveys include autonomous phase-sensitive radio echo sounder (ApRES) deployments to measure ice-shelf basal melt rates, seismic surveys with geopebbles to determine the ice base and seabed depths for supporting the gravity survey and future AUV operation under Getz Ice Shelf, and helicopter gravity field observations to provide wide area estimates of water depth below ice shelves. The ApRES deployment and seismic experiment were performed at four sites on the western part of Getz Ice Shelf and three two-hour helicopter gravimetry survey flights were flown over Getz Ice Shelf. Individual observation data will be used to complement more precise measurements of ice-shelf basal melt rates and insight into geological boundaries and structures in the Getz Ice Shelf region.

# 5.1 Introduction

The Getz Ice Shelf study includes moorings and CTD casts along the edges of the ice shelf. This chapter describes the activities aiming to study the ice shelf by measuring its basal melt rate using autonomous phase-sensitive radio echo sounders (ApRES), and determining the subglacial bathymetry using surface seismic shots and helicopter gravimeter survey flights. The three methods are complementary: the seismics give accurate point measurements of ice base and seabed depths, airborne gravimetry gives information about the large-scale bathymetry between these shots, and ApRES gives detailed time series of basal melting and freezing at these points.

Although the original plan was to survey both the western and eastern sides of Getz Ice Shelf, poor weather and lack of time meant that we were only able to reach the western Getz. There we visited four sites for ApRES deployment and seismic survey, and flew three gravity flights. The site positions, along with planned and actual gravity flight lines are shown in Figure 5.1. Waypoints for the eight Getz Ice Shelf sites, along with three positions on Thwaites Ice Shelf, are given in Table 5.1.

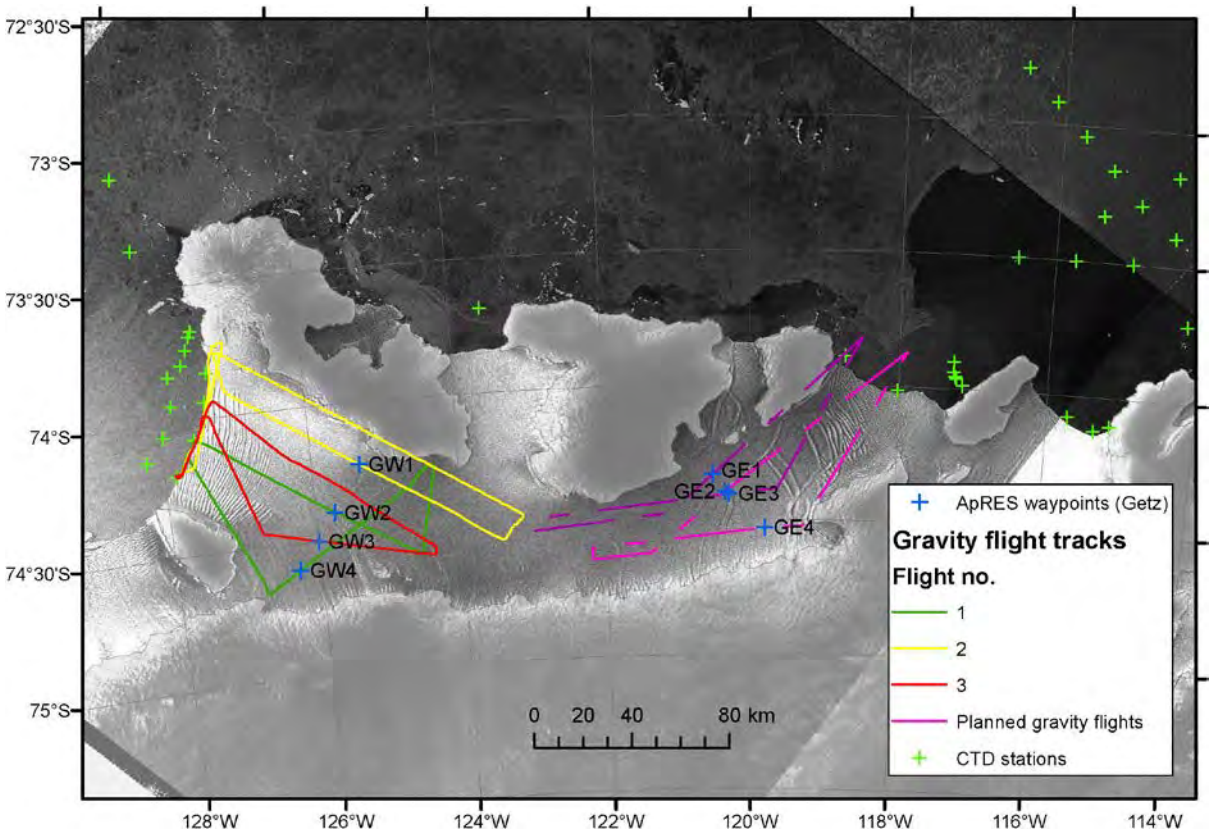


Figure 5.1. Sentinel-1A SAR image of Getz Ice Shelf from Dec. 2015, with ANA06B CTD stations, ApRES/seismics waypoints and actual and planned gravity flight lines superimposed.

Table 5.1. ApRES / seismics waypoints for three regions: western Getz Ice Shelf (GW), eastern Getz Ice Shelf (GE), and Thwaites Ice Shelf (THW)

| Site | Latitude | Longitude | Site | Latitude | Longitude | Site | Latitude | Longitude |
|---|---|---|---|---|---|---|---|---|
| GW1 | 74° 13.800' S | 125° 21.000' W | GE1 | 74° 19.940' S | 120° 31.176' W | THW1 | 75° 04.872' S | 105° 27.240' W |
| GW2 | 74° 24.000' S | 125° 44.400' W | GE2 | 74° 23.737' S | 120° 20.839' W | THW2 | 75° 00.420' S | 105° 34.020' W |
| GW3 | 74° 30.000' S | 126° 00.000' W | GE3 | 74° 24.307' S | 120° 17.482' W | THW3 | 75° 17.946' S | 106° 08.580' W |
| GW4 | 74° 36.000' S | 126° 18.000' W | GE4 | 74° 31.800' S | 119° 48.000' W | | | |

# 5.2 Autonomous Phase-sensitive Radio Echo Sounders (ApRES)

*Lead author: Povl Abrahamsen (BAS)*

Four ApRES units were deployed on ANA06B, on the western side of Getz Ice Shelf. They were all supplied and assembled by British Antarctic Survey in Cambridge in 2015, and use the latest "RMB2" hardware, with firmware version 102. The original plan was to deploy ten radars; five were purchased by KOPRI and five by the University of Bergen. Batteries were supplied by the University of Bergen, and antenna masts and memory cards by the University of Gothenburg.

## Instruments and methods

The radars were installed into 1-m deep holes dug into the snow, with a 60x100 cm sheet of 12-mm plywood above the radar and battery. Batteries used were Sun Xtender PVX-1080T 108-Ah absorbed glass mat (AGM) batteries, charged before deployment with a Defa MarineCharger 1x7 three-stage battery charger. The charger was supposed to charge in three stages, at constant currents of 7, 3.5, and 2 A, before going to a float voltage of 13.5 V. However, we found that it actually charged at closer to 7.5, 2.5, and 2 A, with the first two stages taking only a few minutes for most of the (unused) batteries, and the third stage taking 4-6 hours. It was somewhat confusing that the LED on the charger, which was supposed to be "yellow" at stage three, actually was more orange, and difficult to distinguish from red.

Each radar was connected to compact GPS and Iridium antennas mounted on a 6-m long aluminium pole (Figure 5.2a), with orange plastic flags installed to aid in recovery.

Memory cards for the radars were purchased in Christchurch at short notice; the most suitable cards available were Sandisk Extreme 60 MB/s 16 GB cards. These are rated to -25°C; while this exact model has not previously been tested with ApRES, the similar Sandisk Extreme Pro has been used successfully. In the future care must be taken to purchase (more) suitable industrial cards in advance. The cards were from three batches, manufactured in weeks 16, 18, and 20 of 2015. Two radars have cards from the same batch installed; in the others, cards from two different batches were installed as a precaution against manufacturing variations or defects.

The radars were connected to two cavity-backed bowtie antennas (Figure 5.2b), measuring 60x70x30 cm when assembled. The assembly consists of two copper triangles soldered to a circuit board with a balun and mounted on a polycarbonate roofing sheet using double-faced tape; this is placed in the bottom of the corrugated plastic box, with reinforcing plastic pieces above, and an aluminium reflector at the top of the box. During the passage south, the wooden box containing the antennas was damaged on deck, resulting in seawater ingress into the box, and slight mechanical damage to one plastic panel (not overlapping the copper element or circuit board). After this, the antennas were brought indoors, the baluns rinsed in milli-Q, and continuity between the two sides of the balun was tested. During these tests one antenna was found to have a poor connection between the copper triangle and balun board; this was bridged by soldering a piece of wire to the copper and one side of the transformer on the circuit board. The remaining antennas appeared to have survived their ordeal on deck without any damage. The antennas were buried 20 cm beneath the snow, in a 50 cm deep hole, approximately 4 m from the radar, with a total separation of 8 m between the antenna centres. The magnetic bearing along the line between the antennas was measured using a hand-held compass and noted below.

The deployment positions, settings, and other notes are given in Table 5.2. At each site, the radars were first turned on in attended mode, connected to a laptop. Test bursts of varying RF attenuation (with AF gain at -14 dB) were done to determine the correct settings. In both cases, an attenuation of 20 dB (on a range from 0-31.5 dB) was most appropriate; this was also the default setting used on the remaining units. Then one hundred bursts were fired using the chosen settings; the profiles from these bursts are shown in Figure 5.3. These data were transferred to the computer to determine the "triples" setting, which sets the bin ranges for data to be sent back by Iridium. Once the settings were finalised, the configuration file was updated on the radar, the computer was disconnected, and the radar started in autonomous mode. The first data acquisition was observed (to see that the red LED was blinking), then the radar and battery were buried.

The data is presently handled by Iridium service provider Rockblock and sent to the gmail address UGOT_Iridium@gmail.com from where it can be accessed by all project partners. Additional e-mail addresses or IP addresses can be added as hosts at no extra charge. The IMEI numbers for the modems are given in Table 5.2.

## Deployments on ANA06B

One deployment flight took place on 27 Jan 2016 to the western side of Getz Ice Shelf. After we initially landed on the ice at Getz West 2 (GW2), set up the seismic equipment, and dug the holes for the radar, the helicopter flew back to the ship to collect the radar equipment itself. This was subsequently installed as described above. We then deported the remaining equipment and flew to Getz West 3 (GW3). There we started digging while the helicopter returned to collect the cached equipment. A similar procedure was followed for the following sites.

At sites Getz West 1 (GW1) and 4 (GW4) all three laptops we had brought run out of battery. As we had no working laptops to set up the ApRES, they were started with the default configuration file set up on the ship. This had assumed a base depth above 650 m, and will need to be changed by Iridium to more appropriate settings based on the initial data transmitted back.

After GW1, we returned to the ship, carrying all survival equipment and tools. Unfortunately, poor weather and time constraints prevented the deployment of further radars on the eastern Getz or Thwaites Ice Shelf. The remaining six radars are being shipped back to KOPRI for deployment on the next Amundsen Sea cruise.

## Recommendations for the next deployment

Firstly, more dedicated time must be allocated to this activity if it is to have any chance of success. We cannot rely on having good weather at the exact time that the ship happens to be at an appropriate position for flights to the ice shelf.

The tolerance of the mast poles is very tight, making it difficult to assemble them in the field. Slightly larger tolerance should be given, and a file may need to be brought into the field to adjust the ends of the poles if required.

a

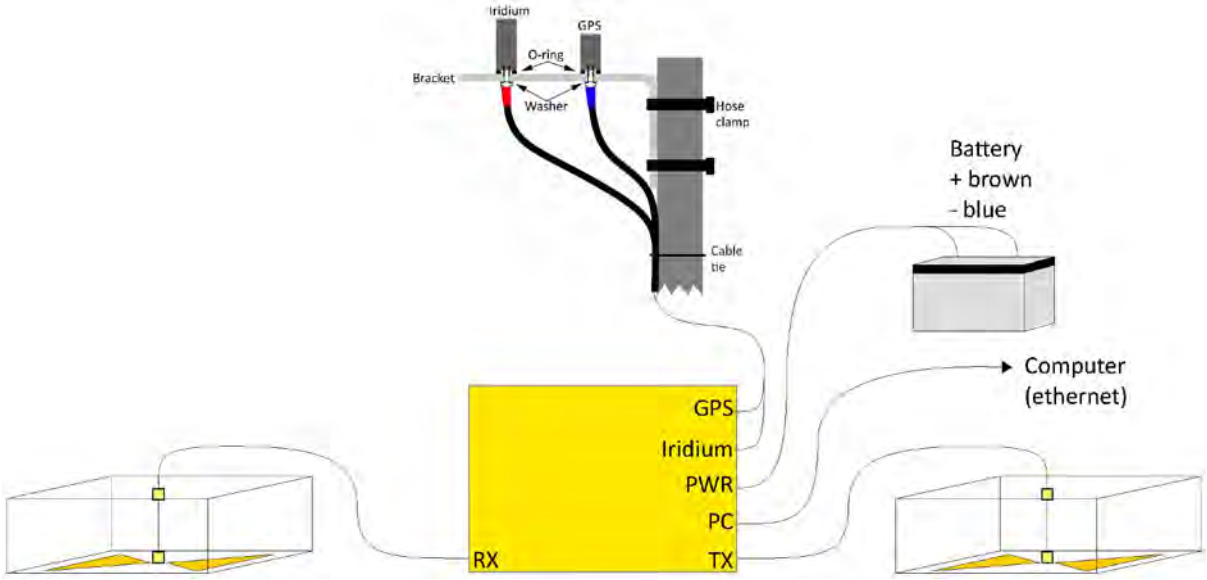


b

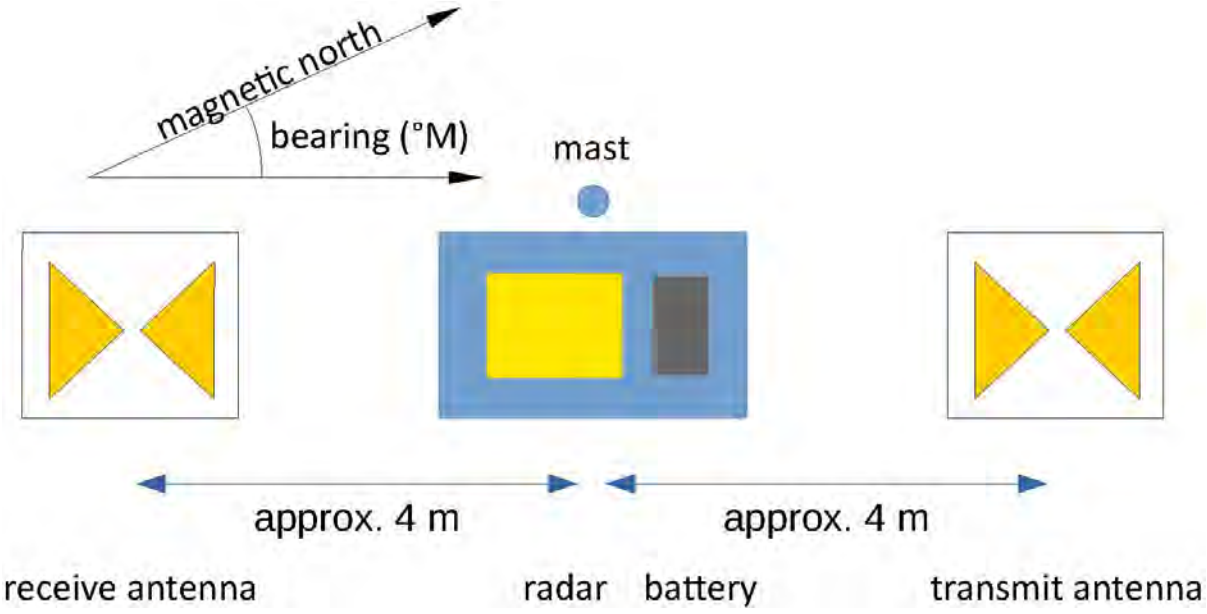


Figure 5.2. a) schematic of an ApRES site, showing the wiring connections on each radar. b) layout of each site, with respect to magnetic north. Drawings are not to scale.

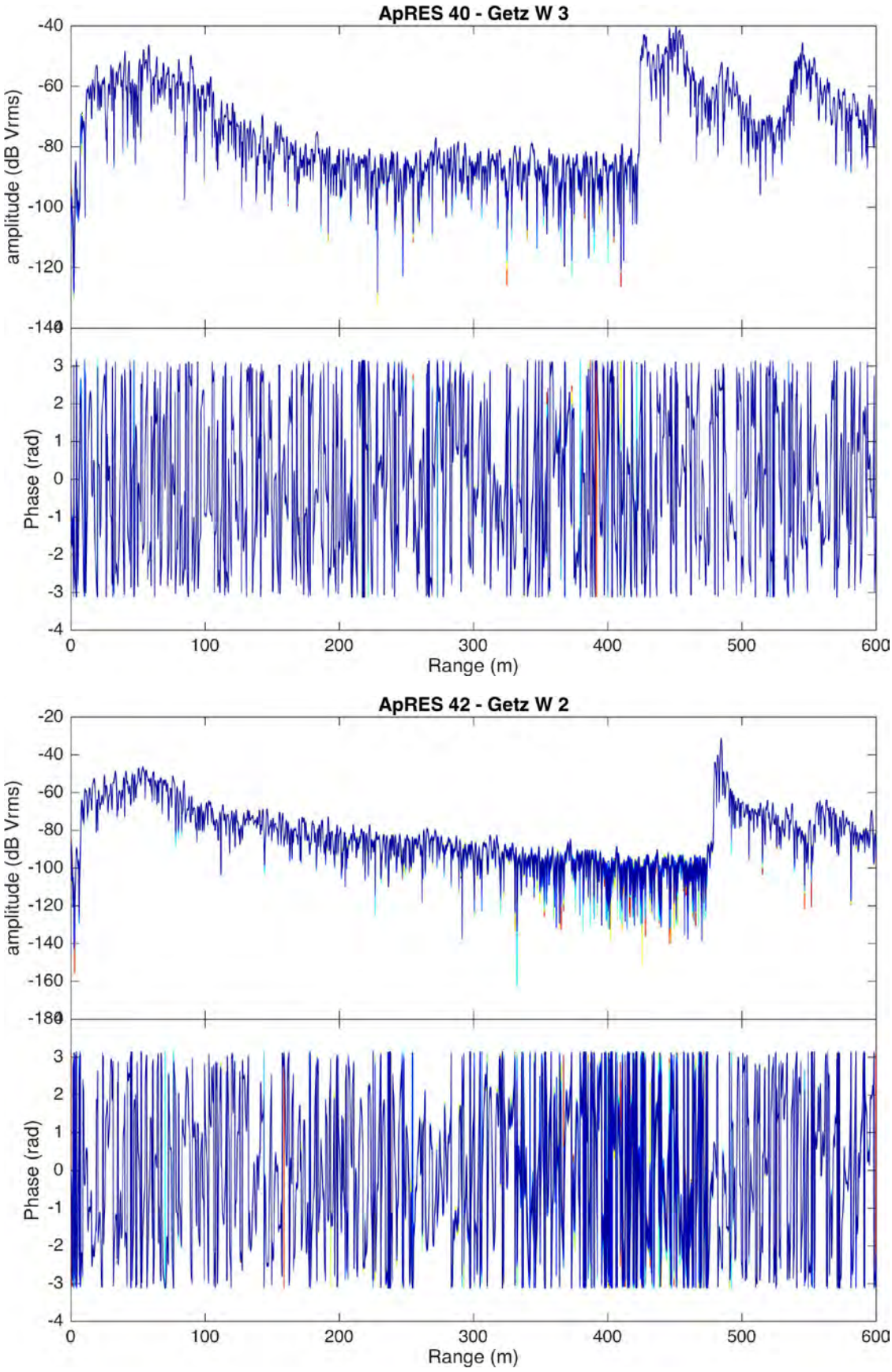


Figure 5.3. Initial 100-burst samples from sites Getz W 2 and 3. Individual chirps are shown, rather than averages.

Table 5.2. Locations and settings used on the ApRES radars

| Site | Serial no. & card | Owner | Iridium IMEI | Latitude | Longitude | Antenna orientation (°M) | Start date & time (UTC) | Approximate base depth (m) | Triples ("start, interval, end" for range bins of data transmitted back) | Notes |
|---|---|---|---|---|---|---|---|---|---|---|
| | 37*‡ | B | 524470 | | | | | | | [1] |
| | 38*‡ | B | 427780 | | | | | | | |
| | 39*‡ | B | 428770 | | | | | | | |
| GW3 | 40*‡ | B | 421770 | 74°29.982'S | 125°59.938'W | 035° | 27 Jan 2016, 11:55 | 424 | 45,5,100,100,20,380,380,3,450 | |
| GW2 | 42*‡ | B | 520520 | 74°23.993'S | 125°44.312'W | 077° | 27 Jan 2016, 09:36 | 479 | 45,5,100,100,20,450,450,3,520 | [2] |
| | 43*‡ | K | 522210 | | | | | | | |
| GW4 | 44*† | K | 420770 | 74°36.018'S | 126°17.931'W | 138° | 27 Jan 2016, 13:55 | unknown | 46,8,100,100,20,650,650,5,800 | |
| GW1 | 45** | K | 525450 | 74°13.808'S | 125°20.930'W | 073° | 27 Jan 2016, 15:58 | unknown | 46,8,100,100,20,650,650,5,800 | |
| | 46*† | K | 525420 | | | | | | | |
| | 47** | K | 520160 | | | | | | | |

Memory card batches: 1516250261G(*), 1518950175G(†), 1520350260D(‡)
Instrument owners are the University of Bergen (B) and KOPRI (K)
IMEI numbers in the table are prefixed by 300234063

[1] Power switch difficult to turn on, but OK once on.
[2] One piece of foam inside the box was missing; a suitable replacement was made on board.

# 5.3 Seismic surveys at the ApRES sites

*Lead author: Karen Assmann (UGOT)*

## Instruments and methods

On ANA06B seismic surveys were performed at each of the ApRES deployment sites to determine the position of the bedrock in order to support the gravity surveys and future AUV work under Getz ice shelf (see Figure 5.4 for a map and positions). We used a set of 13 wireless geophones called geopebbles that were developed and built at Pennsylvania State University by Shridhar Anandakrishnan and Peter Burkett and kindly loaned to the University of Gothenburg for this expedition. After training and tests in Gothenburg the geopebbles were charged and the batteries disconnected before transport to prevent them from discharging fully. When disconnecting the battery on fir12 we found that the thin grey wire connecting the GPS receiver to the circuit board had become detached and therefore operated with an array of 11 geopebbles (fir00-fir14) plus birch05 as a base.

The batteries were reconnected when we reached the Amundsen polynya on 19 January. The geopebbles were then taken on deck so they could find their GPS position and time locks. GPS positions on the display of the instruments were found to be inaccurate, but those on the display of the zstatus.py script agreed with the handheld and the ship's GPS, as did the GPS time. We had a training session with all possible personnel where we also performed a quality check with zQChdf.py in which all geopebbles used in the training session performed well. The geopebbles were then switched off and recharged.

## Experiments on Getz Ice Shelf

We performed seismic surveys at the four ApRES sites deployed on the western Getz Ice Shelf on 27 January 2016 between 08:30 and 15:30 UTC. The geopebbles were taken out on deck approximately one hour before being loaded into the helicopter and successfully achieved GPS locks on time and position (zstatus.py). The UNIX clocks were set with setclock.sh. The geopebbles were left switched on for the duration of the field session and switched off back on board Araon after all four sites were completed.

At the first site we did a huddle test with the geopebbles and found that they locked GPS position and time successfully on zstatus.py. We performed two quality checks with zQChdf.py with hammer blows timed within the 5 sec recording window. The sound source was a 3.5 kg sledgehammer and a 5 mm thick square steel plate with an edge length of 40 cm.

The geopebbles were then deployed along a 100 m long line at intervals of 10 m in numerical order with the writing on the geopebbles facing to the right of the line (Figure 5.4). We used a pulk sled to deploy the geopebbles. Small holes were dug to bring the top of the geopebbles level with the snow (Figure 5.5). After attaching the dedicated metal spikes to their bases, we pressed the geopebbles into the snow to ensure contact of their bases with the snow. The first set of 10 hammer blows was performed 10 m out from fir00, a second set of 10 sledgehammer blows halfway between fir05 and fir06 and the last set 10 m off the other end of the line at fir14 (Figure 5.4). Times of the first hammer blows of each set were recorded in UTC. Positions and times recorded on the deck sheet are summarized below (Table 5.3), as well as the start times and lengths used to extract the sets of hammer blows from the raw-files into hdf-files. The same array setup was used at all four sites. The sites were completed in the order GW2, GW3, GW4 and GW1.

Snow conditions were wind packed, but reasonably soft at the surface with icy patches 15-20 cm below the surface. Site GW4 was slightly more hard-packed, while site GW1 had patches of soft snow and hard-pack/ice. There were light winds at the first sites that decreased further towards the later ones.

The battery pack for the wireless router used to communicate with the geopebbles proved to only provide enough power for the first two sites, so we were only able to check GPS times and not positions for sites GW4 and GW1.

When downloading the data after our return to Araon, we discovered that the setclock.sh script had failed to reset the UNIX clocks on the geopebbles to the current date. Instead the data was recorded into files with names that indicated recording dates between October and December 2015. We used a perl script supplied by Peter Burkett to identify the appropriate raw-files that contained our sites and extracted the appropriate time intervals into hdf files and ascertained the presence of all sites and signals in the data. The data will be processed at Pennsylvania State University.

Table 5.3. Summary of positions and times of the seismics sites. Shown are both target positions of the sites and the actual position of the sites as determined by handheld GPS. Also shown are the times recorded on the deck sheet for each set of hammer blows as well as the GPS time in the data files for the start of the data gather to extract data from the raw files

| Site | Position | | Location / time |
|---|---|---|---|
| | Target Position | | 125°21.000'W, 74°13.800'S |
| | GPS Position | | 125°20.921'W, 74°13.809'S |
| GW1 | | fir00 | 15:25, 10 hammer blows (hdf gather: 15:22:30, 70sec) |
| | Base Position | fir05/06 | 15:27, 10 hammer blows (hdf gather: 15:25:30, 70sec) |
| | | fir14 | 15:31, 10 hammer blows (hdf gather: 15:29:00, 80sec) |
| | Target Position | | 125°44.400'W, 74°24.000'S |
| | GPS Position | | 125°44.374'W, 74°23.996'S |
| GW2 | | fir00 | 08:30, 10 hammer blows (hdf gather: 08:30:00, 120sec) |
| | Base Position | fir05/06 | 08:36, 10 hammer blows (hdf gather: 08:36:00, 120sec) |
| | | fir14 | 08:42, 10 hammer blows (hdf gather: 08:42:00, 120sec) |
| | Target Position | | 126°00.000'W, 74°30.000'S |
| | GPS Position | | 125°59.956'W, 74°29.986'S |
| GW3 | | fir00 | 11:36, 10 hammer blows (hdf gather: 11:35:00, 120 sec) |
| | Base Position | fir05/06 | 11:42, 10 hammer blows (hdf gather: 11:40:30, 90 sec) |
| | | fir14 | 11:45, 10 hammer blows (hdf gather: 11:43:30, 80 sec) |
| | Target Position | | 126°18.000'W, 74°36.000'S |
| | GPS Position | | 126°17.930'W, 74°36.016'S |
| GW4 | | fir00 | 13:29, 10 hammer blows (hdf gather: 13:27:30, 120 sec) |
| | Base Position | fir05/06 | 13:33, 10 hammer blows (hdf gather: 13:30:50, 80 sec) |
| | | fir14 | 13:36, 10 hammer blows (hdf gather: 13:34:10, 80 sec) |

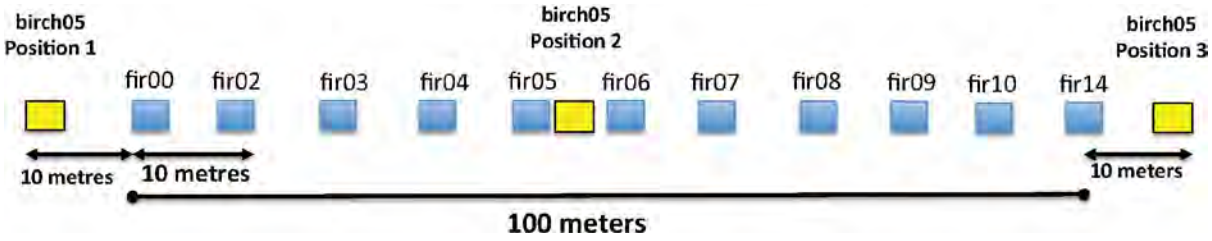


Figure 5.4. Sketch of the seismics array with placement of the base, birch05, and the sound source for each of the sets of hammer blows.

Figure 5.5. Pulk sled with geopebbles. The seismics line with snow from the holes that the geopebbles were placed into can be seen in the background.

## 5.4 Airborne gravimetry

*Lead author: Thomas Richter (UTIG)*

### Introduction

Precise measurement of the earth's gravity field from fixed and rotary wing aircraft has become a standard method to efficiently collect gravity data for both commercial and academic uses in the last twenty years. The University of Texas Institute for Geophysics (UTIG) in collaboration with the Korea Polar Research Institute (KOPRI) and the University of Gothenburg (UGOT) deployed an airborne gravimeter on board the IBRV Araon for the ANA06B cruise with two major goals,

engineering and scientific. The engineering goal was to demonstrate the technical and logistical feasibility of airborne gravimetric operations from a ship at sea, which to our knowledge had not been attempted before. If successful, the technique provides a method to reach areas in the polar regions which are difficult to reach via land based aircraft and inaccessible for direct observation by shipboard instrumentation. The scientific goal was to obtain gravimetric data over the Getz Ice Shelf in support of the UGOT/KOPRI /UiB (University of Bergen) seismic and radar projects of ANA06B. Gravity field observations can provide wide area estimates of water depth below ice shelves which complement the more precise seismic and radar observations, as well as insight into geological boundaries and structures. Five two-hour flights for data collection over the Getz Ice Shelf were in the pre-cruise plan.

## Instruments and methods

The instrumentation deployed consisted of a Gravimetric Technologies GT-1A airborne gravimeter and supporting auxiliary equipment. The GT-1A is a modern technology gravimeter designed for moving platform usage (ships and aircraft). It consists of a sensitive vertical axis accelerometer supported and kept aligned with local vertical by an inertial platform stabilized in all three axes, along with control and data recording subsystems. The GT-1A also uses real-time GPS inputs to assist the inertial measurement unit in stabilizing the sensor platform. The GT-1A had been previously installed aboard a large number of fixed and rotary wing aircraft including land-based AS350B helicopters similar to those scheduled for deployment aboard the IBRV Araon, and UTIG has been operating GT-1A and GT-2A gravimeters in Antarctica aboard fixed wing aircraft since 2012.

The GT-1A was installed aboard the helicopter identified as ZK-HJV at the aircraft's home base at the Helicopters New Zealand facility in Nelson, New Zealand. From there it was flown to Christchurch and onto the IBRV Araon. The GT-1A and its auxiliary equipment are mounted inside the AS350B in the location of the rear passenger seat and the instrument occupies all of the helicopter's rear seating area (Figure 5.6). Other than the physical installation, the only other interface required with the helicopter is the provision of 28 VDC power and installation of a dedicated GPS antenna. After installation but without being powered up the GT-1A does not require special care and the helicopter can be flown normally.

Prior to operation the GT-1A requires a 48-hour initialization and warm-up process and during the time period of possible gravity operations the GT-1A must be kept powered up. Long term power for when the helicopter is parked and not providing generator power to the instrument must be provided by an external source of 28 VDC or 110/220 VAC power. The instrument requires fairly calm seas for initialization for the first few hours, and the initialization process aboard a ship at sea was one of the points of investigation of the deployment.

The GT-1A was powered up and initialized at sea on 16 January, ten days after the IBRV Araon left port and after the passage through the relatively rough Southern Ocean into the calmer Amundsen Sea. The power up and initialization process went without problem and the instrument rapidly stabilized into operational condition. After this power up sequence the GT-1A was kept continuously powered using an extension cord to a 220VAC outlet in the helicopter hangar. In addition to power, the GT-1A also requires continuous connection to a GPS antenna while the ship is in motion in order to remain stabilized. During flight the GT-1A is connected to a GPS antenna installed for that purpose in the upper left window of the aircraft. When the aircraft is in the ship's hangar GPS reception was not possible with the aircraft antenna and a separate antenna was temporarily mounted just outside the hangar door with the antenna cable extended through available space (about 5 mm) under the movable hangar section (Figure 5.7). This provision of continuous GPS signal to the GT-1A during ship operation was another logistical requirement to be evaluated during the deployment. As it turned out,

the system worked satisfactorily with this simple arrangement, however a more secure arrangement for GPS signal provision inside the hangar should be implemented for future deployments.

When the helicopter was moved out of the hangar for flight operations the long extension cord for 220VAC power was extended during aircraft roll out and the GPS signal feed to the GT-1A was switched from the external to the aircraft mounted antenna. Both of these operations proved to be without difficulty. After aircraft engine start, the extension cord was removed from the GT-1A and the system was ready for flight. The system does not require an operator or pilot attention during flight.

## Gravimetric survey on ANA06B

The first flight of the helicopter from the ship with the GT-1A powered up occurred on 21 January when its helicopter was used for logistical support of the Automatic Weather Station team during their trip ashore. The helicopter with the GT-1A carried a sling load to shore. The GT-1A was powered up but no data was recorded as the flight parameters were unsuitable for gravity data collection. Post flight evaluation of the GT-1A showed that the system remained stable and operational during the flight and was adapted successfully to the ship and helicopter flight environment.

The first gravity data acquisition flights occurred over the night of 27-28 January in concert with the UGOT and BAS team expedition to the western part of the Getz Ice Shelf for on-site seismic and radar operations. The helicopter flew three consecutive flights of about two hours each, returning to the ship for refueling between them.

In addition to the equipment aboard the helicopter, the GT-1A system has a specification for a GPS base station to provide reference data for post flight processing of the GPS data collected onboard the aircraft. The base station is normally stationary on a land base near the area of gravimetric data collection. This is to provide for differential GPS (DGPS) processing of the GPS data. Though this is a requirement in the system specification, UTIG has had satisfactory results without base station data in Antarctica, however base station data is highly desired, ideally from a location with clear view of the sky in all directions and with no nearby structures. For the flights from the IBRV Araon of 27 January two GPS base stations were used, one temporarily installed aboard the ship (Figure 5.8) and one carried to the ice shelf by the expedition team. Evaluation of the GPS base station aboard the ship for gravity data use was a point of investigation for this deployment. The ship remained in a stationary location during the gravity data acquisition flights; however it did have continuous slight movements due to wind and wave action. The GPS base station carried to the ice shelf by the expeditionary team was moved to each of the four operating locations of the team as the team progressed, not ideal for the GPS data, but as required by the logistics of the operation. During the periods of movement the base station data is lost.

During the three flights of 27-28 January approximately 950 line-kilometers of gravity data were acquired (Figure 5.9). All the equipment, GT-1A and the onboard and base GPS stations appear to have performed nominally, as designed. Final data reduction has to be done back at the UTIG home offices with access to powerful GPS data reduction software and high bandwidth access to Internet repositories of the GPS satellite orbital parameters. However, preliminary data reduction done onboard the Araon indicates that the entire gravimetric system (helicopter, GT-1A, GPS receivers) performed well and high quality data was acquired. The gravity data acquired while the on-shore base station was stationary (about 65% of the total) could be processed to a high degree aboard the ship and produced good results (Figure 5.10). The base station data acquired from the (slightly) moving ship, while complete and of high quality on its own, was determined to be inadequate for gravity data use without more powerful data reduction facilities available on shore. Techniques to utilize the ship board base station data will be part of a further investigation post cruise. As mentioned, UTIG has

obtained satisfactory gravity results without GPS base station data through the execution of post field processing so it is expected that the entire set of data acquired during the flights will be successfully processed into gravity field information in the summer of 2016.

Poor weather in the operating area precluded any additional gravity data acquisition flights during the cruise and the gravity equipment was unloaded without incident from the helicopter on 03 February, at which time the helicopter was returned to standard configuration.

Overall this test of helicopter gravity acquisition from the IBRV Araon appears to be a solid success, meeting the best of expectations for it. The author (and lead engineer) would like to heartily thank the master and crew of the IBRV Araon, the KOPRI, UGOT, UiB, and BAS science teams, and the personnel of Helicopters New Zealand for all their assistance and cooperation in the deployment of this novel and rather demanding piece of equipment aboard ship.

## References

Greenbaum, J. S., Blankenship, D. D., Young, D. A., Richter, T.G., Roberts, J. L., Aitken, A. R. A., Legresy, B., Schroeder, D. M., Warner, R. C., van Ommen, T. D., and Siegert, M. J., 2015, Ocean access to a cavity beneath Totten Glacier in East Antarctica, Nature Geoscience, 8, 294–298, 10.1038/ngeo2388

Figure 5.6. GT-1A installed aboard AS350B onboard RV Araon.

Figure 5.7. GPS antenna for the GT-1A while the helicopter was hangered. The rigid framed backpack strapped to the helo deck proved to be adequate as an antenna mount and sufficiently nonintrusive to other deck operations.

Figure 5.8. Base station GPS receiver and antenna installed on Compass Deck of RV Araon during gravity data acquisition flights.

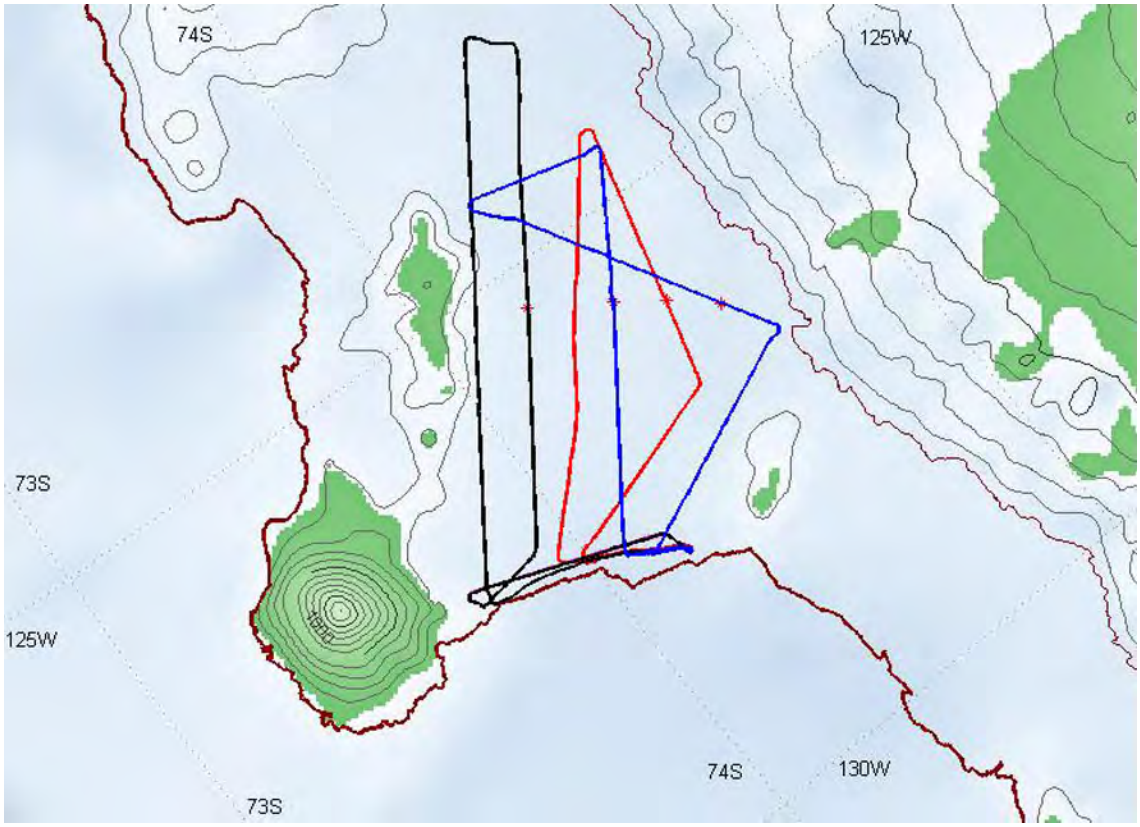


Figure 5.9. Tracks of the three 27-28 January flights over the western part of the Getz Ice Shelf. Red stars show the locations of the seismic/radar sites.

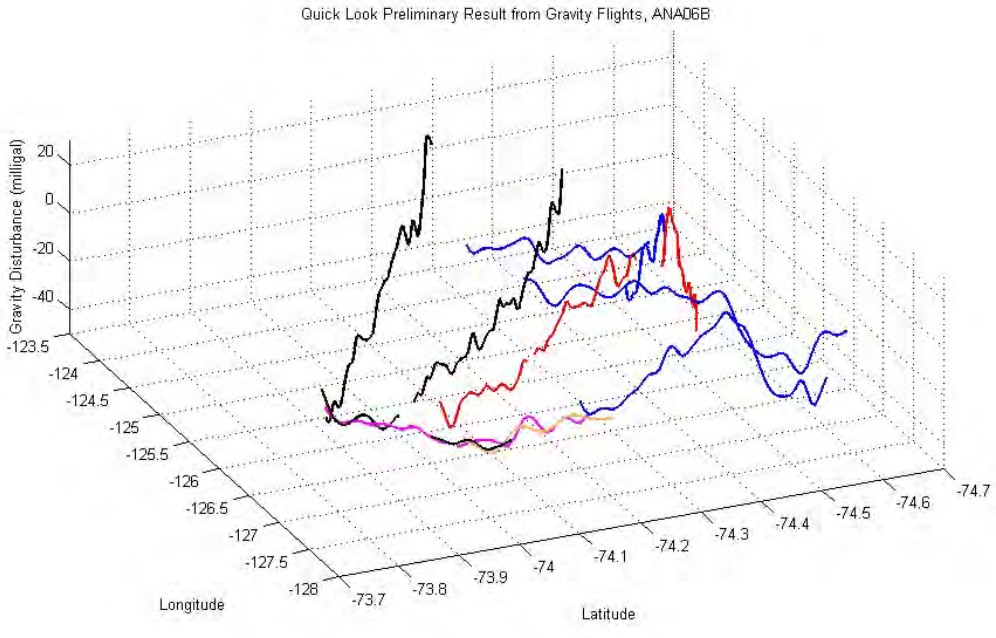


Figure 5.10. Plot of gravity field strengths obtained from the flights of 27-28 January, field processed using the ice shelf base station GPS reference.

# Chapter 6
# Atmospheric Science and Glaciology

T. Choi, S.B. Hong, Y.D. Cho, and S.H. Haam

Korea Polar Research Institute (KOPRI), Incheon 406-840, Korea

## 요약문

서남극 지역 기후변화에 대한 대기과정의 역할 이해를 위해 연안 지역에서의 실측 그리고 특히, 연안 돔 지역에서의 빙하 코어 시추가 필요하다. 이에 대한 사전 연구를 위해 4명의 연구원이 베어 반도(Bear Peninsula)의 무어 돔(Moore Dome)과 카니스티오 반도(Canisteo Peninsula) 주변 린지 섬(Lindsey Island)를 방문하였다. 무어 돔에서의 활동은 2016년 1월 21일 11시부터 ~ 1월 23일 16시까지의 약 53시간 이루어졌다. 활동 기간 날씨가 좋지 않아, 당초 계획했던 지점보다 북서쪽 8 km 떨어진 곳에서 현장 활동이 이루어졌고, GPR 탐사는 수행되지 못하였다. 약 11.5 m 높이의 자동기상관측시스템(AWS)이 설치되었고 (S74°17′41.3″/W111°30′00.8″), 남동쪽으로 약 230 m 떨어진 곳에서10 m 깊이 펀 코어(firn coring)를 시추하였다 (S74°17′45.8″ / W111°29′37.5″). AWS에서는 두 높이에서의 풍향, 풍속, 기온, 상대습도, 기압과 한 높이에서의 지표 복사 및 적설 관측이 이루어진다. 일 평균값 중 일부는 이리듐을 통해 극지연구소로 전송되며, 10분 평균 자료는 2년 후 방문 시 회수될 예정이다. 펀 코어는 총 18번의 시추를 통해 10.10m 깊이의 펀 코어를 시추하였다. 펀층 모델을 통해 계산한 결과 약 4-6년 동안의 기록을 복원할 수 있을 것으로 예상된다.

한편, 린지 섬 방문은 2016년 2월 2일 14 시 ~ 2월 2일 16시 30분에 이루어졌으며, 2008년 설치된 AWS (73° 36′ 4.32″ S/ 103° 01′ 15.18″ W)와 2012년 설치된 플럭스 시스템(S 73°36′37.505″, W 103°02′40.55″)을 모두 철수 하였다. AWS는 강풍에 의해 쓰러져 있었고, 2개의 풍향풍속계는 타워로부터 떨어진 곳에서 발견되었다. 반면에, 플럭스 시스템은 타워는 완전히 휘어져 있었고, 3차원초음파풍속계와 고속반응습도계에는 부식이 있었고, 순복사계는 눈에 부분 묻혀있었다. 다만, 자료집록기에 저장된 자료는 회수할 수 있었다.

## Abstract

To better understand the role of atmospheric processes on climate change on West Antarctica, field activities at two coastal areas, Amundsen Sea was planned in 2015/16 summer season. The first activity was carried out at Moore dome, Bear Peninsula from January 21 to 23. Overall, the weather was bad over Moore Dome and helicopter flight was very limited. Therefore, the study site was decided at an area, which was to the northwest ~8 km away from the planned one. 11-m high automatic weather station was set up and 10-m firn coring was made. However, GPR survey was not made due to limited time by bad weather.

The second activity was carried out at Lindsey Island for two and half hour on February 2. Both automatic weather station and flux system were destroyed and then were recovered. Different from the situation in 2011/12, much more penguins, skua and seals were found at the island.

## Purpose and aims

Air temperature over West Antarctica is known to have increased moderately over past decades. However, it seems rather complicated to identify the dominant and direct cause for the warming. Studies on climate change have been limited by lack of measurements including ice coring over West Antarctica, particularly on the coastal area, which has experienced significant mass loss. To better understand the role of atmospheric processes on climate change on West Antarctica, ice coring is needed at coastal domes as well as long-term meteorological measurements. For this, installation of automatic weather station and firn-core sample are needed as survey research. The aim in 2015/16 is to install an automatic weather station, GPR survey beneath the dome area and sample 10-m long firn core at Moore Dome, a coastal dome in the Bear Peninsula. Another aim is to retrieve data from automatic weather station installed in 2008 and flux system in 2012 as well as to recover both systems at Lindsey Island.

## Material and Methods

Activity at Moore Dome, Bear Peninsula

A research team of an atmospheric scientist, a glaciologist, a technician and a safety guard visited the Moore Dome site from 21 to 23 in January. To access the area, Araon, an Korean Ice- breaking research vessel anchored near the Dotson Iceshelf. Low visibility over snow covered the Moore dome limited helicopter flights between the site and Araon and finally, activity area was decided at an area to the northwest ~ 8 km away from the planned one. After four flights including one survey flight and two flights for cargo, field work started before noon. First, base camp was set up for stay and a 12 m high tower (S74°17′41.3″/W111°30′00.8″) was erected near the camp until late night on 21. It snowed with strong wind in the next morning and field activity was not resumed until early afternoon. Two researchers started to install meteorological instruments on the tower. The other researchers (a glaciologist and a safety guard) moved to an area to the southeast 230 m away from the camp for firn coring (S74°17′45.8″/W111°29′37.5″). According to weather forecast, the dispatch was advanced from 24 to the morning on 23. Simultaneous field work at both area was carried out over the night and was finished about 6 o'clock for firn coring with a depth of ~ 10m and 9 o'clock for the AWS. Unfortunately, ground penetrating radar (GPR) survey was not executed due to limited time and bad weather condition. Until early afternoon there were a few of flights for the return to Araon. The research team returned to Araon around 16 o'clock.

## Description of AWS

Figure 6.1 shows the installed AWS on January 22, 2016 (UTC). Instruments are summarized at Table 6.1. All data are sampled at every 30-second except for snow height, which is sampled twice a day. 900-Ahr Lithium batteries and 500-Ahr rechargeable batteries are used to provide the AWS with 12VDC power with three 20 W solar panels. A net radiaometer is mounted at a highest level with its sensor facing south to avoid shadow effects by other instruments and reflected shortwave radiation by the solar panels facing north. 10-minute and daily averaged data are stored in the data logger and daily averaged data are transmitted to the KOPRI by using iridium transmitter. 10-min averaged data will be retrieved during the next visit.

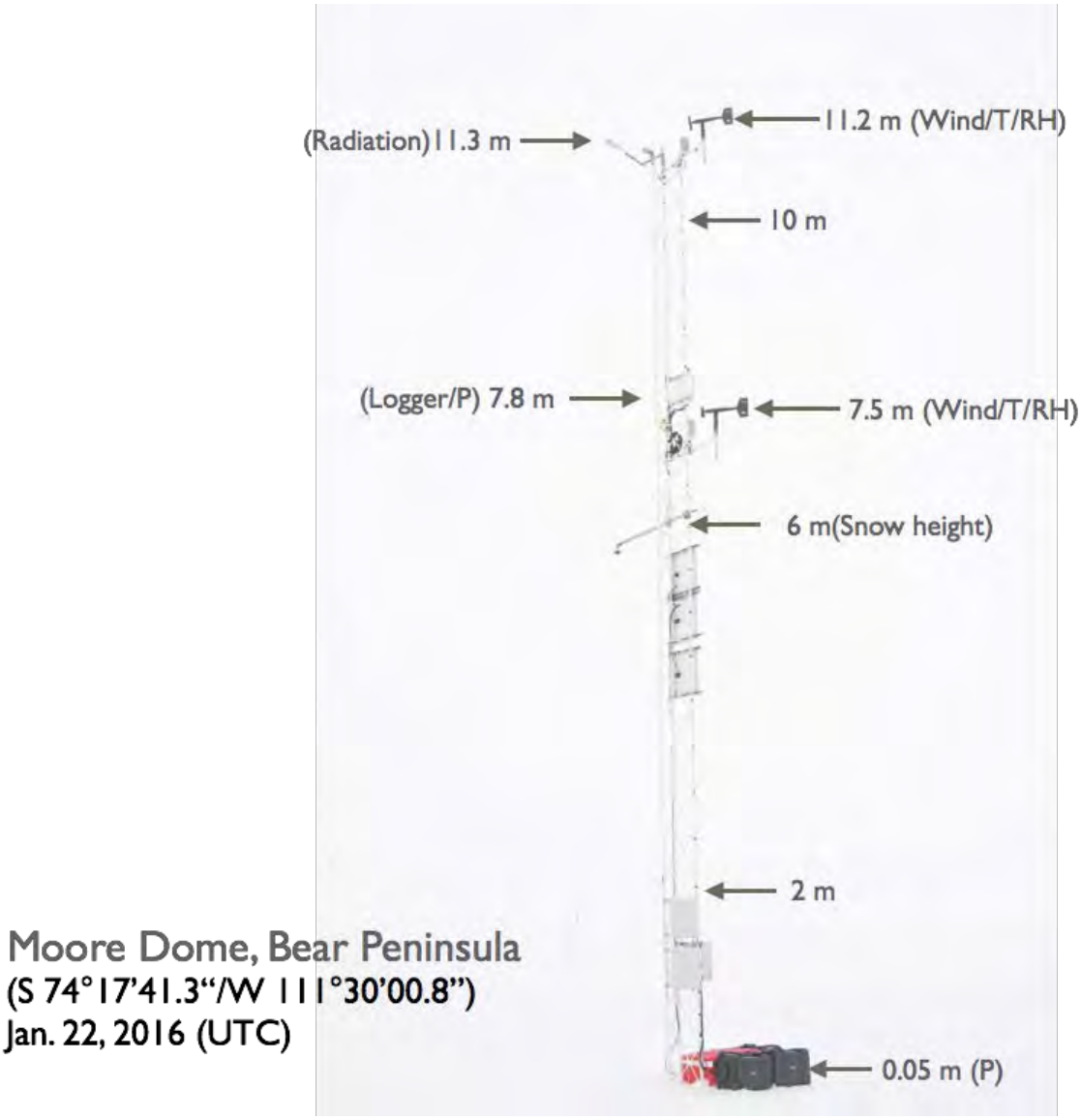


Figure 6.1. Automatic weather station at the Moore Dome, Bear Peninsula.

Table 6.1. Summary of instruments

| Instruments | Model | Manufacturer |
|---|---|---|
| Wind monitor | Wind monitor-HD Alpine 05108-45 | RM Young |
| Temperature/humidity Probe | HMP155 | Vaisala |
| Snow height sensor | SR50A | Campbell Scientific Inc. |
| Barometer | PTB110 | Vaisala |
| Net radiometer | CNR-4 | Kipp & Zonen |
| Logger | CR1000 | Campbell Scientific Inc. |

## Description of firn coring activity

Figure 6.2 shows the result of core processing in the field. 18 firn coring runs were undertaken using a hand auger (Model No. Auger 0417, Japan) and the final depth of firn coring was ~ 10.10 m. The firn coring was conducted at the site to the southeast 230 m away from the camp (S74°17′45.8″/W111°29′37.5″). The core catchers, core catcher spring, cutters, and P5 shoe were assembled and rod holder was also installed at the drilling site. The firn core was drilled with an average core depth of ~ 50cm and the total drilling time was ~10hrs. Figure 6.3 indicates the relationship between age and depth estimated from firn densification model. The initial snow density (~373 g $cm^{-3}$) and annual mean atmospheric temperature (~ -15℃) were assumed based on the slope of regression line between density and depth of surface snow layer and measurement result of USA AWS installed at the bear peninsula (Lat: 74.56S, Lon: 111.89W Elev: 312m). The age at the bottom of firn core was estimated to be ~ 2012-2010.

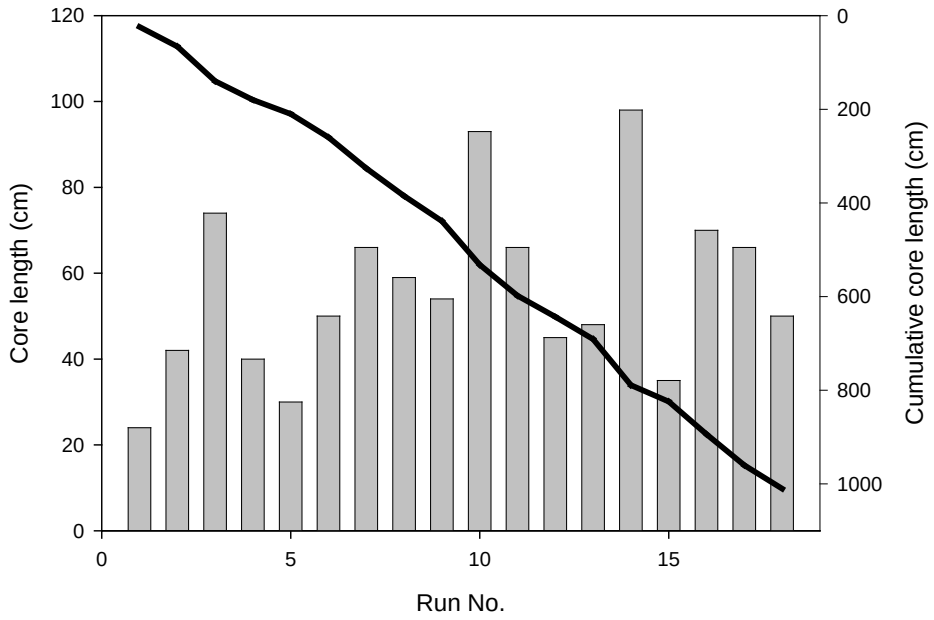


Figure 6.2. The core length per each run (bar) and cumulative core length (line).

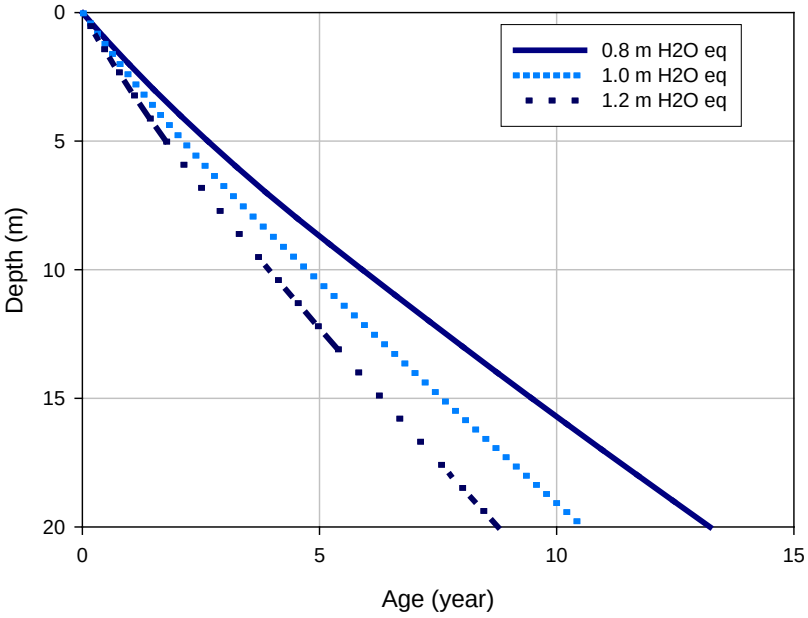


Figure 6.3. Modelled age-depth relationship (Mean annual temperature: ~ -15℃, Initial density: ~ 0.373 g $cm^{-3}$).

## Activity at the Lindsey Island

Field activity to recover an AWS and an Flux system as well as to retrieve their data was carried out within two hours in the afternoon on February 2. First, three researchers visited the Flux site (S73°36′36.6″, W103° 02′13.2″). The system was half-buried by snow and the tower was completely bent. Control boxes for 3-D sonic anemometer and krypton hygrometer formed rust. A net radiometer was buried in the snow. 3-D sonic anemometer, krypton hygrometer, net radiometer and data logger were recovered. The logger was still working and the data from the logger were retrieved later. Two more researchers joined the work at AWS site (S73°36′4.14″, W103°01′15.3″). AWS fell down and two anemometers were found a few meters away from the tower. All instruments were recovered and data from the data logger were retrieved later. Different from the situation in 2012, much more penguins, skua and seals were found at the island.

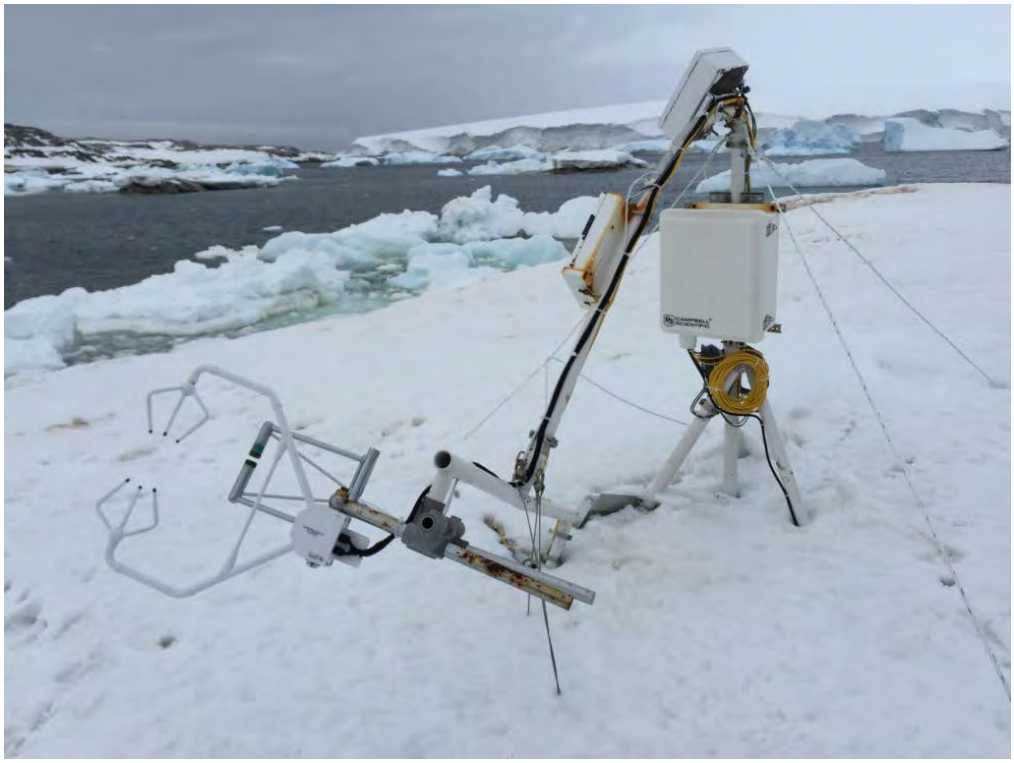

Figure 6.4. Flux system at Lindsy Island on February 2, 2016.

Figure 6.5.  AWS at Lindsey Island on February 2, 2016.

# Chapter 7
# Ocean Optics

DaeHyeok Lee and Hyun-cheol Kim

*Korea Polar Research Institute, Korea*

## 요약문

서남극 해역의 폴리냐에서 높은 일차생산력이 보고 되고 있다. 폴리냐에서의 높은 일차생산은 남극해가 탄소 순환에 있어 중요한 역할을 하고 있다는 증거이기도 하다. 하지만, 폴리냐 내 일차생산력의 대부분은 해색원격탐사(Ocean Color)기술로 부터 유추되는 추정치에 근거하고 있다. 중위도권에서 해색원격탐사의 역활은 많은 현장 검정을 통해 높은 신뢰도를 제공하고 있으나 남극의 경우 절대적으로 부족한 현장 관측 경험치 및 광학특성을 이용한 원격탐사 (해색원격탐사) 특성상 낮은 태양 고도와 이에 따른 입사광선의 특징은 고위도권 해색원격탐사의 신뢰도면에서 해결되어야 하는 숙제이다. 본 연구는 이러한 광학기반 해색원격탐사 자료의 검보정을 통해 해색원격탐사의 신뢰도를 높이는 것이다. 현장에서 광학특성에 기여하는 인자들(식물플랑크톤과 부유성 입자 등에 의한 흡광과 CDOM 등 용해된 물질에 의한 흡광)을 측정하였다. 또한 식물플랑크톤의 정량 추정에 사용되는 엽록소 농도를 측정하였다. 이와 동시에 위성에서 측정된 수출광량의 정밀도를 평가하기 위해, 해수 내 광학특성을 측정(Free-falling optical profiler)하여, 고위도권 해수속의 광학특성에 의한 해수면 수출광량을 연구선의 항적을 따라 연속 측정(Above water optical system) 하였다.

## Introduction

Optical properties are important factors reflecting the physical processes related to the solar energy absorption and distribution in ocean and sea ice. The data of optical properties can be used to analyze the influence from biomasses, including phytoplankton and algae within the light field. Also, the light absorption and scattering influence the heat transportation and dispersion in the ocean. On the other hand, the optical data, together with the analysis for the inherent optical property of particles in the water, can be used for calibration and validation of visible remote sensing data.

In this cruise, we tried to get bio-optical relationships to improve ocean color data quality by observing inherent optical properties (IOPs) of water such as absorptions by phytoplankton, suspended sediment (SS), and colored dissolved organic matters (CDOM), and apparent optical properties (AOPs) of water such as downward irradiances ($E_d$) and upwelling radiance ($L_u$).

Our major aim in this study was to collect bio-optical data in conjunction with measurements of CDOM, phytoplankton and detrital absorption in support of NASA's efforts to develop robust empirical and semi-analytic algorithms for ocean color products in high latitude regions. This effort is a part of longer strategic objective of understanding the impacts of changing climate on biological oceanographic processes in the Amundsen Sea using ocean color satellite data.

For this purpose, we prepared the instruments for inherent optical properties, apparent optical

properties, and reflectivity to implement the cruise. Our observations include the optical profiles in water. In this chapter, we will introduce our instrumentations and observations, and the potential results.

The optical properties of the ocean and sea ice in these areas are linked with the water structure. The optical properties might describe the details of the waters from variety of spectral data.

The optical observations were performed at about 41 stations as shown in Figure 7.1.

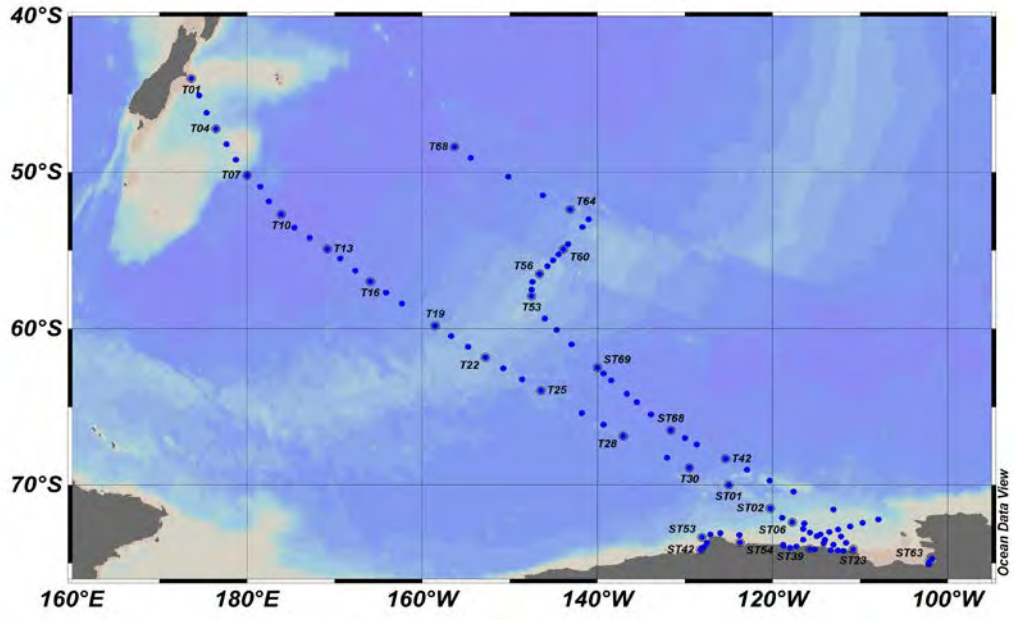


Figure 7.1. A station map for optical observation (T: Underway, ST: station).

## Materials and methods

Ocean optical observation: IOPs

We sampled about 123 waters at about 41 stations (with 3 depths of surface, subsurface chlorophyll maximum, and bottom within euphotic depth) and intermediate sites between stations in underway route. To measure inherent optical properties (IOPs) of water, seawater volumes of 200 ~ 1,000 ml were filtered on 25 mm glass-fiber filters (Whatman GF/F). For absorption by CDOM, seawater volumes of 50 ml were filtered onto disposable syringe filter unit of Advantec (cellulose acetate, 0.45 μm).

Optical densities of total particulate matters were measured directly on the wet filters by methods of Truper and Yentch (1967) with a double-beam recording spectrophotometer (Cary100, Agilent Technologies) in a spectral range 250 ~ 800 nm (spectrum resolution was 1 nm). The filter was placed in front of diffusing windows adjacent to an end-on photomultiplier of large surface area. For a reference blank and baseline variations, an unused wetted filter was taken as were automatically corrected. After the measurement of optical density of total pigments, the spectral absorption by nonalgal material was measured separately with method of Kishino et al. (1985). The filter was placed in absolute methyl-alcohol in order to extract pigments.

Ocean optical observation: AOPs

For the measuring of apparent optical properties (AOPs) of water, we deployed hyperspectral radiometer (TriOS, Figure 7.2) with a spectral range of 280 ~ 950 nm (TriOS) of downward irradiance ($E_d$), upwelling radiance ($L_u$) and upwelling irradiance ($E_u$). For the reference as ambient irradiance variation, downward irradiance ($E_s$) was measured on deck, where was not a shaded place of Araon. The instrument deployed through the A-frame at the stern of the Vessel. The deploying speed was 10 m/min. This data will be able to be used for calibrations and validations of currently operating ocean color remote sensing data.

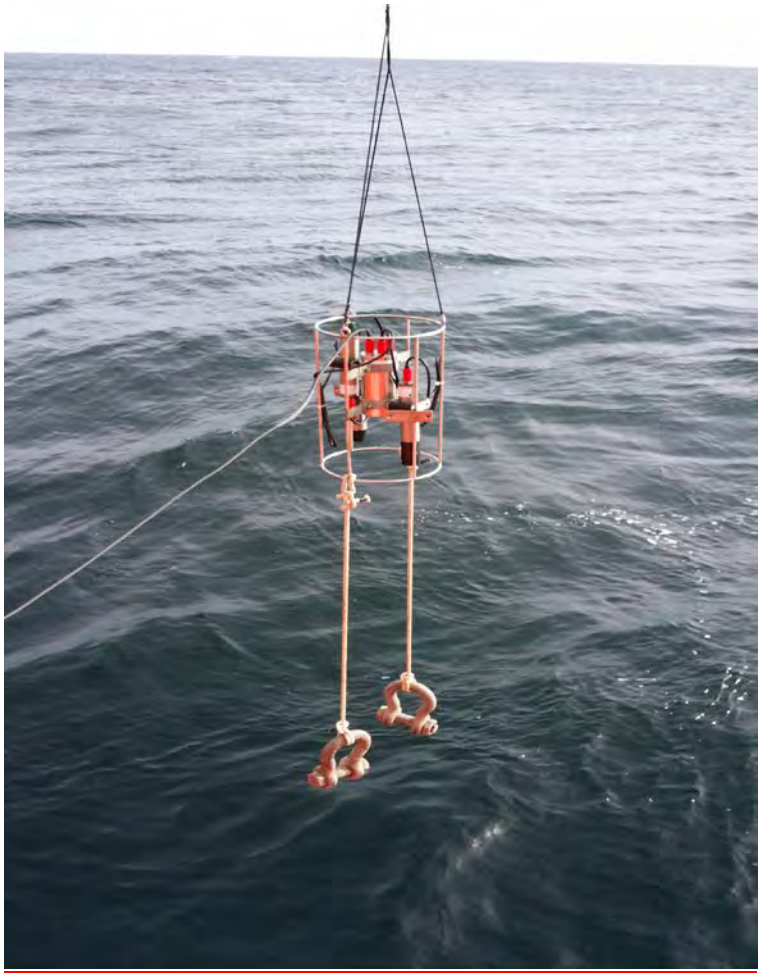

Figure 7.2. Deploy of hyper-spectroradiometer (TriOS).

## Preliminary results (or expected results)

Ocean Optical observation: IOPs

The results from the IOPs will be able to show the bio-optical characteristics in water at each station and at each depth of the water sample.

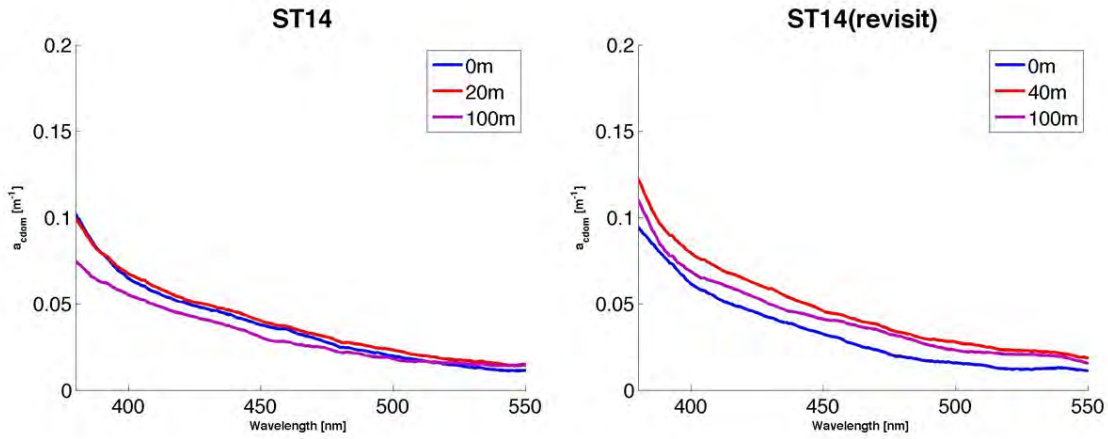


Figure 7.3. An example of colored dissolved organic matter at the station 14.

Ocean Optical observation: AOPs

The results from the AOPs, i.e. data from TriOS, will be able to reflect the continuous bio-optical characteristics of water surface and the bio-optical profiles at the operated station.

## Summary and conclusions

During this cruise, calibration/validation of satellite remote sensing ocean color data were collected. The IOPs reflected the bio-optical characteristics in water at the selected depths. The results from the AOPs such as data from TriOS showed continuous bio-optical characteristics of water surface and the bio-optical profiles at the operated stations. We are going to use these filed data for further detailed examination and correction of satellite data.

## References

Kishino, M., N. Okami, M. Takahashi, and S. Ichimura, 1986. Light utilization efficiency and quantum yield of phytoplankton in a thermally stratified sea. Limnol. Oceangr., 31, 557-566.

Truper, H. G. and C.S. Yentsch, 1967. Use of glass fiber filters for the rapid preparation of in vivo absorption spectra of photosynthetic bacteria. J. Bact.94, 1255-12.

# Appendix I. Cruise participants and contact information

| | Name | Affilation | Email |
|---|---|---|---|
| 1 | SangHoon Lee | Korea Polar Research Institute, Korea | shlee@kopri.re.kr |
| 2 | Tae Siek Rhee | Korea Polar Research Institute, Korea | rhee@kopri.re.kr |
| 3 | Doshik Hahm | Korea Polar Research Institute, Korea | hahm@kopri.re.kr |
| 4 | Kyoung-Ho Cho | Korea Polar Research Institute, Korea | kcho@kopri.re.kr |
| 5 | Tae Wan Kim | Korea Polar Research Institute, Korea | twkim@kopri.re.kr |
| 6 | Jisoo Park | Korea Polar Research Institute, Korea | jspark@kopri.re.kr |
| 7 | Hyoung Sul La | Korea Polar Research Institute, Korea | hsla@kopri.re.kr |
| 8 | Sun-Yong Ha | Korea Polar Research Institute, Korea | syha@kopri.re.kr |
| 9 | Jinyoung Jung | Korea Polar Research Institute, Korea | jinyoungjung@kopri.re.kr |
| 10 | DongYup Kim | Korea Polar Research Institute, Korea | dykim@kopri.re.kr |
| 11 | Chang Sin Kim | Korea Polar Research Institute, Korea | cskim@kopri.re.kr |
| 12 | Youngju Lee | Korea Polar Research Institute, Korea | yjulee@kopri.re.kr |
| 13 | Eric Potvin | Korea Polar Research Institute, Korea | ericpotvin@kopri.re.kr |
| 14 | Intae Kim | Korea Polar Research Institute, Korea | ikim@kopri.re.kr |
| 15 | Jung-Ok Choi | Korea Polar Research Institute, Korea | jochoi@kopri.re.kr |
| 16 | Hee Won Yang | Korea Polar Research Institute, Korea | yhw@kopri.re.kr |
| 17 | Jun Oh Min | Korea Polar Research Institute, Korea | jomin@kopri.re.kr |
| 18 | Eunho Ko | Korea Polar Research Institute, Korea | ehko@kopri.re.kr |
| 19 | Seungjun Lee | Korea Polar Research Institute, Korea | lsjbenthos@gmail.com |
| 20 | Hyo Sub Choi | Korea Polar Research Institute, Korea | Hyosub.hufs@gmail.com |
| 21 | Nag Won Heo | Korea Polar Research Institute, Korea | Ddum2000@hanmail.net |
| 22 | Ah Young Ku | Korea Polar Research Institute, Korea | nayrtic@naver.com |
| 23 | Yeonju Hwang | Korea Polar Research Institute, Korea | hyj1007@kopri.re.kr |
| 24 | Tae Jin Choi | Korea Polar Research Institute, Korea | ctjin@kopri.re.kr |
| 25 | Sang Bum Hong | Korea Polar Research Institute, Korea | hong909@kopri.re.kr |
| 26 | Su Hwan Kim | Korea Polar Research Institute, Korea | idsuhwan@kopri.re.kr |
| 27 | DaeHyeok Lee | Korea Polar Research Institute, Korea | dae-hyuk@kopri.re.kr |
| 28 | Suk Hyun Haam | NEOSEA Tec. | Haam6481@gmail.com |
| 29 | Jae Hak Lee | Korea Institute of Ocean Science and Technology | jhlee@kiost.ac.kr |
| 30 | Dong Guk Kim | Korea Institute of Ocean Science and Technology | kdk21ca@kiost.ac.kr |
| 31 | Jin Hyun Jeong | Korea Institute of Ocean Science and Technology | pujjh@kiost.ac.kr |
| 32 | Jung-Ho Hyun | Hanyang University, Korea | hyunjh@hanyang.ac.kr |
| 33 | Sung-Han Kim | Hanyang University, Korea | shkim1778@hanmail.net |
| 34 | Euo-Jung Jung | Hanyang University, Korea | jeongf21@naver.com |
| 35 | Bumsoo Kim | Seoul National University, Korea | kbs3257@snu.ac.kr |
| 36 | Joo-Han Gwak | Chungbuk National University, Korea | mnter89@gmail.com |
| 37 | Dong Jun Jang | Chungnam National University, Korea | jdjun07@gmail.com |
| 38 | Kyoung Kyu Park | Chungnam National University, Korea | p2k@nate.com |
| 39 | Dabin Lee | Pusan National University, Korea | ldb1370@pusan.ac.kr |
| 40 | You Dong Cho | Korean Alpine Club | youdong@hanmail.net |
| 41 | Young-Hyang Park | LOCEAN, Museum of Natural History, France | yhpark@mnhn.fr |
| 42 | Isabelle Durand | LOCEAN, Museum of Natural History, France | idurand@mnhn.fr |
| 43 | Elin D. Chiche | Unversity of Bergen, Norway | elin@gfi.uib.no |
| 44 | Nicole Waite | Rutgers University, USA | waite@marine.rutgers.edu |
| 45 | Thomas G. Richter | University of Texas at Austin, USA | Tom.richter@utexas.edu |
| 46 | Anna K. Wåhlin | University of Gothenburg, Sweden | anna@marine.gu.se |
| 47 | Karen M. Assmann | University of Gothenburg, Sweden | Karen.assmann@marine.gu.se |
| 48 | Einar P. Abrahamsen | British Antarctic Survey, UK | epab@bas.ac.uk |

# Appendix II. Group photo